# Phenomenology of thermally produced hot and cold dark relics in naturalness-motivated extensions of the Standard Model

Michał Łukawski

Doctoral dissertation prepared under the supervision of
**dr hab. Marcin Badziak, prof. ucz.**
at the Institute of Theoretical Physics, Faculty of Physics, University of Warsaw

**February 2025**

# Acknowledgements

First and foremost, I am profoundly grateful to my supervisor, dr hab. Marcin Badziak, prof. ucz. for his unwavering guidance and patience throughout our six years of collaboration. Your contributions to the thesis cannot be overstated. I do not doubt that you have been the most impactful person in my academic career and I will never forget who introduced me to the beauty of axion physics and supersymmetry. I am truly grateful for the opportunities, knowledge, and insights you have provided.

I am sincerely grateful to the University of Warsaw and the National Science Center for their financial support, which was instrumental in making this research possible. Access to international conferences and the academic community has been invaluable in achieving the quality of research presented in this dissertation.

I would also like to extend my thanks to my collaborators Giovanni Grilli di Cortona and Keisuke Harigaya whose expertise has greatly contributed to the scientific level achieved in this thesis. Working alongside you has been both a privilege and a pleasure.

I am deeply grateful to my collaborator Robert Ziegler, for hosting me at the Karlsruhe Institute of Technology. I am truly thankful for the life-changing experience it provided and for the invaluable lessons I learned during my time there. I also deeply appreciate the warm welcome and hospitality I received at KIT.

A heartfelt thanks to the RL group for their continuous support and inspiration throughout my academic journey, beginning with our undergraduate studies. We did it, guys! I owe a special debt of gratitude to Paweł Pajewski and Michał Ryczkowski, with whom I first understood the quantum harmonic oscillator. You are always an inspiration, and I know I will continue to recall, and have, our discussions for the rest of my life.

I cannot fully express my gratitude for my family, and especially to my parents, who catalyzed my growth in childhood and never slowed me down. You gave me the freedom I hope I have used well. A loud and cheerful thanks to my sister for her constant support throughout my scientific journey. You were the one who showed me what a function is when I was little and I will always remember how you predicted my future in physics.

Last but not least, I would like to express my gratitude to my soulmate Paulina Michalak for her patience and unwavering faith in me. I will always remember our after-breakfast walks as the symbol of our PhD studies. You are the reason why anything is happening and I could never have achieved it without you.

This work was partially supported by the National Science Centre, Poland, under research grant no. 2020/38/E/ST2/00243.

**Abstract**

In the thesis, we investigate the phenomenology of two classes of models motivated by the naturalness criterion that feature thermal production of dark relics: astrophobic axion models and supersymmetric Twin Higgs models.
We first analyse the production of astrophobic axions which avoid astrophysical bounds by suppressing couplings to electrons and nucleons without increasing the axion decay constant. Since astrophobic axions have suppressed coupling to pions, they are primarily produced in lepton-flavour violating decays and lepton scatterings, however non-negligible contribution from kaon scatterings is generically also present. Depending on the axion mass, the population of axions acts as dark radiation or warm dark matter, which we take into account by exploiting mass-dependent bound on axions energy density parametrized by the additional effective number of neutrinos, $\Delta N_{\rm eff}$. We demonstrate that in astrophobic axion models with 2 Higgs doublets, the cosmological bound reads $f_a \gtrsim 8 \times 10^6$ GeV, and is weaker or comparable to the astrophysical constraint on axion-muon and axion-photon couplings, depending on specific couplings of the model. We show that the predicted sensitivities of future CMB experiments will significantly improve the cosmological bound probing up to $f_a \simeq 10^8$ GeV. Furthermore, we discuss how the generalization of the model to include three Higgs doublets allows for additional suppression of mentioned couplings, further relaxing astrophysical bounds and allowing for eV-scale axion mass. We categorize 3HDM astrophobic axion models based on their suppressed couplings and analyse their phenomenologies. Most astrophobic models are within the reach of Simons Observatory or the CMB-S4, and/or within the reach of IAXO or even BabyIAXO. In the naturally astrophobic model, axions are produced solely via non-perturbative effects which remain challenging to calculate exactly. Our estimate for cosmological bound can be as strong as $f_a \gtrsim 5 \times 10^6$ GeV for vanishing strange quark coupling, which potentially allows for explaining baryon asymmetry via axiogenesis and providing a non-relativistic population of axions playing the role of the DM produced via kinetic misalignment mechanism.
Next, we study two dark matter candidates produced via freeze-out in SUSY TH models: the twin stau and the twin neutralino. The former particle is charged under twin electromagnetism mediated by the massless photon. We found that mostly right-handed twin stau with a mass between 400 and 500 GeV is a viable DM candidate, satisfying direct detection, collider, astrophysical, and cosmological constraints. We discuss the collider signatures of the twin stau DM scenario and the prospects of probing it with future direct detection experiments, highlighting that LZ will probe most natural regions of the parameter space, corresponding to fine-tuning better than a few percent. We demonstrate that twin bino-dominated neutralino is also a valid DM candidate and show that overproduction can be relaxed by introducing $\mathbb{Z}_2$ symmetry breaking in the Yukawa sector, which does not spoil the solution to the hierarchy problem while alleviating the dark radiation problem. Similarly to twin stau DM, this scenario will best be probed by direct detection experiments. The LZ experiment will explore the most natural regions of the parameter space, corresponding to fine-tuning better than 10%.
In the thesis, we demonstrate that cosmological observations provide powerful constraints on models featuring thermal production of dark relics, probing energy scales inaccessible to ground-based experiments. By combining astrophysical, laboratory, and cosmological observations, we perform a complete analysis of the models, highlighting the intricate interplay between particle physics models and cosmology.

## Streszczenie

W niniejszej rozprawie doktorskiej badamy fenomenologię dwóch klas modeli motywowanych kryterium naturalności, które wykazują termiczną produkcję ciemnych reliktów: modele astrofobicznych aksjonów oraz supersymmetryczne modele Twin Higgs.

W pierwszej kolejności analizujemy produkcję astrofobicznych aksjonów, które unikają astrofizycznych ograniczeń przez tłumienie sprzężeń do elektronów i nukleonów bez zwiększania stałej rozpadu aksjonu. Ponieważ astrofobiczne aksjony mają tłumione sprzężenia do pionów, są głównie produkowane w rozpadach łamiących liczby leptonowe oraz w rozproszeniach leptonów, z generycznie obecnym niezaniedbywalnym wkładem z rozproszeń kaonów. W zależności od masy aksjonu, populacja aksjonów zachowuje się jako ciemne promieniowanie lub ciepła ciemna materia, co uwzględniamy wykorzystując ograniczenie na gęstość energii aksjonów zależne od masy, sparametryzowane przez dodatkową efektywną liczbę neutrin, $\Delta N_{\rm eff}$. Wykazujemy, że w astrofobicznych modelach aksjonowych z 2 dubletami Higgsa, ograniczenie kosmologiczne wynosi $f_a \gtrsim 8 \times 10^6$ GeV i jest słabsze lub porównywalne do ograniczeń astrofizycznych na sprzężenia aksjon-mion i aksjon-foton, w zależności od dokładnych sprzężeń modelu. Pokazujemy, że przewidywane czułości przyszłych eksperymentów CMB znacznie poprawią ograniczenie kosmologiczne, badając zakres do $f_a \simeq 10^8$ GeV. Ponadto omawiamy, jak uogólnienie modelu do trzech dubletów Higgsa umożliwia dodatkowe tłumienie wspomnianych sprzężeń, dalej osłabiając ograniczenia astrofizyczne i umożliwiając masę aksjonu rzędu eV. Klasyfikujemy modele astrofobicznych aksjonów w 3HDM na podstawie ich tłumionych sprzężeń i analizujemy ich fenomenologię. Większość modeli astrofobicznych jest w zasięgu obserwowalności Simons Observatory lub CMB-S4, oraz/lub w zasięgu IAXO lub nawet BabyIAXO. W modelu naturalnie astrofobicznym aksjony są produkowane wyłącznie poprzez efekty nieperturbacyjne, których obliczenie pozostaje wyzwaniem. Nasza estymacja ograniczenia kosmologicznego może być tak silna jak $f_a \gtrsim 5 \times 10^6$ GeV dla zanikającego sprzężenia z dziwnym kwarkiem, co potencjalnie pozwala na wyjaśnienie asymetrii barionowej poprzez aksjogenezę i zapewnienie nierelatywistycznej populacji aksjonów odgrywających rolę ciemnej materii produkowanej poprzez mechanizm kinetic misalignment.

Następnie badamy dwóch kandydatów na ciemną materię produkowanych poprzez mechanizm freeze-out w supersymetrycznych modelach Twin Higgs: twin stau oraz twin neutralino. Twin stau jest naładowany względem bliźniaczego elektromagnetyzmu, mediowanego przez bezmasowy foton. Nasze badania wykazały, że głównie prawoskrętne twin stau o masie między 400 a 500 GeV stanowi możliwego kandydata na ciemną materię, spełniając ograniczenia wynikające z detekcji bezpośredniej, doświadczeń w zderzaczach, astrofizyki i kosmologii. Dyskutujemy sygnatury zderzeniowe scenariusza z ciemną materią w postaci twin stau oraz perspektywy badania tego scenariusza za pomocą przyszłych eksperymentów detekcji bezpośredniej, podkreślając, że eksperyment LZ zbada większość naturalnych obszarów przestrzeni parametrów, odpowiadających dostrajaniu lepszemu niż kilka procent. Wykazujemy, że zdominowane przez twin bino neutralino również stanowi potencjalnego kandydata na ciemną materię i pokazujemy, że nadprodukcja może zostać złagodzona poprzez wprowadzenie złamania symetrii $\mathbb{Z}_2$ w sektorze Yukawy, co nie narusza rozwiązania problemu hierarchii, jednocześnie łagodząc problem promieniowania ciemnego. Podobnie jak w przypadku ciemnej materii w postaci twin stau, ten scenariusz zostanie najlepiej zbadany za pomocą eksperymentów detekcji bezpośredniej. Eksperyment LZ zbada większość naturalnych obszarów przestrzeni parametrów, odpowiadających dostrajaniu lepszemu niż 10%.

W pracy doktorskiej wykazujemy, że obserwacje kosmologiczne dostarczają silnych ograniczeń na modele charakteryzujące się termiczną produkcją ciemnych reliktów, badając skale energii niedostępne dla eksperymentów naziemnych. Łącząc obserwacje astrofizyczne, laboratoryjne i kosmologiczne, przeprowadzamy kompletną analizę modeli, podkreślając złożoną interakcję między modelami fizyki cząstek a kosmologią.

# Contents


**Acronyms** **1**

**1 Introduction** **2**

**2 Necessity for BSM** **8**
- 2.1 Naturalness . . . 8
- 2.2 Strong CP-problem . . . 9
  - 2.2.1 Symmetry structure of QCD . . . 9
  - 2.2.2 Low energy limit of QCD . . . 11
  - 2.2.3 $U(1)_A$ problem and the instantons . . . 15
  - 2.2.4 The theta vacuum . . . 19
  - 2.2.5 Chiral anomaly . . . 20
  - 2.2.6 Strong CP problem . . . 22
- 2.3 Hierarchy problem . . . 24
  - 2.3.1 Fine-tuning measure . . . 27
- 2.4 Dark matter . . . 28
  - 2.4.1 Evidence for the existence of dark matter . . . 28
  - 2.4.2 Relic density . . . 31
  - 2.4.3 Direct detection . . . 33
  - 2.4.4 Indirect detection . . . 33
- 2.5 Summary . . . 34

**3 Axions** **36**
- 3.1 Peccei-Quinn solution . . . 36
- 3.2 QCD axion . . . 37
  - 3.2.1 DFSZ model . . . 38
  - 3.2.2 QCD axion below PQ symmetry breaking scale . . . 42
- 3.3 Axion properties below chiral symmetry breaking scale . . . 43
  - 3.3.1 Coupling to pions . . . 46
  - 3.3.2 Coupling to kaons . . . 48
- 3.4 Constraints on axion couplings . . . 49
- 3.5 Cosmology with axions . . . 52
  - 3.5.1 Topological defects . . . 52
  - 3.5.2 Misalignment mechanism . . . 53
- 3.6 Summary . . . 54

**4 Astrophobic axions** **55**
- 4.1 Scalar potential of generalized DFSZ models . . . 56
- 4.2 Quark sector in astrophobic axion models . . . 57
  - 4.2.1 Quark sector in 2HDM . . . 59

4.2.2 Quark sector in 3HDM . . . 62
4.3 Lepton sector in astrophobic axion models . . . 63
4.3.1 Lepton sector in 2HDM . . . 65
4.3.2 Lepton sector in 3HDM . . . 65
4.4 Summary of astrophobic axion model . . . 68
4.4.1 Summary of astrophobic axion 2HDMs . . . 69
4.4.2 Summary of astrophobic axion 3HDMs . . . 70

**5 Hot axions contribution to the dark radiation** **73**
5.1 Contribution to $\Delta N_{\text{eff}}$ from massless species . . . 73
5.2 Massive axion and the CMB . . . 78
5.3 Explicit contributions to the Boltzmann equation for axion . . . 78
5.3.1 Lepton scatterings . . . 78
5.3.2 Flavor violating lepton decay . . . 82
5.3.3 Pion scattering . . . 83
5.3.4 Kaon scattering . . . 85
5.4 Freeze-in and freeze-out production of axions . . . 86
5.5 Axion contribution to the effective number of neutrinos . . . 87
5.5.1 Model-independent analysis of axion contribution to $\Delta N_{\text{eff}}$ . . . 87
5.5.2 2HDM . . . 89
5.5.3 3HDM . . . 91
5.5.4 $\Delta N_{\text{eff}}$ from the Naturally Astrophobic QCD Axion . . . 95
5.6 Summary . . . 97

**6 Supersymmetry and Twin Higgs mechanism** **99**
6.1 Twin Higgs mechanism . . . 99
6.2 Supersymmetry . . . 103
6.2.1 Minimal Supersymmetric Standard Model . . . 106
6.2.2 Soft supersymmetry breaking . . . 106
6.3 Supersymmetric Twin Higgs . . . 108
6.3.1 F-term SUSY TH . . . 108
6.3.2 D-term SUSY TH . . . 109
6.3.3 Fine-tuning in SUSY TH models . . . 110
6.4 Summary . . . 111

**7 Twin supersymmetric dark matter** **113**
7.1 Twin stau DM . . . 113
7.1.1 Mass of (twin) stau . . . 113
7.1.2 Self-interactions of twin stau . . . 114
7.1.3 Direct detection . . . 116
7.1.4 Thermal abundance . . . 117
7.1.5 Lifetime of stau . . . 119
7.1.6 Results . . . 124
7.2 Twin neutralino DM . . . 132
7.2.1 Mass of (twin) neutralino . . . 133
7.2.2 Direct detection . . . 133
7.2.3 Thermal abundance . . . 135
7.2.4 Results . . . 135

**8 Conclusions** **139**

**A Elements of QFT** **143**
A.1 Divergence of Chern-Simons current . . . 143
A.2 Non-linear sigma model for mesons . . . 145
A.3 Cross sections, decay widths . . . 149
A.3.1 Scattering $2 \to 2$ . . . 149
A.4 Noether theorem . . . 152
A.5 Spontaneous symmetry breaking and Goldstone theorem . . . 153
A.5.1 Alternative proof of Goldstone theorem . . . 154

**B Cosmology of Homogenous Universe** **157**
B.1 Geometry of homogenous Universe . . . 157
B.2 Thermodynamics of early Universe . . . 159
B.3 Boltzmann equation . . . 160
B.4 Collision term . . . 163
B.4.1 Special cases of collision term . . . 164
B.5 Boltzmann equations in supersymmetric models . . . 168

# Acronyms

**SSB** Spontaneous symmetry breaking

**NGB** Nambu-Goldstone boson

**ChPT** Chiral perturbation theory

**EW** Electroweak

**VEV** Vacuum expectation value

**DM** Dark matter

**LHC** Large Hadron Collider

**PQ** Peccei-Quinn

**SUSY** Supersymmetry

**TH** Twin Higgs

**2HDM** Two Higgs doublet model

**3HDM** Three Higgs doublet model

**QCD** Quantum chromodynamics

**SM** Standard model

**MSSM** Minimal Supersymmetric Standard Model

**pNGBs** pseudo-Nambu-Goldstone bosons

**QCDPT** Quantum Chromodynamics Phase Transition

**LO** Leading order

**NLO** Next-to leading order

**BBN** Big Bang Nucleosynthesis

**LFV** Lepton flavour violation

**CMB** Cosmic microwave background

**EoM** Equation of Motion

**RHS** Right-hand side

**LHS** Left-hand side

**CM** Center of mass

# Chapter 1

# Introduction

The twentieth century was a period of rapid development of fundamental physics, with the rise of quantum mechanics and relativity leading towards the formulation of Quantum Field Theory. The development of electroweak theory in the '60s and QCD in the '70s led to the construction of what is now known as the Standard Model of particle physics. Crucially, the theory of electroweak interactions required the existence of a new scalar particle responsible for generating gauge boson masses via the Brout-Englert-Higgs (BEH) mechanism. The particle, later named 'Higgs particle', triggered the spontaneous breaking of electroweak symmetry by acquiring a non-vanishing VEV. Famously, in 2012, a scalar particle with properties of the Higgs boson was observed by both CMS [1] and ATLAS [2] experiments at the Large Hadron Collider. A year later, the Nobel Prize in physics was awarded to Peter Higgs and François Englert for their contribution to the discovery of the BEH mechanism.

While the discovery of the Higgs boson is the most recent successful prediction of the SM, it certainly is not the only one. The BEH mechanism predicted the masses of $W$ and $Z$ bosons, which are in agreement with recent measurements at LHC, see Ref. [3][1]. Moreover, in the 70s, the existence of the top quark was predicted by Kobayashi and Maskawa [9], which was later confirmed at Fermilab in 1995 [10, 11]. Most notably, the measurement of the electron magnetic dipole moment, obtaining loop corrections from QED, is in astonishing agreement with the measurement with relative accuracy of around $10^{-13}$ [12]. Also, the existence of the charm quark was correctly predicted in the 70s, and of the gluon in the 60s. Quite generally, the agreement between the theoretical predictions of the Standard Model and the measurements is outstanding, see Tab. 10.4 in Ref. [13]. However, the Standard Model does not account for the masses of neutrinos and does not include the gravitational interactions. Moreover, the electroweak scale is not stable in the Standard Model and cannot be reproduced without precise fine-tuning of the parameters. Therefore, the Standard Model must necessarily be viewed as incomplete, placing us in exciting times in the history of particle physics.

A pivotal concept in particle physics is naturalness, a theoretical criterium inferred from viewing the Standard Model as an effective field theory. Considering the parameters of the model as emergent from a more fundamental theory, the order of magnitude of those parameters can often be deduced. If our expectation is far from the measured value, it may signal the existence of a more fundamental model. In particular, the symmetries of the theory are often reflected in the suppression of some effective interaction, and such hints may be leveraged in constructing BSM models.

[1] CDF at Fermilab Tevatron found significant discrepancy between measured mass of $W$ boson and SM prediction, but is also in tension with other measurements [4]. For review, see Refs. [5–7]. However, preliminary results from CMS at LHC found agreement with SM prediction and previous measurements [8].

On the other hand, the General Relativity proposed by Albert Einstein in 1915 was a revolution of its own. The spacetime metric was promoted to a dynamical object determined by the distribution of matter, rather than a static background, with dynamics captured by the Einstein equation. In the early years, General Relativity correctly predicted the precession of Mercury's perihelion and the bending and redshifting of light in curved spacetime. Moreover, it correctly predicted the existence of black holes, with evidence in the form of gravitational waves from black hole mergers, also predicted by General Relativity, first observed in 2015 at LIGO experiment [14]. The Nobel Prize in physics in 2017 has been awarded to Rainer Weiss, Kip Thorne, and Barry Barish for their contribution to the LIGO experiment.

General Relativity allowed for studying the evolution of the Universe as a whole, assuming isotropy and homogeneity. The derivation of Friedmann–Lemaître–Robertson–Walker solution [15–20] to the Einstein equation marked the beginning of modern cosmology. The discovery of the expansion of the Universe in the 20s confirmed the non-static nature of the Universe and ultimately led to the theory of the Big Bang. The history of the Universe can be studied using methods of statistical mechanics in the non-Riemannian geometry of FLRW. In early times, as the energy density of the Universe was large and the average frequency of interactions between particles, determined by the Standard Model of particle physics, was shorter than the rate of expansion of the Universe, equilibrium was maintained between different particle species. Since in the expanding Universe, as time passed the density of particles decreased, the interaction rate between particles dropped, and some species went out of equilibrium. In particular, interactions between baryon-electron plasma and photons ceased to maintain thermal equilibrium at recombination at $T = 0.3$ eV, leaving behind a population of neutral hydrogen atoms, and photons known as Cosmic Microwave Background. The process in which a population of particles ceases to be in thermal contact with a Standard Model bath is known as freeze-out and is the most common thermal mechanism of particle production. Another famous example of freeze-out is the neutrino decoupling around $T = 1$ MeV when scatterings via weak interactions became inefficient. Since neutrinos are stable, they have been redshifting ever since the freeze-out, constituting the neutrino cosmic background. Measurements of temperature anisotropies of Cosmic Microwave Background are currently the most robust observations used to determine the cosmological parameters. So far all observations are consistent with $\Lambda$CDM model, the Standard Model of Cosmology, which is a Universe dominated by the cosmological constant with sizable contribution from non-relativistic matter [21]. The thermal history of the Universe also allows for predicting the mass abundances of nuclei produced in the Big Bang nucleosynthesis, in good agreement with observations (see however the lithium problem, Ref. [22]).

Cosmology is inherently linked to particle physics due to scatterings governed by QFT within the thermal bath. Many problems in particle physics cannot be approached without referring to cosmology, and vice versa. In particular, dark matter is a hypothetical form of matter, constituting the vast majority of all matter, required to match astrophysical and cosmological observations. We infer the existence of dark matter through its gravitational interactions, observed on scales ranging from individual galaxies to cosmological distances probed by observation of the Cosmic Microwave Background. Dark matter cannot interact electromagnetically, as this would make it visible, and it cannot interact strongly, as such interactions with the photon-baryon plasma in the early Universe would disrupt large-scale structure formation. Moreover, interactions between dark matter and visible matter must be weak to satisfy the stringent bounds set by direct detection experiments on the interaction cross section with electrons and nucleons. Crucially, no particle of the Standard Model can play the role of dark matter. While neutrinos at first glance may seem to be a candidate, they are relativistic and cannot be seeds for large-scale structure formation. This brings us to an important distinction between hot relics, like neutrinos, which are relativistic at decoupling, and non-relativistic cold relics which may play a role of dark matter. Besides dark matter, other problems shared by particle physics and cosmology include, but are not restricted to, matter-antimatter asymmetry, the origin of dark energy, and inflation.

The equilibrium established in the early times of the Universe had a significant consequence: any particle coupled to the SM must have necessarily been thermally produced in the early Universe. In particular, if they are stable, at the timescale of the age of the Universe, a background of those particles should be present today in analogy to the CMB or neutrino background. Therefore, freeze-out has become a leading framework for generating the population of cold relics. In particular, for years the leading class of candidates for dark matter have been Weakly Interacting Massive Particles (WIMPs) produced via freeze-out at temperatures typically between 1-100 GeV. In the freeze-out, the increase of the interaction rate delays the decoupling, consequently reducing the final abundance of the relic.

On the other hand, if initially the particle's abundance vanishes, scatterings within the thermal bath may produce a population of particles. Provided that scatterings are never efficient enough to bring particles to equilibrium, this mechanism of production is named freeze-in [23]. In the freeze-in, the increase in the interaction rate leads to an increase in the final abundance of the relic.

Importantly, since very large temperatures have been present in the early Universe, heavy particles beyond the reach of LHC could have been produced. Therefore, cosmological observations may be used to probe energies orders of magnitude beyond the reach of current and future experiments. However, since they rely on observations of a single instance of the Universe's evolution and determine the energy density of the particle, cosmological observations lack the robustness to distinguish between different particle models, constituting complementary observations to ground-based experiments. The accurate measurements of the CMB temperature power spectrum in experiments such as Planck mission [21, 24] allowed for precise determination of the cosmological parameters in $\Lambda$CDM model. Incorporating cosmological hints in studying the phenomenology of particle models is now a standard approach.

In this thesis, we will study the thermal production in two models realizing naturalness criterium: axion model, explaining the smallness of CP violation in strong interactions, and Supersymmetric Twin Higgs model explaining the stability of electroweak scale under quantum corrections without fine-tuning. We will consider thermal production via freeze-out in SUSY TH, and via freeze-in/freeze-out in axion model. In freeze-out production, as opposed to freeze-in, the final density of thermally produced relic is independent of the initial condition. The central equation governing the out-of-equilibrium dynamics in the early Universe is the Boltzmann equation, describing the time evolution of number densities.

The first class of models which we will consider consists of axions. Axions were proposed to solve the strong CP problem via the Peccei-Quinn mechanism [25–30], which we will cover in detail. Axion models have rich phenomenology, in particular, axions produced non-thermally via misalignment or kinetic misalignment mechanisms may play a role of the dark matter [31–36], the symmetry breaking patterns may lead to the formation of topological defects in the early Universe [37–42], and the axiogenesis may generate baryon asymmetry [36, 43–46]. In general, axions have sizable couplings to nucleons due to the irreducible gluon coupling required to solve the strong CP problem. Those couplings and electron coupling lead to an efficient production of axions in stars and supernovae, altering their evolution. Astrophysical models can be used to constrain the magnitude of those couplings [47–57]. In a broad class of models, these bounds are the strongest, ruling out a large portion of parameter space. In particular, the thermal production of axions is suppressed so much in generic axion models, that the resulting population of axions is undetectable.

However, it is possible to construct models, named astrophobic axion, which feature suppressed couplings to nucleons and electrons, relaxing the strongest of bounds [58–61]. In the simplest implementation, astrophobia requires lepton flavour violation, which not only allows for constraining the models with ground-based experiments but also features efficient production of axions in the early Universe via decays of the heavy tau lepton. In the thesis, we will cover the construction of astrophobic axion models, categorizing the models by the couplings and collecting all phenomenologically relevant constraints. The thermal production of astrophobic axions is particularly interesting, since at recombination the resulting population is relativistic for small axion masses, while for relatively large axion masses behaves as warm dark matter [62]. We will solve the Boltzmann equation involving all relevant processes, in particular the kaon scatterings which have often been neglected in the past (however, see Ref. [63]). The density of axions is parametrized by the effective number of neutrinos, $N_{\rm eff}$, which is constrained by the CMB observations and will be the central object of our analysis.

The second class of models, which features an interesting thermal production, are supersymmetric Twin Higgs models [64–71], motivated by the Hierarchy Problem.

While the instability of the EW scale under quantum corrections is widely considered as one of the most severe problems of the SM [72, 73], the naturalness criterium can be leveraged to constrain the possible extensions of the SM. In particular, supersymmetry is well-known to alleviate the Hierarchy Problem by canceling the large corrections to the mass of the Higgs with contributions from supersymmetric partners. However, the cancellation is efficient only above the energy scale of supersymmetry breaking, which is constrained by the null results of LHC searches for strongly interacting SUSY partners like squarks. As a result, the minimal implementations of supersymmetry require fine-tuning of the parameters, which undermines the primary motivation for considering SUSY. Nonetheless, supersymmetry is an attractive extension of the SM, not only allowing for unification of fundamental interactions but also providing a candidate for quantum gravity theory by means of local supersymmetry known as supergravity. Moreover, from the theoretical standpoint, it is appealing that supersymmetry is the only possible spacetime symmetry extension of the Poincaré group [74].

On the other hand, the Twin Higgs mechanism [75, 76] protects the EW scale by promoting the Higgs boson to the Nambu-Goldstone boson of spontaneously broken global symmetry of the potential. The symmetry arises accidentally due to the introduction of a twin sector, with the couplings related to the coupling in the visible sector via discrete $\mathbb{Z}_2$ symmetry. The mass of the Goldstone bosons is protected from large quantum correction, and the Hierarchy Problem is postponed to the scale of global symmetry breaking. The $\mathbb{Z}_2$ symmetry relating sectors must be softly broken to match the observed properties of the Higgs boson, which results in misalignment of the Higgses' VEVs. Consequently, the masses of particles in the twin sector can be expressed in terms of the masses of particles in the visible sector and the ratio of those VEVs. The Twin Higgs model has rich phenomenology, due to the abundance of particles in the twin sector. In particular, many dark matter candidates in Twin Higgs models have been studied over the last decade [77–92].

Often, additional model building is required to satisfy all constraints, in particular, breaking of twin electromagnetism is often necessary to suppress self-interactions. However, the Twin Higgs model suffers the Hierarchy Problem same as the SM, with large quantum corrections to the scale of the global symmetry breaking, instead of the EW scale. In other words, the Twin Higgs mechanism is by itself incomplete and requires UV completion at large energies.

The possibility of double protection of the EW scale has been studied extensively in the past. The idea is to combine the two mechanisms protecting the mass of the Higgs from large quantum corrections to reduce the fine-tuning in models solving the Hierarchy Problem. Well-studied possibilities are combinations of supersymmetry with little Higgs [93–97] or twin Higgs with composite models [98–103]. In this thesis, we will consider double protection of the EW scale by supersymmetry and Twin Higgs mechanism [64, 65, 68–71]. In certain realizations of Supersymmetric Twin Higgs, the electroweak scale is safe from large correction up to the Planck scale while the fine-tuning can be of order 10% [70].

Interestingly, if the lightest supersymmetric particle resides in the twin sector, it is a candidate for dark matter [104]. Twin LSP particles are produced via a freeze-out mechanism involving annihilations, coannihilations, and resonances. It is interesting to investigate what is possible improvement in twin SUSY DM when compared to MSSM DM. Therefore, we chose two particles we have investigated in detail, whose MSSM partners cannot constitute dark matter in the simplest and natural scenarios.

Our first choice is twin stau, the $\mathbb{Z}_2$ partner of supersymmetric partner of tau lepton. The MSSM stau cannot be dark matter due to the electromagnetic charge, which would make it visible and thus directly observable. On the other hand, twin stau is charged under twin electromagnetism and is a potentially viable candidate for the dark matter, as it does not interact efficiently with baryon-photon plasma and has suppressed couplings to the SM nucleons, avoiding tight bounds from direct detection experiments. Interestingly, twin stau coupling to twin photon induces sizable self-interactions which are constrained by the ellipticity measurements of dark matter halo. Without a detailed analysis of twin stau thermal production, it is impossible to assess if it can constitute all dark matter without additional model building.

Another twin SUSY candidate for dark matter which we will consider is the twin neutralino, the mixture of $\mathbb{Z}_2$ partners of of gauginos and higgsinos. In the MSSM, only tight regions of the parameter space allow for successful neutralino DM [105], which is significantly relaxed in the SUSY TH model. In particular, in part of the parameter space thermalization occurs via chirality-suppressed stau exchange, with the mass of stau constrained by LEP. The lower limit on stau mass suppresses the annihilation cross section and consequently leads to the overproduction of dark matter, which can be avoided in the SUSY TH [106].

In Chapter 2 we provide extensive motivation for models considered in the thesis, focusing on the strong CP problem, the Hierarchy Problem, and dark matter. Chapter 3 introduces the Peccei-Quinn solution to the strong CP problem and reviews the details of the DFSZ axion model, while Chapter 4 covers the construction of astrophobic axion models. Chapter 5 presents the original results of this thesis, discussing the thermal production of astrophobic axions in the early Universe. In Chapter 6 we cover the Twin Higgs mechanism and Supersymmetry, emphasizing their role in addressing the Hierarchy Problem. Finally, in Chapter 7 we analyze the parameter space of twin stau and twin bino as dark matter candidates, accounting for all relevant constraints, in particular the direct detection bounds and their thermal abundance. Finally, in Chapter 8 we conclude the findings of the thesis and discuss its limitations.

We also provide appendices at the end of the thesis, where we collect results used throughout the thesis. Appendix A includes some results from QFT, particularly the construction of the Chiral Perturbation Theory at leading order and proofs of Noether and Goldstone theorems. Appendix B covers elements of Cosmology, in particular in Appendix B.3 we discuss the Boltzmann equation and derive several examples of collision terms.

# Chapter 2

# Necessity for BSM

In this chapter, we lay out the motivation for models considered in the thesis. In Sec. 2.1 we discuss the naturalness, as a criterion for BSM. In Sec. 2.2 we review the QCD and low-energy limit of strong interaction, ultimately stating the strong CP problem. In Sec. 2.3 we discuss in detail corrections to the mass of the Higgs boson arising in the SM, and how they signal a Hierarchy Problem. Finally, in Sec. 2.4 we review the observational evidence for the existence of DM and experimental efforts towards its detection.

## 2.1 Naturalness

In the 1930s, Dirac proposed the Large Numbers Hypothesis, concerning relations between large, dimensionless numbers [107]. While his idea turned out to be wrong, it has been pivotal in understanding how effective parameters originate from fundamental theories. In modern understanding, the Dirac naturalness states, that the parameters of the fundamental theory are expected to be of order $\mathcal{O}(1)$. In QFT, any parameter in the effective theory emerges as a consequence of integrating out heavy fields. A special value of parameter $p$ in the effective theory, e.g. $p \simeq 0$, reflects the properties of the fundamental theory, such as symmetries. In other words, the values of parameters should be comprehensible from the more fundamental theory, suggesting the existence of a mechanism explaining observed values. Of course, this idea should be used with caution, as it could be that the observed parameter is fundamental with no deeper explanation. Nonetheless, Dirac's naturalness could be used as a guiding principle for constructing high-energy theories, especially when experimental evidence for new physics is limited.

For a specific UV theory, an emergent observable $\mathcal{O}(p_i)$ depends on the parameters $p_i$ of the fundamental theory. If the observed value of $\mathcal{O}$ is reproduced only in a tight region of parameter space, we say a theory is fine-tuned. In other words, the theory is fine-tuned if it requires precise adjustments of its parameters $p_i$ to match experimental observations, and even small deviations in $p_i$ could lead to significant changes in the observable $\mathcal{O}$, potentially rendering the theory inconsistent with observations. Fine-tuning indicates a lack of robustness in the model and a need for additional model building explaining the tuning of the parameters. We will quantify the fine-tuning measure in Sec. 2.3.1 in the context of the Hierarchy Problem.

An example of Dirac unnatural parameter is the electron Yukawa coupling, $y_e \simeq 10^{-5}$, which is orders of magnitude below natural top Yukawa, $y_t \simeq 1$. This suggests that the Yukawas are not fundamental parameters, but emerge from a more fundamental theory, explaining the observed hierarchy.

On the other hand, the notion of technical naturalness, also called 't Hooft naturalness, is more restrictive [108]. It relies on the understanding of the quantum corrections and can be stated as [109]: "If a symmetry of the theory is enlarged in the limit of some parameter $p \to 0$, the parameter $p$ is technically natural". The rationale behind this definition is that the beta function of a technically natural parameter is proportional to this parameter. An example of technically natural parameters are masses of fermions, since in the limit $m_f \to 0$ chiral symmetry is restored. The corrections to the fermion masses are schematically $\delta m_f \propto m_f \log \Lambda/m_f$, and since chiral symmetry is only broken by $m_f$, the correction to this parameter vanishes in the limit of vanishing fermion mass. In the SM, the masses of the fermions are fixed by the Yukawa couplings, which are therefore technically natural. This property is significant since it allows understanding that some, perhaps Dirac unnatural, value of a parameter is set at large energies corresponding to the more fundamental theory, $\Lambda^{\rm UV}$. The relations between the Yukawas, in particular the hierarchies such as $y_e/y_t \simeq 10^{-5}$, could be established by the unknown physics at $\Lambda^{\rm UV}$ and remain stable upon running to the EW scale. In principle, hierarchies of technically natural parameters are considered less severe, because it suffices to introduce a mechanism at GUT or Planck scales explaining those values and the running will not spoil the solution.

On the other hand, parameters such as the mass of the Higgs boson are not technically natural. Even if we set the mass of the Higgs to $m_h = 125$ GeV at the Planck scale, the running effects will spoil this solution, by contributing $\mathcal{O}(M^{\rm Pl})$ to the mass of the Higgs at EW scale, as will be discussed in Sec. 2.3. Moreover, in many extensions of the SM, the observed mass of the Higgs requires fine-tuning, indicating that it is also Dirac unnatural.

## 2.2 Strong CP-problem

In this section, we will review the physics of one of the most important questions in particle physics: why strong interactions preserve the combination of charge and parity conjugations. To arrive at the strong CP problem, we will review the symmetries of the QCD in Sec. 2.2.1 and what these imply in the low energy spectrum of the QCD in Sec. 2.2.2. In sections 2.2.3 and 2.2.4 we will follow the development of understanding of vacuum in non-abelian gauge theories. We will cover the connection between the instantons and the chiral anomaly in Sec. 2.2.5, and finally in Sec. 2.2.6 we will state the strong CP problem.

### 2.2.1 Symmetry structure of QCD

Quantum chromodynamics is the theory of strong interaction, with non-abelian, colour $SU(3)_C$ gauge group. There are six quark flavours, thus the lagrangian is given by

$$\mathcal{L}_{\rm QCD} = \sum_{q=u,d,s,c,b,t} \bar{q}(iD_\mu \gamma^\mu - m_q)q - \frac{1}{4} G^a_{\mu\nu} G^{a\mu\nu} \,. \tag{2.1}$$

The covariant derivative is defined as $D_\mu = \partial_\mu - \frac{i}{2} g_s A^a_\mu \lambda^a$ and gluon field strength $G_{\mu\nu} = \partial_\mu A_\nu - \partial_\nu A_\mu + g_s f^{abc} A^a_\mu A^b_\nu$, where $\lambda^a$ are Gell-Mann matrices and $f^{abc}$ are structure constants of $SU(3)_C$ defined by

$$\left[\frac{\lambda^a}{2}, \frac{\lambda^b}{2}\right] = i f^{abc} \frac{\lambda^c}{2} \,. \tag{2.2}$$

The only non-zero structure constants are

$$\begin{aligned}
&f^{123} = 1\,,\\
&f^{147} = f^{246} = f^{257} = f^{345} = -f^{156} = -f^{367} = \frac{1}{2}\,,\\
&f^{458} = f^{678} = \frac{\sqrt{3}}{2}\,,
\end{aligned} \tag{2.3}$$

along with those obtained by permutations of indices.
The anticommutator of Gell-Mann matrices defines the totally symmetric tensor $d^{abc}$

$$\{\lambda^a, \lambda^b\} = \frac{4}{3}\delta^{ab} + 2d^{abc}\lambda^c\,, \tag{2.4}$$

where only non-zero values, up to permutations, are [110]

$$\begin{aligned}
&d^{118} = d^{228} = d^{338} = -d^{888} = \frac{1}{3}\,,\\
&d^{146} = d^{157} = d^{256} = d^{344} = d^{355} = -d^{366} = -d^{377} = \frac{1}{2}\,,\\
&d^{448} = d^{558} = d^{668} = d^{778} = -\frac{1}{2\sqrt{3}}\,.
\end{aligned} \tag{2.5}$$

A useful identity for the product of Gell-Mann matrices holds

$$\lambda^a\lambda^b = 2\delta^{ab}/3 + (d^{abc} + if^{abc})\lambda^e\,. \tag{2.6}$$

Each quark field is a $SU(3)_C$ triplet $q^T = (q_r, q_g, q_b)$ with gauge transformation

$$q \to q' = U(x)q = \exp\left(-i\theta^a(x)\frac{\lambda^a}{2}\right)\begin{pmatrix} q_r \\ q_g \\ q_b \end{pmatrix}\,, \tag{2.7}$$

where $U(x) \in SU(3)_C$. Gauge fields also transform under $SU(3)_C$

$$\begin{aligned}
&A_\mu \to A'_\mu = A'^a_\mu\frac{\lambda^a}{2} = U(x)A_\mu U^\dagger(x) - \frac{i}{g_s}\partial_\mu U(x)U^\dagger(x)\,,\\
&G_{\mu\nu} = G^a_{\mu\nu}\frac{\lambda^a}{2} \to U(x)G_{\mu\nu}U^\dagger(x)\,.
\end{aligned} \tag{2.8}$$

As a result, the covariant derivative transforms the same as a quark field, while the gluonic term is invariant under gauge transformations

$$\begin{aligned}
&D_\mu q \to U(x)D_\mu q\,,\\
&-\frac{1}{2}\mathrm{Tr}(G_{\mu\nu}G^{\mu\nu}) \to -\frac{1}{2}\mathrm{Tr}(G_{\mu\nu}G^{\mu\nu})\,,
\end{aligned} \tag{2.9}$$

where invariance of gluonic lagrangian follows from the cyclic property of trace.

The Gell-Mann matrices $\lambda^a$ are:

$$\lambda_1 = \begin{pmatrix} 0 & 1 & 0 \\ 1 & 0 & 0 \\ 0 & 0 & 0 \end{pmatrix}, \quad \lambda_2 = \begin{pmatrix} 0 & -i & 0 \\ i & 0 & 0 \\ 0 & 0 & 0 \end{pmatrix}, \quad \lambda_3 = \begin{pmatrix} 1 & 0 & 0 \\ 0 & -1 & 0 \\ 0 & 0 & 0 \end{pmatrix}$$

$$\lambda_4 = \begin{pmatrix} 0 & 0 & 1 \\ 0 & 0 & 0 \\ 1 & 0 & 0 \end{pmatrix}, \quad \lambda_5 = \begin{pmatrix} 0 & 0 & -i \\ 0 & 0 & 0 \\ i & 0 & 0 \end{pmatrix}, \quad \lambda_6 = \begin{pmatrix} 0 & 0 & 0 \\ 0 & 0 & 1 \\ 0 & 1 & 0 \end{pmatrix}$$

$$\lambda_7 = \begin{pmatrix} 0 & 0 & 0 \\ 0 & 0 & -i \\ 0 & i & 0 \end{pmatrix}, \quad \lambda_8 = \frac{1}{\sqrt{3}} \begin{pmatrix} 1 & 0 & 0 \\ 0 & 1 & 0 \\ 0 & 0 & -2 \end{pmatrix}.$$

The renormalization group equation of strong gauge couplings is

$$\mu \frac{dg_s}{d\mu} = \beta(g_s) = \beta_V(g_s) + \beta_F(g_s)\,, \tag{2.10}$$

where $\mu$ is renormalization scale and beta functions $\beta_V$ and $\beta_F$ encode corrections from vectors and fermions, respectively.

Famously, in the $G = SU(N)$ gauge theory the contributions to the beta function from vectors in adjoint representation and fermions in representation $R$ are [111, 112]

$$\begin{aligned} \beta_V &= -\frac{g_s^3}{16\pi^2}\frac{11}{3}C_2(G)\,, \\ \beta_F &= -\frac{g_s^3}{16\pi^2}\frac{4}{3}\frac{C_2(R)d(R)}{r}\,, \end{aligned} \tag{2.11}$$

where, $d(R)$ is dimension of representation $R$, $r$ is a number of generators of $G$ and $C_2(G)$ and $C_2(R)$ are quadratic Casimir operator of adjoint and $R$ representations, respectively. For $G = SU(3)_C$, we have $C_2(G) = 3$, $r = 8$, $d(R) = 3$ and $C_2(R) = (N^2-1)/2N = 4/3$, implying that the beta function of strong coupling is

$$\beta(g_s^2) = -\frac{g_s^3}{16\pi^2}\left(11 - \frac{2}{3}n_f\right), \tag{2.12}$$

where $n_f$ is a number of fermions in fundamental representation. Defining $\alpha_s = g_s^2/4\pi$, the renormalization group equation can be rewritten as

$$\mu \frac{d\alpha_s}{d\mu} = -\frac{\alpha_s^2}{2\pi}\left(11 - \frac{2}{3}n_f\right), \tag{2.13}$$

with solution for $n_f = 6$ [113]

$$\alpha_s(\mu) = \frac{2\pi}{7}\frac{1}{\ln\frac{\mu}{\Lambda_{\text{QCD}}}}\,. \tag{2.14}$$

The above equation is valid above the Landau pole $\mu > \Lambda_{\text{QCD}}$, where $\Lambda_{\text{QCD}}$, can be found by measuring $\alpha_s$ at any scale and using that boundary condition. The property of the gauge coupling to fall with the energy is called asymptotic freedom. On the other hand, at low energies, the coupling blows up, and perturbative expansion in gauge coupling breaks down. This motivates using alternative methods, such as Chiral Perturbation Theory (ChPT), for computation of QCD observables at low energies.

### 2.2.2 Low energy limit of QCD

To study the low energy meson spectrum of the QCD, it is necessary to integrate out heavy quarks using equations of motion. The masses of quarks are given in 2.1, and clearly charm, bottom, and top quarks are quite heavier than nucleon, $m_N \simeq 1$ GeV. In the low energy limit, the momentum of heavy quarks is small, and the Dirac equation is dominated by the mass

$$(iD_\mu\gamma^\mu - m)q = 0 \xrightarrow{-i\partial_\mu q \simeq 0} g_s A_\mu \gamma^\mu q - imq = 0 \to q(x) = 0\,, \tag{2.15}$$

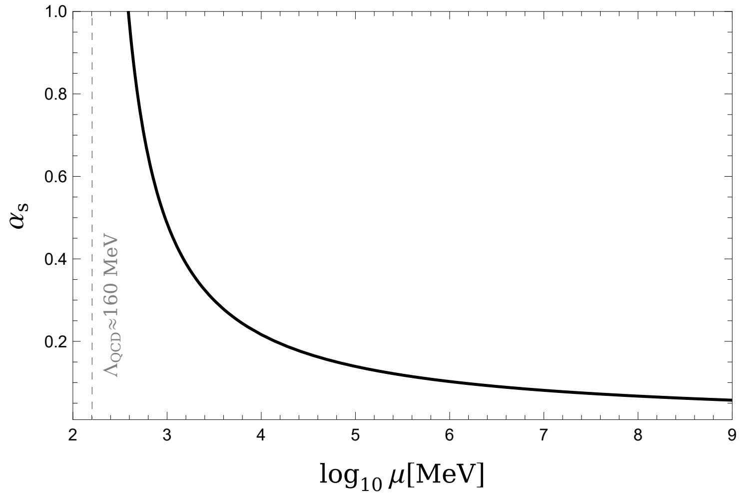


Figure 2.1: Running of $\alpha_s$ at leading order, Eq. (2.14). In the limit $\mu \to \infty$ the coupling vanishes, while as we approach the Landau pole, which we approximate in the plot with $\Lambda_{\rm QCD} \simeq 160$ MeV, the coupling blows up and the theory becomes non-perturbative.

| | | |
|---|---|---|
| Up ($u$) $m_u = 2.16^{+0.49}_{-0.26}$ MeV | Strange ($s$) $m_s = 93.4^{+8.6}_{-3.4}$ MeV | Top ($t$) $m_t = 172.69 \pm 0.30$ GeV |
| Down ($d$) $m_d = 4.67^{+0.48}_{-0.17}$ MeV | Charm ($c$) $m_c = 1.27 \pm 0.02$ GeV | Bottom ($b$) $m_b = 4.18^{+0.03}_{-0.02}$ GeV |

Table 2.1: Quark masses according to Particle Data group [114]. Up, down, and strange quarks are much lighter than the nucleon, while charm, bottom, and top are well above 1 GeV.

where we have demanded that EoMs are satisfied for all gluon configurations $A_\mu$. Using EoMs we can integrate out heavy quarks by setting them to zero in the QCD lagrangian Eq. (2.1). Therefore, the effective lagrangian below the nucleon scale is

$$\mathcal{L} = \sum_{q=u,d,s} \bar{q}(iD_\mu\gamma^\mu - m_q)q - \frac{1}{4}G^a_{\mu\nu}G^{a\mu\nu}\,. \tag{2.16}$$

We will study the chiral limit of the QCD, thus it will be advantageous to express quark fields in Weyl basis via left- and right-handed fermions. The projection operators are defined

$$\begin{aligned} P_L &= \frac{1}{2}\Big(1-\gamma^5\Big)\,, \\ P_R &= \frac{1}{2}\Big(1+\gamma^5\Big)\,, \end{aligned} \tag{2.17}$$

where $\gamma^5 = i\gamma^0\gamma^1\gamma^2\gamma^3$.[1] The projection operators satisfy $P^2_{L/R} = P_{L/R}$, $P_{L/R}P_{R/L} = 0$ and $P_L + P_R = \mathbb{1}$. With these properties, we can decompose any Dirac quark as $q =$

[1]note that $\gamma^5$ is Hermitian $(\gamma^5)^\dagger = -i(\gamma^3)^\dagger(\gamma^2)^\dagger(\gamma^1)^\dagger(\gamma^0)^\dagger = i\gamma^3\gamma^2\gamma^1\gamma^0$. Since $\{\gamma^\mu,\gamma^\mu\} = g^{\mu\nu}$ we end up with $(\gamma^5)^\dagger = \gamma^5$.

$P_L q + P_R q = q_L + q_R$. Also note that

$$\begin{aligned} \bar{q}_L &= (P_L q)^\dagger \gamma^0 = q^\dagger P_L \gamma^0 = q^\dagger \gamma^0 P_R = \bar{q} P_R \,, \\ \bar{q}_R &= (P_R q)^\dagger \gamma^0 = q^\dagger P_R \gamma^0 = q^\dagger \gamma^0 P_L = \bar{q} P_L \,. \end{aligned} \tag{2.18}$$

where we have used $\{\gamma^5, \gamma^\mu\} = 0$ after third equality sign in both lines. It follows that the quark lagrangian can be rewritten by inserting $\mathbb{1} = P_L + P_R$

$$\begin{aligned} \mathcal{L}_{\text{quark}} &= \sum_{q=u,d,s} [\bar{q}(P_L + P_R)(i\partial_\mu \gamma^\mu - m_q)(P_L + P_R)q] = \\ &= \sum_{q=u,d,s} [i\bar{q} P_L \partial_\mu \gamma^\mu P_R q + i\bar{q} P_R \partial_\mu \gamma^\mu P_L q - m_q(\bar{q} P_L P_L q + \bar{q} P_R P_R q)] = \\ &= \sum_{q=u,d,s} [i\bar{q}_L \partial_\mu \gamma^\mu q_L + i\bar{q}_R \partial_\mu \gamma^\mu q_R + m_q(\bar{q}_L q_R + \bar{q}_R q_L)] \,, \end{aligned} \tag{2.19}$$

where we have used $P_{L/R}\gamma^\mu = \gamma^\mu P_{R/L}$, and the orthogonality of the projection operators when going from first to second line. We have dropped interactions with gluons, which are irrelevant for the discussion of chirality. An important feature of the lagrangian is that the mixing between left- and right-handed quarks is mediated by the quark masses. It means that in the limit $m_q \to 0$ the lagrangian splits into distinct, chiral parts. Moreover, for vanishing masses the quarks are indistinguishable (note that we neglect the electroweak interaction as well), and a unitary transformation which rotates $q = u, d, s$ into each other is a classical symmetry of lagrangian. The splitting of the lagrangian implies that in the chiral limit, the symmetry is a global $U(3)_L \times U(3)_R$, with quarks forming fundamental representations $(\mathbf{3}, 1)$ and $(1, \mathbf{3})$

$$\begin{aligned} q_L &= \begin{pmatrix} u_L \\ d_L \\ s_L \end{pmatrix} \to q'_L = \exp\Big(-i\Big(\theta^a_L \frac{\lambda^a}{2} + \theta_L\Big)\Big) \begin{pmatrix} u_L \\ d_L \\ s_L \end{pmatrix}, \\ q_R &= \begin{pmatrix} u_R \\ d_R \\ s_R \end{pmatrix} \to q'_R = \exp\Big(-i\Big(\theta^a_R \frac{\lambda^a}{2} + \theta_R\Big)\Big) \begin{pmatrix} u_R \\ d_R \\ s_R \end{pmatrix}, \end{aligned} \tag{2.20}$$

where $\lambda^a$ are again Gell-Mann matrices, and we have intentionally separated generators according to $U(3)_{L/R} \simeq SU(3)_{L/R} \times U(1)_{L/R}$ for later convenience. The Noether theorem ensures that global symmetry implies a conservation law, see Appendix A.4. For the quickest way to find conserved currents, consider an infinitesimal *local* transformation, which in leading order is

$$\begin{aligned} q_L \to q'_L = q_L + \delta q_L = q_L - i\Big(\theta^a_L(x) \frac{\lambda^a}{2} + \theta_L(x)\Big) q_L \,, \\ q_R \to q'_R = q_R + \delta q_R = q_R - i\Big(\theta^a_R(x) \frac{\lambda^a}{2} + \theta_R(x)\Big) q_R \,. \end{aligned} \tag{2.21}$$

For now, let's simply write those transformations as $q_l \to q_l + \delta q_l$, where $l = L, R$. The kinetic terms in the lagrangian transform as

$$i\bar{q}_l \partial\!\!\!/ q_l \to i(\bar{q}_l + \delta\bar{q}_l)\partial\!\!\!/(q_l + \delta q_l) = i\bar{q}_l \partial\!\!\!/ q_l + i\delta\bar{q}_l \partial\!\!\!/ q_l + i\bar{q}_l \partial\!\!\!/ \delta q_l + \mathcal{O}(\delta q_l^2) \,. \tag{2.22}$$

Noether currents are found from the variation of the lagrangian involving the spacetime derivative of the transformation parameter $\partial_\mu \theta_{L/R}$. Hence, we can only look at the third term in Eq. (2.22) involving $\not{\partial}\delta q_l$, which evaluates to

$$\delta\mathcal{L} \supset \bar{q}_R\Big(\partial_\mu\theta^a_R\frac{\lambda^a}{2} + \partial_\mu\theta_R\Big)\gamma^\mu q_R + \bar{q}_L\Big(\partial_\mu\theta^a_L\frac{\lambda^a}{2} + \partial_\mu\theta_L\Big)\gamma^\mu q_L\,. \tag{2.23}$$

The conserved currents are therefore

$$\begin{aligned} J^{a,\mu}_L &= \frac{\partial\delta\mathcal{L}}{\partial(\partial_\mu\theta^a_L)} = \bar{q}_L\frac{\lambda^a}{2}\gamma^\mu q_L\,,\\ J^{a,\mu}_R &= \frac{\partial\delta\mathcal{L}}{\partial(\partial_\mu\theta^a_R)} = \bar{q}_R\frac{\lambda^a}{2}\gamma^\mu q_R\,,\\ J^{\mu}_L &= \frac{\partial\delta\mathcal{L}}{\partial(\partial_\mu\theta_L)} = \bar{q}_L\gamma^\mu q_L\,,\\ J^{\mu}_R &= \frac{\partial\delta\mathcal{L}}{\partial(\partial_\mu\theta_R)} = \bar{q}_R\gamma^\mu q_R\,. \end{aligned} \tag{2.24}$$

It is common to combine the left and right currents into vector and axial currents, inserting $q_{L/R} = P_{L/R}q$ in formulas above

$$\begin{aligned} J^{a,\mu}_V &= J^{a,\mu}_R + J^{a,\mu}_L = \bar{q}\gamma^\mu\frac{\lambda^a}{2}q\,,\\ J^{a,\mu}_A &= J^{a,\mu}_R - J^{a,\mu}_L = \bar{q}\gamma^\mu\gamma^5\frac{\lambda^a}{2}q\,,\\ J^{\mu}_V &= J^{\mu}_R + J^{\mu}_L = \bar{q}\gamma^\mu q\,,\\ J^{\mu}_A &= J^{\mu}_R - J^{\mu}_L = \bar{q}\gamma^\mu\gamma^5 q\,. \end{aligned} \tag{2.25}$$

Those current correspond to the symmetry transformations analogous to Eq. (2.20) belonging to $SU(3)_V \times SU(3)_A \times U(1)_V \times U(1)_A \simeq U(3)_V \times U(3)_A$.

Reintroducing the quark masses $m_q$, we can find the classical divergences of scalar and pseudoscalar currents

$$\partial_\mu J^\mu_V = 0\,, \tag{2.26}$$
$$\partial_\mu J^\mu_A = \sum_q 2im_q\bar{q}\gamma^5 q\,, \tag{2.27}$$

where equalities hold upon using the quark EoMs. Clearly, in the limit $m_q \to 0$, the axial current is also conserved. The charge corresponding to each of the currents is defined as a spatial integral of the current density

$$Q^a_i = \int d^3x J^{a,0}_i\,. \tag{2.28}$$

The axial and vector charges are given by

$$\begin{aligned} Q^a_V &= Q^a_R + Q^a_L\,,\\ Q^a_A &= Q^a_R - Q^a_L\,, \end{aligned} \tag{2.29}$$

which transform differently under parity transformation :

$$\begin{aligned} PQ^a_V P^{-1} &= P(Q^a_R + Q^a_L)P^{-1} = Q^a_L + Q^a_R = Q^a_V\,,\\ PQ^a_A P^{-1} &= P(Q^a_R - Q^a_L)P^{-1} = Q^a_R + Q^a_L = -Q^a_A\,. \end{aligned} \tag{2.30}$$

Let $|i,+\rangle$ be single particle, QCD eigenstate with positive parity

$$\begin{aligned} H_{\text{QCD}}|i,+\rangle &= E_i|i,+\rangle \,, \\ P|i,+\rangle &= +|i,+\rangle \,. \end{aligned} \tag{2.31}$$

We can construct a state $|\phi\rangle = Q_A^a|i,+\rangle$ with the same energy but opposite parity

$$\begin{aligned} H_{\text{QCD}}|\phi\rangle &= H_{\text{QCD}}Q_A^a|i,+\rangle = E_iQ_A^a|i,+\rangle = E_i|\phi\rangle \,, \\ P|\phi\rangle &= PQ_A^a|i,+\rangle = PQ_A^aP^{-1}P|i,+\rangle = -Q_A^a(+|i,+\rangle) = -|\phi\rangle \,. \end{aligned} \tag{2.32}$$

In the first line we have used the commutation of Hamiltonian and axial charge, and in the second line the parity of axial charge Eq. (2.30). A symmetry transformation corresponding to charge $Q_A$ in the leading order is

$$\Phi_i \to \Phi_i - i\epsilon^a t_{ij}^a \Phi_j \,, \tag{2.33}$$

where $t_{ij}^a$ are generators of $U(3)_A$ acting in the field space, $t_{ij}^a = \lambda_{ij}^a/2$ for $a = 1, \ldots, 8$ and $t_{ij}^0 = 1$. The above transformation implies the commutation relation between charge and field $[Q_A^a, \phi_i] = -t_{ij}^a\phi_j$. A similar relation holds between the creation operators, $[Q_A^a, a_i^\dagger] = -t_{ij}^a b_j^\dagger$. We justify the usage of different symbols for creation operators on both sides by noting that $b_j^\dagger$ must create a single particle state of opposing parity. Expanding

$$|\phi\rangle = Q_A^a a_k^\dagger|0\rangle = ([Q_A^a, a_k^\dagger] + a_k^\dagger Q_A^a)|0\rangle = -t_{kj}^a b_j^\dagger|0\rangle \,, \tag{2.34}$$

where the last equality holds if $Q_A^a|0\rangle = 0$. Under this assumption, the spectrum of chiral QCD consists of degenerate particles, created by $a_i^\dagger$ and $b_i^\dagger$, of opposing parities. Note that since the correspondence holds at the level of creation operators, this really means doubling of the spectrum of QCD. However, the parity doubling is not observed in nature, e.g. proton and neutron, which have similar masses, both have $P = 1$. We conclude that we have made a mistake by assuming that the vacuum is annihilated by axial charges. As a matter of fact, it is sufficient to assume that the QCD vacuum is not invariant under axial transformations

$$Q_A^a|0\rangle \neq 0 \,, \tag{2.35}$$

to solve the doubling parity problem. The reason is that the spontaneous symmetry breaking implies the existence of massless Goldstone bosons. These bosons are created by charges corresponding to the generators of the broken symmetry. Thus, while for any chiral QCD state, there exists a degenerate state of opposite parity, this state consists of several particles, including massless Goldstone bosons. Hence, parity doubling is a real phenomenon, but the degeneracy does not hold for single-particle states.

Another viewpoint is that if the vacuum state and Hamiltonian are symmetric under axial transformations, we can always construct states with opposite parity by applying the axial charge to those states. However, since the vacuum is not symmetric under $U(3)_A$ , applying the axial charge creates new, massless particles within the state.

### 2.2.3 $U(1)_A$ problem and the instantons

Non-invariance of the ground state under axial transformation inevitably leads to the presence of massless particles, as predicted by Goldstone theorem [115].

As shown in Appendix A.5, the Goldstone theorem states that there exists a massless boson to each generator of the broken symmetry. Thus, we expect to observe $\dim(U(3)_A) = 9$ approximately massless pseudoscalar particles in the low-energy spectrum of QCD. The

| Meson Name | Quark Content | Mass [MeV] | Spin | Parity |
|---|---|---|---|---|
| $\pi^+$ | $u\bar{d}$ | $139.57039 \pm 0.0001$ | 0 | $-1$ |
| $\pi^0$ | $(u\bar{u} - d\bar{d})/\sqrt{2}$ | $134.9768 \pm 0.0005$ | | |
| $K^+$ | $u\bar{s}$ | $493.677 \pm 0.016$ | | |
| $K^0$ | $(d\bar{s} - s\bar{d})/\sqrt{2}$ | $497.611 \pm 0.013$ | | |
| $\eta$ | $(u\bar{u} + d\bar{d} - 2s\bar{s})/\sqrt{6}$ | $547.862 \pm 0.017$ | | |
| $\eta'$ | $(u\bar{u} + d\bar{d} + s\bar{s})/\sqrt{3}$ | $957.78 \pm 0.06$ | | |

Table 2.2: Table of mesons according to Ref. [114], with their masses, spins, and parities. The masses of all mesons except for $\eta'$ are well below the mass of the neutron, $m_n \simeq 939.6$ GeV.

correction to the masses of Goldstone bosons should emerge as a result of the explicit chiral symmetry breaking by non-zero quark masses and should be small compared to masses of other particles in the low-energy spectrum. Indeed, looking at the meson spectrum in Tab. 2.2 we may verify that masses of $\pi^\pm, \pi^0, K^\pm, K^0, \overline{K}^0, \eta$ are substantially smaller than neutron mass $m_n \simeq 939.6$ GeV. Large chiral symmetry breaking strange quark mass results in a larger mass of mesons composed of $s$, kaons, and eta.

However, the $\eta'$ with mass $m_{\eta'} \sim 960$ GeV is even heavier than neutron and proton. This large mass cannot be accounted for with the explicit breaking of chiral symmetry by quark masses. Because of the apparent lack of Goldstone boson corresponding to the generator of the subgroup $U(1)_A \subset U(3)_A$, this issue is known as $U(1)_A$-problem.

In the mid-70s, Polyakov was involved in understanding the confinement through pseudoparticle configuration of gauge fields [116]. The famous BPST instanton solution has been shown to exist in Euclidean continuation of non-abelian Yang-Mills theories [117]. Within a year, t'Hooft realized that instantons lead to observable effect also in Minkowski spacetime, breaking explicitly axial symmetry [118]. An additional source of explicit symmetry breaking was the reason why the mass of the corresponding Goldstone boson was so large, solving the $U(1)_A$-problem. Furthermore, Jackiw and Rebbi found, that instantons in Minkowski spacetime are quantum mechanical-like objects corresponding to tunneling between topologically distinct, degenerate vacua [119]. They proposed the existence of a vacuum state as a superposition of those vacua, parametrized by an angle.

We will follow this historical development in the following sections.

Firstly, we will look for a classical solution to the equations of motion of Yang-Mills theory in Euclidean space. The continuation of Minkowski space-time into Euclidean space-time is obtained by Wick rotation $t \to it_E$. As a result, the action transforms $iS \to -S_E$. We will drop the indices of Euclidean on objects such as $A_\mu^{a,E}$ or $G_{\mu\nu}^{a,E}$ for clarity, but keep in mind that all formulas in this section hold in Euclidean continuation of Minkowski spacetime. The classical solutions will correspond to non-perturbative field configurations, which motivates the rescaling of fields $A_\mu \to A_\mu/g_s$ so that $G_{\mu\nu} \to G_{\mu\nu}/g_s$. The QCD action becomes

$$S^E = \frac{1}{2g_s^2} \int d\Omega \int r^3 dr \, \mathrm{Tr}\left(G_{\mu\nu} G^{\mu\nu}\right), \tag{2.36}$$

which is finite if $G_{\mu\nu}$ falls off faster than $1/r^2$:

$$G_{\mu\nu} \xrightarrow{x\to\infty} \mathcal{O}(r^{-2-\epsilon}), \tag{2.37}$$

for $\epsilon > 0$. The boundary of the action in the Euclidean space should correspond to the vacuum configuration. Besides a trivial $A_\mu = 0$, the same condition is satisfied for any pure gauge, which from Eq. (2.8) reads

$$A_\mu^a \to iU\partial_\mu U^\dagger + \mathcal{O}(r^{-1-\epsilon}) \,, \tag{2.38}$$

where $U \in G = SU(3)$ and we have accounted for the fact, that for field strength to fall off faster than $1/r^2$, the potential must fall off faster than $1/r$. We have used $\partial_\mu U U^\dagger = -U\partial_\mu U^\dagger$ for notational agreement with Ref. [120]. This condition holds at the boundary of Euclidean $\mathbb{R}^4$, which is a 3-sphere. We may focus on field configurations constructed from a subgroup of the gauge group $SU(2) \subset SU(3)$. Because $SU(2)$ is homeomorphic to 3-sphere $S_3$, the gauge field configurations $A_\mu$ are maps between two 3-spheres. Such maps are characterized by a winding number defined [120]

$$n_w = -\frac{1}{24\pi^2}\int d^3\theta \epsilon^{ijk}\mathrm{Tr}\big(U(\partial_i U^\dagger)U(\partial_j U^\dagger)U(\partial_k U^\dagger)\big) \,. \tag{2.39}$$

An example of the field configuration with winding number $n_w$ can be found by considering pure gauges generated by 'hedgehog' [121, 122]

$$U(\vec{x}) = \exp\Big(if(r)\sigma^a\hat{x}^a\Big) = \cos(f(r))\mathbb{1} + i\sin(f(r))\sigma^a\hat{x}^a \,, \tag{2.40}$$

where $\hat{x}^a = x^a/r$ and $f(r)$ is any function satisfying $f(r=0) = n_w\pi$ and $f(r\to\infty) = 0$.

On the other hand, Chern-Simons current is defined

$$K_\mu = 4\epsilon^{\mu\nu\alpha\beta}\mathrm{Tr}\Big(A_\nu\partial_\alpha A_\beta - \frac{2}{3}iA_\nu A_\alpha A_\beta\Big) \,. \tag{2.41}$$

Because the indices $\alpha$ and $\beta$ are contracted with totally antisymmetric tensor, we may rewrite the trace using antisymmetrization

$$K_\mu = 4\epsilon^{\mu\nu\alpha\beta}\mathrm{Tr}\Big(\frac{1}{2}A_\nu(\partial_\alpha A_\beta - \partial_\beta A_\alpha) - \frac{2}{3}iA_\nu\cdot\frac{1}{2}[A_\alpha, A_\beta]\Big) \,. \tag{2.42}$$

We can now use the definition of the rescaled field strength

$$G_{\alpha\beta} = \partial_\alpha A_\beta - \partial_\beta A_\alpha - i[A_\alpha, A_\beta] \,, \tag{2.43}$$

to express the Chern-Simons current as

$$\begin{aligned} K_\mu &= 2\epsilon^{\mu\nu\alpha\beta}\mathrm{Tr}\Big(A_\nu G_{\alpha\beta} + \frac{i}{3}A_\nu\cdot[A_\alpha, A_\beta]\Big) = \\ &= 2\epsilon^{\mu\nu\alpha\beta}\mathrm{Tr}\Big(A_\nu G_{\alpha\beta} + \frac{2i}{3}A_\nu A_\alpha A_\beta\Big) \,, \end{aligned} \tag{2.44}$$

where in the last line we have removed the commutator contracted with a totally antisymmetric tensor, effectively multiplying by 2. Using Eq. (2.37) and Eq. (2.38), the Chern-Simons current at the boundary of $\mathbb{R}^4$ is

$$\begin{aligned} K_\mu &\xrightarrow{x\to\infty} \frac{4i}{3}\epsilon^{\mu\nu\alpha\beta}\mathrm{Tr}A_\nu A_\alpha A_\beta = \\ &= \frac{4}{3}\epsilon^{\mu\nu\alpha\beta}\mathrm{Tr}\big(U(\partial_\nu U^{-1})U(\partial_\alpha U^{-1})U(\partial_\beta U^{-1})\big) \,, \end{aligned} \tag{2.45}$$

Working in the temporal gauge, $A_0 = U\partial_0 U^\dagger = 0$ and $K_i = 0$, let us look at the surface integral of the Chern-Simons current over the boundary of $\mathbb{R}^4$, adjusting the multiplicity for later convenience

$$\begin{aligned}\frac{1}{32\pi^2}\int d\sigma_\mu K^\mu = \frac{1}{32\pi^2}\int d^4x\partial_\mu K^\mu = \frac{1}{32\pi^2}\int dt\frac{d}{dt}\int d^3x K_0 = \\ = \frac{1}{24\pi^2}\int dt\int d^3x\epsilon^{ijk}\mathrm{Tr}(U(\partial_i U^{-1})U(\partial_j U^{-1})U(\partial_k U^{-1})) = n_w^+ - n_w^- \,,\end{aligned} \tag{2.46}$$

where we have used Gauss law in the first step, and in the last equality we have used the definition of winding number Eq. (2.39), evaluated at past and future infinities, $n_w^+$, and $n_w^-$, respectively. The conclusion is that Chern-Simons currents correspond to changes in the topological charge, given by the winding number. Moreover, using results from Appendix A.1 we can define an instanton number $n$ as

$$n \equiv n_w^+ - n_w^- = \frac{1}{32\pi^2}\int d^4x\partial_\mu K^\mu = \frac{1}{16\pi^2}\int d^4x\mathrm{Tr}\, G_{\mu\nu}\widetilde{G}^{\mu\nu}\,, \tag{2.47}$$

which is gauge invariant. As a result, the instanton number cannot be changed by the gauge transformation. Since for any winding number $n_w$, field strength vanishes $G_{\mu\nu} = 0$, it means that the distinct vacua cannot be transformed into each other without crossing an energy barrier with $G_{\mu\nu} \neq 0$.

We can now look at specific field configurations which minimize the QCD action by noting, that we can write the QCD action

$$\frac{1}{2g_s^2}\int d^4x\mathrm{Tr}G_{\mu\nu}G^{\mu\nu} = \frac{1}{2g_s^2}\int d^4x\frac{1}{2}\mathrm{Tr}\Big(\Big(G_{\mu\nu} \pm \widetilde{G}^{\mu\nu}\Big)^2 \mp G_{\mu\nu}\widetilde{G}_{\mu\nu}\Big)\,, \tag{2.48}$$

where we have used

$$\begin{aligned}\widetilde{G}_{\mu\nu}\widetilde{G}^{\mu\nu} =& \frac{1}{4}G^{\mu\nu}G_{\alpha\beta}\epsilon_{\mu\nu\delta\gamma}\epsilon^{\alpha\beta\delta\gamma} = \frac{1}{4}G^{\mu\nu}G_{\alpha\beta}2\Big(\delta_\mu^\alpha\delta_\nu^\beta - \delta_\mu^\beta\delta_\nu^\alpha\Big)\\ =& \frac{1}{2}(G_{\mu\nu}G^{\mu\nu} - G_{\nu\mu}G^{\mu\nu}) = G_{\mu\nu}G^{\mu\nu}\,.\end{aligned} \tag{2.49}$$

In the second equality we have used the formula for a scalar product of totally antisymmetric tensors $\epsilon_{\mu\nu\delta\gamma}\epsilon^{\alpha\beta\delta\gamma} = 2\Big(\delta_\mu^\alpha\delta_\nu^\beta - \delta_\mu^\beta\delta_\nu^\alpha\Big)$, and $G_{\mu\nu} = -G_{\nu\mu}$ in last line. With that in mind, Eq. (2.48) consists of two terms, positive $(G \pm \widetilde{G})^2$ and topologically invariant $G\widetilde{G}$. Hence, solutions that minimize the action obey

$$G_{\mu\nu} = \mp\widetilde{G}_{\mu\nu}\,. \tag{2.50}$$

The action of self-dual field configurations is then determined by the instanton number

$$\mathcal{S} = \frac{8\pi^2|n|}{g_s^2}\,. \tag{2.51}$$

Above shows, that Euclidean action is minimized for field configurations labeled by $n = n_w^+ - n_w^-$. Such configurations connect topologically distinct vacua, mediating between vacuum in the past with winding number $n_w^-$ and vacuum in the future with winding number $n_w^+$.

The explicit form of the solution with $n = 1$ is BPST instanton given by gauge potential [117]

$$A_\mu^a(x) = \frac{2\eta_{a\mu\nu}x_\nu}{x^2 + \rho^2}\,, \tag{2.52}$$

where $\rho$ is parametrizing the size of the instanton and 't Hooft symbol is defined as

$$\eta_{a\mu\nu} = \begin{cases} \epsilon_{a\mu\nu} & \mu,\nu = 1,2,3 \\ \delta_{a\mu} & \nu = 4 \\ -\delta_{a\nu} & \mu = 4 \\ 0 & \nu = \mu = 4 \end{cases} . \tag{2.53}$$

The field strength for that solution is

$$\left(G^a_{\mu\nu}\right)^2 = \frac{192\rho^2}{\left(x^2+\rho^2\right)^4} , \tag{2.54}$$

which falls off as $1/x^4$, hence is well localized even though $A_\mu \sim 1/x$. The name instanton comes from the fact, that this field configuration is localized not only in space but also in time (so the transition is instantaneous). Instanton with $n = -1$ is given by the same formulas but with replacing $\eta$ with

$$\overline{\eta}_{a\mu\nu} = \begin{cases} \epsilon_{a\mu\nu} & \mu,\nu = 1,2,3 \\ -\delta_{a\mu} & \nu = 4 \\ \delta_{a\nu} & \mu = 4 \\ 0 & \nu = \mu = 4 \end{cases} . \tag{2.55}$$

To sum up, we have found an infinite set of QCD vacua, characterized by a winding number $n_w$. Field configurations connecting topologically distinct vacua of the QCD via the Euclidean path are characterized by a difference of winding number, called instanton numbers , $n = n_w^+ - n_w^-$. Instanton number can be expressed in terms of gauge invariant divergence of the Chern-Simons current, which highlights the physical significance of the solution. We have also recalled the explicit form of the solution of EoMs realizing $n = 1$ BPST instanton.

### 2.2.4 The theta vacuum

The classical solution to equations of motions in Euclidean space corresponds to tunnelings in Minkowski spacetime [123]. Thus, solutions found above correspond to tunnelings between degenerate, topologically distinct vacua in QCD.

Since the Chern-Simons current is not gauge invariant, the winding number $n_w$ is not gauge invariant either. In particular, there exists a gauge transformation such that

$$U^{(1)}|n_w\rangle = |n_w + 1\rangle . \tag{2.56}$$

We have also seen that vacua with different winding numbers are separated by an energy barrier. It motivates the introduction of gauge invariant vacuum as a linear combination

$$|\theta\rangle = \sum_{n_w=-\infty}^{n_w=\infty} e^{in_w\theta}|n_w\rangle , \tag{2.57}$$

where $\theta$ is a continuous parameter taking values between 0 and $2\pi$. We can verify the gauge invariance of this state by acting with transformation Eq. (2.56)

$$\begin{aligned} U^{(1)}|\theta\rangle = \sum_{n_w=-\infty}^{n_w=\infty} e^{in_w\theta}U^{(1)}|n_w\rangle = \sum_{n_w=-\infty}^{n_w=\infty} e^{in_w\theta}|n_w+1\rangle = \\ = e^{-i\theta}\sum_{n_w=-\infty}^{n_w=\infty} e^{in_w\theta}|n_w\rangle = e^{-i\theta}|\theta\rangle , \end{aligned} \tag{2.58}$$

where we have relabelled the summation index $n_w \to n_w + 1$ in the next to last step. We investigate the effect of the $\theta$-vacuum on the QCD action by considering amplitude for transition from $\theta$ to $\theta'$

$$\begin{aligned}\langle\theta'|e^{-iH_{\mathrm{QCD}}t}|\theta\rangle &= \sum_{m_W} e^{im_W\theta'} \sum_{n_w} e^{-in_w\theta}\langle m_W|e^{-iH_{\mathrm{QCD}}t}|n_w\rangle \\ &= \sum_{m_W,n_w} e^{im_W(\theta'-\theta)}e^{-i(n_w-m_W)\theta}\int DA_\mu^{[n_w-m_W]}e^{i\int d^4x\mathcal{L}+JA}\,,\end{aligned} \tag{2.59}$$

where we have expressed the amplitude via path integral over all gauge field configurations $DA_\mu^{[n_w-m_W]}$ with instanton number $n_w - m_W$, and $J$ is the source current. By relabelling the index $\nu = n_w - m_W$ and performing sum over $m_W$ we find

$$\langle\theta'|e^{-iH_{\mathrm{QCD}}t}|\theta\rangle = \delta(\theta-\theta')\sum_\nu \int DA_\mu^\nu e^{-i\nu\theta+i\int d^4x\mathcal{L}+JA}\,. \tag{2.60}$$

It follows, that $\theta$ cannot be changed by any process and is therefore a fundamental parameter of the QCD. We can now use Eq. (2.47) to find, that the effect of $\theta$-vacuum of the action is captured by an additional $\theta$-term in the QCD Lagrangian

$$\mathcal{L}_{\mathrm{QCD}}^{\mathrm{eff}} = \mathcal{L} - \frac{\theta}{16\pi^2}\mathrm{Tr}G_{\mu\nu}\tilde{G}^{\mu\nu}\,. \tag{2.61}$$

By rescaling the gauge field $A_\mu \to g_s A_\mu$, and evaluating the trace we find the usual form of the theta term [113, 124, 125]

$$\mathcal{L}_\theta = \frac{\theta g_s^2}{32\pi^2}G_{\mu\nu}^a\tilde{G}^{a\mu\nu}\,. \tag{2.62}$$

### 2.2.5 Chiral anomaly

We have discussed the global symmetries $U(3)_L \times U(3)_R$ of massless QCD at the classical level. However, chiral symmetries are explicitly broken by a quantum effect known as anomaly [119].

The chiral anomaly can be viewed as non-invariance of the path integral measure under axial transformations. For simplicity, we will consider the chiral limit of QED, which can be generalized to non-abelian gauge theory. Consider an expectation value of an arbitrary operator $\mathcal{O}$, as a path integral

$$\langle\mathcal{O}\rangle = \int D\psi D\bar{\psi}DA_\mu\mathcal{O}\exp\left(i\int d^4x\big(-\frac{1}{4}F_{\mu\nu}F^{\mu\nu} + i\bar{\psi}\not{\partial}\psi\big)\right). \tag{2.63}$$

The action is invariant under axial rotation

$$\begin{aligned}\psi &\to \exp(i\beta\gamma^5)\psi = \Delta\psi\,,\\ \bar{\psi} &\to \bar{\psi}\exp(i\beta\gamma^5) = \bar{\psi}\Delta\,.\end{aligned} \tag{2.64}$$

We can simply focus on the transformation properties of fermion measure $D\psi D\bar{\psi}$. Since fermions anticommute, the fermionic paths are represented by Grassmann variables. A change of variables in the Grassmann integral yields the inverse of the Jacobian determinant, $J = \det\Delta$, [126]

$$\int D\psi D\bar{\psi} \to \int D\psi D\bar{\psi}|J|^{-2}\,. \tag{2.65}$$

We can use the known representation of the determinant

$$\det\Delta = \exp\mathrm{Tr}\log\Delta = \exp\Big(\mathrm{Tr}\big(\beta(\hat{x})\gamma^5\big)\Big)\,. \tag{2.66}$$

To evaluate the trace over the continuous index we may use

$$\mathrm{Tr}(\hat{x}) = \int d^4x \langle x|\hat{x}|x\rangle \,, \tag{2.67}$$

so that the Jacobian is given by

$$\det\Delta = \exp\left(\mathrm{Tr}\int d^4x\beta(x)\gamma^5\right), \tag{2.68}$$

where the trace is now just the Dirac trace since integral already accounts for a trace of the continuous operator $\hat{x}$. We regularize the integral with a cut-off dependent exponential

$$\log\det\Delta = \lim_{\Lambda\to\infty}\mathrm{Tr}\int d^4x\beta(x)\gamma^5\exp\left(\frac{\not{\Pi}^2}{\Lambda^2}\right), \tag{2.69}$$

where we have introduced a gauge covariant momentum $\Pi_\mu = (-i\partial_\mu - eA_\mu)$, which is related to the covariant derivative by $\Pi_\mu = -iD_\mu$. Using $\Pi_\mu$ allows for retaining the gauge invariance.

Using known formula relating interactions of spinors and scalars with gauge field $\not{D}^2 = D^2 + eF_{\mu\nu}\sigma^{\mu\nu}/2$ we have [113]

$$\not{\Pi}^2 = \Pi^2 - \frac{e}{2}F_{\mu\nu}\sigma^{\mu\nu} \,. \tag{2.70}$$

Plugging that into formula for Jacobian

$$\begin{aligned}\log\det\Delta &= \lim_{\Lambda\to\infty}\mathrm{Tr}\int d^4x\beta(x)\gamma^5\exp\left(\frac{\Pi^2}{\Lambda^2}\right)\exp\left(-\frac{e}{2}\frac{F_{\mu\nu}\sigma^{\mu\nu}}{\Lambda^2}\right) = \\ &= \lim_{\Lambda\to\infty}\mathrm{Tr}\int d^4x\beta(x)\gamma^5\exp\left(\frac{\Pi^2}{\Lambda^2}\right)\left(1 - \frac{e}{2\Lambda^2}F_{\mu\nu}\sigma^{\mu\nu} + \frac{e^2}{8\Lambda^4}F_{\mu\nu}F_{\alpha\beta}\sigma^{\mu\nu}\sigma^{\alpha\beta} + \mathcal{O}\Big((\frac{1}{\Lambda^6}\Big)\right).\end{aligned} \tag{2.71}$$

The last term of the expansion is symmetric with respect to change $F_{\mu\nu} \leftrightarrow F_{\alpha\beta}$, so we can consider only the symmetric part of the sigma part of $\sigma^{\mu\nu}\sigma^{\alpha\beta}$. Symmetrization of the sigma matrices is $\{\sigma^{\mu\nu},\sigma^{\alpha\beta}\}/2 = g^{\mu\alpha}g^{\nu\beta} - g^{\nu\alpha}g^{\mu\beta} + i\gamma^5\epsilon^{\mu\nu\alpha\beta}$, which combined with the field strength tensor yields

$$F_{\mu\nu}F_{\alpha\beta}\sigma^{\mu\nu}\sigma^{\alpha\beta} = 2F_{\mu\nu}F^{\mu\nu} + i\gamma^5\epsilon^{\mu\nu\alpha\beta}F_{\mu\nu}F_{\alpha\beta} \,. \tag{2.72}$$

Plugging this result in Eq. (2.71), the first two terms in the bracket, as well as the first term from Eq. (2.72), vanish under trace because $\mathrm{Tr}[\gamma^5] = \mathrm{Tr}[\gamma^5\gamma^\mu\gamma^\nu] = 0$. On the other hand, because $\mathrm{Tr}[(\gamma^5)^2] = \mathrm{Tr}[1] = 4$, from the second term of Eq. (2.72) we have

$$\log\det\Delta = i\int d^4x\beta(x)\frac{4e^2}{8}\epsilon^{\mu\nu\alpha\beta}F_{\mu\nu}F_{\alpha\beta}\lim_{\Lambda\to\infty}\frac{1}{\Lambda^4}\exp\left(\Pi^2/\Lambda^2\right). \tag{2.73}$$

In order to evaluate the limit consider expectation value

$$\lim_{\Lambda\to\infty}\frac{1}{\Lambda^4}\langle x|\exp\left(\Pi^2/\Lambda^2\right)|x\rangle = \lim_{\Lambda\to\infty}\frac{1}{\Lambda^4}\int\frac{d^4k}{(2\pi)^4}\langle x|\exp\left((\hat{p}-eA)^2/\Lambda^2\right)|k\rangle\langle k\,|\,x\rangle \,, \tag{2.74}$$

where we have inserted the complete set of momentum states. In the limit of infinite cut-off quadratic and linear terms in the gauge field vanish in the exponential. Using $\langle x\,|\,k\rangle = \langle k\,|\,x\rangle^* = \exp(i\vec{p}\cdot\vec{x})$ and performing Wick's rotation to imaginary time we find

$$\lim_{\Lambda\to\infty}\frac{1}{\Lambda^4}\int\frac{d^4k}{(2\pi)^4}\exp\left(\frac{k^2}{\Lambda^2}\right) = \lim_{\Lambda\to\infty}\frac{i}{\Lambda^4}\int\frac{d^4k_E}{(2\pi)^4}\exp\left(\frac{k_E^2}{\Lambda^2}\right), \tag{2.75}$$

which is simply a fourth power of Gaussian integral

$$\begin{aligned}\lim_{\Lambda\to\infty}\frac{i}{\Lambda^4}\int\frac{d^4k_E}{(2\pi)^4}\exp\left(\frac{k_E^2}{\Lambda^2}\right) &= \lim_{\Lambda\to\infty}\frac{i}{\Lambda^4}\left(\int\frac{dk_E}{2\pi}\exp\left(\frac{k_E^2}{\Lambda^2}\right)\right)^4 = \\ &= \lim_{\Lambda\to\infty}\frac{i}{\Lambda^4}\frac{\left(\sqrt{\pi\Lambda^2}\right)^4}{(2\pi)^4} = \frac{i}{16\pi^2}\,.\end{aligned}\tag{2.76}$$

Finally we can put everything together accounting for $(-1)$ factor from $\mathcal{J}^{-1}$ and original spacetime integral becomes

$$|\mathcal{J}|^{-1} = \exp\left(-i\int d^4x\beta(x)\frac{e^2}{32\pi^2}\epsilon^{\mu\nu\alpha\beta}F_{\mu\nu}F_{\alpha\beta}\right).\tag{2.77}$$

Hence, as a result of the anomalous transformation, the action is shifted

$$\int D\psi D\bar{\psi}DA\mathcal{O}\exp\left(i\int d^4x(-\frac{1}{4}F_{\mu\nu}F^{\mu\nu}+i\bar{\psi}\not{\partial}\psi-i\int d^4x\beta(x)\frac{e^2}{16\pi^2}\epsilon^{\mu\nu\alpha\beta}F_{\mu\nu}F_{\alpha\beta}\right).\tag{2.78}$$

The non-invariance of lagrangian under the chiral transformation is also manifested by the non-vanishing divergence of the axial current found from Eq. (A.77)

$$\partial^\mu J^A_\mu = -\frac{e^2}{16\pi^2}\epsilon^{\mu\nu\alpha\beta}F_{\mu\nu}F_{\alpha\beta}\,.\tag{2.79}$$

This non-perturbative result agrees with the 1-loop calculation of pion decay to two photons:

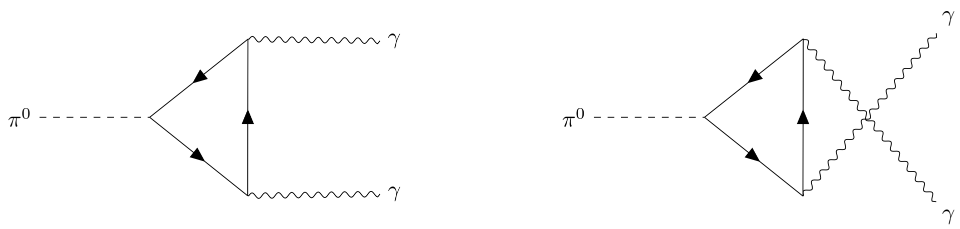


The result of the calculation is interpreted as the expectation value of composite operator $\bar{q}\gamma^5 q$ in the presence of external electromagnetic fields [113]

$$\langle A|\bar{q}\gamma^5 q|A\rangle = i\frac{e^2}{32\pi^2 m}\epsilon^{\mu\nu\alpha\beta}F_{\mu\nu}F_{\alpha\beta}\,,\tag{2.80}$$

which after using divergence of axial current, Eq. (2.26), gives

$$\langle A|\partial^\mu J^A_\mu|A\rangle = -\frac{e^2}{16\pi^2}\epsilon^{\mu\nu\alpha\beta}F_{\mu\nu}F_{\alpha\beta}\,.\tag{2.81}$$

### 2.2.6 Strong CP problem

We have seen that non-perturbative instanton effects induce $G\widetilde{G}$ term to the lagrangian Eq. (2.62). However, this term is not invariant under chiral transformation due to chiral anomaly

$$\begin{aligned}m\bar{q}q &\to me^{2i\alpha}\bar{q}q\,,\\ \theta\frac{g^2}{32\pi^2}G^a_{\mu\nu}\tilde{G}^{a,\mu\nu} &\to \left(\theta-2\alpha\right)\frac{g^2}{32\pi^2}G^a_{\mu\nu}\tilde{G}^{a,\mu\nu}\,.\end{aligned}\tag{2.82}$$

Of course, physical observables cannot depend on field redefinitions, which motivates the introduction of chiral invariant

$$\bar{\theta} = \theta + \arg\det M_u M_d \,, \tag{2.83}$$

where $M_u, M_d$ denote the $3 \times 3$ mass matrices of up and down type quarks so that the argument of the determinant picks up all complex phases of quark masses. Note, that by making the appropriate chiral transformation, we can move $\bar{\theta}$ between the quark masses and $G\widetilde{G}$ term. This freedom allows us to choose a suitable framework for our specific needs.

Firstly, let us explicitly show the CP transformation of $G\widetilde{G}$ term. Recall that the CP transformation for gluon field $A_\mu$ and partial derivatives are

$$\begin{aligned} &\text{CP: } A_i(\vec{x},t) \to -A_i(-\vec{x},t), \qquad && A_0(\vec{x},t) \to A_0(-\vec{x},t)\,, \\ &\text{CP: } \qquad\qquad \partial_i \to -\partial_i, && \partial_0 \to \partial_0\,. \end{aligned} \tag{2.84}$$

Since the anomaly term involves contraction with a totally antisymmetric tensor, it will involve the sum of non-zero terms with exactly one time-like contraction. Schematically,

$$\epsilon^{\mu\nu\alpha\beta} G_{\mu\nu} G_{\alpha\beta} = \sum \epsilon^{0ijk} G_{0i} G_{jk}, \tag{2.85}$$

where we intentionally don't specify the summed indices. Using the definition of field strength we have

$$\begin{aligned} G_{0i} &= \partial_0 A_i - \partial_i A_0 + g f^{abc} A_0^a A_i^b \to -\partial_0 A_i + \partial_i A_0 - g f^{abc} A_0^a A_i^b = -G_{0i}\,, \\ G_{ij} &= \partial_i A_j - \partial_j A_i + g f^{abc} A_i^a A_j^b \to \partial_i A_j - \partial_j A_i + g f^{abc} A_i^a A_j^b = G_{ij}\,. \end{aligned} \tag{2.86}$$

Combining those, we have

$$\text{CP: } \epsilon^{\mu\nu\alpha\beta} G_{\mu\nu} G_{\alpha\beta} \to -\epsilon^{\mu\nu\alpha\beta} G_{\mu\nu} G_{\alpha\beta}\,, \tag{2.87}$$

which proves that the $\theta$-term is odd under CP transformation.

In Appendix A.1 we prove that this term is a total derivative and does not affect the perturbation theory. However, this CP violation has a significant effect on neutron electric dipole moment (nEDM) $d_n$, which is CP odd observable in low-energy QCD[2]. Since the neutron is an effective degree of freedom below the confinement scale, non-perturbative effects affect its couplings.

This estimate closely follows [125]. We will work in a basis where $\bar{\theta}$ is absorbed in the quark masses. Lorentz invariant lagrangian for nEDM has form

$$\mathcal{L}_{\text{nEDM}} = -\frac{i}{2} d_n \bar{n} \sigma^{\mu\nu} \gamma^5 n F_{\mu\nu}\,, \tag{2.88}$$

It is a dimension 5 operator and is suppressed by the applicability scale of EFT, roughly the mass of neutron $m_n$. The photon must couple to a charged particle, thus there should be a loop factor $1/16\pi^2$ and EM coupling $e$. On top of that, we include the CP-violating phase in the quark mass matrix by inserting dimensionless $m_q e^{i\bar{\theta}}/m_n$. Combining those the estimate is

$$\mathcal{L}_{\text{nEDM}} = \frac{e}{16\pi^2} \frac{m_q e^{i\bar{\theta}}}{m_n} \frac{1}{m_n} \bar{n} \sigma^{\mu\nu} \gamma^5 n F_{\mu\nu} m\,, \tag{2.89}$$

[2] Intuitively, one can understand why this parameter measures CP-violation by considering a classical electric dipole moment $\vec{d} = q\vec{p}$ with displacement vector $\vec{p}$ pointing from negative to positive charge. The charge conjugation $C: q \to -q, \vec{p} \to -\vec{p}$, while parity flips only vector $P: q \to q, \vec{p} \to -\vec{p}$. Combining, we have $\text{CP}: q\vec{p} \to -q\vec{p}$

which upon expanding to leading order in $\bar{\theta}$ gives approximate nEDM

$$|d_n| \simeq \frac{1}{8\pi^2}\frac{m_q}{m_n^2}\bar{\theta}e \sim 10^{-4}\ \bar{\theta}\ e\ \mathrm{GeV}^{-1}\,. \tag{2.90}$$

We have taken $m_q = (m_u + m_d + m_s)/3 \simeq m_s/3$ in last equality. This rough estimate is enough to indicate the problem, because the bound on the nEDM [127]

$$|d_n| < 1.8 \times 10^{-26}\ \mathrm{e\ cm} \simeq 10^{-12}\ e\ \mathrm{GeV}^{-1}\,, \tag{2.91}$$

implying $\bar{\theta} < 10^{-8}$! Rigorous calculations lead to even stronger limits, in particular in baryon chiral perturbation theory is [128]

$$|d_n| < 5.5 \times 10^{-3}\bar{\theta}\ e\ \mathrm{GeV}^{-1}\,, \tag{2.92}$$

implying

$$\bar{\theta} < 1.8 \times 10^{-10}\,. \tag{2.93}$$

The QCD sum rules give the same order of magnitude result [129]

$$|d_n| < 2.1 \times 10^{-3}\bar{\theta}\ e\ \mathrm{GeV}^{-1}\,, \tag{2.94}$$

implying

$$\bar{\theta} < 4.7 \times 10^{-10}\,. \tag{2.95}$$

Even though the QCD predicts the generic existence of CP violation, it is absent. The inexplicable smallness of $\bar{\theta}$ suggests that there could be new physics, which explains this peculiar value. As it is a fine-tuning issue, it is always possible to argue that it is just a coincidence that the two unrelated quantities, $\theta$ and $\arg\det M_u M_d$, perfectly cancel out. However, in the era of limited clues for new physics, every hint is priceless, as discussed in Sec. 2.1.

## 2.3 Hierarchy problem

The scalar potential of the Standard Model is

$$V(H, H^\dagger) = -m^2 H^\dagger H + \lambda\Big(H^\dagger H\Big)^2\,, \tag{2.96}$$

which is minimized at $\langle H^\dagger H\rangle = v^2/2 = m^2/2\lambda$. The Higgs doublet expanded around the new minimum is

$$H = \begin{pmatrix} G^\pm \\ \frac{1}{\sqrt{2}}(v + h + iG^0) \end{pmatrix}\,, \tag{2.97}$$

and can be inserted into the potential Eq. (2.96). Neglecting the would-be-Goldstone bosons $G^i$ yields the potential for the real Higgs

$$V(h) = \frac{1}{2}m_h^2 h^2 + m\sqrt{\lambda}h^3 + \frac{\lambda}{4}h^4\,, \tag{2.98}$$

where $m_h^2 = 2m^2$ is the mass of the Higgs boson and $\lambda$ is the quartic self-coupling of the Higgs doublet. The Higgs doublet couples to the SM fermions via Yukawa interactions

$$\mathcal{L}_{\text{yuk}} = \bar{d}\mathbf{y_d}HQ + \bar{u}\mathbf{y_u}\widetilde{H}Q + \bar{e}\mathbf{y_e}HL\,, \tag{2.99}$$

where $u, d, e$ are right-handed components of the fermion fields and $Q, L$ are left-handed quark and lepton doublets, respectively. After SSB, we can substitute Eq. (2.97) obtaining Yukawa interactions of type

$$\mathcal{L}_{\rm yuk} = \frac{y_f}{\sqrt{2}} \bar{f} f h \,. \tag{2.100}$$

The Higgs also couples to the electroweak gauge bosons via covariant derivative

$$\mathcal{L} = (D_\mu H)^\dagger (D^\mu H) \supset \frac{g^2}{4} W^+ W^- h^2 + \frac{g^2 + g'^2}{4} Z^2 h^2 \,, \tag{2.101}$$

where $D_\mu H = \partial_\mu - i g \tau^a W^a_\mu/2 - i g' B_\mu/2$.

Each of the above couplings contributes to the self-energy of the Higgs doublet. Some quadratically divergent loop diagrams include

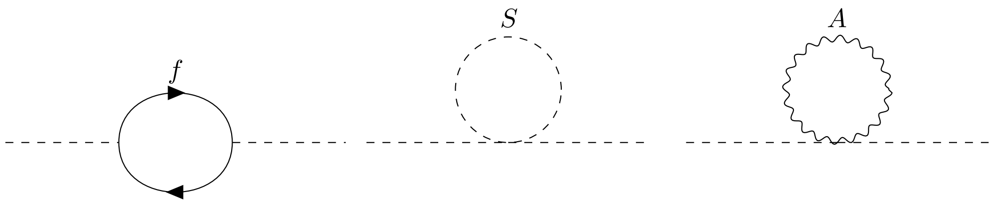


Let us start with the calculation of the scalar loop diagram from the Higgs self-interaction quartic term in Eq. (2.98), which contributes to the Higgs self-energy

$$\Pi_s(p^2) = \left(-i\frac{\lambda}{4}\right) \times 4 \times 3 \int \frac{d^4 k}{(2\pi)^4} \frac{i}{k^2 - m_h^2} = \frac{3 i \lambda}{16\pi^4} \int \frac{k_E^3 dk_E d\Omega}{k_E^2 + m_h^2} \,, \tag{2.102}$$

where $4 \times 3$ is the combinatoric factor and in the last step we have gone to the Euclidean time, $\tau = it$. Integrating over the solid 3-angles, $\int d\Omega = 2\pi^2$, and regularizing the divergent integral by introducing the hard, Euclidean cut-off $\Lambda_E$ results in

$$\Pi_s(p^2) = \frac{3 i \lambda}{16\pi^2} \left( \Lambda_E^2 - 2 m_h^2 \ln\left(\frac{\Lambda_E}{m_h}\right)\right) \simeq \frac{3\lambda}{16\pi^2} \Lambda^2 + \mathcal{O}\left(\ln \frac{\Lambda^2}{m_h^2}\right) , \tag{2.103}$$

where we have neglected a small $m_h/\Lambda$ term in the logarithm. Keeping only the quadratic term, and using the formula for the mass of the Higgs, $m_h = 2\lambda v^2$ gives

$$\delta m_h^2(h) = \frac{3}{16\pi^2 v^2} \Lambda^2 m_h^2 \,. \tag{2.104}$$

The fermion diagram gives

$$\begin{aligned}
\Pi_f(p^2) &= -\left(-i\frac{y_f}{\sqrt{2}}\right)^2 \times 2 \times n_g \int \frac{d^4 k}{(2\pi)^4} \frac{i^2 \mathrm{Tr}\left[\left(\left(\not{p} + \not{k}\right) + m_f\right)(\not{k} + m_f)\right]}{\left((p+k)^2 - m_f^2\right) \cdot \left(k^2 - m_f^2\right)} = \\
&= -4 y_f^2 n_g \int \frac{d^4 k}{(2\pi)^4} \frac{k^2 + m_f^2}{(k^2 - m_f^2)^2} = -4 y_f^2 n_g \int \frac{d^4 k}{(2\pi)^4} \left( \frac{1}{k^2 - m_f^2} + \frac{2 m_f^2}{(k^2 - m_f^2)^2} \right) = \\
&= -\frac{y_f^2 n_g}{4\pi^2} \left( \Lambda^2 - 2 m_f^2 \ln\left(\frac{\Lambda}{m_f}\right) - y_f^2 m_f^2 + 2 m_f^2 \ln\left(\frac{\Lambda}{m_f}\right)\right) = \\
&= -\frac{y_f^2 n_g}{4\pi^2} \left( \Lambda^2 - y_f^2 m_f^2 \right) \simeq -\frac{n_g}{8\pi^2 v^2} \Lambda^2 m_f^2 \,,
\end{aligned} \tag{2.105}$$

where $n_g$ is the number of internal degrees of freedom ($n_g = 3$ for quarks), and in the last line we have used $m_f^2 = y_f^2 v^2/2$. Finally, the gauge loop contributes to the Higgs self-energy

$$\begin{aligned}\Pi_A(p^2) &= -\frac{ig^2}{4} \times 2 \times n_g \int \frac{d^4k}{(2\pi)^4} \frac{-ig_{\mu\nu}\left(g^{\mu\nu} - \frac{k^\mu k^\nu}{k^2}\right)}{k^2 - m_A^2} = \\ &= -\frac{3g^2 n_g}{32\pi^2}\left(\Lambda^2 - 2m_A^2 \ln\left(\frac{\Lambda}{m_A}\right)\right) \simeq -\frac{3}{8\pi^2 v^2} n_g \Lambda^2 m_A^2 \,,\end{aligned} \tag{2.106}$$

where $m_A$ is vector boson mass and $n_g$ is the number of degrees of freedom, $n_g = 2(1)$ for $W(Z)$ boson.

The complete quadratically divergent contribution to the Higgs mass, involving contributions from would-be-Goldstones can be written as [72, 130, 131]

$$\delta m_h^2 = \frac{3}{8\pi^2 v^2}\Lambda^2\left(4m_t^2 - m_h^2 - m_Z^2 - 2m_W^2\right). \tag{2.107}$$

The vanishing of the above is known as Veltman condition [72] and has been speculated to be satisfied in the past. However, measurements of the mass of the top quark rule out this possibility since

$$\left(4m_t^2 - m_h^2 - m_Z^2 - 2m_W^2\right) \simeq (300 \text{ GeV})^2 \,. \tag{2.108}$$

As a result, the mass of the Higgs obtains large corrections from the UV scales. It means, that in the SM viewed as an effective theory, the high energy scales do not decouple. In particular, any heavy particle coupled to the Higgs contributes to the mass of the Higgs. Assuming that there is no new physics up to the scale of quantum gravity, $M_{\text{pl}} \simeq 10^{19}$ GeV, requires that the bare mass of the Higgs boson is also of similar magnitude, and by miraculous cancellation between those two we observe the Higgs with mass $m_h \simeq 125$ GeV. Because the whole SM spectrum is related to the mass of the Higgs via the Higgs mechanism, all SM particles inherit the UV sensitivity.

The correction to the mass of the Higgs from the SM particles, assuming the validity of SM up to $\Lambda = 5$ TeV, gives

$$\delta m_h^2 \simeq (1.7 \text{ TeV})^2 \,, \tag{2.109}$$

which already requires that the bare mass of the Higgs is tuned within 1 part in about 200. Even assuming that New Physics canceling the quadratic divergencies enters around 2 TeV, the fine-tuning is at a percent level. It is debatable how much fine-tuning is acceptable, but it is widely believed, that fine-tuning of one part in $10^{30}$, as predicted for $\Lambda = M_{\text{pl}}$ is truly problematic. Solutions to the hierarchy problem must cancel the quadratic divergences above some scale $\Lambda_{\text{HP}}$, usually leaving some residual tuning from finite corrections of order $\delta m_h^2 \simeq \Lambda_{\text{HP}}^2/16\pi^2$.

Note, that it isn't sufficient to set the mass of the Higgs at 125 GeV at any particular scale because running it to another scale will quickly diverge from the observed EW scale. The solution to the Hierarchy Problem requires the cancellation of the quadratically divergent correction at all scales.

We do not need to rely on the hard cut-off regularization to understand the hierarchy problem. The one-loop running of the mass of the Higgs from $\mu$ to $Q$ is [13]

$$\delta m_h^2 = \sum_i g_i (-1)^{2s_i} \frac{\lambda_i^2 m_i^2}{32\pi^2} \log\left(\frac{Q^2}{\mu^2}\right), \tag{2.110}$$

where $s_i$ is spin and $\lambda_i$ is coupling constant to the Higgs, $g_i$ is a number of internal degrees of freedom, and the sum runs over all particles with masses $m_i^2$, that are coupled to the Higgs via terms $\lambda_i^2 h^2 \phi_i^2/2$. In practice, any heavy particle coupled to the Higgs induces large corrections, which means that precise fine-tuning is necessary to keep $m_h \simeq 125$ GeV in any BSM theory.

This miraculous cancellation of the corrections to the mass of the Higgs suggests a special property of the UV theory, which can be leveraged in the theoretical searches for BSM physics.

### 2.3.1 Fine-tuning measure

In the Sec. 2.1 we have discussed how fine-tuning indicates the unnaturalness of a theory. We will now consider the fine-tuning in greater depth. To quantify the fine-tuning of observable $\mathcal{O}$ with respect to parameters $p_i$, Ref. [132] considered what is now known as the Barbieri-Giudice measure, defined as

$$\Delta_{\rm BG}(p_i) = \left| \frac{p_i}{\mathcal{O}(p_i)} \frac{\partial \mathcal{O}}{p_i} \right| , \tag{2.111}$$

which was first used in Ref. [133]. A large value of $\Delta_{\rm BG}$ indicates the high sensitivity of $\mathcal{O}$ on $p_i$, so the values of $p_i$ must be carefully selected to match the observation, indicating fine-tuning. Following example from Ref. [132], demanding that $\Delta_{\rm BG} < 10$ allows for cancellation up to one order of magnitude. We can convert the Eq. (2.111) to percent via

$$\text{fine} - \text{tuning} = 100\%/\Delta_{\rm BG} \,. \tag{2.112}$$

Consequently, $\Delta_{\rm BG} = 10$ implies that there is 10% tuning of parameters. Since Eq. (2.111) is defined for each of the parameters $p_i$, the total fine-tuning is obtained by picking the largest one

$$\Delta_{\rm BG} = \max_i(\Delta_{\rm BG}(p_i)) \,. \tag{2.113}$$

If there is more than one independent source of tuning of the model, the total tuning is obtained multiplicatively

$$\Delta_{\rm tot} = \prod_i \Delta_i \,. \tag{2.114}$$

We can now calculate the fine-tuning of the electroweak scale in the SM. The largest correction to the mass of the Higgs comes from the loops involving the top quark from Eq. (2.107). The correction to the EW VEV is

$$\delta v^2 = \frac{\delta m_h^2}{4\lambda} = \frac{3 y_t^2}{16\pi^2 \lambda} \Lambda^2 \,. \tag{2.115}$$

Plugging that into Eq. (2.111) we obtain

$$\Delta_{\rm SM} = \left| \frac{\Lambda^2}{v^2} \frac{\partial v^2}{\Lambda^2} \right| = \frac{3 y_t^2}{16\pi^2 \lambda v^2} \Lambda^2 \,, \tag{2.116}$$

where we have treated the cut-off as a physical mass threshold. For $\Lambda = 5$ TeV we have $\Delta_{\rm SM} = 60$ and the tuning is worse than 5%, while for $\Lambda = 10$ TeV we obtain $\Delta_{\rm SM} = 240$ and tuning is at the sub-percent level.

## 2.4 Dark matter

Dark matter is yet an unknown component of the Universe, which certainly interacts gravitationally, and has suppressed couplings to photons. Dark matter behaves as a non-relativistic gas of particles and hence is an example of a cold relic. In section 2.4.1 we will briefly review the evidence for the existence of the DM at different scales and in Sec. 2.4.2 we will present the most common mechanism of thermal production of DM via freeze-out and define the density of DM which quantifies its energy density. Finally, in Sec. 2.4.3 and Sec. 2.4.4 we will review strategies for detecting DM and probing its interactions.

### 2.4.1 Evidence for the existence of dark matter

The presence of DM can be observed at various scales, ranging from individual galaxies and galaxy clusters to cosmological distances. In this section, we will briefly review the most significant hints on the existence of the dark matter, for exhaustive analysis see Ref. [134, 135].

**Rotation curves of spiral galaxies**

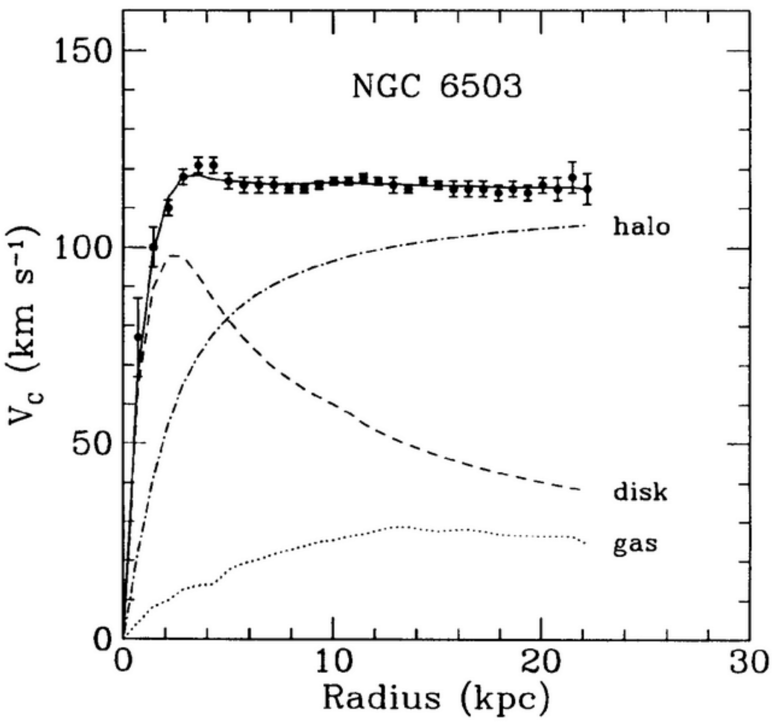


Figure 2.3: Rotation curve of NGC 6503 galaxy from Ref. [136]. The curves from gas (dotted), disc (dashed), and dark matter halo (dash-dotted) are shown. Including the dark matter halo allows for agreement with the observation.

One of the most compelling evidence for the existence of dark matter is also the one that was first identified, the rotational curves of the galaxies measured by Fritz Zwicky [137]. The circular velocities of stars as a function of distance from the center of the galaxy are found using

$$v(r) = \sqrt{\frac{4\pi G \int_0^r r'^2 dr' \rho(r')}{r}}\,, \tag{2.117}$$

where $\rho(r')$ is the density of galactic matter. The above implies that beyond the optical disc of the galaxy, where $\rho(r) \simeq 0$, the circular velocities of the stars should fall as $\sim 1/\sqrt{r}$. However, the observations give $v(r) \sim$ const at large $r$, see Fig. 2.3, suggesting that the density does not vanish at large $r$. Interestingly, it is sufficient to assume that besides the visible disc of matter, there is also a halo of non-luminous matter extending beyond the radius of the disc, which can also be read from Fig. 2.3. The simplest example of the dark matter halo profile, which fixes the rotational curves, is the singular isothermal sphere profile with scaling $\rho_{\text{halo}} \sim 1/r^2$.

The Ref. [138] analyzed around 1100 rotation curves, finding signals of DM halo in galaxies with masses spanning six orders of magnitude.

### Galaxy clusters

Galaxy clusters are gravitationally bound structures consisting of up to thousands of galaxies. Those clusters are permeated by the intercluster medium composed of hot plasma, emitting X-ray photons. The analysis of the optical images allows for the estimation of the mass of the visible matter in the galaxy clusters. On the other hand, by measuring the gravitational lensing induced by the whole system, the total mass of the galaxy cluster can be calculated. The visible matter tends to constitute 10-20% of the total mass of the galaxy clusters [134]

The existence of the dark matter is also favored by the observation of the galaxy cluster merger 1E0657-558 [139] known as Bullet Cluster. Because dark matter does not have strong self-interaction, as opposed to baryonic matter, it propagates mostly undisturbed after the collision. The authors combine the observation of the gravitational lensing maps of the object, which encodes information about its total mass, with the visible matter distribution from the Chandra X-ray observatory. As a result, the spatial offset of the center of total mass to the center of visible, baryonic mass is observed at a statistical significance of $8\sigma$. [3]. A similar analysis of the MACSJ0025.4-1222 merging cluster found the offset between centers of mass with the significance of $4\sigma$ [142]. Galaxy cluster mergers are considered to be one of the strongest evidence for the existence of dark matter [135].

### Cosmic Microwave Background

The photons emitted at the recombination encode the information about the evolution of perturbations at different scales. The temperature anisotropies in the Cosmic Microwave Background (CMB) can be measured to very high accuracy and mapped to the power spectrum. The shape of the spectrum is determined by the composition of the Universe, allowing for testing cosmological models.

[3] While bullet cluster observations are widely believed to be strong evidence for dark matter, some implementations of Modified Newtonian dynamics (MOND) are not necessarily in conflict with those observations [140]. Nonetheless, DM remains the simplest hypothesis explaining all observations as MOND theories often struggle to account for observed CMB anisotropies, gravitational lensing and matter power spectrum [141].

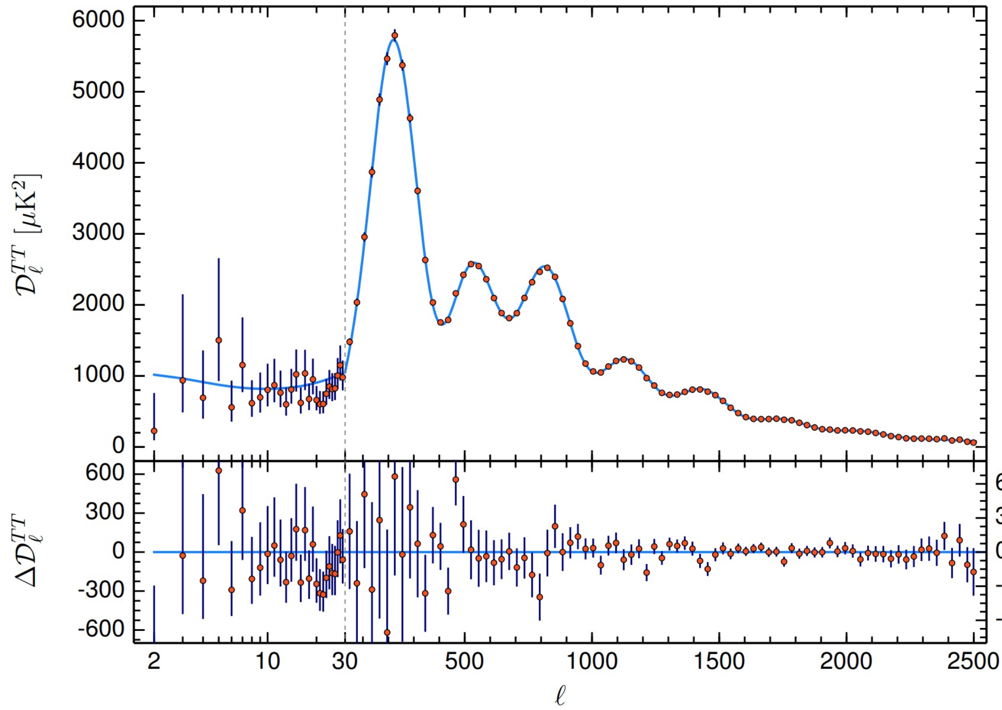


Figure 2.4: Planck 2018 CMB temperature power spectrum (upper panel) and the residual with respect to the model (lower panel). The continuous curve is the best TT,TE,EE+lowE+lensing fit to ΛCDM model. The plot from Ref. [21].

In particular, the effects of dark matter are distinct from other energy deposits, as it interacts only gravitationally, at the same time redshifting like non-relativistic matter. This is in contrast to the relativistic neutrinos and self-interacting photon-baryon fluid. The effect of the dark matter on the CMB power spectrum is mostly captured by the height of the first two peaks, affected by the time of matter-radiation equality [143].

The relic density of dark matter, as defined in Appendix B.1, can be reliably estimated in the ΛCDM model using CMB data from Planck satellite [21]

$$\Omega_{\mathrm{CDM}} h^2 = 0.11933 \pm 0.00091\,, \tag{2.118}$$

which is roughly 6 times larger than the baryon abundance $\Omega_b h^2 = 0.02242 \pm 0.00014$ [21], in agreement with the expectation from rotational curves of galaxies, that DM density should dominate over luminous matter density.

### Big Bang Nucleosynthesis

The production of light nuclei (D, $^3$He, $^4$He and $^7$Li) in the early Universe, known as Big Bang Nucleosynthesis, is a well understood process. The key parameter in the standard cosmology determining the ratios of the elements is the baryon-to-photon ratio $\eta = \eta_{10} \times 10^{-10}$. The observed value [144]

$$\eta_{10} = 6.129 \pm 0.039\,, \tag{2.119}$$

allows for precise determination of the density of baryons, $\Omega_b h^2 = 0.02239 \pm 0.00014$, in agreement with Planck results. Combining this result with CMB observations of the total matter density, $\Omega_m h^2 \simeq 0.14$, results in the conclusion that a larger part of the matter is non-baryonic [13].

Big Bang Nucleosynthesis provides an overall consistency check for the ΛCDM model combined with the Standard Model of particle physics. Moreover, the great agreement of the predictions to the observations provides constraints on the new physics [145].

**Large-scale structure formation**

The dark matter as a pressureless fluid forms gravitational wells, which pull the baryonic matter, leading to galaxy formation. In particular, the seeding of the Universe by DM is essential for reproducing the galaxy clustering observed by Sloan Digital Sky Survey [146, 147].

The energy density with perturbation $\delta\rho$ in a fluid of background density $\bar{\rho}$ is

$$\rho = \bar{\rho} + \delta\rho\,. \tag{2.120}$$

The early evolution of matter perturbations, provided they are sufficiently small to neglect higher order terms, can be described by linearized non-relativistic, barotropic fluid equations in the Fourier space [143]

$$\ddot{\delta}(\mathbf{k},t) + 2H\dot{\delta}(\mathbf{k},t) + c_s^2\left(\frac{k^2}{a^2} - k_J^2(t)\right)\delta = 0\,. \tag{2.121}$$

where $\delta = \delta\rho/\bar{\rho}$ is linear density contrast, $c_s$ is the sound speed of the fluid, $H = \dot{a}/a$ is Hubble parameter and the physical Jeans wavenumber is defined

$$k_J(t) = \frac{\sqrt{4\pi G\bar{\rho}(t)}}{c_s}\,, \tag{2.122}$$

and corresponds to the characteristic scale above which gravitational interactions dominate the evolution of density perturbations. For large wavenumber $k$, the Jeans scale can be dropped, and the equation becomes the damped harmonic oscillator with time-dependent friction. On the other hand, for small $k$ gravity dominates and perturbations can grow with details depending on the Hubble constant. In particular, the growth of the perturbations with scale factor in the radiation dominated era is logarithmic, $\delta \sim \log a$, while in the matter dominated era is linear, $\delta \sim a$.

The correlation function of the density contrast in the Fourier space defines the matter power spectrum, which encodes the information about the scaling of the perturbations at different scales. The dark matter enters the picture, as it is the main component of the non-relativistic matter. As such, its energy density affects the matter-radiation equality, which sets the position of the maximum of the power spectrum.

Combining the data from the matter power spectrum and the CMB anisotropies is in good agreement with the ΛCDM model [21, 148]. Moreover, the matter-radiation equality determines the total matter density, which combined with the BBN measurements of baryon density indicates that the majority of matter is non-baryonic [143].

### 2.4.2 Relic density

Let us derive some basic formulae for the abundance of thermally produced dark matter candidate $\chi$ following a classic review paper, Ref. [104]. We will assume, that the production was dominated by annihilation processes, $\chi\chi \leftrightarrow \bar{X}X$. This choice is motivated by the fact, that under certain assumptions (see Appendix B.5) the Boltzmann equations for a set of particles can be rewritten in the form of Boltzmann equation with an effective annihilation process.

The Boltzmann equation for number density $n_\chi$ takes the form

$$\frac{dn_\chi}{dt} + 3Hn_\chi = -\langle\sigma v\rangle\Big(n_\chi^2 - (n_\chi^{\text{eq}})^2\Big)\,, \tag{2.123}$$

where $n_\chi^{\text{eq}}$ is equilibrium number density, and $\langle\sigma v\rangle$ is thermally averaged annihilation cross section defined by Eq. (B.4.65) and $H$ is the Hubble parameter. For the sake of simplicity and to present the most basic properties of the solution to Eq. (2.123), let's assume that $\langle\sigma v\rangle$ = const. At high temperatures, $T \gg m_\chi$, the number density scales $\propto T^3$, while the Hubble goes as $\propto T^2$. Hence, the RHS of the equation dominates the expansion term $3Hn_\chi$, and the number density is dragged toward equilibrium. At later times, when the temperature drops below the mass of the DM candidates, $T \ll m_\chi$, the equilibrium number density of $\chi$ exponentially drops and the RHS of Eq. (2.123) is negligible. The $\chi$s are free-streaming, while being red-shifted by the expansion of the Universe, $n_\chi \propto T^3$. Such production is called freeze-out, as with the drop of the temperature the interactions cease and the comoving number density, $Y_\chi \equiv n_\chi/s$, becomes constant with time.

The relic abundance is set only by the time of the decoupling of $\chi$ from the thermal bath, $T_d$. Defining the annihilation rate as $\Gamma = \langle\sigma v\rangle n_\chi$, the approximate condition for freeze-out is

$$\Gamma(T_d) = H(T_d)\,. \tag{2.124}$$

Quite generally for weakly interacting massive particles with mass $\mathcal{O}(100)$ GeV, the freeze-out temperature is in the range $T_d/m_\chi \in (20, 25)$. Approximating $s(T) = 0.4g_*(T)T^3$, $H = 1.66g_*^{1/2}T^2/M_{\text{pl}}$, where $g_*$ is the effective number of relativistic degrees of freedom, defined by Eq. (B.2.29), and $M_{\text{pl}} \simeq 10^{19}$ GeV is the Planck mass, we find that comoving number density is

$$Y_\chi \simeq \frac{100}{g_*(T_d)^{1/2}M_{pl}m_\chi\langle\sigma v\rangle}\,. \tag{2.125}$$

The present mass density is defined

$$\Omega_\chi h^2 = \frac{m_\chi n_\chi}{\rho_c} = \frac{Y_\chi s_0 m_\chi}{\rho_c} = \frac{100 s_0}{g_*(T_d)^{1/2}M_{\text{pl}}\rho_c\langle\sigma v\rangle}\,, \tag{2.126}$$

where we have used that $Y_\chi(T_d) = Y_\chi(T_0)$, for the current temperature of the Universe $T_0$ and we have introduced current entropy density $s_0$ and critical density $\rho_c$. Most importantly, the result shows that the relic density is inversely proportional to the annihilation cross section. Stronger interactions keep $\chi$ longer in thermal equilibrium, with the equilibrium number density falling as $T^3$. The later annihilations freeze out , the smaller the number density at the time of decoupling. The scaling of relic abundance with an effective cross section also implies, that as we increase the mass of the DM, the Boltzmann suppression of $\langle\sigma v\rangle$ becomes more efficient, and relic abundance is enhanced. This is the leading effect of DM mass on the relic density, while small logarithmic corrections arise in numerical solutions to the freeze-out equation, Eq. (2.124).

We can approximate the relic density [104]

$$\Omega_\chi h^2 \simeq \frac{3\times 10^{-27}\text{cm}^3\ \text{s}^{-1}}{\langle\sigma v\rangle} \simeq \frac{2.5\times 10^{-10}\ \text{GeV}^{-2}}{\langle\sigma v\rangle}\,. \tag{2.127}$$

For a process mediated by a weak scale particle, parameterized by $\langle\sigma v\rangle \sim \alpha^2/(100\ \text{GeV})^2 = 10^{-4}\alpha^2\ \text{GeV}^{-2}$, the observed relic abundance, $\Omega h^2 \simeq 0.1$, is obtained for $\alpha \sim 5\times 10^{-3}$. Remarkably, for a natural value of the gauge coupling, $g \simeq 0.3$, we have $\alpha = g^2/4\pi \sim 5\times 10^{-3}$. This coincidence, named the WIMP (Weakly Interacting Massive Particle) miracle, sourced by the expectation of new particles at around weak scale, has driven decades of research. The WIMP paradigm has been the leading framework for the construction of DM models, as well as one of the main targets of experimental efforts [39,104,143,149–151].

### 2.4.3 Direct detection

Direct detection experiments aim to measure the interaction of dark matter particles with ordinary matter. Detectors of DD experiments are usually placed underground to reduce the noise from cosmic radiation and are designed to identify the events of DM scatterings of atomic nuclei.

Few of the main categories of DD experiments rely on scintillator crystal, cryogenic, or scintillator noble gas detectors. Reviews of DD experiments can be found in Ref. [152–154]

Scintillator crystal detectors absorb the energy from the scattering with DM and re-emit in the form of light. Examples of scintillator DD experiments involve DAMA/LIBRA [155, 156], KIMS [157, 158] and COSINE-100, designed to validate the annual modulation signal found in DAMA/LIBRA [159, 160]. It should be stressed that the signal has never been detected by another experiment and is not widely considered a detection of DM.

In cryogenic crystal detectors, such as CRESST [161, 162] or CDMS [163, 164], the DM particle excites the crystal lattice, disturbing its superconductivity.

Finally, in noble gas time-projection chambers (either liquid, gas, or dual phase), such as Xenon [165, 166], LZ [167, 168] and PandaX [169, 170], the scattering of DM on the atomic nuclei results in excitation of the nuclei which relaxes to the ground state by emitting a photon which can be observed by photon detectors.

DD experiments set bounds on the non-relativistic scattering cross section for a process $\mathrm{DM} + N \to \mathrm{DM} + N$. On the plot in Fig. 2.5 we present limits on the cross section from DD experiments, including those used in this thesis. Note, that the bounds are strongest around $m_{\mathrm{DM}} \sim \mathcal{O}(30)$ GeV.

Following Ref. [154], the differential cross section for DM-nucleus scatterings can be decomposed in the spin-dependent and spin-independent parts

$$\frac{d\sigma}{dE_R} = \frac{m_{\mathrm{nuc}}}{2\mu^2 v^2}\left(\sigma_0^{\mathrm{SI}} F_{\mathrm{SI}}^2(E_R) + \sigma_0^{\mathrm{SD}} F_{\mathrm{SD}}^2(E_R)\right), \tag{2.128}$$

where $\mu = m_{\mathrm{DM}} m_{\mathrm{nuc}}/(m_{\mathrm{DM}} + m_{\mathrm{nuc}})$ is the DM-nucleus reduced mass, $E_R$ is the recoil energy of the event, and $F(E_R)$ is form factor encoding dependence of cross section on the momentum transfer and $v$ the velocity of the DM in the rest frame of experiment. The reduced mass is maximized for $m_{\mathrm{DM}} = m_{\mathrm{nuc}}$, which for xenon gives the best sensitivity around $m_{\mathrm{DM}} \simeq 130$ GeV. The details of the experiment such as the energy threshold of the detector shift the maximal sensitivity to masses around 30 GeV [153].

### 2.4.4 Indirect detection

Indirect searches for DM aim to observe the SM products of decays or scatterings coming from regions of high concentrations of DM. As discussed above, the freeze-out of DM often involves annihilations, DM+DM→SM+SM, which keep DM in thermal equilibrium until decoupling. Consequently, it is feasible to detect the products of similar processes occurring at later times in DM-dense regions, such as the centers of galaxies or galaxy clusters. However, the dependence of the observed signals on the distribution of dark matter leads to relatively large uncertainties in the predictions [172].

The indirect detection can be categorized by the products of DM decays or annihilations. One possibility is to look for high energy gamma-rays in experiments such as Fermi Large Area Telescope [173, 174], H.E.S.S.-II [175–177], MAGIC [178, 179] or VERITAS [180]. Those searches look at the spectrum deviations from the astrophysical background.

Another possibility is to observe cosmic rays in the form of charged particles such as protons and positrons in an Alpha Magnetic Spectrometer on the International Space

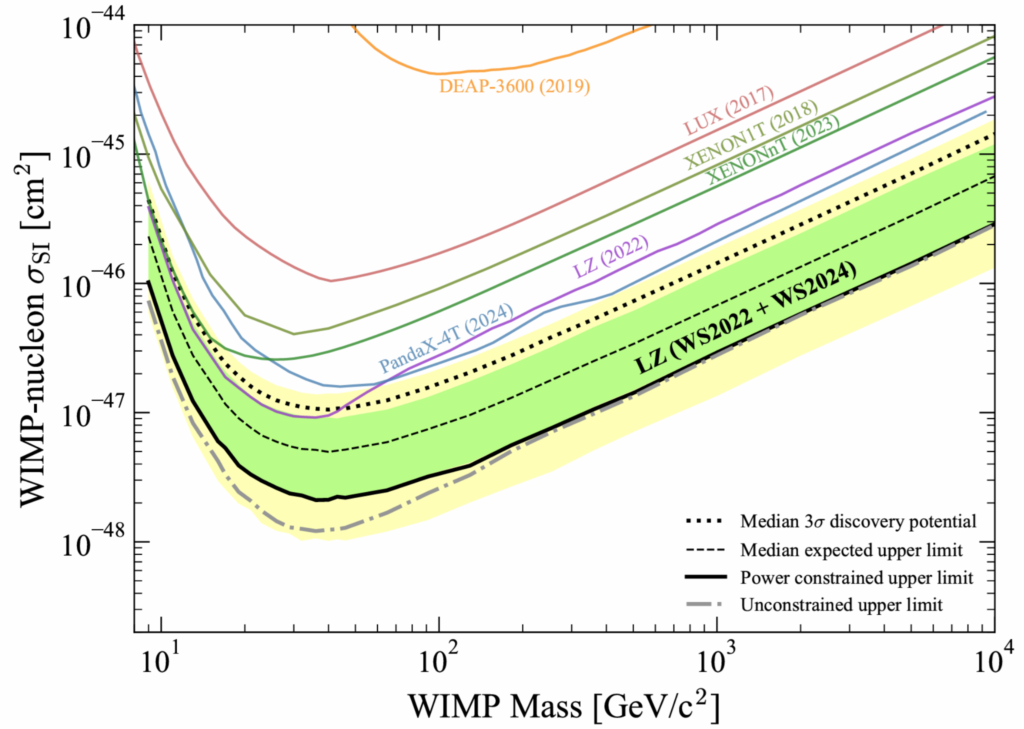


Figure 2.5: Compilation of DM-nucleon spin-independent cross section limits from DD experiments, including bounds used in the thesis labeled Xenon1T [165] and LZ (2022) [168]. Plot from Ref. [171].

Station [181, 182], PAMELA [183] or Pierre-Auger Observatory [184]. In contrast to the gamma-ray and neutrino observations, cosmic rays cannot be used to determine the source of the signal.

Finally, high energy neutrinos can be produced in the weak interactions of DM (in particularly WIMP) and could be observed in Super-Kamiokande [185–187], IceCube [188–191] or ANTARES experiments [192–194]. Search for neutrino flux correlated with the DM-dense regions allows constraining the DM interactions.

## 2.5 Summary

In this chapter, we have argued for the necessity of physics beyond the Standard Model, focusing on the strong CP problem, the hierarchy problem, and dark matter. The first two are examples of naturalness issues, which we discussed in the context of Dirac and 't Hooft naturalness principles. Additionally, we examined the vacuum properties of QCD, parameterized by the vacuum $\theta$ angle. We also demonstrated how axial symmetry is broken both spontaneously and by the chiral anomaly, highlighting the interplay between quark mass phases and the anomaly term. Finally, we have shown that the measurement of the neutron electric dipole moment requires a precise cancellation between the two unrelated contributions to the CP violating parameter $\bar{\theta}$, which remains unexplained in the SM.

Furthermore, we have discussed in detail the sensitivity of the EW scale to the UV corrections, explicitly calculating some of the corrections to the mass of the Higgs. We showed that for UV scales $\Lambda = 5\text{TeV}$, the corrections to the Higgs mass exceed the observed value of $m_h = 125\text{GeV}$ by an order of magnitude. The hierarchy problem suggests that the SM is incomplete, and by leveraging the naturalness criterion some properties of the UV theories can be deduced.

Finally, we have covered the most straightforward indication of the incompleteness of the SM, the unknown nature of the dark matter. We presented arguments supporting the existence of dark matter at various scales and reviewed experimental efforts aimed at its detection.

# Chapter 3

# Axions

This chapter will introduce the PQ solution to the strong CP problem, starting with proving the Vafa-Witten theorem in Sec. 3.1. We review the QCD axion's properties in Sec. 3.2, focusing on the DFSZ axion. Furthermore, we present effective axion couplings in the ChPT in Sec. 3.3 and the most stringent constraints, which are relevant for Chapter 4 in the Sec. 3.4. Finally, we shortly review the cosmological implications of axions in Sec. 3.5.

The author is not aware of a step-by-step analytical derivation of axion-pion coupling in peer-reviewed papers, which can be found in Sec. 3.3.1. Moreover, we present a result for effective axion-kaon coupling derived by author in Sec. 3.3.2 for general axion-quark couplings.

## 3.1 Peccei-Quinn solution

A modern understanding of Peccei-Quinn solution of the strong CP-problem [25,26] relies on a theorem proven by Vafa and Witten [195]. We will closely follow the original paper in this section.

Consider a vector-like theory with lagrangian $\mathcal{L}$, such as QCD (unlike electroweak interactions, which differentiate left- and right-handed fermions). Moreover, consider a parity odd hermitian operator $X$, which enters the lagrangian with coupling $\lambda$. An example of such an operator is the CP-violating term $G\widetilde{G}$.

Performing a Wick rotation to the imaginary time, the path integral becomes a partition function of a system. Moreover, the parity odd operator $X$ picks up an imaginary unit $i$ (in the $G\widetilde{G}$ term Levi-Civita symbol picks up $i$), resulting in

$$e^{-VE(\lambda)} = \int DA^a_\mu D\Psi D\bar{\Psi} \exp\left( - \int d^4x \mathcal{L}_{\rm QCD} + i\lambda X \right), \tag{3.1}$$

where we have explicitly displayed the $\lambda$-dependence of the energy, and $V$ denotes the volume of Euclidean spacetime. Integrating out the massive fermions in vector-like theories results in positive Jacobian [196]

$$e^{-VE(\lambda)} = \int DA^a_\mu \det\left( \not{D} + M \right) \exp\left( - \int d^4x \frac{1}{4} G^a_{\mu\nu} G^{a,\mu\nu} + i\lambda X \right). \tag{3.2}$$

The right-hand side is positive except for the complex phase from the $X$ term. Using $\int f \leqslant \int |f|$, we have

$$e^{-VE(\lambda)} \leqslant e^{-VE(\lambda=0)} \to E(0) \leqslant E(\lambda), \tag{3.3}$$

and the minimal energy is achieved for parity conserving theory, $\lambda = 0$. Note, that in the above discussion, $\lambda$ is just a parameter, not a dynamical object. From this also follows, that parity cannot be spontaneously broken in QCD because the VEV of arbitrary P-violating operator X is zero at minimum. Let us quote the original paper: "*This is essential for the viability of the axion approach to the strong CP problem, in which the vacuum angle is a dynamical variable and relaxes to the value that minimizes the energy*".

The radiative effects of weak interactions, which distinguish between left- and right-handed fermions (thus making the determinant in Eq. (3.2) not necessarily positive), are expected to contribute to a non-zero value of $\bar{\theta}$. The leading term arises at 3-loop level at $\mathcal{O}(\alpha_s G_F^2)$ and was estimated at [197]

$$\delta\bar{\theta} \sim 4 \times 10^{-19}\,, \tag{3.4}$$

which means that $\bar{\theta} \simeq 0$ is radiatively stable. This contribution is still many orders of magnitude below the sensitivity of nEDM experiments, Eq. (2.90).

## 3.2 QCD axion

The Peccei-Quinn solution of the strong CP problem relies on the introduction of a global, chiral symmetry, $U(1)_{\mathrm{PQ}}$, along with extending the scalar sector of the SM. The $U(1)_{\mathrm{PQ}}$ symmetry is not only broken explicitly by the chiral anomaly but also spontaneously by the VEV of a scalar particle. The Goldstone theorem ensures, that the breaking of the symmetry implies the emergence of a scalar spin-0 particle called the axion, which shifts under $U(1)_{\mathrm{PQ}}$. Vafa-Witten theorem ensures that the VEV of axion is at CP-conserving value, that is $\bar{\theta} = \langle a \rangle = 0$.
This general mechanism can be implemented in a variety of ways, most notably the Peccei-Quinn-Weinberg-Wilczek (PQWW) model extends the scalar sector by a single $SU_L(2)$ doublet [25–28]. The weak isospin conservation implies that one of the Higgs doublets, $H_u$, couples to up-type quark and the other, $H_d$, to down-type quarks, leaving two possibilities of coupling leptons to one of those[1]. However, this minimal setup implies that the scale at which axion emerges as a physical degree of freedom is just the EW scale, $f_a \simeq \sqrt{v_u^2 + v_d^2} \simeq 246$ GeV. Axion is an effective degree of freedom, and by the dimensional analysis all axion couplings (beside the anomaly, which explicitly breaks $U(1)_{\mathrm{PQ}}$) are of form

$$\text{axion couplings} \propto \frac{\partial_\mu a}{f_a}\,, \tag{3.5}$$

where $f_a$ is the scale of $U(1)_{\mathrm{PQ}}$ breaking. As a result, axion couplings in the PQWW model are suppressed by the relatively low EW scale and from early days have been in tension with beam dump experiments and meson decay [198]. Collider ALP searches, exploiting axion-photon coupling, totally rule out PQWW axion [199].

Those results motivate models of invisible axion, whose interactions are suppressed by the scale of new physics unrelated to the EW interactions.

An example of invisible axion is KSVZ model [29, 30], which extends SM by a scalar singlet $\Phi$ and a vector-like quark, $Q = Q_L + Q_R$, which is in fundamental representation of $SU_C(3)$ and singlet under EW interactions $SU_L(2) \times U_Y(1)$. The singlet scalar is coupled to $Q$ by Yukawa interactions, and under the assumption that $\Phi$ obtains a VEV that breaks PQ symmetry at scale $v_a$, it generates the mass of the quark $m_Q \simeq v_a y_{\Phi\bar{Q}Q}$. As a result of the spontaneous breaking of PQ symmetry, a Goldstone boson emerges, which

[1] A PQWW model with three Higgs doublets has been considered [198], the third doublet giving mass to leptons

we identify with axion. Crucially, since the quark is charged under QCD, axion couples to gluons and photons. The anomaly coupling to gluons allows for solving the strong CP problem, as discussed above, by absorbing the CP-violating $\bar{\theta}$ angle into the definition of axion. A distinguishing feature of the KSVZ model is that there are no derivative coupling interactions between axion and SM particles. It follows from the fact, that the only fields charged under PQ symmetry in minimal implementations are BSM particles, vector-quarks, and the scalar. However, chiral anomaly induces KSVZ axion coupling to gluons, which in turn results in axion couplings to hadrons. In literature, the notion of hadronic axion usually denotes the low energy limit of a KSVZ-like model, without specifying the exact form of UV completion.

### 3.2.1 DFSZ model

The minimal implementation of the PQ mechanism, PQWW model, yields axion phenomenology excluded. A possible extension of the PQ mechanism is the introduction of a complex scalar, SM gauge singlet $\phi$ besides the two Higgs doublets $H_u$ and $H_d$. The idea is that the $\phi$ obtains VEV of scale, which is unrelated to the EW scale and potentially large. The NGB of broken $U(1)_{\rm PQ}$ has couplings suppressed by the scale at which it emerges as an effective degree of freedom. This suppression can yield an axion invisible in current experiments.

To be more specific, let $H_u, H_d$ be $SU_L(2)$ doublets with $Y(H_u) = Y(H_d) = -1/2$ and $\phi$ be SM gauge singlet. The most general, renormalizable potential respecting gauge symmetry will be of form

$$V(H_u, H_d, \phi) = V(|H_u|, |H_d|, |\phi|)\,. \tag{3.6}$$

This potential has large global symmetry, with a $U(1)$ group corresponding to each of the scalars, $U_{H_u}(1) \times U_{H_d}(1) \times U_\phi(1)$:

$$H_u \to e^{i\theta_u} H_u, \qquad H_d \to e^{i\theta_d} H_d, \qquad \phi \to e^{i\theta_\phi}\phi\,, \tag{3.7}$$

where we have fixed the unphysical normalization of the charges $X_i = 1$. We can explicitly break this symmetry to $U_Y(1)\times U(1)_{\rm PQ}$ by adding a term coupling explicitly Higgs doublets

$$V_b = H_u^\dagger H_d \mathcal{O}_\phi\,, \tag{3.8}$$

where operator $\mathcal{O}_\phi \in \{\phi, \phi^2, \phi^*, (\phi^*)^2\}$. The combination $H_u^\dagger H_d$ is $U_Y(1)$ invariant, but is not invariant under $U_{H_u}(1) \times U_{H_d}(1)$. By choosing the $\mathcal{O}$, we fix the $U(1)_{\rm PQ}$ charges of the scalars

$$X_{H_u} = X_{H_d} \pm \{X_\phi, 2X_\phi\}\,. \tag{3.9}$$

One usually chooses $X_\phi = 1$, which in turn fixes the normalization of all the charges. The scalars transform under the Peccei-Quinn symmetry according to

$$H_u \to e^{iX_{h_u}\theta_u} H_u, \qquad H_d \to e^{iX_{h_d}\theta_d} H_d, \qquad \phi \to e^{iX_\phi\theta_\phi}\phi\,. \tag{3.10}$$

The Yukawa couplings are generation blind in the DFSZ model and are simply

$$\mathcal{L}_{\rm Yuk} = -Y_u \bar{q}_L H_u u_R - Y_d \bar{q}_L \tilde{H}_d d_R - \begin{cases} Y_e \bar{L}\tilde{H}_d e_R\,, & \text{DFSZ-I} \\ Y_e \bar{L}\tilde{H}_u e_R\,, & \text{DFSZ-II} \end{cases} \tag{3.11}$$

where $\tilde{H}_i = i\sigma^2 H^*$. The two models differ by which Higgs doublet leptons couple to. In order to retain the invariance of the lagrangian under PQ symmetry, the symmetry must be chiral

$$u \to e^{-i\theta_{\rm PQ}X_{h_u}\gamma_5/2}u\,, \qquad d \to e^{i\theta_{\rm PQ}X_{h_d}\gamma_5/2}d\,, \qquad l \to e^{i\theta_{\rm PQ}X_{h_{d(u)}}\gamma_5/2}l\,, \tag{3.12}$$

where for leptons transform with $X_d$ ($X_u$) for DFSZ-I (DFSZ-II). Note, that since we have chosen $Y(H_u) = Y(H_d) = -1/2$, the charges of down quarks and leptons have inverted signs as compared to Ref. [125].

By construction, the minimum of the potential spontaneously breaks the PQ symmetry such that all scalars obtain VEVs $\langle H_i \rangle = v_i$, $\langle \phi \rangle = v_\phi$. The fields can be parameterized as

$$H_i = \begin{pmatrix} \frac{1}{\sqrt{2}}(v_i + h_i) \\ h_i^+ \end{pmatrix} e^{ia_i/v_i} \,, \qquad \phi = \frac{1}{\sqrt{2}}\Big(v_\phi + \rho\Big) e^{ia_\phi/v_\phi} \,. \tag{3.13}$$

To find the NGB of broken $U(1)_{\mathrm{PQ}}$ we will use the Goldstone theorem from Appendix A.5.1. We have proven that the NGB state is produced by acting on the vacuum state with the Noether current corresponding to the broken generator

$$\langle a(\vec{p}) | J_\mu(x) | \Omega \rangle = i p_\mu v_a e^{i\vec{p}\cdot\vec{x}} \,. \tag{3.14}$$

It follows that the derivative of the axion field can be written as

$$v_{\mathrm{PQ}} \partial_\mu a = J_\mu^{\mathrm{PQ}} \,. \tag{3.15}$$

The PQ current can be found by letting the PQ transformation parameter depend on 4-position (cf. Appendix A.4)

$$J_\mu^{\mathrm{PQ}} = \frac{\partial \delta \mathcal{L}}{\partial(\partial^\mu \theta^{\mathrm{PQ}})} \,. \tag{3.16}$$

Let us figure it out step by step. Note, that the $\partial_\mu \theta^{\mathrm{PQ}}$ may only arise from the kinetic terms. Moreover, to find the composition of the axion we can focus only on the scalar contribution since only those can donate a bosonic degree of freedom. The contribution to $J_\mu^{\mathrm{PQ}}$ from kinetic term of any scalar $\Phi_i$

$$\begin{aligned} (\partial_\mu \Phi_i)^\dagger (\partial_\mu \Phi_i) \to &(\partial_\mu \Phi_i)^\dagger (\partial_\mu \Phi_i) + (-iX_i \partial_\mu \theta) \Phi_i^\dagger \partial^\mu \Phi_i + \Phi_i^\dagger (iX_i \partial_\mu \theta) \partial \Phi_i \\ &\to \delta \mathcal{L} = -i(\partial_\mu \theta) X_i \Phi_i^\dagger \overleftrightarrow{\partial_\mu} \Phi_i \,. \end{aligned} \tag{3.17}$$

where we have used notation $g \overleftrightarrow{\partial_\mu} f = g(\partial_\mu f) - (\partial_\mu g) f$. From Eq. (3.16), the scalar contributions to the current is

$$J_\mu^{\mathrm{PQ}} = \sum_{\text{scalars } i} -iX_i \Phi_i^\dagger \overleftrightarrow{\partial_\mu} \Phi_i \,. \tag{3.18}$$

We anticipate, based on the transformation law of NGB, that a combination of phases of fields will constitute the NGB. We will evaluate the current only on field $\phi$ setting the radial field to 0:

$$\begin{aligned} \phi^\dagger \overleftrightarrow{\partial_\mu} \phi =& \frac{1}{2} v_\phi e^{-ia_\phi/v_\phi} \left( v_\phi \left( i \frac{\partial_\mu a_\phi}{v_\phi} \right) e^{ia_\phi/v_\phi} \right) \\ &- \frac{1}{2} v_\phi e^{ia_\phi/v_\phi} \left( v_\phi \left( -i \frac{\partial_\mu a_\phi}{v_\phi} \right) e^{-ia_\phi/v_\phi} \right) \\ =& v_\phi^2 \left( i \frac{\partial_\mu a_\phi}{v_\phi} \right) = i v_\phi \partial_\mu a_\phi \,. \end{aligned} \tag{3.19}$$

A similar calculation can be performed for Higgs doublets, which combined with Eq. (3.18) results in the final formula

$$v_{\mathrm{PQ}} \partial_\mu a = \sum_i X_i v_i \partial_\mu a_i \,. \tag{3.20}$$

Therefore, the composition of axion is given by

$$a = \sum_i X_i \frac{v_i}{v_{\rm PQ}} a_i \,. \tag{3.21}$$

At this point, it is clear how construction with an additional singlet allows for hiding the axion. Given that $v_u, v_d \ll v_\phi$, axion is primarily composed of the phase of the singlet, and only small components of the axion are the phases of Higgses related to the EW scale. The PQ symmetry is realized non-linearly on Goldstone bosons $a_i \to a_i + \theta^{\rm PQ} X_i v_i$, so that the axion transforms as

$$a \to a + \theta^{\rm PQ} v_{\rm PQ} \,. \tag{3.22}$$

A similar discussion leads to a formula for would-be NGB, which gives mass to the $Z^0$:

$$Z^0_{\rm long} = \sum_i Y_i \frac{v_i}{v} a_i \,, \tag{3.23}$$

where $Y_i$ is the hypercharge of $H_i$. Since we do not want to have large axion-Z boson mixing, we will demand that those linear combinations are orthogonal. This orthogonality is necessary, as it ensures that Landau-Yang theorem [200, 201] holds. Otherwise, mixing between Z boson and photon would induce the Z decay into two photons via anomaly term. Keeping in mind that $Y_\phi = 0$, the condition is

$$\sum_i X_i v_i \cdot Y_i v_i = 0 \,, \tag{3.24}$$

which for $Y_u = Y_d = -1/2$ gives condition for PQ charges

$$X_{h_u} v_u^2 + X_{h_d} v_d^2 = 0 \,. \tag{3.25}$$

Recall that $v_u = v \sin\beta$, $v_d = v\cos\beta$. Hence, the charges are related

$$X_{h_u} = X \cos^2\beta \qquad\qquad X_{h_d} = -X \sin^2\beta \,, \tag{3.26}$$

where $X$ is just normalization fixed by the condition Eq. (3.8), $X_{h_u} - X_{h_d} = \pm\{1, 2\}$. After SSB, Yukawas can be written as

$$\mathcal{L}_{\rm yuk} = -m_u \bar{u}_L u_R e^{iX_u a/v_{PQ}} - m_d \bar{d}_L d_R e^{iX_d a/v_{PQ}} - m_e \bar{e}_L e_R e^{iX_{u/d} a/v_{PQ}} \,. \tag{3.27}$$

It is convenient to reparametrize fermions by field-dependent chiral rotation

$$u \to e^{-i\gamma_5 X_{h_u} a/2v_{PQ}} u, \qquad d \to e^{i\gamma_5 X_{h_d} a/2v_{PQ}} d, \qquad e \to e^{i\gamma_5 X_{h_{u/d}} a/2v_{PQ}} e \,, \tag{3.28}$$

which removes axion from the fermion mass terms. As a result, PQ symmetry acts only on axion according to Eq. (3.22). We have seen that the divergence of the current is then found by differentiating the Lagrangian with respect to the transformation parameter, Eq. (A.77),

$$\partial^\mu J^{\rm PQ}_\mu = \frac{\partial \mathcal{L}}{\partial \theta^{\rm PQ}} = \frac{\partial \mathcal{L}}{\partial(\partial_\mu a)} \frac{\partial(\partial_\mu a)}{\partial \theta^{\rm PQ}} + \frac{\partial \mathcal{L}}{\partial a} \frac{\partial a}{\partial \theta^{\rm PQ}} \,. \tag{3.29}$$

The first term vanishes, while $\partial a/\partial\theta^{\rm PQ} = v_{\rm PQ}$. The chiral PQ symmetry is anomalous under EM and QCD

$$\frac{\partial \mathcal{L}}{\partial a} v_{\rm PQ} = N \frac{g_s^2}{16\pi^2} G_{\mu\nu} \widetilde{G}^{\mu\nu} + E \frac{e^2}{16\pi^2} F_{\mu\nu} \widetilde{F}^{\mu\nu} \,, \tag{3.30}$$

where $N$ and $E$ are color and electromagnetic anomaly coefficients, respectively. Each field $\Psi$ contributes to the anomalies with [125]

$$N_\Psi = X_\Psi d(\mathcal{I}_\Psi) T(\mathcal{C}_\Psi)\,, \tag{3.31}$$
$$E_\Psi = X_\Psi d(\mathcal{C}_\Psi) (Q^{\mathrm{EM}})^2, \tag{3.32}$$

where $d(\mathcal{C}_\Psi)$ and $d(\mathcal{I}_\Psi)$ are dimensions of colour and weak isospin representations of $\Psi$, $T(\mathcal{C}_\Psi)$ is Dynkin index of colour representation and $Q^{\mathrm{EM}}$ is electromagnetic charge. For a single generation, we have

$$N_{u_R} + N_{u_L} = (X_{u_R} - X_{u_L}) \cdot 1 \cdot \frac{1}{2} = \frac{X_{h_u}}{2} = \frac{X}{2} c_\beta^2\,, \tag{3.33}$$
$$N_{d_R} + N_{d_L} = (X_{d_R} - X_{d_L}) \cdot 1 \cdot \frac{1}{2} = \frac{X_{h_d}}{2} = \frac{X}{2} s_\beta^2\,, \tag{3.34}$$

where we have used $T(\mathcal{C}_q) = 1/2$, $d(\mathcal{C}_q) = 3$ and $d(\mathcal{I}_q) = 1$. Summing over all 3 generations gives

$$N = \sum_\Psi N_\Psi = \frac{3}{2} X\,. \tag{3.35}$$

Similarly for electromagnetic anomaly from a single generation we have

$$E_{u_R} + E_{u_L} = X_{h_u} \cdot 3 \cdot \left(\frac{2}{3}\right)^2 = \frac{4}{3} X c_\beta^2\,, \tag{3.36}$$
$$E_{d_R} + E_{d_L} = X_{h_d} \cdot 3 \cdot \left(-\frac{1}{3}\right)^2 = \frac{1}{3} X s_\beta^2\,, \tag{3.37}$$
$$E_{e_R} + E_{e_L} = \begin{cases} -X_{h_d} \cdot 1 \cdot (-1)^2 = X s_\beta^2 & \text{DFSZ-I} \\ -X_{h_u} \cdot 1 \cdot (-1)^2 = -X c_\beta^2 & \text{DFSZ-II} \end{cases}, \tag{3.38}$$

where we have used $d(\mathcal{C}_q) = 3$, $Q_u^{\mathrm{EM}} = 2/3$, $Q_d^{\mathrm{EM}} = -1/3$ and $Q_e^{\mathrm{EM}} = -1$. Putting everything together and accounting for 3 generations we arrive at

$$E = \begin{cases} 4X & \text{for DFSZ-I} \\ 2X & \text{for DFSZ-II} \end{cases}. \tag{3.39}$$

Integrating Eq. (3.30) yields axion anomaly couplings

$$\mathcal{L} = \frac{\alpha_s}{8\pi f_a} a G_{\mu\nu} \widetilde{G}^{\mu\nu} + \frac{E}{N} \frac{\alpha_{\mathrm{em}}}{8\pi f_a} a F_{\mu\nu} \widetilde{F}^{\mu\nu}\,, \tag{3.40}$$

where we have defined the axion decay constant by rescaling it with the color anomaly coefficient, $f_a = v_{\mathrm{PQ}}/2N$. The coupling of an axion to the color anomaly is essential for the solution of a strong CP problem. Even though the Witten-Vafa theorem ensures that the energy is minimized for $\langle a \rangle = 0$, we will derive axion potential in Sec. 3.3 using ChPT to see that play out in action.

The fermion field redefinitions Eq. (3.28) induce derivative axion-fermion couplings

$$\begin{aligned} i\bar{f}\gamma^\mu \partial_\mu f \to & i\bar{f} e^{-iX_f a/2v_{\mathrm{PQ}}} \gamma^\mu \left(\partial_\mu e^{-i\gamma^5 X_f a/2v_{\mathrm{PQ}}} f\right) \\ &= i\bar{f}\gamma^\mu \partial_\mu f + \frac{\partial_\mu a}{2v_{\mathrm{PQ}}} X_f \bar{f} \gamma^\mu \gamma^5 \partial_\mu f\,. \end{aligned} \tag{3.41}$$

Hence, the axion fermion couplings in DFSZ models are

$$\mathcal{L}_{\text{leptons}} = \frac{\partial_\mu a}{2f_a} C_u \bar{u}\gamma^\mu\gamma^5\partial_\mu u + \frac{\partial_\mu a}{2f_a} C_d \bar{d}\gamma^\mu\gamma^5\partial_\mu d + \frac{\partial_\mu a}{2f_a} C_e \bar{e}\gamma^\mu\gamma^5\partial_\mu e\,, \tag{3.42}$$

where we have defined the couplings as

$$C_f = X_f/2N\,. \tag{3.43}$$

For DFSZ models with cubic coupling, $X = \pm 1$ in Eq. (3.26), the fermion couplings are fixed

$$C_u = \pm\frac{1}{3}\cos^2\beta\,, \qquad C_d = \pm\frac{1}{3}\sin^2\beta\,, \qquad C_e = \begin{cases} \pm\frac{1}{3}\sin^2\beta\,, & \text{DFSZ-I} \\ \mp\frac{1}{3}\cos^2\beta\,, & \text{DFSZ-II} \end{cases}. \tag{3.44}$$

### 3.2.2 QCD axion below PQ symmetry breaking scale

Generalizing results from the previous section, the axion lagrangian can include flavor-violating couplings to fermions

$$\mathcal{L} = \frac{1}{2}(\partial_\mu a)^2 + \frac{a}{f_a}\frac{\alpha_s}{8\pi}G_{\mu\nu}\tilde{G}^{\mu\nu} + \frac{E}{N}\frac{a}{f_a}\frac{\alpha_{\text{em}}}{8\pi}F_{\mu\nu}\tilde{F}^{\mu\nu} + \frac{\partial_\mu a}{2f_a}\overline{f}_i\gamma^\mu\Big(C^V_{ij} + C^A_{ij}\gamma_5\Big)f_j\,, \tag{3.45}$$

where couplings are rescaled by the color anomaly coefficients in analogy to Eq. (3.43) and can be written in terms of independent PQ charges of left- and right-handed fermions

$$C^V_{u_iu_j} = \frac{C^{u_R}_{ij} + C^{u_L}_{ij}}{2N}\,, \qquad C^A_{u_iu_j} = \frac{C^{u_R}_{ij} - C^{u_L}_{ij}}{2N}\,, \tag{3.46}$$

$$C^V_{d_id_j} = \frac{C^{d_R}_{ij} + C^{d_L}_{ij}}{2N}\,, \qquad C^A_{d_id_j} = \frac{C^{d_R}_{ij} - C^{d_L}_{ij}}{2N}\,, \tag{3.47}$$

$$C^V_{e_ie_j} = \frac{C^{e_R}_{ij} + C^{e_L}_{ij}}{2N}\,, \qquad C^A_{e_ie_j} = \frac{C^{e_R}_{ij} - C^{e_L}_{ij}}{2N}\,. \tag{3.48}$$

We define the LFV coupling, for $i \neq j$, as

$$C_{ij} = \sqrt{\left(C^A_{ij}\right)^2 + \left(C^V_{ij}\right)^2}\,. \tag{3.49}$$

Note, that flavor-diagonal vector couplings are non-physical, as the interaction may be written as

$$\mathcal{L} \supset \frac{\partial_\mu a}{2f_a}C^V_{ii}\overline{f}_i\gamma^\mu f_i = \frac{C^V_{ii}}{2f_a}\partial^\mu a J^V_\mu = -\frac{C^V_{ii}}{2f_a}a\partial^\mu J^V_\mu = 0\,, \tag{3.50}$$

where $J^V_\mu$ is vector current defined in Eq. (2.25) and we have integrated by parts in the second step and used the conservation of vector current in the last equality. Therefore, axion couples diagonally to fermions only via axial interaction

$$C_i = C^A_{ii}\,, \tag{3.51}$$

which agrees with result in Eq. (3.43) in DFSZ model.

## 3.3 Axion properties below chiral symmetry breaking scale

After SSB of PQ symmetry the effective lagrangian of axion interactions, neglecting leptons, is composed of Eq. (3.40) and Eq. (3.41)

$$\mathcal{L} = \frac{1}{2}(\partial_\mu a)^2 + \frac{a}{f_a}\frac{g_s^2}{32\pi^2}G\tilde{G} + \frac{1}{4}g^0_{a\gamma}aF\tilde{F} + C_q\frac{\partial_\mu a}{2f_a}\bar{q}\gamma^\mu\gamma^5 q - \bar{q}Mq\,, \tag{3.52}$$

where $M$ is the light quark mass matrix in flavour space $q^T = (u, d, s)$, and we have used $\alpha_s = g_s^2/4\pi$ and we have defined axion-photon coupling

$$g^0_{a\gamma} = \frac{\alpha_{\rm em}}{2\pi f_a}\frac{E}{N}\,. \tag{3.53}$$

The chiral rotation

$$q \longrightarrow e^{i\gamma_5\frac{a}{2f_a}Q^a}q\,, \tag{3.54}$$

where $Q^a$ is a matrix in the flavor space, shifts the gluon coupling

$$\frac{a}{f_a}\frac{g_s^2}{32\pi^2}G\tilde{G} \to \frac{a}{f_a}\frac{g_s^2}{32\pi^2}(1-\mathrm{Tr}Q^a)G\tilde{G}\,. \tag{3.55}$$

Hence, by choosing a matrix with $\mathrm{Tr}Q^a = 1$ we can cancel the axion-gluon coupling. This rotation also shifts the axion-photon coupling as

$$-\frac{1}{4}g^0_{a\gamma}aF\tilde{F} \to -\frac{1}{4}\left(g^0_{a\gamma} - 2N_c\frac{\alpha_{\rm em}}{2\pi f_a}\mathrm{Tr}\Big(Q^aQ^2\Big)\right)aF\tilde{F}\,, \tag{3.56}$$

where $Q = \mathrm{diag}(2/3, -1/3, -1/3)$ is the EM charge matrix of the quarks, and $N_c = 3$ is a number of colours. We can rewrite the axion-photon coupling as

$$-\frac{1}{4}g_{a\gamma}aF\tilde{F} = -\frac{1}{4}\frac{\alpha_{\rm em}}{2\pi f_a}C_\gamma aF\tilde{F}\,, \tag{3.57}$$

where, for $Q^a = \mathrm{diag}(Q^a_u, Q^a_d, Q^a_s)$

$$C_\gamma = \frac{E}{N} - C_\gamma^{\rm QCD}, \qquad C_\gamma^{\rm QCD} = \frac{2}{3}(4Q^a_u + Q^a_d + Q^a_s)\,. \tag{3.58}$$

The field-dependent chiral rotation also induces a derivative axion-quark coupling according to Eq. (3.41), resulting in shifting of couplings

$$C_q\frac{\partial_\mu a}{2f_a}\bar{q}\gamma^\mu\gamma^5 q \to \Big(C_q - Q^a_q\Big)\frac{\partial_\mu a}{2f_a}\bar{q}\gamma^\mu\gamma^5 q\,. \tag{3.59}$$

Finally, the axion-quark lagrangian after chiral rotation is

$$\mathcal{L} = \frac{1}{2}(\partial_\mu a)^2 + \frac{1}{4}g_{a\gamma}aF\tilde{F} + \Big(C_q - Q^a_q\Big)\frac{\partial_\mu a}{2f_a}\bar{q}\gamma^\mu\gamma^5 q - \bar{q}M_a q\,, \tag{3.60}$$

where the rotated quark mass matrix is axion-dependent

$$M_a = e^{iQ^a a/2f_a}Me^{iQ^a a/2f_a}\,. \tag{3.61}$$

To study the effective axion interactions within ChPT we can neglect the axion-photon couplings, and use Eq. (A.44) to write down the LO of chiral lagrangian including axion [125]

$$\mathcal{L} = \frac{f_\pi^2}{4}\left(\mathrm{Tr}(D^\mu U^\dagger D_\mu U) + 2B\mathrm{Tr}(UM_a^\dagger + M_aU^\dagger)\right) + \frac{\partial_\mu a}{2f_a}c_a\mathrm{Tr}\left(\frac{if_\pi^2}{2}\lambda_a(U\partial^\mu U^\dagger - U^\dagger\partial^\mu U)\right), \tag{3.62}$$

where we parametrize Goldstones via

$$U = \exp\left(\frac{i}{f_\pi}\begin{pmatrix}\pi^0 + \eta/\sqrt{3} & \sqrt{2}\pi^+ & \sqrt{2}K^+ \\ \sqrt{2}\pi^- & -\pi^0 + \eta/\sqrt{3} & \sqrt{2}K^0 \\ \sqrt{2}K^- & \sqrt{2}\overline{K}^0 & -2\eta/\sqrt{3}\end{pmatrix}\right). \tag{3.63}$$

The axial couplings can be arranged in a linear combination of Gell-Mann matrices and unit matrix,

$$\begin{aligned} c = &\begin{pmatrix} C_u - Q_u^a & 0 & 0 \\ 0 & C_d - Q_d^a & 0 \\ 0 & 0 & C_s - Q_s^a \end{pmatrix} = \\ = &\frac{1}{3}\mathrm{Tr}(c)\mathbf{1} + \frac{1}{2}\mathrm{Tr}(c\lambda_3)\lambda_3 + \frac{1}{2}\mathrm{Tr}(c\lambda_8)\lambda_8 = c_a\lambda_a\,. \end{aligned} \tag{3.64}$$

Note, that besides the derivative coupling, all axion dependence is encoded in the mass term

$$\mathrm{Tr}\Big(UM_a^\dagger + M_aU^\dagger\Big) = \mathrm{Tr}\Big(Ue^{-i\frac{a}{2f_a}Q_a}M^\dagger e^{-i\frac{a}{2f_a}Q_a} + e^{i\frac{a}{2f_a}Q_a}Me^{i\frac{a}{2f_a}Q_a}U^\dagger\Big)\,. \tag{3.65}$$

Let us examine the leading term in the axion field by expanding the exponentials:

$$\begin{aligned} \mathcal{L}_{M_a^\dagger} \simeq &\frac{f_\pi^2 B}{2}\mathrm{Tr}\Big(U\Big(1 + i\frac{a}{2f_a}Q_a\Big)M^\dagger\Big(1 + i\frac{a}{2f_a}Q_a\Big)\Big) \\ = &\frac{f_\pi^2 B}{2}\Big(\mathrm{Tr}\Big(UM^\dagger\Big) + i\frac{a}{2f_a}\mathrm{Tr}\Big(U\{Q_a, M^\dagger\}\Big)\Big), \\ \mathcal{L}_{M_a} \simeq &\frac{f_\pi^2 B}{2}\mathrm{Tr}\Big(\Big(1 - i\frac{a}{2f_a}Q_a\Big)M\Big(1 - i\frac{a}{2f_a}Q_a\Big)U^\dagger\Big) \\ = &\frac{f_\pi^2 B}{2}\Big(\mathrm{Tr}\Big(MU^\dagger\Big) - i\frac{a}{2f_a}\mathrm{Tr}\Big(\{Q_a, M\}U^\dagger\Big)\Big)\,. \end{aligned} \tag{3.66}$$

In the physical $SU_L(2)$-gauge the mass matrix is real and diagonal, hence we set $M^\dagger = M$. We can now exploit the freedom of choosing matrix $Q_a$, by setting $Q_a = M^{-1}/\mathrm{Tr}M^{-1}$. As a result, the anticommutator $\{Q_a, M\} = 2/\mathrm{Tr}M^{-1}$ is proportional to the unit matrix. This simplifies the lagrangian involving leading axion term

$$\begin{aligned} \mathcal{L}_a^{(1)} &= i\frac{f_\pi^2 B}{2}\frac{a}{2f_a}\Big(\mathrm{Tr}(U\{Q_a, M\}) - \mathrm{Tr}\Big(\{Q_a, M\}U^\dagger\Big)\Big) \\ &= i\frac{f_\pi^2 B}{4f_a}a\mathrm{Tr}\Big(U\frac{2}{\mathrm{Tr}M^{-1}} - \frac{2}{\mathrm{Tr}M^{-1}}U^\dagger\Big) = \\ &= i\frac{f_\pi^2 B}{2f_a\mathrm{Tr}M^{-1}}a\mathrm{Tr}\Big(U - U^\dagger\Big) \simeq i\frac{f_\pi^2 B}{2f_a\mathrm{Tr}M^{-1}}a\mathrm{Tr}\Big(\Big(1 + i\frac{\pi^a}{f_\pi}\frac{\lambda^a}{2}\Big) - \Big(1 - i\frac{\pi^a}{f_\pi}\frac{\lambda^a}{2}\Big)\Big) = \\ &= -\frac{f_\pi B}{2f_a\mathrm{Tr}M^{-1}}a\pi^a\mathrm{Tr}\lambda^a = 0\,. \end{aligned} \tag{3.67}$$

In the third line, we have expanded $U(x)$ in the leading order of Goldstone modes and in final equality we have used $\mathrm{Tr}\lambda^a = 0$. In the absence of linear axion term, the $a - \pi^0$ and $a - \eta$ mixings vanish. Explicitly, the matrix avoiding mixing is

$$Q_a = M^{-1}/\mathrm{Tr}M^{-1} = \begin{pmatrix} \frac{1}{1+z+w} & 0 & 0 \\ 0 & \frac{z}{1+z+w} & 0 \\ 0 & 0 & \frac{w}{1+z+w} \end{pmatrix}, \tag{3.68}$$

where we have defined mass ratios

$$z = m_u/m_d = 0.465(24)\,, \tag{3.69}$$
$$w = m_u/m_s = 0.023(1)\,, \tag{3.70}$$

where numerical values are obtained in $N_f = 2{+}1{+}1$ lattice QCD [202] and the number in parenthesis indicates the uncertainty. Moreover, note that axion potential can be written as series

$$V(a) = V_0 + \frac{dV}{da}a + \frac{d^2V}{da^2}\frac{a^2}{2} + \dots\,. \tag{3.71}$$

Since we have shown that the are no linear couplings, it means that the $dV/da = 0$. That is, the axion field $a$ is indeed an excitation around the minimum $\langle a\rangle = 0$. This is an explicit demonstration of the Vafa-Witten theorem in action, as the minimum of axion preserves CP symmetry by ensuring that the complex phase of quark masses vanishes.

This choice of $Q^a$ in Eq. (3.68) also fixes the axion-photon interaction, which from Eq. (3.58) reads

$$C_\gamma^{\rm QCD} = \frac{2}{3}\frac{4+z+w}{1+z+w}\,. \tag{3.72}$$

Since PQ symmetry is anomalous, we expect that the axion is not massless. Indeed, $aG\widetilde{G}$ the term, which explicitly breaks PQ symmetry, generates axion mass according to Appendix A.5.1. After the chiral rotation Eq. (3.54) anomaly is transferred to the quark mass matrix and we can find the mass of the axion by expanding mass term Eq. (3.65) to quadratic order in axion modes

$$\begin{aligned}
\mathcal{L}_{M_a^\dagger} &\simeq \frac{f_\pi^2}{2}B\mathrm{Tr}\left(U\left(1 - i\frac{a}{2f_a}Q_a + \frac{1}{2}\left(-i\frac{a}{2f_a}Q_a\right)^2\right)M^\dagger\left(1 - i\frac{a}{2f_a}Q_a + \frac{1}{2}\left(-i\frac{a}{2f_a}Q_a\right)^2\right)\right),\\
\mathcal{L}_{M_a} &\simeq \frac{f_\pi^2}{2}B\mathrm{Tr}\left(\left(1 + i\frac{a}{2f_a}Q_a + \frac{1}{2}\left(i\frac{a}{2f_a}Q_a\right)^2\right)M\left(1 + i\frac{a}{2f_a}Q_a + \frac{1}{2}\left(i\frac{a}{2f_a}Q_a\right)^2\right)U^\dagger\right).
\end{aligned} \tag{3.73}$$

We can set Goldstone bosons of $SU(3)_A$ to zero, $U(x) = \mathbb{1}$, to find

$$\begin{aligned}
\mathcal{L}_{M_a^\dagger} &= \frac{f_\pi^2}{2}B\left(-i\frac{a}{2f_a}\right)^2\mathrm{Tr}(Q_aMQ_a + Q_aQ_aM)\,,\\
\mathcal{L}_{M_a} &= \frac{f_\pi^2}{2}B\left(-i\frac{a}{2f_a}\right)^2\mathrm{Tr}(Q_aMQ_a + Q_aQ_aM)\,.
\end{aligned} \tag{3.74}$$

Finally, adding the contributions from both terms and identifying the mass term $\mathcal{L}_{\text{axion mass}} = m_a^2a^2/2$ we find

$$m_a^2 = B\frac{f_\pi^2 m_u}{f_a^2(1+z+w)}\,. \tag{3.75}$$

The mass parameter $B$ is fixed by the mass of the pion, which in leading order in $w$ gives

$$B = m_\pi^2\left(\frac{z}{m_u(1+z)} + \frac{w(-1+z)}{4m_u(1+z)^2}\right), \tag{3.76}$$

we finally get the formula for the mass of the axion in 3-flavour ChPT

$$m_a^2 = \frac{f_\pi^2 m_\pi^2}{4f_a^2}\frac{4z - w(1-z)}{(1+z)(1+z+w)}\,, \tag{3.77}$$

which in the limit $w \to 0$ simplifies to well known formula [27]

$$m_a = \frac{f_\pi m_\pi}{f_a}\frac{\sqrt{z}}{(1+z)} \simeq 0.583 \text{ eV}\left(\frac{10^7 \text{ GeV}}{f_a}\right), \tag{3.78}$$

where in last equality we have used values $z = 0.48$, $m_\pi = 134.98$ MeV and $f_\pi = 92.3$ MeV. The state-of-the-art formula obtained at NLO of ChPT gives [203]

$$m_a = 5.70(6)(4) \text{ eV}\left(\frac{10^7 \text{ GeV}}{f_a}\right), \tag{3.79}$$

where the error in the first bracket corresponds to uncertainties in the estimation of $z$ and the second corresponds to an error in the determination of renormalized NLO couplings in ChPT lagrangian.

### 3.3.1 Coupling to pions

We will show the analytical, step-by-step derivation of axion-pion coupling, rarely found in the literature (however, see Ref. [204]). Axion coupling to Goldstone bosons of $SU(3)_A$ come from the axial current Eq. (3.62)

$$\mathcal{L}_{\text{axial}} = \frac{\partial^\mu a}{2f_a} c_a \text{Tr}\left(\frac{i f_\pi^2}{2}\lambda^a\Big(U\partial_\mu U^\dagger - U^\dagger\partial_\mu U\Big)\right). \tag{3.80}$$

Expanding in Goldstones and keeping terms with three fields we find

$$U\partial_\mu U^\dagger \simeq -\frac{i}{2f_\pi^3}\pi^a\lambda^a\partial_\mu(\pi^b\lambda^b)^2 - \frac{i}{6f_\pi^3}\partial_\mu(\pi^a\lambda^a)^2 + \frac{i}{2f_\pi^3}(\pi^a\lambda^a)^2\partial_\mu\pi^b\lambda^b\,. \tag{3.81}$$

All terms are imaginary, so adding hermitian conjugation results in multiplication by 2

$$U\partial_\mu U^\dagger - U^\dagger\partial_\mu U = -\frac{i}{f_\pi^3}\pi^a\lambda^a\partial_\mu(\pi^b\lambda^b)^2 - \frac{i}{3f_\pi^3}\partial_\mu(\pi^a\lambda^a)^2 + \frac{i}{f_\pi^3}(\pi^a\lambda^a)^2\partial_\mu\pi^b\lambda^b\,. \tag{3.82}$$

Firstly, consider terms involving $(\pi^a\lambda^a)^2$. Goldstones are spin-0 real fields, they commute with each other, hence we can only look at the symmetric part of Gell-Mann matrices

$$\pi^a\pi^b\lambda^a\lambda^b = \pi^a\pi^b\lambda^{(a}\lambda^{b)} = \frac{1}{2}(\pi^a\pi^b\{\lambda^a,\lambda^b\}) = \frac{1}{2}\left(\frac{4}{3}\pi^a\pi^a + 2\pi^a\pi^b d^{abc}\lambda^c\right), \tag{3.83}$$

where we have used $\{\lambda^a,\lambda^b\} = 4\delta^{ab}/3 + 2d^{abc}\lambda^c$, cf. Eq. (2.4). In particular, using this result in the first term of Eq. (3.82) we find

$$-\frac{i}{f_\pi^3}(\pi^d\lambda^d)\partial_\mu\Big(\pi^a\pi^b\lambda^a\lambda^b\Big) = -\frac{1}{2}\frac{i}{f_\pi^3}\left(\frac{8}{3}\partial_\mu\pi^a\pi^a\pi^d\lambda^d + 2d^{abc}\partial_\mu(\pi^a\pi^b)\pi^d\lambda^d\lambda^c\right). \tag{3.84}$$

We want to find axion-pion interactions, so indices are restricted $a,b,d \in \{1,2,3\}$. Note, that the only non-zero totally symmetric tensors of $SU(3)$ with two indices restricted to $SU(2)$ are $d^{118} = d^{228} = d^{338}$, which fixes the index $c = 8$, cf. Eq. (2.5). We may now use Eq. (2.6), $\lambda^d\lambda^c = 2\delta^{dc}/3 + (d^{dce} + if^{dce})\lambda^e = 2\delta^{d8}/3 + (d^{d8e} + if^{d8e})\lambda^e$. By noting, that there is no structure constant of $SU(3)$ involving indices $1, 2, 3$ and $8$, cf. Eq. (2.3), and setting $\delta^{d8} = 0$ we have $\lambda^d\lambda^8 \to \delta^{de}\lambda^e/\sqrt{3}$. Using the above we find

$$\begin{aligned}-\frac{i}{f_\pi^3}(\pi^d\lambda^d)\partial_\mu\Big(\pi^a\pi^b\lambda^a\lambda^b\Big) &= -\frac{i}{2f_\pi^3}\left(\frac{8}{3}\partial_\mu\pi^a\pi^a\pi^d\lambda^d + 2\delta^{ab}\left(\frac{1}{\sqrt{3}}\right)^2\partial_\mu(\pi^a\pi^b)\pi^d\delta^{de}\lambda^e\right) = \\ &= -\frac{i}{2f_\pi^3}\left(\frac{8}{3}\partial_\mu\pi^a\pi^a\pi^d\lambda^d + \frac{4}{3}\partial_\mu\pi^a\pi^a\pi^d\lambda^d\right) = -\frac{2i}{f_\pi^3}\Big(\partial_\mu\pi^a\pi^a\Big)\Big(\pi^d\lambda^d\Big)\,.\end{aligned} \tag{3.85}$$

Focusing on the third term in Eq. (3.82) we have

$$
\begin{aligned}
\frac{i}{f_\pi^3}\Big(\pi^a\pi^b\lambda^a\lambda^b\Big)\partial_\mu\pi^d\lambda^d =& \frac{i}{2f_\pi^3}\left(\pi^a\pi^b\left(\frac{4}{3}\delta^{ab}+2d^{abc}\lambda^c\right)\right)\partial_\mu\pi^d\lambda^d = \\
=& \frac{i}{2f_\pi^3}\left(\frac{4}{3}\pi^a\pi^a\partial_\mu\pi^d\lambda^d+2\pi^a\pi^b d^{abc}\partial_\mu\pi^d\lambda^d\lambda^c\right) = \\
=& \frac{i}{2f_\pi^3}\left(\frac{4}{3}\pi^a\pi^a\partial_\mu\pi^d\lambda^d+2\left(\frac{1}{\sqrt{3}}\right)^2\pi^a\pi^b\delta^{ab}\partial_\mu\pi^d\delta^{dc}\right) = \\
=& \frac{i}{f_\pi^3}(\pi^a\pi^a)(\partial_\mu\pi^d\lambda^d)\,,
\end{aligned}
\tag{3.86}
$$

where in the first line we have used Eq. (2.6), and in going from the second line to the third line we have again used that index $c=8$, and that $d^{ii8}=1/\sqrt{3}$.

Moving on to the cubic pion term from Eq. (3.82), because pions commute with each other, only the symmetric part of the Gell-Mann matrices product contributes

$$
\frac{i}{3f_\pi^3}\partial_\mu\Big(\pi^a\pi^b\pi^c\lambda^a\lambda^b\lambda^c\Big) = \frac{i}{3!\cdot 3f_\pi^3}\partial_\mu\Big(\pi^a\pi^b\pi^c\lambda^{(a}\lambda^b\lambda^{c)}\Big)\,. \tag{3.87}
$$

We can construct such symmetrization by combining the following objects

$$
\Lambda^{abc} = \{\lambda^a,\{\lambda^b,\lambda^c\}\}\,, \tag{3.88}
$$

which are symmetric under $b\leftrightarrow c$, as well as under $abc\leftrightarrow bca$. We can combine three such objects, each for a pair of indices. However, since every permutation will be covered twice, we include a factor of 1/2

$$
\lambda^{(a}\lambda^b\lambda^{c)} = \frac{1}{2}\Big(\Lambda^{abc}+\Lambda^{cab}+\Lambda^{bac}\Big)\,. \tag{3.89}
$$

By using the commutator of Gell-Mann matrices we have

$$
\begin{aligned}
\Lambda^{abc} =& \{\lambda^a,\frac{4}{3}\delta^{bc}+2d^{bcd}\lambda^d\} = \frac{8}{3}\lambda^a\delta^{bc}+2d^{bcd}\{\lambda^a,\lambda^d\} = \\
=& \frac{8}{3}\lambda^a\delta^{bc}+\frac{8}{3}d^{bca}+4d^{bcd}d^{ade}\lambda^e\,.
\end{aligned}
\tag{3.90}
$$

Combining the $\Lambda$'s we find that symmetrization is

$$
\begin{aligned}
\lambda^{(a}\lambda^b\lambda^{c)} = \frac{1}{2}\bigg(&\frac{8}{3}\Big(\lambda^a\delta^{bc}+\lambda^b\delta^{ac}+\lambda^c\delta^b\Big)+\frac{8}{3}\Big(d^{abc}+d^{bac}+d^{cab}\Big)+ \\
&+4\Big(d^{bcd}d^{ade}+d^{abd}d^{cde}+d^{acd}d^{bde}\Big)\,.
\end{aligned}
\tag{3.91}
$$

The contraction of one index of a totally symmetric tensor can be found in Ref. [205]

$$
3d_{ijk}d_{pqk} = \delta_{ip}\delta_{jq}+\delta_{iq}\delta_{jp}-\delta_{ij}\delta_{pq}+f_{ipm}f_{jqm}-f_{iqm}f_{jpm}\,, \tag{3.92}
$$

which simplifies if we take into account that indices will be contracted with the pion fields, and we can neglect the terms involving structure constants. Specifying to our case Eq. (3.90), we find

$$
\begin{aligned}
d^{bcd}d^{ade} &= (\delta_{ba}\delta_{ce}+\delta_{be}\delta_{ca}-\delta_{bc}\delta_{ae})/3\,, \\
d^{abd}d^{cde} &= (\delta_{ac}\delta_{be}+\delta_{ae}\delta_{bc}-\delta_{ab}\delta_{ce})/3\,, \\
d^{acd}d^{bde} &= (\delta_{ab}\delta_{ce}+\delta_{ae}\delta_{cb}-\delta_{ac}\delta_{be})/3\,.
\end{aligned}
\tag{3.93}
$$

Upon adding all those together we find

$$d^{bcd}d^{ade} + d^{abd}d^{cde} + d^{acd}d^{bde} = (\delta_{ab}\delta_{ce} + \delta_{ae}\delta_{bc} + \delta_{ac}\delta_{be})/3\,. \tag{3.94}$$

Finally, plugging that result into Eq. (3.91) and combining with Eq. (3.87) we find

$$\begin{aligned}\frac{i}{3f_\pi^3}\partial_\mu\Big(\pi^a\pi^b\pi^c\lambda^a\lambda^b\lambda^c\Big) &= \frac{i}{3!\cdot 3f_\pi^3}\partial_\mu\Bigg(\pi^a\pi^b\pi^c\Bigg(\frac{1}{2}\Bigg(\frac{8}{3}\Big(\lambda^a\delta^{bc} + \lambda^b\delta^{ac} + \lambda^c\delta^b\Big) + \\ &+ \frac{8}{3}\Big(d^{abc} + d^{bac} + d^{cab}\Big) + 4\delta_{ab}\delta_{ce} + \delta_{ae}\delta_{bc} + \delta_{ac}\delta_{be}\Bigg) = \\ &= \frac{i}{3!\cdot 3f_\pi^3}\partial_\mu\Bigg(\frac{8}{3}\cdot 3(\pi^a\pi^a)(\pi^b\lambda^b) + \frac{4}{3}\cdot 3(\pi^a\pi^a)(\pi^b\lambda^b)\Bigg) = \\ &= \frac{i}{3f_\pi^3}\partial_\mu\Big((\pi^a\pi^a)(\pi^b\lambda^b)\Big)\,,\end{aligned} \tag{3.95}$$

where we have used the fact that for $d^{123} = 0$ (Eq. (2.5)). Finally we may combine results from Eq. (3.85), Eq. (3.86) and Eq. (3.95) to find

$$U\partial^\mu U^\dagger - U^\dagger\partial^\mu U \simeq \frac{4i}{3f_\pi^3}\Big(\partial_\mu\pi^b(\pi^a\pi^a) - \pi^b(\pi^a\partial_\mu\pi^a)\Big)\lambda^b\,, \tag{3.96}$$

The axial current, after relabelling the indices is thus given by

$$\begin{aligned}\mathcal{L}_{\text{axial}} &= \frac{\partial^\mu a}{2f_a}\frac{if_\pi^2}{2}c_a\mathrm{Tr}\Bigg(\frac{4i}{3f_\pi^3}\Big(\partial_\mu\pi^b(\pi^c\pi^c) - \pi^b(\pi^c\partial_\mu\pi^c)\Big)\lambda^a\lambda^b\Bigg) = \\ &= -\frac{2}{3}\frac{\partial_\mu a}{f_af_\pi}c_a\Big(\partial_\mu\pi^b(\pi^c\pi^c) - \pi^b(\pi^c\partial_\mu\pi^c)\Big)\delta^{ab}\,.\end{aligned} \tag{3.97}$$

Taking into account the Kronecker delta with restricted $b$ index and Eq. (3.64), we have $c_a\delta^{ab} = c_3$, which can be further evaluated, using Eq. (3.64), $c_3 = \mathrm{Tr}(c\lambda_3)/2 = (C_u - Q_u^a - C_d + Q_d^a)/2$. Note that these terms are independent of the $C_s$.

Using definitions of physical pions $\pi^0 = \pi^3$ and $\pi^\pm = (\pi^1 \mp i\pi^2)/\sqrt{2}$ we find

$$\mathcal{L}_{\text{axial}} = -\frac{C_u - C_d - Q_u^a + Q_d^a}{3f_\pi f_a}(\partial_\mu a)\Big(2\partial_\mu\pi_0\pi_+\pi_- - \pi_0\partial_\mu\pi_+\pi_- - \pi_0\pi_+\partial_\mu\pi_-\Big)\,. \tag{3.98}$$

Identifying coefficient rescaled by the $f_\pi f_a$ as axion pion coupling and using explicit form of $Q_a$ from Eq. (3.68), we obtain the known result [206]

$$C_\pi = -\frac{1}{3}\Big(C_u - C_d - \frac{1-z}{1+z+w}\Big)\,. \tag{3.99}$$

We often abbreviate the formula for pion coupling by using

$$\partial[\pi\pi\pi]_\mu = 2\partial_\mu\pi_0\pi_+\pi_- - \pi_0\partial_\mu\pi_+\pi_- - \pi_0\pi_+\partial_\mu\pi_-\,. \tag{3.100}$$

The full axion-pion lagrangian beyond at NLO of ChPT has been found in Ref. [207].

### 3.3.2 Coupling to kaons

We will not attempt the analytic derivation of axion-kaon coupling by hand. Instead, we have used Mathematica [208] code to expand the axial current in Eq. (3.62) up to three meson fields. Working with generic axion-quark couplings $C_u, C_d, C_s$ we find

$$\begin{aligned}\mathcal{L}_{aK} =&\frac{\partial^\mu a}{12 f_a f_\pi}\Bigg(\Big(C_u - C_d - \frac{1-z}{1+z+w}\Big)\times\\ &\times\Big(K^0\pi^0\partial_\mu\bar{K}^0 + 3\sqrt{2}K^+\pi^-\partial_\mu\bar{K}^0 + K^+\pi^0\partial_\mu K^- - 3\sqrt{2}K^0\pi^+\partial_\mu K^- +\\ &+ \bar{K}^0\pi^0\partial_\mu K^0 - 3\sqrt{2}\bar{K}^0\pi^-\partial_\mu K^+ - 2\bar{K}^0K^0\partial_\mu\pi^0 + 3\sqrt{2}K^-\pi^+\partial_\mu K^0 +\\ &+ K^-\pi^0\partial_\mu K^+ - 2K^-K^+\partial_\mu\pi^0\Big) - \Big((C_u + C_d - 1 - 2C_s + \frac{3w}{1+z+w})\Big)\times\\ &\times\Big(K^0\pi^0\partial_\mu\bar{K}^0 - \sqrt{2}K^+\pi^-\partial_\mu\bar{K}^0 - K^+\pi^-\partial_\mu K^- - \sqrt{2}K^0\pi^+\partial_\mu K^-\\ &+ \bar{K}^0\pi^0\partial_\mu K^0 - \sqrt{2}\bar{K}^0\pi^-\partial_\mu K^+ - 2\bar{K}^0K^0\partial_\mu\pi^0 + 2\sqrt{2}\bar{K}^0K^+\partial_\mu\pi^-\\ &\sqrt{2}K^-\pi^+\partial_\mu K^0 - K^-\pi^0\partial_\mu K^+ + 2K^-K^+\partial_\mu\pi^0 + 2\sqrt{2}K^-K^0\partial_\mu\pi^+\Big)\Bigg).\end{aligned} \tag{3.101}$$

For approximate values $z = 1/2$, $w = 0$ this coupling takes form

$$\begin{aligned}\mathcal{L}_{aK} =&\frac{\partial_\mu a}{12 f_a f_\pi}\Bigg(\Big(C_u - C_d - \frac{1}{3}\Big)\Big(3\sqrt{2}K^+\pi^-\partial^\mu\bar{K}^0 - 3\sqrt{2}K^0\pi^+\partial^\mu K^-\\ &+ \bar{K}^0\pi^0\partial^\mu K^0 - 3\sqrt{2}\bar{K}^0\pi^-\partial^\mu K^+ - 2\bar{K}^0K^0\partial^\mu\pi^0 + 3\sqrt{2}K^-\pi^+\partial^\mu K^0\\ &+ K^-\pi^0\partial^\mu K^+ - 2K^-K^+\partial^\mu\pi^0 + \pi^0K^0\partial^\mu\bar{K}^0 + \pi^0K^+\partial^\mu K^-\Big)\\ &- \Big(C_u + C_d - 1 - 2C_s\Big)\Big(K^0\pi^0\partial^\mu\bar{K}^0 - \sqrt{2}K^+\pi^-\partial^\mu\bar{K}^0 - K^+\pi^0\partial^\mu K^-\\ &+ \sqrt{2}K^0\pi^+\partial^\mu K^- + \bar{K}^0\pi^0\partial^\mu K^0 - \sqrt{2}\bar{K}^0\pi^-\partial^\mu K^+ - 2\bar{K}^0K^0\partial^\mu\pi^0\\ &+ 2\sqrt{2}\bar{K}^0K^+\partial^\mu\pi^- - \sqrt{2}K^-\pi^+\partial^\mu K^0 + K^-\pi^0\partial^\mu K^+ - 2K^-K^+\partial^\mu\pi^0\\ &- 2\sqrt{2}K^-K^0\partial^\mu\pi^+\Big)\Bigg).\end{aligned} \tag{3.102}$$

For reasons explained in Chapter 4, in models of astrophobic axions the charges are fixed $C_u = 2/3$, $C_d = 1/3$, and the matrix Eq. (3.64) is $c = \mathrm{diag}(0, 0, C_s)$. In such case, the only contribution to axion-kaon coupling comes from strange quark charge

$$\begin{aligned}\mathcal{L}_{aK} = \frac{\partial_\mu a}{6 f_a f_\pi}C_s\Big(&\overline{K}^0(\pi^0\partial^\mu K^0 - 2K^0\partial^\mu\pi^0 - \sqrt{2}\pi^-\partial^\mu K^+ + 2\sqrt{2}K^+\partial^\mu\pi^-) -\\ &- K^-(\sqrt{2}\pi^+\partial^\mu K^0 - 2\sqrt{2}K^0\partial^\mu\pi^+ + \pi^0\partial^\mu K^+ - 2K^+\partial^\mu\pi^0) +\\ &+ K^0\pi^0\partial^\mu\overline{K}^0 - \sqrt{2}K^0\pi^+\partial^\mu K^- - \sqrt{2}K^+\pi^-\partial^\mu\overline{K}^0 - K^+\pi^0\partial^\mu K^-\Big).\end{aligned} \tag{3.103}$$

Hence, in astrophobic axion models, axion-kaon coupling is mainly controlled by the strange coupling. In case of vanishing strange coupling, $C_s = 0$ only the term linear in $w$ from Eq. (3.101) gives irreducible, suppressed contribution to the kaon coupling.

## 3.4 Constraints on axion couplings

We are now in the position to list the constraints on axion couplings. Let us collect in one place all axion lagrangian of phenomenological relevance below QCD scale, that is axion-photon coupling Eq. (3.56), nucleon axial couplings in analogy to Eq. (3.41), general lepton couplings from the last term of Eq. (3.45) and pion coupling Eq. (3.98),

$$\begin{aligned}\mathcal{L} = C_\gamma \frac{a}{f_a}\frac{\alpha_{\rm em}}{8\pi}F\tilde{F} + \frac{\partial_\mu a}{2f_a}(C_n\overline{n}\gamma^\mu\gamma_5 n + C_p\overline{p}\gamma^\mu\gamma_5 p)\\ + \frac{\partial_\mu a}{2f_a}\bar{l}_i\gamma^\mu\Big(C^V_{ij} + C^A_{ij}\gamma_5\Big)l_j + \frac{C_\pi}{f_a f_\pi}\partial_\mu a\partial[\pi\pi\pi]^\mu\,,\end{aligned} \tag{3.104}$$

where $C_n, C_p, C_\gamma$ effective axion couplings to neutron, proton, and photon respectively, come from UV coefficient matching. Axion-fermion couplings are given by Eq. (3.49) and Eq. (3.51). We have intentionally neglected the kaon interaction, Eq. (3.101) which is not subject to tight constraints. Expressing the effective couplings in terms of UV couplings gives [60, 209]

$$C_p + C_n = 0.40(4)\left(0.95(C_u + C_d) + 0.05 - \frac{1+z}{1+z+w}\right) - 2\delta\,, \tag{3.105}$$

$$C_p - C_n = 1.273(2)\left(C_u - C_d - \frac{1-z}{1+z+w}\right), \tag{3.106}$$

$$C_\pi = -\frac{1}{3}\left(C_u - C_d - \frac{1-z}{1+z+w}\right), \tag{3.107}$$

$$C_\gamma = |E/N - 2.07(4)|\,, \tag{3.108}$$

where up and down quark charges are given by Eq. (3.51) and $\delta$ is contribution from other quarks, dominated by strange quark and typically of order $\mathcal{O}(0.01)$ [58,60]. Below, we will list all relevant constraints on axion couplings.

### Axion nucleon couplings

Axion nucleon couplings are generically present in axion models, as axion gluon coupling, necessary to solve the strong CP problem, induces couplings to protons and neutrons. Axion nucleon couplings are constrained by the duration of neutrino burst in supernova SN1987A [54] and cooling of neutron stars [57]. Axion emission provides an additional energy sink in the stellar evolution, cooling the neutron stars. On the other hand, energy sink in the form of axion emission in supernova leads to suppressed neutrino burst duration. Those two bounds have similar magnitude, and we will focus only on SN1987A, which is [54]

$$0.61g^2_{ap} + g^2_{an} + 0.53g_{an}g_{ap} < 8.26\times 10^{-19}\,, \tag{3.109}$$

where $g_{ai} \equiv C_i m_i/f_a$ with $i = n, p$. In particular, for $C_n = 0$ the bound is

$$\frac{f_a}{C_p} \gtrsim 8\times 10^8~\text{GeV}\,, \tag{3.110}$$

and for $C_p = 0$ the bound gives

$$\frac{f_a}{C_n} \gtrsim 10^9~\text{GeV}\,. \tag{3.111}$$

As a benchmark, in the KSVZ model $C_p \approx -0.47$, and $f_a$ is constrained to be above about $4\times 10^8$ GeV. These are usually among the strongest bounds in axion models.

### Pion coupling

The pion coupling is not independent of nucleon couplings. Indeed, we can approximate

$$C_\pi = -\frac{1}{4}(C_p - C_n)\,, \tag{3.112}$$

which is largest for $C_n = -C_p$, giving $C_\pi = -C_p/2$. This allows us to approximate a bound on pion coupling

$$\frac{f_a}{C_\pi} \gtrsim 2 \times 10^9 \text{ GeV}\,. \tag{3.113}$$

### Electron coupling

The axion-electron coupling is constrained by investigation of the shape of the white dwarf luminosity function, giving the lower bound [210]

$$\frac{f_a}{|C_e|} \gtrsim 2 \times 10^9 \text{ GeV}\,. \tag{3.114}$$

This bound is of similar order as bounds from nucleon couplings Eq. (3.109).

### Muon coupling

The axion-muon coupling is constrained by the SN1987A data [55, 56] which gives a conservative lower bound [55]:

$$\frac{f_a}{|C_\mu|} \gtrsim \frac{1}{2} \times 10^{7.5} \text{ GeV} \approx 1.6 \times 10^7 \text{ GeV}\,. \tag{3.115}$$

As we will see in Chapter 4, in astrophobic axion models this bound is often one of the strongest.

### Photon coupling

The stellar evolution in globular clusters sets constraint on the axion-photon coupling: [53]

$$g_{a\gamma} < 0.66 \times 10^{-10} \text{ GeV}^{-1}\,, \tag{3.116}$$

which in terms of $C_\gamma$ is

$$\frac{f_a}{|C_\gamma|} > 1.8 \times 10^7 \text{ GeV}\,. \tag{3.117}$$

Under the assumption that axions make up all DM in the Universe, the James Webb Space Telescope can be used to constrain the indirect detection of axion decay into photons [211–214]. For axion in the mass range from 0.18 eV to 2.6 eV ($f_a$ from $2.2\times10^6$ to $3.2\times10^7$) the end-of-mission sensitivity will be roughly [211]

$$g_{a\gamma} \lesssim 5.5 \times 10^{-12} \text{ GeV}^{-1}\,. \tag{3.118}$$

Note, that heavy axion can constitute the whole DM if produced by decay domain walls [215, 216], parametric resonance [34] or kinetic misalignment [35].

Axion-photon coupling is also constrained by helioscopes, searching for solar axions produced via Primakoff. Axions would be converted into photons in the magnetic field of the detector. Examples of helioscopes include CAST, which gives bound $g_{a\gamma} < 0.66 \times 10^{-11}$ GeV$^{-1}$ for $m_a < 0.02$ eV [217], and IAXO whose sensitivity should allow for probing axion-photon coupling down to $g_{a\gamma} \sim 10^{-12}$ GeV$^{-1}$ for similar axion masses [218]. A compilation of up-to-date limits on the axion-photon coupling may be found in Ref. [219].

#### Flavor-violating couplings

Collider experiments that search for missing energy in rare lepton decays have constrained flavor-violating axion couplings Eq. (3.49). The strongest constraint is set by experiments searching for $\mu \to ea$ decays. Depending on the chirality structure of the axion couplings, the strongest bounds come from either TRIUMF [220] or TWIST [221] experiments. For purely left-handed or right-handed couplings upper bounds at 95% C.L. read [222]

$$\frac{2f_a}{|C_{\mu e}|} \geqslant 1.0 \times 10^9 \text{ GeV} \qquad \text{for } C^V_{\mu e} = -C^A_{\mu e}\,, \tag{3.119}$$

$$\frac{2f_a}{|C_{\mu e}|} \geqslant 4.9 \times 10^9 \text{ GeV} \qquad \text{for } C^V_{\mu e} = C^A_{\mu e}\,. \tag{3.120}$$

Constraints from flavor-violating $\tau$ decays are much weaker. The strongest constraints have been recently provided by Belle-II [223] which result in the following lower bounds at 95% C.L.

$$\frac{f_a}{|C_{\tau e}|} \gtrsim 3.6 \times 10^6 \text{ GeV} \tag{3.121}$$

for tau-electron, and

$$\frac{f_a}{|C_{\tau\mu}|} \gtrsim 4.65 \times 10^6 \text{ GeV} \tag{3.122}$$

for tau-muon coupling.

Belle-II is expected to improve the luminosity to 50 ab$^{-1}$ [223]. By rescaling the current expected bounds accordingly, we may estimate the expected sensitivity to flavor-violating $\tau$ couplings [209]

$$\frac{f_a}{|C_{\tau e}|} \gtrsim 1.6 \times 10^7 \text{ GeV}\,, \tag{3.123}$$

$$\frac{f_a}{|C_{\tau\mu}|} \gtrsim 1.7 \times 10^7 \text{ GeV}\,. \tag{3.124}$$

## 3.5 Cosmology with axions

Axions may play a crucial role at different stages of the evolution of the early Universe. In particular, axions produced in several ways may play a role of the cold DM, providing the main cosmological motivation for the PQ solution to the strong CP problem [31–36]. Scenarios with the radial mode of PQ scalar field playing the role of inflaton have been considered [224–228]. On the other hand, as discussed in this thesis, axions produced thermally around QCDPT could contribute to the dark radiation.

Rich phenomenology of axion models has been studied excessively over the years. We will not try to cover it in detail, but in this section, we will review and cite some of the established results and provide references for interested readers.

### 3.5.1 Topological defects

Depending on the relation between axion decay constant $f_a$ and the Gibbons-Hawking temperature of the Universe during inflation, $T_I = H_I/2\pi$ [229, 230], topological defects may lead to observable effects. If PQ symmetry is unbroken during inflation, it breaks at later times, meaning that the PQ scalar singlet $\phi$ (in DFSZ and KSVZ models) obtains a VEV $\langle\phi\rangle = v_\phi e^{i\alpha/f_a}$. The phases of VEVs, $\theta_{\text{PQ}} = \alpha/f_a$, at causally disconnected patches of the Universe are uncorrelated, and since axion does not have potential above QCDPT there is no preferred value, and they uniformly populate the range $[0, 2\pi]$. Famously, the breaking of $U(1)$ symmetry results in the formation of cosmic strings via the Kibble mechanism [37]. It can be understood by noting that the spacetime-dependent VEV of the PQ scalar, $\langle\phi\rangle(x) = v_\phi e^{i\theta_{\rm PQ}(x)}$, must be a single-valued function, hence tracking this function along a closed loop, its phase must change continuously by a factor of $\Delta\theta_{\rm PQ} = 2\pi$. Contracting the loop should preserve this property, but when shrunk to a point the change from $\Delta\theta_{\rm PQ} = 2\pi$ to $\Delta\theta_{\rm PQ} = 0$ cannot be continuous. It suggests, that within the loop there is a point where $\Delta\theta_{\rm PQ}$ is not defined, that is $\langle\phi\rangle = 0$. In three space-like dimensions, by shifting the loop, we find a one-dimensional path with vanishing VEV called cosmic string. Those strings are tubes of false vacuum and, therefore have non-zero energy density, which for non-relativistic stings scales as $a^{-2}$ but quickly dissipates via emission of gravitational waves or non-relativistic axions. Nets of strings can have intricate interactions involving collisions and collapses, which could leave either a background of gravitational waves (see e.g. recent study in Ref. [231]) or a relic density of non-relativistic axions, contributing to the DM [38–40].

The axion potential after SSB of $U(1)_{\rm PQ}$ has a residual, discrete $Z(N)$ symmetry. This symmetry is reflected in $N_{DW} = N$ degenerate vacua of the axion potential generated after the QCDPT. Spontaneous symmetry breaking to the discrete symmetry leads to the formation of domain walls attached to the net of cosmic strings. Domain walls can be stable and could contribute to the energy density of the Universe, especially since their energy density scales as $a^{-2}$ with no other energy sink. Domain walls therefore quickly come to dominate the energy density of the Universe, posing a problem to the axion models with $N_{DW} > 1$ [41]. The problem arises only if inflation takes place before domain wall formation since otherwise rapid expansion of the universe homogenizes the axion field [42]. Alternatively, by introducing explicit $Z(N)$ breaking, the degeneracy of the vacua is removed, and domain walls become unstable [41].

### 3.5.2 Misalignment mechanism

A cold population of axions may be produced in the non-thermal process of misalignment. After SSB of the PQ symmetry, the axion field obtains non-zero VEVs, $a_i = \langle a\rangle$. The axion equation of motion in an expanding Universe is

$$\ddot{a} + 3H\dot{a} + m_a(T)^2 a = 0\,, \tag{3.125}$$

where we have neglected the axion decay into photons (justified for relatively large $f_a$). The mass of the axion vanishes at high temperatures and is generated only after the QCDPT. Therefore, assuming $\dot{a} = 0$, at large $T$ we have

$$\ddot{a} + 3H\dot{a} = 0 \to a = a_i = \text{const}\,. \tag{3.126}$$

On the other hand, when the temperature drops enough and $m_a(T) \gtrsim 3H$, the approximate equation is

$$\ddot{a} + m_a(T)^2 a = 0\,, \tag{3.127}$$

and axion field oscillates with frequency $m_a$. Such coherent oscillation corresponds to condensate, which in the expanding Universe behaves as a non-relativistic gas with energy density scaling $\rho_a \sim a^{-3}$. As a result, axions produced by misalignment mechanism have been proposed as a DM candidate [31–33]. The relic density of axions produced in this way, for $f_a < 2 \times 10^{15}$ GeV is [230]

$$\Omega_a h^2 \simeq 2 \times 10^4 \left(\frac{f_a}{10^{16}\ \text{GeV}}\right)^{7/6} \langle a_i^2\rangle\,. \tag{3.128}$$

For natural initial displacement, $\langle a_i^2 \rangle \sim 1$, the correct relic abundance is obtained for $f_a \sim 10^{11}$ GeV.

Dropping the assumption of vanishing initial field velocity, $\dot{a} \neq 0$, allows for very efficient production of axions even for small axion decay constant, $f_a \ll 10^8$ [35]. The initial axion velocity may be easily induced by higher dimensional operators or UV completion with supersymmetry.

## 3.6 Summary

In this chapter, we have introduced the PQ solution to the strong CP problem and discussed in detail the axion properties within DFSZ model. Axion-pion and axion-kaon couplings below the scale of chiral symmetry breaking were derived, with the latter constituting an original result of this thesis. Moreover, we have collected constraints on axion couplings coming from astrophysical observations and ground-based experiments. For completeness, we have included some known results from axion cosmology, particularly we discussed the axion produced via (kinetic) misalignment mechanism as DM candidate.

# Chapter 4

# Astrophobic axions

We have seen in the previous chapter, that a generic axion model with $C_n, C_p, C_e = \mathcal{O}(1)$ is constrained by the astrophysical observations, implying a lower bound on axion decay constant of order $\mathcal{O}(10^9 \text{ GeV})$. However, those constraints may also be satisfied if couplings vanish, $C_n, C_p, C_e \simeq 0$, allowing for a wider range of $f_a$. Such models have been called astrophobic axions, as they evade most stringent astrophysical bounds coming from SN1987A, neutron star and white dwarf cooling [58].

The motivation for considering such models include the possibility of axiogenesis with correct DM abundance from kinetic misalignment mechanism [60], relaxation of axion quality problem [232–234] and distinct flavor violating signals in high precision experiments [58]. Moreover, as shown in Ref. [209], thermal production of astrophobic axions leaves a characteristic imprint in the CMB.

The defining condition of nucleophobia is the vanishing of Eqs. (3.105) and (3.106). For simplicity, let us approximate the parentheses in those equations [58]

$$\begin{aligned} C_p + C_n &\simeq 0.40(4)(C_u + C_d - 1) = 0\,, \\ C_p - C_n &\simeq 1.273(2)\left(C_u - C_d - \frac{1-z}{1+z}\right) = 0\,, \end{aligned} \tag{4.1}$$

where we have neglected a small $\delta$ contribution from quark sea and correction of order $w = m_u/m_s$. Just to show that such models exist, we will approximate Eq. (3.69) with $z \simeq 1/2$ so that $(1-z)/(1+z) = 2/3$. One can see that for quark charges $C_u = 2/3$, $C_d = 1/3$ nucleophobia conditions are satisfied. Note that the axion pion coupling is proportional to the linear combination $C_p - C_n$, Eq. (3.107), thus nucleophobic axions are also pionphobic.

Besides supernova bound on axion-nucleon couplings, one of the strongest astrophysical constraints is set on axion-electron coupling by white dwarf luminosity function Eq. (3.114). To efficiently allow for values of $f_a$ below $10^8$ GeV, this coupling must also be suppressed. Models with two Higgs doublets, suppress this coupling by tuning the flavor structure of axion-lepton coupling against the lepton Yukawa sector. Electrophobia in 2HDM necessarily implies LFV, opening up the possibility of probing astrophobic axions by ground-based flavor experiments and, as we will show in the following chapter, by cosmological observations.

In this chapter, we provide detailed construction of astrophobic axion models. In the simplest implementation astrophobia can be achieved with 2 Higgs doublets, with generation-dependent PQ charges. We will discuss how LFV is necessarily present in 2HDM astrophobic models, and how it can be avoided in 3HDM. This technical chapter will lay the foundations for systematic analysis of the phenomenology of astrophobic axions. In particular, using formulas for axion couplings we will identify cosmologically interesting astrophobic axion models which allow for sizable production of thermal axions, discussed in Chapter 5.

In this chapter, we review the construction of astrophobic axion models following Ref. [209]. In Sec. 4.1 we discuss the scalar sector in generalized DFSZ axion models with $n$ Higgs doublets. In Sec. 4.2 we introduce useful parametrization of axion-quark couplings which we utilize in Sec. 4.2.1 and Sec. 4.2.2 where we derive axion-quark couplings in 2HDM and 3HDM astrophobic axion models, respectively. In particular, plots on Fig. 4.1 presenting the possible relaxation of fine-tuning in 3HDM constitute the original results of the chapter. Finally, in Sec. 4.3 we discuss the lepton sector of potentially astrophobic axion models with explicit derivations of lepton-axion couplings in Sec. 4.3.1 and Sec. 4.3.2 for 2HDM and 3HDM, respectively.

## 4.1 Scalar potential of generalized DFSZ models

The generalization of DFSZ models includes $n$ Higgs doublets $h_i$, $i = 0, 1, ..., n-1$ and a singlet $\phi$. The scalar potential of each scalar $\Phi_i$ has form

$$\mathcal{L}_i = m_i^2 \Phi_i^2 - \lambda \Phi_i^4 \,, \tag{4.2}$$

which is $U(1)_i$ symmetric. In total, the symmetry of generalized DFSZ potential is hence $U(1)_h^n \times U(1)_\phi$. By introducing couplings between the scalars, we may break the symmetry down to single $U(1)_{\rm PQ}$, identified with Peccei-Quinn symmetry. Considering only renormalizable operators, the general couplings may be written as

$$\mathcal{L} \ni \sum_{i,j} A_{ij} h_i^\dagger h_j \mathcal{O}_{ij}, \qquad \mathcal{O}_{ij} \in \{\phi, \phi^2, \phi^*, \phi^{*2}\} \,. \tag{4.3}$$

Denoting the PQ charge of Higgs doublet $h_i$ with $X_i$, we can write any charge in terms of $X_0$ and $X_\phi$, by trading $n-1$ charges for parameters $A_i$:

$$X_i = X_0 + A_i X_\phi, \qquad A_i = \pm 1, \pm 2, \ldots, \pm 2(n-1) \,. \tag{4.4}$$

The maximal value of $A_i$ is obtained if we couple e.g. $h_0^\dagger h_1 \phi^2$, $h_1^\dagger h_2 \phi^2$ etc.

Similarly to Eq. (3.23), we demand that the axion is orthogonal to the would-be Goldstone boson eaten by the Z boson. Recall that

$$\begin{aligned} a &= \sum_{\text{doublets}} X_i \frac{v_i}{v_{\rm PQ}} a_i + X_\phi \frac{v_\phi}{v_{\rm PQ}} a_\phi \,, \\ Z &= \sum_{\text{doublets}} Y_i \frac{v_i}{v} a_i \,, \end{aligned} \tag{4.5}$$

where $a_i$ are phases of the scalars $h_i$, $a_\phi$ is phase of $\phi$, $v_{\rm PQ}$ is VEV of the PQ singlet, $v$ is EW VEV, and $Y_i$ are weak hypercharges. Since $v$ and $v_{\rm PQ}$ are only normalization factors, we can choose to rescale $a$ by $v_{\rm PQ}/v$. The orthogonality condition becomes

$$\sum_{i,\text{ doublets}} X_i Y_i \frac{v_i^2}{v^2} = Y \sum_{i,\text{ doublets}} X_i \frac{v_i^2}{v^2} = 0 \,, \tag{4.6}$$

where in the last step we have used the freedom to set universal weak hypercharges of doublets. Plugging in our parametrization of charges Eq. (4.4) we find

$$\begin{aligned} 0 = \sum_i (X_0 + A_i X_\phi) \frac{v_i^2}{v^2} = X_0 \sum_i \frac{v_i^2}{v^2} + X_\phi \sum_i A_i \frac{v_i^2}{v^2} = X_0 + X_\phi \sum_i A_i \frac{v_i^2}{v^2} \\ \to X_0 = -X_\phi \sum_i A_i \frac{v_i^2}{v^2} \,. \end{aligned} \tag{4.7}$$

As a result, we find that individual charges $X_i$, as found from Eq. (4.4) are functions of continuous parameters $v_i/v$. However, the differences between any charges are integers:

$$X_i - X_j = X_0 + A_i X_\phi - X_0 - A_j X_\phi = X_\phi(A_i - A_j)\,. \tag{4.8}$$

In the following sections, we will see that this property guarantees that anomaly coefficients $E$ and $N$ are integers, which is consistent with their topological origin.

## 4.2 Quark sector in astrophobic axion models

We will assume that the quark Yukawa sector must be consistent with **2+1** flavor structure. It means that we can pick indices 1,2 to denote the symmetric flavor structure, while index 3 corresponds to flavor which breaks the universality. With that in mind, we can write down the most general Yukawa sector

$$\begin{aligned}\mathcal{L} = &- y^u_{33}\overline{q}_{L3}u_{R3}h^u_{33} - y^u_{3a}\overline{q}_{L3}u_{Ra}h^u_{3a} - y^u_{a3}\overline{q}_{La}u_{R3}h^u_{a3} - y^u_{ab}\overline{q}_{La}u_{Rb}h^u_{ab}\\ &+ y^d_{33}\overline{q}_{L3}d_{R3}\tilde{h}^d_{33} + y^d_{3a}\overline{q}_{L3}d_{Ra}\tilde{h}^d_{3a} + y^d_{a3}\overline{q}_{La}d_{R3}\tilde{h}^d_{a3} + y^d_{ab}\overline{q}_{La}d_{Rb}\tilde{h}^d_{ab} + \text{h.c.}\,,\end{aligned} \tag{4.9}$$

where $\tilde{h}_i = i\sigma^2 h_i^*$, index $a = 1,2$, $h^{u/d}_{ij} \in \{h_1, h_2, ...\}$, e.g. $h^u_{3a} = h_2, h^d_{33} = h_1$ etc. The idea is that the quark bilinears must couple to one of the Higgses indexed by $i,j$. Schematically, we can use the matrix notation to express the Yukawas

$$y_u \sim \begin{pmatrix} h^u_{ab} & h^u_{a3} \\ h^u_{3a} & h^u_{33}\end{pmatrix}, \qquad\qquad y_d \sim \begin{pmatrix} h^d_{ab} & h^d_{a3} \\ h^d_{3a} & h^d_{33}\end{pmatrix}. \tag{4.10}$$

PQ invariance of the Yukawa sector implies that the charges are not independent, and eight conditions for charges must be satisfied. Fermion charges are fixed in terms of Higgses charges and $X_{q_3}$:

$$\begin{aligned} X_{u_a} = -X_{h^u_{3a}} + X_{q_3}\,, \qquad X_{d_a} = X_{h^d_{3a}} + X_{q_3}\,, \qquad X_{q_a} = -X_{h^u_{33}} + X_{h^u_{a3}} + X_{q_3}\,,\\ X_{u_3} = -X_{h^u_{33}} + X_{q_3}\,, \qquad X_{d_3} = X_{h^d_{33}} + X_{q_3}\,. \end{aligned} \tag{4.11}$$

The remaining three conditions are consistency conditions relating Higgs charges

$$X_{h^u_{33}} - X_{h^u_{a3}} = X_{h^u_{3a}} - X_{h^u_{ab}} = X_{h^d_{a3}} - X_{h^d_{33}} = X_{h^d_{ab}} - X_{h^d_{3a}}\,. \tag{4.12}$$

In analogy with (3.28), we perform the axion-dependent, chiral redefinition which removes axion from fermions mass terms

$$f \to f e^{iX_f a/v_{PQ}}. \tag{4.13}$$

This redefinition induces anomalous couplings to gluons, photons

$$\mathcal{L}_{\text{anom}} = N\frac{a}{v_{\text{PQ}}}\frac{\alpha_s}{4\pi}G_{\mu\nu}\tilde{G}^{\mu\nu} + E\frac{a}{v_{\text{PQ}}}\frac{\alpha_{\text{em}}}{4\pi}F_{\mu\nu}\tilde{F}^{\mu\nu}\,, \tag{4.14}$$

where the anomaly coefficients Eq. (3.31) and Eq. (3.32) are

$$\begin{aligned} 2N &= 4X_{q_a} - X_{u_3} - 2X_{u_a} - X_{d_3} - 2X_{d_a}\\ &= 2X_{h^u_{ab}} + X_{h^u_{33}} - 2X_{h^d_{ab}} - X_{h^d_{33}}\,, \end{aligned} \tag{4.15}$$

$$\begin{aligned} E &= E_Q + E_L\\ &= \frac{5}{3}(2X_{q_a} + X_{q_3}) - \frac{4}{3}(2X_{u_a} + X_{u_3}) - \frac{1}{3}(2X_d + X_{d_3}) + E_L\\ &= \frac{8}{3}X_{h^u_{ab}} + \frac{4}{3}X_{h^u_{33}} - \frac{2}{3}X_{h^d_{ab}} - \frac{1}{3}X_{h^d_{33}} + E_L\,. \end{aligned} \tag{4.16}$$

We included also a generic contribution from the charged lepton sector $E_L$, to be discussed in Sec. 4.3. Note, that since Eq. (4.8) holds, the anomaly coefficients are integers.

By analogy with (3.41), the chiral rotation Eq. (4.13) induces a derivative axion-fermion couplings from the kinetic terms, which in the flavor interaction basis are

$$\mathcal{L} = \frac{\partial_\mu a}{v_{\rm PQ}}\Big[\overline{u}_i\gamma^\mu\Big(\tilde{C}^q_{ij}P_L + \tilde{C}^u_{ij}P_R\Big)u_j + \overline{d}_i\gamma^\mu\Big(\tilde{C}^q_{ij}P_L + \tilde{C}^d_{ij}P_R\Big)d_j\Big]\,, \tag{4.17}$$

where couplings can be expressed in terms of Higgs charges, in the matrix notation

$$\begin{aligned}
\tilde{C}^q &= \Big(X_{h^u_{33}} - X_{h^u_{a3}} - X_{q_3}\Big)\mathbb{1} + \mathrm{diag}(0,0,X_{h^u_{a3}} - X_{h^u_{33}})\,,\\
\tilde{C}^u &= \Big(X_{h^u_{3a}} - X_{q_3}\Big)\mathbb{1} + \mathrm{diag}(0,0,X_{h^u_{33}} - X_{h^u_{3a}})\,,\\
\tilde{C}^d &= \Big(-X_{h^d_{3a}} - X_{q_3}\Big)\mathbb{1} + \mathrm{diag}(0,0,X_{h^d_{3a}} - X_{h^d_{33}})\,.
\end{aligned} \tag{4.18}$$

In this way, we have split the charges into the part which is proportional to the unit matrix and the term which only alters the third entry. For example, to obtain first raw of Eq. (4.18) we use $X_{q_a} = -X_{h^u_{33}} + X_{h^u_{a3}} + X_{q_3}$ which sign must be adjusted due to $i^2$ factor coming from chiral redefinition, cf. Eq. (3.41). For the third entry, $X_{q_3}$, one must compensate by removing $X_{h^u_{33}}$ and $X_{h^u_{a3}}$.

Alternatively, we can write Eq. (4.18) using indices as

$$\begin{aligned}
\tilde{C}^q_{ij} &= \Big(X_{h^u_{33}} - X_{h^u_{a3}} - X_{q_3}\Big)\delta_{ij} + (X_{h^u_{a3}} - X_{h^u_{33}})\delta_{i3}\delta_{j3}\,,\\
\tilde{C}^u_{ij} &= \Big(X_{h^u_{3a}} - X_{q_3}\Big)\delta_{ij} + (X_{h^u_{33}} - X_{h^u_{3a}})\delta_{i3}\delta_{j3}\,,\\
\tilde{C}^d_{ij} &= \Big(-X_{h^d_{3a}} - X_{q_3}\Big)\delta_{ij} + (X_{h^d_{3a}} - X_{h^d_{33}})\delta_{i3}\delta_{j3}\,.
\end{aligned} \tag{4.19}$$

The mass matrices are diagonalized with unitary transformations

$$f_i \to V_{ij}f_j, \qquad \text{i.e. } m_f^{\rm diag} = V^\dagger_{fL}m_fV_{fR}. \tag{4.20}$$

It is now clear why it is advantageous to split the charge matrix as in (4.18). The mass diagonalization will only alter the third entry of the charge matrix. Explicitly, in the mass basis, we obtain

$$\mathcal{L} = \frac{\partial_\mu a}{v_{\rm PQ}}\overline{u}\gamma^\mu(C^{u_L}P_L + C^{u_R}P_R)u + \frac{\partial_\mu a}{v_{\rm PQ}}\overline{d}\gamma^\mu\Big(C^{d_L}P_L + C^{d_R}P_R\Big)d\,, \tag{4.21}$$

where

$$\begin{aligned}
C^{u_L}_{ij} &= \Big(X_{h^u_{33}} - X_{h^u_{a3}} - X_{q_3}\Big)\delta_{ij} - \Big(X_{h^u_{33}} - X_{h^u_{a3}}\Big)\xi^{u_L}_{ij}\,,\\
C^{d_L}_{ij} &= \Big(X_{h^u_{33}} - X_{h^u_{a3}} - X_{q_3}\Big)\delta_{ij} - \Big(X_{h^u_{33}} - X_{h^u_{a3}}\Big)\xi^{d_L}_{ij}\,,\\
C^{u_R}_{ij} &= \Big(X_{h^u_{3a}} - X_{q_3}\Big)\delta_{ij} + \Big(X_{h^u_{33}} - X_{h^u_{3a}}\Big)\xi^{u_R}_{ij}\,,\\
C^{d_R}_{ij} &= \Big(-X_{h^d_{3a}} - X_{q_3}\Big)\delta_{ij} + \Big(X_{h^d_{3a}} - X_{h^d_{33}}\Big)\xi^{d_R}_{ij}\,,
\end{aligned} \tag{4.22}$$

where the flavor structure is controlled by the matrices

$$\xi^{f_P}_{ij} \equiv (V_{fP})^*_{3i}(V_{fP})_{3j}\,, \qquad f = u,d,q\,, \qquad P = L,R\,. \tag{4.23}$$

The formula for $\xi$'s is a direct consequence of the Kronecker deltas in Eq. (4.19). Let us work out the properties of the $\xi$ following from the unitarity of $V_{fP}$. The unitarity condition in index notation is

$$V^\dagger_{fP}V_{fP} = \mathbf{1} \to \sum_j\Big(V^*_{fP}\Big)_{ji}V_{jk} = \delta_{ij}. \tag{4.24}$$

1. Since $\delta_{ii} = 1$, $\sum_j (V_{fP})^*_{ji} V_{ji} = \sum_j |(V_{fP})_{ji}|^2 = 1$. On the other hand, $\xi^{f_P}_{ii} = (V_{fP})^*_{3i}(V_{fP})_{3i} = |(V_{fP})_{3i}|^2 > 0$. It follows that

$$0 \leqslant \xi^{f_P}_{ii} \leqslant 1, \qquad \sum_i \xi^{f_P}_{ii} = 1\,. \tag{4.25}$$

2. From $\xi^{f_P}_{ii}\xi^{f_P}_{jj} = (V_{fP})^*_{3i}(V_{fP})_{3i}(V_{fP})^*_{3j}(V_{fP})_{3j} = \xi^{f_P}_{ij}\xi^{f_P*}_{ij}$, and thus

$$|\xi^{f_P}_{ij}| = \sqrt{\xi^{f_P}_{ii}\xi^{f_P}_{jj}}\,. \tag{4.26}$$

Thus, we can find (up to sign) all $\xi^{f_P}_{ij}$ based only on three diagonal entries $\xi^{f_P}_{ii}$, summing up to one. As a result, flavor violation is controlled by 2 independent, real parameters in each sector $u_L, u_R, d_R$. This parametrization is particularly useful, as it allows us to easily identify models with specific couplings, such as astrophobic models, with all information about the flavor structure encoded in a few real parameters. By means of using simple relations Eq. (4.25) and Eq. (4.26) other couplings are easily found.

### 4.2.1 Quark sector in 2HDM

The structure of the Yukawa sector is fixed by the consistency conditions

$$X_{h^u_{33}} - X_{h^u_{a3}} = X_{h^u_{3a}} - X_{h^u_{ab}} = X_{h^d_{a3}} - X_{h^d_{33}} = X_{h^d_{ab}} - X_{h^d_{3a}}\,, \tag{4.27}$$

which can only be fulfilled if in each equation Higgses are pairwise identified. Writing the above in three separate equations

$$\begin{aligned} X_{h^u_{33}} - X_{h^u_{a3}} &= X_{h^u_{3a}} - X_{h^u_{ab}}\,, \\ X_{h^u_{3a}} - X_{h^u_{ab}} &= X_{h^d_{a3}} - X_{h^d_{33}}\,, \\ X_{h^d_{a3}} - X_{h^d_{33}} &= X_{h^d_{ab}} - X_{h^d_{3a}}\,. \end{aligned} \tag{4.28}$$

With at most 3 Higgs doublets, each of these equations can be satisfied in two ways, (e.g. in the first line of Eq. (4.28) $X_{h^u_{33}} = X_{h^u_{3a}}$ or $X_{h^u_{33}} = -X_{h^u_{ab}}$), giving $3 \cdot 2 = 6$ possible models. Another possibility is found by setting Eq. (4.27) to zero, resulting in a total of 7 distinct models consistent with the required flavor structure

$$\begin{gathered} \begin{pmatrix} h_b h_b \\ h_a h_a \end{pmatrix}\begin{pmatrix} h_a h_a \\ h_b h_b \end{pmatrix}, \begin{pmatrix} h_a h_a \\ h_a h_a \end{pmatrix}\begin{pmatrix} h_b h_c \\ h_b h_c \end{pmatrix}, \begin{pmatrix} h_b h_a \\ h_b h_a \end{pmatrix}\begin{pmatrix} h_a h_c \\ h_a h_c \end{pmatrix}, \begin{pmatrix} h_b h_a \\ h_b h_a \end{pmatrix}\begin{pmatrix} h_c h_a \\ h_c h_a \end{pmatrix}, \\ \begin{pmatrix} h_a h_b \\ h_a h_b \end{pmatrix}\begin{pmatrix} h_c h_a \\ h_c h_a \end{pmatrix}, \begin{pmatrix} h_a h_b \\ h_a h_b \end{pmatrix}\begin{pmatrix} h_a h_c \\ h_a h_c \end{pmatrix}, \begin{pmatrix} h_b h_c \\ h_b h_c \end{pmatrix}\begin{pmatrix} h_a h_a \\ h_a h_a \end{pmatrix}. \end{gathered} \tag{4.29}$$

We also restrict to models that potentially have suppressed couplings to nucleons (4.1), which mainly depend on the valence quark couplings $C_u$ and $C_d$. Using definitions Eq. (3.51), Eq. (3.46) and Eq. (3.47) with couplings Eq. (4.22) we have

$$C_u = \frac{1}{2N}\Big[X_{h^u_{ab}} + \Big(X_{h^u_{33}} - X_{h^u_{3a}}\Big)\xi^{u_R}_{11} + \Big(X_{h^u_{3a}} - X_{h^u_{ab}}\Big)\xi^{u_L}_{11}\Big]\,, \tag{4.30}$$

$$C_d = \frac{1}{2N}\Big[-X_{h^d_{ab}} + \Big(X_{h^d_{3a}} - X_{h^d_{33}}\Big)\xi^{d_R}_{11} + \Big(X_{h^d_{ab}} - X_{h^d_{3a}}\Big)\xi^{d_L}_{11}\Big]\,. \tag{4.31}$$

Note, that in the first equation, we have used the consistency condition, Eq. (4.27), to find $X_{h^u_{ab}} = X_{h^u_{3a}} - X_{h^u_{33}} + X_{h^u_{a3}}$, and similarly in the second equation $-X_{h^d_{ab}} = X_{h^d_{3a}} - X_{h^d_{33}} -$

$X_{h^d_{3a}}$. We restrict to models without quark flavor violating, that is, $\xi_{ij} = 0$ for $i \neq j$. It means that at least one of $\xi_{ii}$ must vanish, which combined with properties (4.25) and (4.26) gives $\xi_{11} = 0$ or $\xi_{11} = 1$. We set those conditions uniformly for the $u-$ and $d$-sector.

It might seem very restrictive, however, models with flavor violation in the quark sector are strongly constrained by flavor-violating meson decay experiments, $f_a \gtrsim$ few $\times 10^8$ GeV [235]. As it turns out, see Sec. 5.1, thermal production is efficient only at low temperatures, corresponding to smaller values of $f_a$. Therefore, the thermal abundance is often unobservable for models with quark flavor violation.

The first nucleophobia condition $1 = C_u + C_d$ will narrow down the plethora of models consistent with **2+1** flavor structure (4.29). For $\xi_{11} = 0$:

$$
\begin{aligned}
&C_u + C_d = \frac{1}{2N}\left(X^u_{ab} - X^d_{ab}\right) = 1 \qquad (\xi^{u_L}_{11} = \xi^{u_R}_{11} = \xi^{d_L}_{11} = \xi^{d_R}_{11} = 0)\,,\\
&X_{h^u_{ab}} - X_{h^d_{ab}} = 2N = 2X_{h^u_{ab}} + X_{h^u_{33}} - 2X_{h^d_{ab}} - X_{h^d_{33}},\\
&X_{h^u_{ab}} + X_{h^u_{33}} - X_{h^d_{ab}} - X_{h^d_{33}} = 0\,,
\end{aligned}
$$

where we have used Eq. (4.15) for colour anomaly. This condition can only be satisfied if Higgses are pairwise identified.

Similarly, for $\xi_{11} = 1$ models condition $C_u + C_d = 1$ becomes

$$
\begin{gathered}
X_{h^u_{ab}} - X_{h^d_{ab}} + (X_{h^u_{33}} - X_{h^u_{3a}} + X_{h^u_{3a}} - X_{h^u_{ab}}) + (X_{h^d_{3a}} - X_{h^d_{33}} + X_{h^d_{ab}} - X_{h^d_{3a}}) = 2N\\
(\xi^{u_L}_{11} = \xi^{u_R}_{11} = \xi^{d_L}_{11} = \xi^{d_R}_{11} = 1),
\end{gathered}
$$

$$
\begin{aligned}
&2X_{h^u_{ab}} + X_{h^u_{33}} - 2X_{h^d_{ab}} - X_{h^d_{33}} = X_{h^u_{ab}} - X_{h^d_{ab}} + X_{h^u_{33}} - X_{h^u_{ab}} - X_{h^d_{33}} + X_{h^d_{ab}}\,,\\
&X_{h^u_{ab}} - X_{h^d_{ab}} = 0\,.
\end{aligned}
$$

For the QCD axion, we also need non-vanishing color anomaly $N \neq 0$ to be non-zero, so that $\bar{\theta}$ could be absorbed into the definition of axion. We finally arrive at the following necessary conditions for nucleophobia:

$$
X_{h^u_{ab}} = X_{h^d_{33}} \neq X_{h^u_{33}} = X_{h^d_{ab}} \qquad (\xi^{u_L}_{11} = \xi^{u_R}_{11} = \xi^{d_L}_{11} = \xi^{d_R}_{11} = 0), \tag{4.32}
$$

$$
X_{h^u_{ab}} = X_{h^d_{ab}} \wedge X_{h^u_{33}} \neq X_{h^d_{33}} \qquad (\xi^{u_L}_{11} = \xi^{u_R}_{11} = \xi^{d_L}_{11} = \xi^{d_R}_{11} = 1)\,. \tag{4.33}
$$

Note, that in astrophobic axions color anomaly effectively comes from a single family, as firstly noted in Ref. [58], $2N = X_{h^u_{ab}} - X_{h^d_{ab}}$ for $\xi_{11} = 0$ and $2N = X_{h^u_{33}} - X_{h^d_{33}}$ for $\xi_{11} = 1$.

Comparing to Eq. (4.29), we see that for $\xi_{11} = 0$ only two structures allow for nucleophobia

$$
\begin{aligned}
\text{Q2}: &\qquad y_u \sim \begin{pmatrix} h_a h_a \\ h_b h_b \end{pmatrix}, \qquad y_d \sim \begin{pmatrix} h_b h_b \\ h_a h_a \end{pmatrix},\\
\text{Q3}: &\qquad y_u \sim \begin{pmatrix} h_a h_b \\ h_a h_b \end{pmatrix}, \qquad y_d \sim \begin{pmatrix} h_b h_a \\ h_b h_a \end{pmatrix},
\end{aligned} \tag{4.34}
$$

with $h_a \neq h_b$, while for $\xi_{11} = 1$ there are also only two possible structures

$$
\begin{aligned}
\text{Q1}: &\qquad y_u \sim \begin{pmatrix} h_a h_a \\ h_a h_a \end{pmatrix}, \qquad y_d \sim \begin{pmatrix} h_a h_b \\ h_a h_b \end{pmatrix},\\
\text{Q4}: &\qquad y_u \sim \begin{pmatrix} h_c h_a \\ h_c h_a \end{pmatrix}, \qquad y_d \sim \begin{pmatrix} h_c h_b \\ h_c h_b \end{pmatrix},
\end{aligned} \tag{4.35}
$$

where $h_a \neq h_b, h_c$. This convenient notation allows us to have universal formulas for all Q1-Q4 models, using Eq. (4.22),

$$2N = X_a - X_b\,, \qquad C_u = \frac{X_a}{X_a - X_b}\,, \qquad C_d = \frac{-X_b}{X_a - X_b}\,. \tag{4.36}$$

which manifestly satisfy $C_u + C_d = 1$.

The other condition for nucleophobia, $C_u - C_d = \frac{1}{3}$, requires for all models

$$\frac{1}{3} = \frac{X_a + X_b}{X_a - X_b}\,. \tag{4.37}$$

For 2HDMs, without loss of generality $h_a = h_1$ and $h_b = h_0$, and simplification gives $X_0 = X_1/2$. Using parametrization (4.4) we find

$$\begin{aligned} X_0 = -\frac{1}{2}X_1 = -\frac{1}{2}X_0 - \frac{1}{2}A_1 X_\phi\,, \\ X_0 = -\frac{1}{3}A_1 X_\phi\,. \end{aligned} \tag{4.38}$$

Using the condition of axion-Z orthogonality, Eq. (4.7), we find

$$X_0 = -X_\phi A_1 \frac{v_1^2}{v^2} = -\frac{1}{3}A_1 X_\phi \quad \rightarrow \quad \sin^2\beta \equiv s_\beta^2 = \frac{v_1^2}{v^2} = \frac{1}{3}\,. \tag{4.39}$$

Note, that satisfying Eq. (4.37) requires fine-tuning of the parameters and is not natural.

The value of $A_1$ is unphysical, as it can always be changed by adjusting the PQ charge normalization $X_\phi$. The coupling $h_1^\dagger h_0 \phi$ (equivalent to $A_1 = 1$) results in charges $X_1 = c_\beta^2$ and $X_0 = -s_\beta^2$, which combined with (4.35) and (4.34) results in four models found first in Ref. [58].

As an example, we will present an explicit derivation of couplings in the Q1 model. The up- and down-type diagonal quark couplings are

$$\begin{aligned} C_{u_i} &= \frac{1}{2N}\Big[X_{h^u_{ab}} + \Big(X_{h^u_{33}} - X_{h^u_{3a}}\Big)\xi^{u_R}_{ii} + \Big(X_{h^u_{3a}} - X_{h^u_{ab}}\Big)\xi^{u_L}_{ii}\Big]\,, \\ C_{d_i} &= \frac{1}{2N}\Big[-X_{h^d_{ab}} + \Big(X_{h^d_{3a}} - X_{h^d_{33}}\Big)\xi^{d_R}_{ii} + \Big(X_{h^d_{ab}} - X_{h^d_{3a}}\Big)\xi^{d_L}_{ii}\Big]\,, \end{aligned} \tag{4.40}$$

which for Q1 structure from Eq. (4.35) with $h_a = h_1$ and $h_b = h_0$ gives

$$\begin{aligned} C_{u_i} &= \frac{X_1}{X_1 - X_0} = \frac{X_0 + A_1 X_\phi}{A_1 X_\phi} = \frac{-X_\phi A_1 s_\beta^2 + X_\phi A_1}{A_1 X_\phi} = c_\beta^2\,, \\ C_{d_i} &= \frac{1}{2N}\Big(-X_1 + (X_1 - X_0)\xi^{d_R}_{ii}\Big) = -c_\beta^2 + \xi^{d_R}_{ii}\,, \end{aligned} \tag{4.41}$$

where we have substituted parametrization of charges via Eq. (4.4), $X_1 = X_0 + A_1 X_\phi$, and used axion-Z orthogonality condition Eq. (4.7), $X_0 = -X_\phi A_1 \frac{v_1^2}{v^2} = -X_\phi A_1 s_\beta^2$. In the last equality of the second line, we have utilized $2N = X_1 - X_0$. For off-diagonal couplings we have

$$\begin{aligned} C^A_{u_i \neq u_j} &= \frac{1}{2N}\Big[\Big(X_{h^u_{33}} - X_{h^u_{3a}}\Big)\xi^{u_R}_{ij} + \Big(X_{h^u_{3a}} - X_{h^u_{ab}}\Big)\xi^{u_L}_{ij}\Big]\,, \\ C^A_{d_i \neq d_j} &= \frac{1}{2N}\Big[\Big(X_{h^d_{3a}} - X_{h^d_{33}}\Big)\xi^{d_R}_{ii} + \Big(X_{h^d_{ab}} - X_{h^d_{3a}}\Big)\xi^{d_L}_{ii}\Big]\,, \end{aligned} \tag{4.42}$$

| Model | $E_Q/N$ | $C^A_{u_iu_i}$ | $C^A_{d_id_i}$ | $C^{V,A}_{u_i\neq u_j}$ | $C^{V,A}_{d_i\neq d_j}$ |
|---|---|---|---|---|---|
| Q1 | $2/3+6c_\beta^2$ | $c_\beta^2$ | $\xi^{d_R}_{ii}-c_\beta^2$ | $0$ | $\xi^{d_R}_{ij}$ |
| Q2 | $-4/3+6c_\beta^2$ | $c_\beta^2-\xi^{u_L}_{ii}$ | $-\xi^{d_L}_{ii}+s_\beta^2$ | $\pm\xi^{u_L}_{ij}$ | $\pm\xi^{d_L}_{ij}$ |
| Q3 | $-4/3+6c_\beta^2$ | $c_\beta^2-\xi^{u_R}_{ii}$ | $-\xi^{d_R}_{ii}+s_\beta^2$ | $-\xi^{u_R}_{ij}$ | $-\xi^{d_R}_{ij}$ |
| Q4 | $-10/3+6c_\beta^2$ | $-s_\beta^2+\xi^{u_R}_{ii}$ | $s_\beta^2$ | $\xi^{u_R}_{ij}$ | $0$ |

Table 4.1: Axion couplings in nucleophobic ($C_u \approx 2/3, C_d \approx 1/3$) 2HDMs Q1-Q4, defined in Eq. (4.35) and Eq. (4.34), expressed in terms of flavor parameters $\xi^{q_P}_{ij}$ defined by Eq. (4.23) and vacuum angle $c_\beta \equiv \cos\beta, s_\beta \equiv \sin\beta$. We denote contribution from quarks to the electromagnetic anomaly as $E_Q$.

which for Q1 structure give

$$\begin{aligned} C^A_{u_i\neq u_j} &= 0, \\ C^A_{d_i\neq d_j} &= \frac{1}{2N}\Big[(X_1-X_0)\xi^{d_R}_{ii}\Big] = \xi^{d_R}_{ii}\,, \end{aligned} \tag{4.43}$$

where in the last equality we have again used $2N = X_1 - X_0$. Analogous calculations give predictions in Tab. 4.1. The nucleophobia is achieved by setting the up and down quark couplings, $C_u = 2/3$, $C_d = 1/3$, which can give several distinct nucleophobic models, depending on the quark coupling structure.

### 4.2.2 Quark sector in 3HDM

Extending the scalar sector with another Higgs doublet allows for suppression of nucleon couplings without introducing fine-tuning. We demonstrate it by choosing Higgs couplings $h_1^\dagger h_0\phi^2, h_2^\dagger h_0\phi^\dagger$ (corresponding to $A_1 = 2$, $A_2 = -1$). Choosing $h_a = h_1$, $h_b = h_2$ we find that condition from Eq. (4.37) is

$$\frac{X_1+X_2}{X_1-X_2} = \frac{2X_0/X_\phi + A_1X_\phi + A_2X_\phi}{A_1X_\phi - A_2X_\phi} = \frac{2X_0/X_\phi + A_1 + A_2}{A_1 - A_2} = \frac{1}{3} + \frac{2}{3}\frac{X_0}{X_\phi}\,. \tag{4.44}$$

Clearly, the nucleophobia is achieved for $X_0 \ll 0$. Expressing the second term in terms of VEVs using Eq. (4.7)

$$\frac{X_0}{X_\phi} = -\sum_i A_i \frac{v_i^2}{v^2} = \frac{v_2^2}{v^2} - 2\frac{v_1^2}{v^2}\,, \tag{4.45}$$

which can be parametrized by vacuum angles, $\beta_1$ and $\beta_2$,

$$\frac{X_0}{X_\phi} = s_1^2c_2^2 - 2c_1^2c_2^2 = c_2^2(s_1^2+c_1^2-3c_1^2) = c_2^2(1-3c_1^2)\,, \tag{4.46}$$

where we have abbreviated $s_i = \sin\beta_i$ and $c_i = \cos\beta_i$ and $v_0 = s_2 v, v_1 = c_1c_2v, v_2 = s_1c_2v$. Exactly how small $X_0$ can be is only limited by the perturbativity of Yukawas. In Q1-Q4 models the strongest constraint comes from top and bottom Yukawas

$$\begin{aligned} y_t &= y_t^{\text{3HDM}} c_1c_2 < \sqrt{16\pi/3} \approx 4.1\,, \\ y_b &= y_b^{\text{3HDM}} s_1c_2 < \sqrt{16\pi/3} \approx 4.1\,, \end{aligned} \tag{4.47}$$

where $y_{t,b}$ are SM Yukawas, while $y_{t,b}^{\text{3HDM}}$ are Yukawas in 3HDM. Those bounds have been obtained in [59]. On the left panel of the plot Fig. 4.1 we show unitarity bounds with

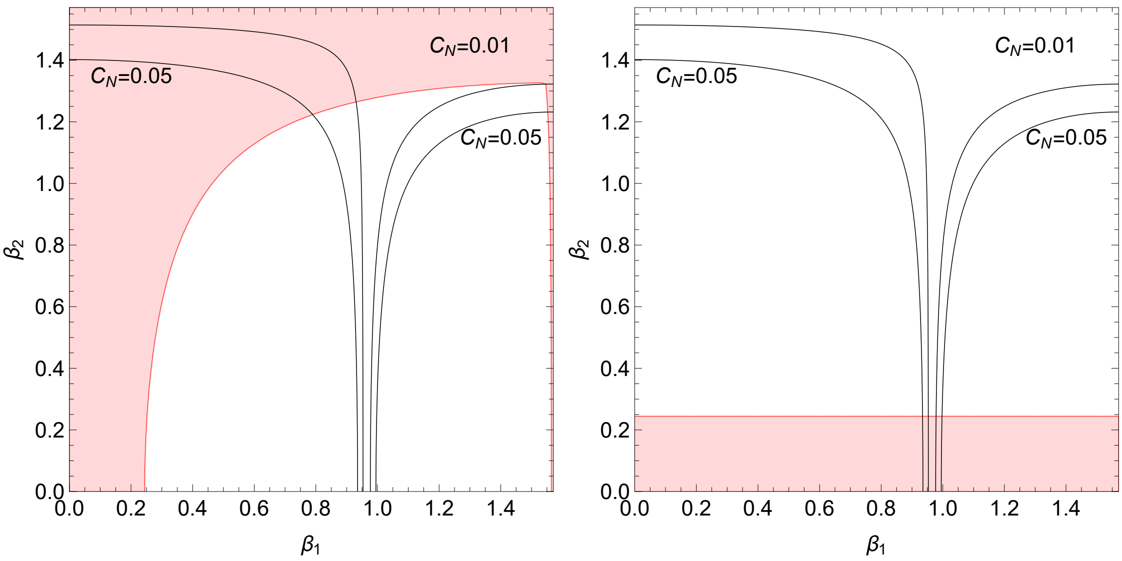


Figure 4.1: Contours of a constant $C_N$ defined in Eq. (4.48) according to Eq. (4.46) with red region excluded by the unitarity of top and bottom Yukawas Eq. (4.47). The left panel corresponds to Q1-Q4 3HDM models, while the right panel corresponds to the Q5 model with relaxed unitarity constraints. An analogous plot to the left panel was originally included in [59].

contours of combined nucleon coupling [59]

$$C_N = \sqrt{C_n^2 + C_p^2} \simeq \frac{1}{\sqrt{2}} \sqrt{1.27^2 \left( \frac{1}{3} - \frac{1-z}{1+z} - \frac{2}{3} \frac{X_0}{X_\phi} \right)^2 + 4\delta^2}\,, \tag{4.48}$$

where we have used Eq. (3.105) and Eq. (3.105) with $z = 0.48$, $\delta = 0$ and $w = 0$. Taking the supernova bound Eq. (3.111) the allowed values of axion decay constant for $C_N = 0.05$ are

$$f_a \gtrsim 5 \times 10^7 \text{ GeV}\,, \tag{4.49}$$

while for $C_N = 0.01$

$$f_a \gtrsim 10^7 \text{ GeV}\,. \tag{4.50}$$

Note, that $C_N = 0.01$ requires precise tuning of vacuum angle $\beta_1$ to preserve perturbative unitarity in Q1-Q4 models.

However, it is also possible to construct a model, which avoids the unitarity constraint, requiring no fine-tuning at all. Let's denote with Q5 model with $h_c = h_0$ (instead of $h_c = h_2$), in Q4 structure (4.35), while keeping $h_a = h_1$, $h_b = h_2$. The Yukawas couple up and down quarks to the $h_1$ and $h_2$, respectively. As a result, Yukawas are both proportional to $c_2$. On the other hand, all heavy fermions are coupled to the $h_0$, thus the top and bottom SM Yukawas are proportional to $s_2$. On the right panel of Fig. 4.1 we show how the unitarity bound is relaxed, and nucleophobia can be achieved for a wider range of vacuum angles.

## 4.3 Lepton sector in astrophobic axion models

Restricting to a **2+1** flavor structure, the lepton Yukawa sector lagrangian is

$$\mathcal{L} = -y^e_{33} \bar{\ell}_{L3} e_{R3} \tilde{h}^e_{33} - y^e_{3a} \bar{\ell}_{L3} e_{Ra} \tilde{h}^e_{3a} - y^e_{a3} \bar{\ell}_{La} e_{R3} \tilde{h}^e_{a3} - y^e_{ab} \bar{\ell}_{La} e_{Rb} \tilde{h}^e_{ab}\,, \tag{4.51}$$

| Model | $E_Q/N$ | $C^A_{u_iu_i}$ | $C^A_{d_id_i}$ | $C^{V,A}_{u_i\neq u_j}$ | $C^{V,A}_{d_i\neq d_j}$ |
|---|---|---|---|---|---|
| Q1 | $14/3+2X_0$ | $2/3+X_0/3$ | $-2/3-X_0/3+\xi^{d_R}_{ii}$ | $0$ | $\xi^{d_R}_{ij}$ |
| Q2 | $8/3+2X_0$ | $2/3+X_0/3-\xi^{u_L}_{ii}$ | $1/3-X_0/3-\xi^{d_L}_{ii}$ | $\pm\xi^{u_L}_{ij}$ | $\pm\xi^{d_L}_{ij}$ |
| Q3 | $8/3+2X_0$ | $2/3+X_0/3-\xi^{u_R}_{ii}$ | $1/3-X_0/3+\xi^{d_R}_{ii}$ | $-\xi^{u_R}_{ij}$ | $-\xi^{d_R}_{ij}$ |
| Q4 | $2/3+2X_0$ | $-1/3+X_0/3+\xi^{u_R}_{ii}$ | $1/3-X_0/3$ | $\xi^{u_R}_{ij}$ | $0$ |
| Q5 | $2+2X_0$ | $X_0/3+2/3\xi^{u_R}_{ii}$ | $-X_0/3+1/3\xi^{d_R}_{ii}$ | $2/3\xi^{u_R}_{ij}$ | $1/3\xi^{d_R}_{ij}$ |

Table 4.2: Axion couplings in potentially nucleophobic ($C_u \approx 2/3, C_d \approx 1/3$ achieved for $X_0 \simeq 0$) 3HDMs Q1-Q5, defined in Eq. (4.35) and Eq. (4.34), expressed in terms of flavor parameters $\xi^{q_P}_{ij}$ defined by Eq. (4.23) and vacuum angle $c_\beta \equiv \cos\beta, s_\beta \equiv \sin\beta$. The Q5 model is obtained from the Q4 structure and setting $h_c = h_0$. We denote contribution from quarks to the electromagnetic anomaly as $E_Q$.

which in matrix notation gives general Higgs couplings as

$$y_e \sim \begin{pmatrix} h^e_{ab} h^e_{a3} \\ h^e_{3a} h^e_{33} \end{pmatrix} . \tag{4.52}$$

Invariance of the lagrangian fixes 4 relations between the PQ charges of leptons and Higgses

$$\begin{aligned} X_{\ell_3} &= X_{e_3} - X_{h^e_{33}} , \qquad & X_{\ell_3} &= X_{e_a} - X_{h^e_{3a}} , \\ X_{\ell_a} &= X_{e_3} - X_{h_{a3}} , \qquad & X_{\ell_a} &= X_{e_a} - X_{h_{ab}} . \end{aligned} \tag{4.53}$$

Combining the equations in the first column by eliminating $X_{e_3}$ gives

$$X_{\ell_a} = X_{h^e_{33}} - X_{h^e_{a3}} + X_{\ell_3} , \tag{4.54}$$

which together with the first row of Eq. (4.53) gives the following relations between lepton and Higgses charges

$$X_{\ell_a} = X_{h^e_{33}} - X_{h^e_{a3}} + X_{\ell_3} , \qquad X_{e_a} = X_{h^e_{3a}} + X_{\ell_3} , \qquad X_{e_3} = X_{h^e_{33}} + X_{\ell_3} . \tag{4.55}$$

Similarly, combining the second column to eliminate $X_{e_a}$ gives

$$X_{\ell_a} = -X_{h^e_{ab}} + X_{h^e_{a3}} + X_{\ell_3} . \tag{4.56}$$

By combining Eq. (4.54) and Eq. (4.56) we find a single consistency condition

$$X_{h^e_{a3}} - X_{h^e_{33}} = X_{h^e_{ab}} - X_{h^e_{3a}} . \tag{4.57}$$

The electromagnetic anomaly coefficient from leptons $E_L$ is given by

$$E_L = -2X_{h^e_{ab}} - X_{h^e_{33}} , \tag{4.58}$$

By redefinition of leptons according to Eq. (3.28) axion derivative coupling is generated (with flipped sign). The chiral couplings read

$$\begin{aligned} C^{e_L}_{ij} &= \Big(X_{h^e_{a3}} - X_{h^e_{33}} - X_{\ell_3}\Big)\delta_{ij} - \Big(X_{h^e_{a3}} - X_{h^e_{33}}\Big)\delta_{i3}\delta_{j3} , \\ C^{e_R}_{ij} &= \Big(-X_{h^e_{3a}} - X_{\ell_3}\Big)\delta_{ij} + \Big(X_{h^e_{3a}} - X_{h^e_{33}}\Big)\delta_{i3}\delta_{j3} , \end{aligned} \tag{4.59}$$

where we have again intentionally split the coupling into part proportional to $\delta_{ij}$ and the universality breaking entry proportional to $\delta_{i3}\delta_{j3}$. The unitary transformation which diagonalizes the lepton mass matrix $\ell_i \to V^\ell_{ij}\ell_j$ leaves the first term unchanged resulting in couplings

$$
\begin{aligned}
C^{e_L}_{ij} &= \Big(X_{h^e_{a3}} - X_{h^e_{33}} - X_{\ell_3}\Big)\delta_{ij} - \Big(X_{h^e_{a3}} - X_{h^e_{33}}\Big)\xi^{e_L}_{ij}\,, \\
C^{e_R}_{ij} &= \Big(-X_{h^e_{3a}} - X_{\ell_3}\Big)\delta_{ij} + \Big(X_{h^e_{3a}} - X_{h^e_{33}}\Big)\xi^{e_R}_{ij}\,,
\end{aligned} \tag{4.60}
$$

where $\xi^{f_P}_{ij} \equiv (V^{fP})^*_{3i}(V^{fP})_{3j}$ control the flavor structure.

The consistency condition Eq. (4.57) can only be pairwise satisfied, giving 2 possible structures

$$
\begin{aligned}
X_{h_{a3}} = X_{h_{ab}} \equiv X_d \text{ and } X_{h_{33}} = X_{h_{3a}} \equiv X_e\,, \\
X_{h_{a3}} = X_{h_{33}} \equiv X_e \text{ and } X_{h_{ab}} = X_{h_{3a}} \equiv X_d\,.
\end{aligned} \tag{4.61}
$$

The definitions of $X_d, X_e$ are justified by the compact form of electron coupling below. Those models are universal LH ($\xi^{e_R} = 0$) or RH ($\xi^{e_L} = 0$) with lepton charges

$$
y_e \sim \begin{pmatrix} h_d h_e \\ h_d h_e \end{pmatrix} \quad [ER] \qquad \text{or} \qquad y_e \sim \begin{pmatrix} h_d h_d \\ h_e h_e \end{pmatrix} \quad [EL] \tag{4.62}
$$

. Electron coupling Eq. (3.51) with Eq. (3.48) in both models reads

$$
C_e = \frac{1}{2N}\left(-X_d + (X_d - X_e)\begin{cases} \xi^{e_R}_{11} & \text{ER} \\ \xi^{e_L}_{11} & \text{EL} \end{cases}\right). \tag{4.63}
$$

### 4.3.1 Lepton sector in 2HDM

In 2HDM, where both $X_e$ and $X_d$ are non-vanishing, tuning of $\xi_{11}$ is required to suppress electron couplings. There are 2 possibilities for identifying $h_d = h_0$ and $h_e = h_1 = h_d$ with $h_1$ and $h_e = h_0$ giving

$$
\begin{aligned}
\text{EL1}: \qquad & y_e \sim \begin{pmatrix} h_1 h_1 \\ h_0 h_0 \end{pmatrix}, \\
\text{EL2}: \qquad & y_e \sim \begin{pmatrix} h_0 h_0 \\ h_1 h_1 \end{pmatrix}.
\end{aligned} \tag{4.64}
$$

for universal LH models, which gives identical predictions for axion couplings as RH, upon replacing $\xi^{e_L}_{ij} \leftrightarrow \xi^{e_R}_{ij}$. Nucleophobia fixes the Higgs charges in terms of vacuum angle Eq. (4.39), and the final results for lepton couplings are given in Table 4.3. Note that models with single flavor violation cannot be simultaneously electro- and muon-phobic.

### 4.3.2 Lepton sector in 3HDM

In 3HDMs, suppression of the electron coupling can be achieved by simply choosing $h_d = h_0$ ($\xi_{11} = 0$) or $h_e = h_0$ ($\xi_{11} = 1$), since $X_0 \ll 0$, cf. Eq. (4.63). There are 5 distinct

| Model | $E_L/N$ | $C^A_{e_ie_i}$ | $C^{V,A}_{e_i\neq e_j}$ |
|---|---|---|---|
| EL1 | $2-6c^2_\beta$ | $-c^2_\beta+\xi^{e_L}_{ij}$ | $\mp\xi^{e_L}_{ij}$ |
| EL2 | $4-6c^2_\beta$ | $s^2_\beta-\xi^{e_L}_{ij}$ | $\pm\xi^{e_L}_{ij}$ |

Table 4.3: Axion-lepton couplings in potentially electrophobic 2HDM models EL1 and EL2 expressed in terms of flavor parameters $\xi^{q_P}_{ij}$ defined by Eq. (4.23) and vacuum angle $c_\beta\equiv\cos\beta, s_\beta\equiv\sin\beta$. Predictions for ER1 and ER2 couplings are identical, upon $\xi^{e_L}_{ij}\to\xi^{e_R}_{ij}$ and in the last column $\mp\xi^{e_L}_{ij}\to\xi^{e_R}_{ij}, \pm\xi^{e_L}_{ij}\to-\xi^{e_R}_{ij}$. We denote the contribution from leptons to the electromagnetic anomaly as $E_L$. Electrophobia is achieved by tuning $\xi^{e_L}_{11}\approx c^2_\beta$ (E1) and $\xi^{e_L}_{11}\approx s^2_\beta$ (E2).

| Model | $E_L/N$ | $C^A_{e_ie_i}$ | $C^{V,A}_{e_i\neq e_j}$ |
|---|---|---|---|
| E1 | $-4/3-2X_0$ | $-X_0/3-2/3\xi^{e_L}_{ij}$ | $\pm2/3\xi^{e_L}_{ij}$ |
| E2 | $2/3-2X_0$ | $-X_0/3+1/3\xi^{e_L}_{ij}$ | $\mp1/3\xi^{e_L}_{ij}$ |
| E3 | $-2X_0$ | $-X_0/3$ | $0$ |
| E4 | $-8/3-2X_0$ | $-2/3-X_0/3+2/3\xi^{e_L}_{ij}$ | $\mp2/3\xi^{e_L}_{ij}$ |
| E5 | $4/3-2X_0$ | $1/3-X_0/3-1/3\xi^{e_L}_{ij}$ | $\pm1/3\xi^{e_L}_{ij}$ |
| E6 | $-2/3-2X_0$ | $X_0/3+\delta_{i3}/3$ | $\mp\sqrt{2}/3(\delta_{i2}\delta_{j3}+\delta_{i3}\delta_{j2})$ |

Table 4.4: Axion-lepton couplings in potentially electrophobic 3HDM models EL1-6 expressed in terms of flavor parameters $\xi^{q_P}_{ij}$ defined by Eq. (4.23) and vacuum angle $c_\beta\equiv\cos\beta, s_\beta\equiv\sin\beta$. Predictions for ER1-6 couplings are identical, upon $\xi^{e_L}_{ij}\to\xi^{e_R}_{ij}$ and in the last column $\mp\xi^{e_L}_{ij}\to\xi^{e_R}_{ij}, \pm\xi^{e_L}_{ij}\to-\xi^{e_R}_{ij}$. We denote the contribution from leptons to the electromagnetic anomaly as $E_L$. Electrophobia is achieved for $X_0\simeq0$ in E3 model, and additionally $\xi^{e_L}_{11}\approx0$ (E1,E2) or $\xi^{e_L}_{11}\approx1$ (E4,E5). In the E6 model all lepton PQ charges are different.

choices (upon L $\leftrightarrow$ R)

$$\begin{aligned}
\text{E1}:&\quad y_e\sim\begin{pmatrix}h_0h_0\\h_1h_1\end{pmatrix},\\
\text{E2}:&\quad y_e\sim\begin{pmatrix}h_0h_0\\h_2h_2\end{pmatrix},\\
\text{E3}:&\quad y_e\sim\begin{pmatrix}h_0h_0\\h_0h_0\end{pmatrix},\\
\text{E4}:&\quad y_e\sim\begin{pmatrix}h_1h_1\\h_0h_0\end{pmatrix},\\
\text{E5}:&\quad y_e\sim\begin{pmatrix}h_2h_2\\h_0h_0\end{pmatrix}.
\end{aligned}\tag{4.65}$$

In the Table 4.4 we show the charges of the lepton sector in 3HDMs. Note that E1-E3 can be simultaneously electro- and muonphobic, in the absence of lepton flavor violation ($\xi_{33}=1$). Moreover, the E3 model has all couplings to leptons suppressed.

We can also relax the assumption of a **2+1** flavor structure, considering different PQ charges for each of the leptons. The consistency condition analogous to Eq. (4.57) gives two possible coupling structures

$$y_e \sim \begin{pmatrix} h_d h_e h_f \\ h_d h_e h_f \\ h_d h_e h_f \end{pmatrix} \quad [ER] \qquad \text{or} \qquad y_e \sim \begin{pmatrix} h_d h_d h_d \\ h_e h_e h_e \\ h_f h_f h_f \end{pmatrix} \quad [EL]\,. \tag{4.66}$$

Those are different from E1-E5 models only if $h_d \neq h_e \neq h_f$, which gives a simple formula for the electromagnetic anomaly

$$E_L = -X_d - X_e - X_f = -(3X_0 + A_1 + X_2) = -3X_0 - 1\,, \tag{4.67}$$

and

$$E_L/N = -\frac{2}{3}(3X_0 + 1) = -2X_0 - 2/3\,, \tag{4.68}$$

where we have used Eq. (4.35) for $2N = X_1 - X_2$ and Eq. (4.8) with $A_2 = 2, A_1 = -1$. The lepton couplings are given by

$$(C_e^A)_{ij} = \frac{1}{2N} \sum_k (V_{EP}^*)_{ki} (V_{EP})_{kj} X_k\,, \tag{4.69}$$

where $P = L(R)$ for EL (ER) and $X_k = \{X_d, X_e, X_f\}$. We can set both $C_e$ and $C_\mu$ to zero without introducing electron-muon LFV, $C_{e\mu} = 0$. This is achieved by setting $h_d = h_0, h_e = h_1, h_f = h_2$, giving

$$\text{E6}: \qquad y_e \begin{pmatrix} h_0 h_1 h_2 \\ h_0 h_1 h_2 \\ h_0 h_1 h_2 \end{pmatrix} \quad [EL] \qquad \text{or} \qquad y_e \sim \begin{pmatrix} h_0 h_0 h_0 \\ h_1 h_1 h_1 \\ h_2 h_2 h_2 \end{pmatrix} \quad [ER] \tag{4.70}$$

Using Eq. (4.3) and Eq. (4.69) for EL we find

$$(C_e^A)_{ij} = \frac{1}{3}[X_0 \delta_{ij} - (V_{EL}^*)_{2i} (V_{EL})_{2j} + 2 (V_{EL}^*)_{3i} (V_{EL})_{3j}]\,. \tag{4.71}$$

To avoid electron-muon LFV we can choose $V_{EL}$ to be just a rotation in the 2-3 sector,

$$V_{EL} = \begin{pmatrix} 1 & 0 & 0 \\ 0 & c_e & s_e \\ 0 & -s_e & c_e \end{pmatrix}, \tag{4.72}$$

which for $s_e = -\sqrt{1/3}, c_e = \sqrt{2/3}$, gives

$$(C_e^A)_{ij} = \frac{1}{3} X_0 \delta_{ij} + \frac{1}{3} \begin{pmatrix} 0 & 0 & 0 \\ 0 & 0 & \sqrt{2} \\ 0 & \sqrt{2} & 1 \end{pmatrix}. \tag{4.73}$$

We can read off the couplings in the E6 model

$$(C_e^A)_{ii} = \frac{1}{3} X_0 + \frac{1}{3} \delta_{i3}\,, \qquad (C_e^{V,A})_{i \neq j} = \mp \frac{\sqrt{2}}{3} (\delta_{i2} \delta_{j3} + \delta_{i3} \delta_{j2})\,. \tag{4.74}$$

For $X_0 \ll 1$ only $C_\tau$ and $C_{\tau\mu}$ are non-vanishing and the model is electro- and muonphobic.

## 4.4 Summary of astrophobic axion model

In the following sections, we collect all relevant astrophobic models, categorizing them by the suppressed couplings. We will also include an example of derivation of the results presented in the tables.

All presented quark models, denoted with Qn, are nucleophobic (and thus also pionphobic)

$$C_p = C_n \simeq 0 \to C_\pi \simeq 0\,, \tag{4.75}$$

and all lepton models, denoted with Em, are electrophobic

$$C_e \simeq 0\,. \tag{4.76}$$

Astrophobic axion models, denoted as QnEm arise from combining each of the quark sectors with each of the lepton sectors. In particular, the total electromagnetic anomaly coefficient is given by

$$E/N = E_Q/N + E_L/N\,. \tag{4.77}$$

**Example of finding an electrophobic model**

Let us show explicitly how models with suppressed couplings are found. As an example, let us take the simplest example of the lepton sector in the 2HDM. Recall, that nucleophobia fixes $c_\beta^2 = 2/3$, Eq. (4.39), and the lepton couplings in E1 model can be read off from Tab. 4.6, in particular the electron coupling is

$$C_e^A = -\frac{2}{3} + \xi_{11}^{e_L} = 0 \to \xi_{11}^{e_L} = \frac{2}{3}\,. \tag{4.78}$$

Using Eq. (4.25), and assuming that only one other $\xi_{ii} \neq 0$, equivalent to demanding only one source of LFV, we have two possibilities: 1) $\xi_{22}^{e_L} = 1/3$ and $\xi_{33}^{e_L} = 0$ or 2) $\xi_{33}^{e_L} = 1/3$ and $\xi_{22}^{e_L} = 0$. For 1) the flavor diagonal couplings are $C_\mu = -2/3 + 1/3 = -1/3$ and $C_\tau = -2/3$ and the flavor violating couplings are

$$C_{e_{12}}^V = C_{e_{12}}^A = \xi_{12}^{e_L} = \sqrt{\xi_{11}^{e_L}\xi_{22}^{e_L}} = \sqrt{\frac{2}{3}}\,, \tag{4.79}$$

while for 2) the flavor diagonal coupling are $C_\mu = -2/3$ and $C_\tau = -2/3 + 1/3 = -1/3$ and flavor violation is present only in tau-electron sector

$$C_{e_{13}}^V = C_{e_{13}}^A = \xi_{13}^{e_L} = \sqrt{\xi_{11}^{e_L}\xi_{33}^{e_L}} = \sqrt{\frac{2}{3}}\,. \tag{4.80}$$

Using definition of FV coupling in Eq. (3.49) we find that

$$1) \quad C_{\tau e} = \frac{2}{3} \qquad \text{or} \qquad 2) \quad C_{\mu e} = \frac{2}{3}\,. \tag{4.81}$$

A similar reasoning can be applied to the quark sector, demanding that $C_u = 2/3$ and $C_d = 1/3$ in each of the possible flavor structures.

| Model | $E_Q/N$ | $C_c^A$ | $C_s^A$ | $C_t^A$ | $C_b^A$ |
|---|---|---|---|---|---|
| Q1 | 14/3 | 2/3 | -2/3 | 2/3 | -2/3 |
| Q2$_a$ | 8/3 | 2/3 | 1/3 | -1/3 | -2/3 |
| Q2$_b$ | | 2/3 | -2/3 | -1/3 | 1/3 |
| Q2$_c$ | | -1/3 | 1/3 | 2/3 | -2/3 |
| Q2$_d$ | | -1/3 | -2/3 | 2/3 | 1/3 |
| Q3$_a$ | 8/3 | 2/3 | 1/3 | -1/3 | -2/3 |
| Q3$_b$ | | 2/3 | -2/3 | -1/3 | 1/3 |
| Q3$_c$ | | -1/3 | 1/3 | 2/3 | -2/3 |
| Q3$_d$ | | -1/3 | -2/3 | 2/3 | 1/3 |
| Q4 | 2/3 | -1/3 | 1/3 | -1/3 | 1/3 |

Table 4.5: Quark charges $C_q^A$ of astrophobic 2HDM models. All models have $C_u = 2/3$ and $C_d = 1/3$. We have intentionally neglected all models with quark flavor violation, as those models are highly constrained [235] and lead to unobservable $\Delta N_{\text{eff}}$.

| Model | $E_L/N$ | $C_\mu^A$ | $C_\tau^A$ | $C_{\mu e}^A$ | $C_{\tau e}^A$ |
|---|---|---|---|---|---|
| E1L$_a$ | -2 | -1/3 | -2/3 | $\mp\sqrt{2}/3$ | 0 |
| E1L$_b$ | | -2/3 | -1/3 | 0 | $\mp\sqrt{2}/3$ |
| E1R$_a$ | | -1/3 | -2/3 | $\sqrt{2}/3$ | 0 |
| E1R$_b$ | | -2/3 | -1/3 | 0 | $\sqrt{2}/3$ |
| E2L$_a$ | 0 | -1/3 | 1/3 | $\mp\sqrt{2}/3$ | 0 |
| E2L$_b$ | | 1/3 | -1/3 | 0 | $\mp\sqrt{2}/3$ |
| E2R$_a$ | | -1/3 | 1/3 | $\sqrt{2}/3$ | 0 |
| E2R$_b$ | | 1/3 | -1/3 | 0 | $\sqrt{2}/3$ |

Table 4.6: Lepton charges $C_\ell^A$ and lepton flavor violating couplings $C_{\ell\ell'}^A$ of all astrophobic 2HDM. All models are electrophobic, $C_e = 0$.

### 4.4.1 Summary of astrophobic axion 2HDMs

Let us first consider the minimal implementation of astrophobic axion, involving two Higgs doublets. The axion-quark couplings can be found in Tab. 4.1 and axion-lepton couplings are presented in the Tab. 4.3.

We present the results for possible quark-axion couplings in Tab. 4.5 and lepton-axion couplings in Table 4.3. In total, there are $10 \times 8 = 40$ distinct models obtained by combining each of the quark sectors with each of the lepton sectors. However, since we will consider axion thermal production at the tree level, we can organize the astrophobic 2HDMs by the absolute value of relevant couplings, which significantly reduces the clutter.

In the quark sector, the only relevant coupling that alters the thermal production of axion is the axion-strange coupling, which directly contributes to axion-kaon coupling (see Section 3.3.2). From Table 4.1 we see that $C_s^A = -2/3, 1/3$, which conveniently splits models into two categories.

Heavy quarks do not influence axion abundance because production at high temperatures is ineffective (see Section 5.1), and at low temperatures is Boltzmann-suppressed. This fact greatly simplifies the task of categorizing the astrophobic models and applies to our discussion of 3HDMs as well.

In the lepton sector, we will focus on models with flavor-violation in tau-electron rather than muon-electron. Note, that models with $C_{\mu e}^A \neq 0$ are constrained by TRIUMF [220] and TWIST [221] with lower bound $f_a \gtrsim \text{few} \times 10^8$ GeV. As a result, axion contribution to the effective number of neutrinos is well below the predicted sensitivity of CMB experiments. Therefore, we will focus on models that have lepton flavor violating coupling $C^{A,V}_{\tau e} \neq 0$: $E1L_b$, $E1R_b$ and $E2L_b$, $E2R_b$. The absolute value of this coupling is always $C_{\tau e} = \sqrt{(C^A_{\tau e})^2 + (C^V_{\tau e})^2} = 2/3$ in 2HDMs. It follows that there are two distinct scenarios for thermal axion production from leptons in 2HDM, which we will denote as $E1$ and $E2$, and which only differ by the axion-muon coupling $C_\mu = -2/3, 1/3$.

Finally, the axion photon couplings Eq. (3.108) are controlled by the electromagnetic anomaly coefficient, which takes values

$$\frac{E}{N} = \begin{cases} 14/3 & \text{Q1E2} \\ 8/3 & \text{Q2E2, Q3E2, Q1E1} \\ 2/3 & \text{Q4E2, Q2E1, Q3E1} \\ -4/3 & \text{Q4E1} \end{cases} . \tag{4.82}$$

### 4.4.2 Summary of astrophobic axion 3HDMs

| Model | $E_Q/N$ | $C^A_c$ | $C^A_s$ | $C^A_t$ | $C^A_b$ |
|---|---|---|---|---|---|
| Q1 | 14/3 | 2/3 | -2/3 | 2/3 | -2/3 |
| Q2$_a$ | 8/3 | 2/3 | 1/3 | -1/3 | -2/3 |
| Q2$_b$ | | 2/3 | -2/3 | -1/3 | 1/3 |
| Q2$_c$ | | -1/3 | 1/3 | 2/3 | -2/3 |
| Q2$_d$ | | -1/3 | -2/3 | 2/3 | 1/3 |
| Q3$_a$ | 8/3 | 2/3 | 1/3 | -1/3 | -2/3 |
| Q3$_b$ | | 2/3 | -2/3 | -1/3 | 1/3 |
| Q3$_c$ | | -1/3 | 1/3 | 2/3 | -2/3 |
| Q3$_d$ | | -1/3 | -2/3 | 2/3 | 1/3 |
| Q4 | 2/3 | -1/3 | 1/3 | -1/3 | 1/3 |
| Q5 | 2 | 0 | 0 | 0 | 0 |

Table 4.7: Table of quark charges $C^A_q$ in astrophobic axion 3HDM derived from Table 4.2 assuming no quark flavor violation. All models have $C_u = 2/3$ and $C_d = 1/3$, required by nucleophobia Eq. (4.1). The table is identical to Table 4.5 with an additional Q5 model, obtained from Q4 structure Eq. (4.35) by setting $h_c = h_0$.

| Model | $E_L/N$ | $C^A_\mu$ | $C^A_\tau$ | $C^A_{\mu e}$ | $C^A_{\tau e}$ |
|---|---|---|---|---|---|
| E1$_a$ | -4/3 | -2/3 | 0 | 0 | 0 |
| E1$_b$ | | 0 | -2/3 | 0 | 0 |
| E2$_a$ | 2/3 | 1/3 | 0 | 0 | 0 |
| E2$_b$ | | 0 | 1/3 | 0 | 0 |
| E3 | 0 | 0 | 0 | 0 | 0 |
| E4$_a$ | -8/3 | -2/3 | -2/3 | 0 | 0 |
| E5$_a$ | 4/3 | 1/3 | 1/3 | 0 | 0 |
| E6 | -2/3 | 0 | 1/3 | 0 | $\sqrt{2}/3$ |

Table 4.8: Table of lepton charges $C^A_\ell$ and lepton flavor-violating axion couplings $C^A_{\ell\ell'}$ in astrophobic axion 3HDM derived from Table 4.4. All models are electrophobic, $C_e = 0$.

We can now move on to the generalization of astrophobic axion models to three Higgs doublets. Assuming no quark flavor violation, nucleophobia fixes the possible quark couplings, which are presented in Table 4.7. On the other hand, electrophobia in 3HDMs can be realized by lepton couplings presented in Table 4.8.

The quark sector remains similar to 2HDMs with an additional Q5 model, where all quark couplings, except for $C_u$ and $C_d$, vanish. Consequently, the strange coupling charges, which determine axion-kaon coupling Eq. (3.101) may take three values $C_s = -2/3, 1/3, 0$.

The lepton sector differs substantially in 3HDM. Assuming a **2+1** flavor structure results in no LFV required to suppress the axion-electron coupling. Moreover, besides $C_e$, it is also possible to suppress other lepton couplings. Relaxing the assumption of flavor structure in the E6 model allows for suppression of axion-muon coupling if LFV is reintroduced. We categorize models based on coupling suppression, emphasizing the common phenomenological features of astrophobic models.

### Muonphobia

Axion-muon coupling $C_\mu$ in 2+1 flavor structure is suppressed in $E1_b$, $E2_b$ and $E3$ models, while axion-tau coupling is suppressed in $E1_a$, $E2_a$ and $E3$. Axion-muon coupling is constrained by SN1987A, Eq. (3.115), while axion-tau coupling is unprobed, hence we will be interested in models with $C_\mu = 0$. From now on, we will drop subscript $b$ and denote muonphobic lepton sectors as simply E1, E2, and E3. By combining these lepton sectors with any of the quarks sectors we identify in total 15 muonphobic models. This suppression is realized without LFV $C_{\tau e} = C_{\tau\mu} = 0$. Hence, the distinction between the models comes from axion-tau coupling $C_\tau = -2/3, 1/3, 0$ for E1, E2, E3 and the axion-strange coupling $C_s = -2/3, 1/3, 0$ for (Q1, Q2), (Q2,Q4) and Q5.

The axion-photon coupling determined by the electromagnetic anomaly

$$E/N \in \{16/3, 14/3, 10/3, 8/3, 2, 4/3, 2/3, -2/3\},$$

and can be suppressed in Q5E3 ($E/N = 2$), however, we will consider this very special model separately and call naturally astrophobic axion [60], hence the number of muonphobic models is 14. The lower bound from HB Eq. (3.117) varies in muonphobic models between $10^7$ GeV for $E/N = 8/3$ (Q2E3, Q3E3, Q5E2) and $E/N = 4/3$ (Q2E1, Q3E1, Q4E2) up to $6 \times 10^7$ GeV for $E/N = 16/3$ (Q1E2).

### Photophobia

Axion-photon coupling is suppressed in models with $E/N = 2$ (cf. Eq. (3.108)), realized in Q1E4 and Q4E5 models (neglecting both muon- and photophobic Q5E3 model with distinct phenomenology). The HB bound, Eq. (3.117), in these models allows for $f_a \simeq \mathcal{O}(10^6)$ GeV and the strongest non-cosmological bound comes from axion-muon coupling $C_\mu = -2/3(1/3)$ in Q1E4 (Q4E5) model and allows for $f_a \simeq 8 \times 10^6$ $(4 \times 10^6)$ GeV in Q1E4 (Q4E5).

The photophobic models differ by the axion-strange coupling $C_s = -2/3, (0)$ Q1E4 (Q4E5), axion-muon and axion-tau couplings $C_\mu = C_\tau = -2/3(1/3)$ in Q1E4 (Q4E5) model. Axion-muon couplings set a lower bound $f_a > 4 \times 10^6$ $(8 \times 10^6)$ GeV in Q1E4 (Q4E5) model. Electrophobia in those models is achieved without LFV.

### Properly astrophobic axion

It is possible to simultaneously suppress axion-photon and axion-muon coupling in models with 1+1+1 lepton flavor structure, Q2E6, and Q3E6. Because such suppression indeed escapes all astrophysical constraints, we denote this model as proper astrophobic. Those models differ only by the strange coupling $C_s = 2/3, -1/3$ and predict the LFV, which allows for sizable thermal axion production discussed in the following section. The lower bound on $f_a$ comes from axion-nucleon coupling generated by higher-order corrections and is of order $10^6$ GeV, but the exact value depends on the details of the model and uncertainties of lattice determination of $m_u/m_d$ [60].

### Naturally astrophobic axion

Finally, we consider naturally astrophobic axion realized in model Q5E3 and introduced in Ref. [60]. The only quarks with non-vanishing PQ charges are up and down, with couplings fixed by nucleophobia, $C_u = 2/3$ and $C_d = 1/3$. Most importantly, the condition $X_0 \ll 1$ can be realized without fine-tuning usually required in 3HDM for perturbative unitarity of heavy quark Yukawas as shown in Fig. 4.1. As there are no couplings to leptons, and the electromagnetic anomaly is $E/N = 2$, the astrophysical bounds do not constrain this model and $f_a \simeq 10^6$ GeV may be possible.

It is worth mentioning, that naturally astrophobic axion may be UV completed not only within 3HDM but also with new vector-like quarks [60].

# Chapter 5

# Hot axions contribution to the dark radiation

In this chapter, we will present the original findings published in Ref. [209]. In Sec. 5.1 we introduce the parametrization of axion energy density via the number of effective degrees of freedom, $\Delta N_{\text{eff}}$, and discuss its limitations. In Sec. 5.2 we recall the bound on the effective number of neutrinos from CMB and we discuss how we apply findings from Ref. [62] to the astrophobic axion models. In Sec. 5.3 we review the analytical calculation of scattering and decay rates, which directly enter the Boltzmann equation and, consequently, influence the cosmological abundance of axions. In particular, results in Sec. 5.3.4 are original contributions of this thesis. Finally, in Sec. 5.5 we present the original results of astrophobic axion contribution to the effective number of neutrinos, following the categorization of models introduced in Sec. 4.4.1 and Sec. 4.4.2.

## 5.1 Contribution to $\Delta N_{\text{eff}}$ from massless species

If axions have been in thermal contact with the SM bath, they would be produced in scatterings and decays, behaving as relativistic species, similarly to neutrinos. The Universe with additional, besides neutrinos, hot relics has a larger Hubble parameter at the time of recombination which results in increased dumping of CMB power spectrum [143].

The total radiation energy density is a sum of the contributions of relativistic species

$$\rho_r = \rho_\gamma + \rho_\nu + \rho_a \,, \tag{5.1}$$

where $\rho_\gamma$ is energy density of photons, $\rho_\nu$ is energy density of neutrinos and $\rho_a$ is energy density of axions. We parameterize the axion contribution to radiation energy density with an additional effective number of neutrinos

$$\rho_r = \rho_\gamma \left( 1 + \frac{7}{8} N_{\text{eff}} \left( \frac{T_\nu}{T_\gamma} \right)^{4/3} \Big|_{\text{CMB}} \right) , \tag{5.2}$$

where factor 7/8 comes from energy density of neutrinos, Eq. (B.2.24), and

$$N_{\text{eff}} = N_{\text{eff}}^{\text{SM}} + \Delta N_{\text{eff}} \,, \tag{5.3}$$

where the SM value is $N_{\text{eff}}^{\text{SM}} = 3.0432(2)$ [236], which deviates from 3 because of non-instantaneous neutrino decoupling, neutrino interactions, neutrino oscillations, and QED corrections. Any additional contribution to the effective number of neutrinos must come from new physics and for axions is defined

$$\Delta N_{\text{eff}} = \frac{8}{7}\left(\frac{11}{4}\right)^{4/3}\frac{\rho_a}{\rho_\gamma}\bigg|_{\text{CMB}}. \tag{5.4}$$

For exactly massless species, the latest bound from the CMB is [21]

$$\Delta N_{\text{eff}} < 0.3 \qquad\qquad \text{at } 95\%\ \text{CL}\,, \tag{5.5}$$

while predicted sensitivity of Simons Observatory should reach $\Delta N_{\text{eff}}^{\text{Sim}} = 0.1$ [237]. Eventually, the CMB-S4 experiments will enhance the sensitivity down to $\Delta N_{\text{eff}}^{\text{CMB}-\text{S4}} = 0.054$ [238].
Axions during BBN contribute to the dark radiation since $T_{\text{BBN}} \gg m_a$, and can hence alter the abundances of light elements. This yields a lower limit on $\Delta N_{\text{eff}}$ similar to the CMB bound Eq. (5.5) [239, 240].

Recall, that assuming the equilibrium distribution function, the number density and energy density in relativistic limit are given by (see Appendix B)

$$n_i = g_i\frac{\zeta(3)}{\pi^2}T_i^3\,, \tag{5.6}$$

$$\rho_i = g_i\frac{\pi^2}{30}T_i^4\,, \tag{5.7}$$

where $g_i$ is the number of degrees of freedom of species $i$ and we have accounted for a fact, that if $i$ is not in thermal equilibrium $T_i \neq T_\gamma$. We can eliminate temperature by expressing axion energy density by axion number density

$$\begin{aligned} T_a &= \left(\frac{\pi^2}{\zeta(3)}n_a\right)^{1/3}, \\ \rho_a &= \frac{\pi^2}{30}\left(\frac{\pi^2}{\zeta(3)}n_a\right)^{4/3}. \end{aligned} \tag{5.8}$$

Above, we have used that axion is pNGB with $g_a = 1$. On the other hand, for energy density of photons and total entropy density are (see Appendix B)

$$\rho_\gamma = \frac{\pi^2}{15}T^4\,, \tag{5.9}$$

$$s = g_{*s}(T)\frac{2\pi^2}{45}T^3\,, \tag{5.10}$$

where we have omitted subscript $\gamma$, $T = T_\gamma$, for photons temperature. Using those, we can express the energy density of photons in terms of entropy density, eliminating temperature

$$\rho_\gamma = \frac{\pi^2}{15}\left(\frac{s}{g_{*s}(T)}\frac{45}{2\pi^2}\right)^{4/3}. \tag{5.11}$$

Plugging that to Eq. (5.4) we find

$$\begin{aligned} \Delta N_{\text{eff}} =& \frac{8}{7}\left(\frac{11}{4}\right)^{4/3}\frac{\pi^2}{30}\left(\frac{\pi^2}{\zeta(3)}n_a\right)^{4/3}\frac{15}{\pi^2}\left(\frac{g_{*s}(T)}{s}\frac{2\pi^2}{45}\right)^{4/3} = \\ =& \frac{4}{7}\left(\frac{11}{4}\right)^{4/3}\left(\frac{2\pi^2}{45\zeta(3)}g_{*s}(T)\frac{n_a}{s}\right)\bigg|_{\text{CMB}}^{4/3} = \\ =& \frac{4}{7}\left(\frac{11}{4}\right)^{4/3}\left(\frac{2\pi^2}{45\zeta(3)}g_{*s}(T_{\text{CMB}})Y_a\bigg|_{\text{CMB}}\right)^{4/3}, \end{aligned} \tag{5.12}$$

where in the last equality we have used the definition of comoving number density $Y_a = n_a/s$. The simplified formula might be found by simply letting $g_{*s}(T_{\text{CMB}}) = g_{*s}^{\text{SM}}(T_{\text{CMB}}) = 2 + (7/8) \times 3 \times 2 \times (4/11) = 43/11$ with numerical result

$$\Delta N_{\text{eff}} = 74.85 Y_a^{4/3}\Big|_{\text{CMB}} . \tag{5.13}$$

Moreover, we can find an approximate formula for $\Delta N_{\text{eff}}$, if axions thermalize. The comoving number density is constant if there are no interactions between axions and thermal bath, cf. Sec. 5.3, thus

$$Y_a^{\text{CMB}} = Y_a(T_d) = \frac{n_a(T_d)}{s(T_d)} = \frac{45\zeta(3)}{2\pi^2} g_{*s}(T_d)^{-1} , \tag{5.14}$$

where $T_d$ is the decoupling temperature at which axions freeze-out, and interactions cease. We can estimate this temperature using condition $\Gamma(T_d) = H(T_d)$. Conveniently, we find that for freeze-out scenario $\Delta N_{\text{eff}}$ is simply related to the number of entropic degrees of freedom at the time of decoupling

$$\Delta N_{\text{eff}} \simeq \frac{4}{7}\left(\frac{11}{4}\right)^{4/3} \left(\frac{g_{*s(T_{\text{CMB}})}}{g_{*s(T_d)}}\right)^{4/3} \simeq 13.7 g_{*s}(T_d)^{-4/3} . \tag{5.15}$$

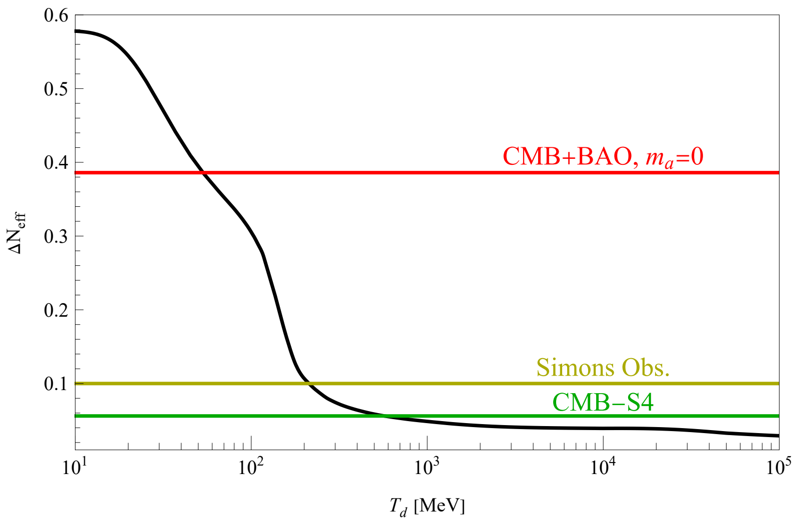


Figure 5.1: Approximate values of $\Delta N_{\text{eff}}$, assuming freeze-out at temperature $T_d$ according to Eq. (5.15) (black). We also include the bound from CMB+BAO [62] assuming massless axion (red) and predicted sensitivities of Simons Observatory [237] (dark yellow) and CMB-S4 [238] (dark green).

However, if axions contribute to relativistic degrees of freedom, they should also be included in the entropic degrees of freedom in Eq. (5.12):

$$g_{*s}(T_{\text{CMB}}) = g_{*s}^{\text{SM}}(T_{\text{CMB}}) + g_{*s}^{a}(T_{\text{CMB}}) . \tag{5.16}$$

To find unknown contribution from axions, note that the entropy density of axions is given by

$$s = \frac{2\pi^2}{45} T_a^3 , \tag{5.17}$$

while their contribution to the entropy density of the thermal bath is given by

$$s = g_{*s}^a(T_\gamma)\frac{2\pi^2}{45}T_\gamma^3\,, \tag{5.18}$$

where we have reintroduced the subscript $\gamma$ to highlight that the temperature of the thermal bath is identified with the temperature of photons. By letting the number of degrees of freedom depend on the temperature, we encode the information about the independent evolution of axions after freeze-out. Of course, those two must be equal due to entropy conservation

$$g_{*s}^a(T)T_\gamma^3 = T_a^3\,, \tag{5.19}$$

from which it follows, that

$$g_{*s}^a(T) = \left(\frac{T_a}{T_\gamma}\right)^3. \tag{5.20}$$

It can be further simplified using Eq. (5.8) and Eq. (5.10)

$$\begin{aligned} g_{*s}^a(T_{\mathrm{CMB}}) = \left(\frac{T_a}{T_\gamma}\right)^3\Big|_{\mathrm{CMB}} &= \frac{\pi^2}{\zeta(3)}n_a\frac{45}{2\pi^2}\frac{g_{*s}(T_{\mathrm{CMB}})}{s} = \frac{2\pi^4}{45\zeta(3)}Y_a(T_{\mathrm{CMB}})g_{*s}(T_{\mathrm{CMB}}) = \\ &= \frac{2\pi^4}{45\zeta(3)}Y_a(T_{\mathrm{CMB}})\Big(g_{*s}^{\mathrm{SM}}(T_{\mathrm{CMB}}) + g_{*s}^a(T_{\mathrm{CMB}})\Big)\,. \end{aligned} \tag{5.21}$$

From that, we can find

$$g_{*s}^a(T_{\mathrm{CMB}}) = \frac{\frac{2\pi^4}{45\zeta(3)}Y_a(T_{\mathrm{CMB}})}{1-\frac{2\pi^4}{45\zeta(3)}Y_a(T_{\mathrm{CMB}})}g_{*s}^{\mathrm{SM}}(T_{\mathrm{CMB}})\,. \tag{5.22}$$

Hence, the total number of entropic degrees of freedom is

$$\begin{aligned} g_{*s}^{\mathrm{SM}}(T_{\mathrm{CMB}}) + g_{*s}^a(T_{\mathrm{CMB}}) &= g_{*s}^{\mathrm{SM}}(T_{\mathrm{CMB}})\left(1+\frac{\frac{2\pi^4}{45\zeta(3)}Y_a(T_{\mathrm{CMB}})}{1-\frac{2\pi^4}{45\zeta(3)}Y_a(T_{\mathrm{CMB}})}\right) = \\ &= \frac{g_{*s}^{\mathrm{SM}}(T_{\mathrm{CMB}})}{1-\frac{2\pi^4}{45\zeta(3)}Y_a(T_{\mathrm{CMB}})}\,. \end{aligned} \tag{5.23}$$

Plugging that into Eq. (5.12) we find our final formula for $\Delta N_{\mathrm{eff}}$:

$$\begin{aligned} \Delta N_{\mathrm{eff}} &= \frac{4}{7}\left(\frac{11}{4}\right)^{4/3}\left(\frac{2\pi^2}{45\zeta(3)}\Big(g_{*s}^{\mathrm{SM}}(T_{\mathrm{CMB}}) + g_{*s}^a(T_{\mathrm{CMB}})\Big)Y_a^{\mathrm{CMB}}\right)^{4/3} = \\ &= \frac{4}{7}\left(\frac{11}{4}\right)^{4/3}\left(\frac{\frac{2\pi^2}{45\zeta(3)}g_{*s}^{\mathrm{SM}}(T_{\mathrm{CMB}})}{1-\frac{2\pi^4}{45\zeta(3)}Y_a(T_{\mathrm{CMB}})}Y_a(T_{\mathrm{CMB}})\right)^{4/3}\,. \end{aligned} \tag{5.24}$$

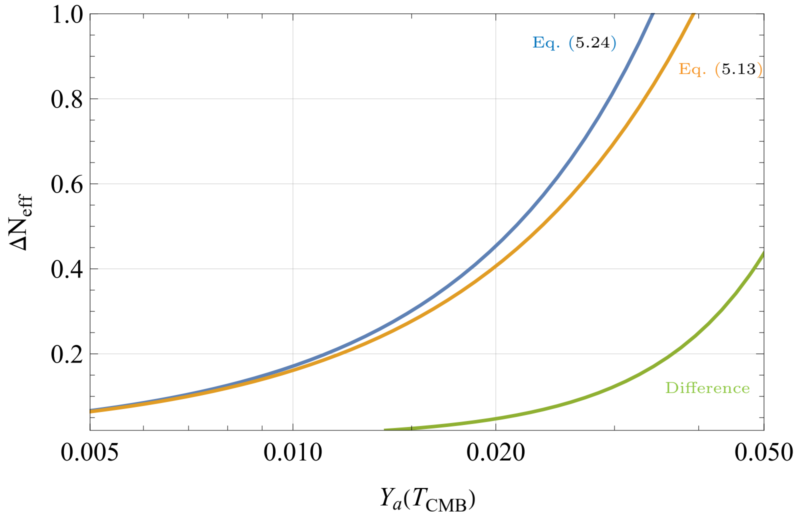


Figure 5.2: A plot comparing formulas for $\Delta N_{\rm eff}$ from equation Eq. (5.24) (blue) and Eq. (5.13) (orange) and their difference (green). At small $Y_a(T_{\rm CMB})$ the axion contribution to the $g_{*s}$ is negligible and the difference between formulas is small, but for large axion abundance, it rapidly grows. In all numerical calculations we use Eq. (5.24).

The axion contribution to the effective number of neutrinos explicitly depends on the $g_{*s}$. However, the bounds we derive do not depend strongly on the exact dependence of $g_{*s}$ on the temperature we use, which has also been noted in [241]. In our numerical calculations we use results from Ref. [242] but we have checked explicitly that using $g_{*s}(T)$ from Ref. [243] doesn't alter our results.

As noted in Ref. [209], formula Eq. (5.24) underestimates contribution to the $\Delta N_{\rm eff}$ in freeze-in. We used the relation between the temperature of axions and number density, Eq. (5.8), which holds as long as axions follow the thermal distribution. Consequently, the typical axion energy is roughly $\rho_a/n_a \sim n_a^{1/3}$, which in freeze-in is smaller than the actual energy of axions produced by thermally by scatterings of SM plasma, $(n_a^{\rm eq})^{1/3} \sim T$. Therefore, we underestimate the axion energy density used in Eq. (5.4) for freeze-in.

More precise estimation of $\rho_a$ can be obtained using

$$\rho_{a,1} = \rho_a^{\rm eq} \frac{n_a}{n_a^{\rm eq}}\,, \tag{5.25}$$

which we will compare with

$$\rho_{a,2} = \frac{\pi^2}{30}\left(\frac{\pi^2 n_a}{\zeta(3)}\right)^{4/3}. \tag{5.26}$$

Taking the ratio and using approximate formula Eq. (5.13) to find

$$\frac{\rho_{a,2}}{\rho_{a,1}} \simeq 0.5\left(\frac{\Delta N_{\rm eff}}{0.05}\right)^{1/4}\left(\frac{g_{*s}(T_{\rm FI})}{10}\right)^{1/3}. \tag{5.27}$$

The most underestimated region is $\Delta N_{\rm eff} < 0.05$. The most underestimated channel turns out to be muon scattering with $g_{*s}(T_{\rm FI}) \simeq 10$. From the formula, it is clear that for the phenomenologically relevant region, which is within the sensitivity of CMB-S4, the underestimation is at most by a factor of 2. However, since in freeze-in $\Delta N_{\rm eff} \sim f_a^{-8/3}$, it translates to change in bounds by at most 30%. This underestimation of $\Delta N_{\text{eff}}$ can be avoided by solving the Boltzmann equation for energy density, instead of number density[1].

## 5.2 Massive axion and the CMB

We have derived the mass of the QCD axion, which is small compared to the particles of the SM. Satisfying the astrophysical constraints usually requires $f_a \gtrsim 4 \times 10^8$ GeV, which translates via Eq. (3.79) to mass $m_a \lesssim 15$ meV. However, since astrophobic axions can be significantly heavier, with the mass of order eV, bounds from the previous section may not apply.

The CMB analysis in Ref. [62] allowed for two additional parameters, the mass of the axion and $\Delta N_{\text{eff}}$, to the standard cosmology. As a result, the authors derived the bound on the axion abundance in the $(m_a, \Delta N_{\text{eff}})$ plane, which we reproduce in Fig. 5.3. For the QCD axion, it can be translated into bound in $(f_a, \Delta N_{\text{eff}})$ plane using Eq. (3.79). In practice, since the $\Delta N_{\text{eff}}$ axis in Fig. 5.3 is neither linear nor logarithmic, we have digitalized the bound in plane $(m_a, T_d)$. Assuming freeze-out of axions, which is justified for larger values of $\Delta N_{\text{eff}}$ and smaller $f_a$, we have used Eq. (5.15) to relate $T_d$ to $\Delta N_{\text{eff}}$. In all results of this section, we will be using this bound which is manifested in mass-dependent bound on the additional number of neutrinos.

## 5.3 Explicit contributions to the Boltzmann equation for axion

In Sec. 5.1, we have shown how the energy density of axions can be parameterized by additional effective degrees of freedom $\Delta N_{\text{eff}}$. The formulas Eq. (5.24) and Eq. (5.12) depend on the comoving number density evaluated at time of recombination $Y_a(T_{\text{CMB}})$, whose evolution is governed by the integrated Boltzmann equation, Eq. (B.3.45)

$$sHx\frac{dY_a}{dx} = \left(1 - \frac{x}{3g_{*s}}\frac{dg_{*s}}{dx}\right)n_a^{\text{eq}}\sum_i \Gamma_i\left(1 - \frac{Y_a}{Y_a^{\text{eq}}}\right), \tag{5.28}$$

where the sum runs over all processes leading to the thermalization of axions and $x = m/T$ with mass $m$ of the heaviest particle involved in thermalization. We choose throughout this chapter $m = m_\tau = 1776.86$ MeV. We assume that initial axions have vanishing axion abundance, which yields the most conservative bound.

We will follow the same momentum convention of Ref. [241], where incoming particles have momentum $p_1$ and $p_2$, outgoing axion has momentum $k$ and another outgoing particle has momentum $p_3$. We have used FeynCalc [245,246] to find the expressions for the squares of amplitudes.

### 5.3.1 Lepton scatterings

There are two tree-level lepton scatterings that produce axions: a) $\ell^\pm\gamma \leftrightarrow \ell^\pm a$ and b) $\ell^+\ell^- \leftrightarrow a\gamma$.

[1]During work on the thesis Ref. [244] have been published which resolves the issue by solving the full Boltzmann equation for the axion distribution function. The energy density, and consequently $\Delta N_{\text{eff}}$ is found via Eq. (B.2.22).

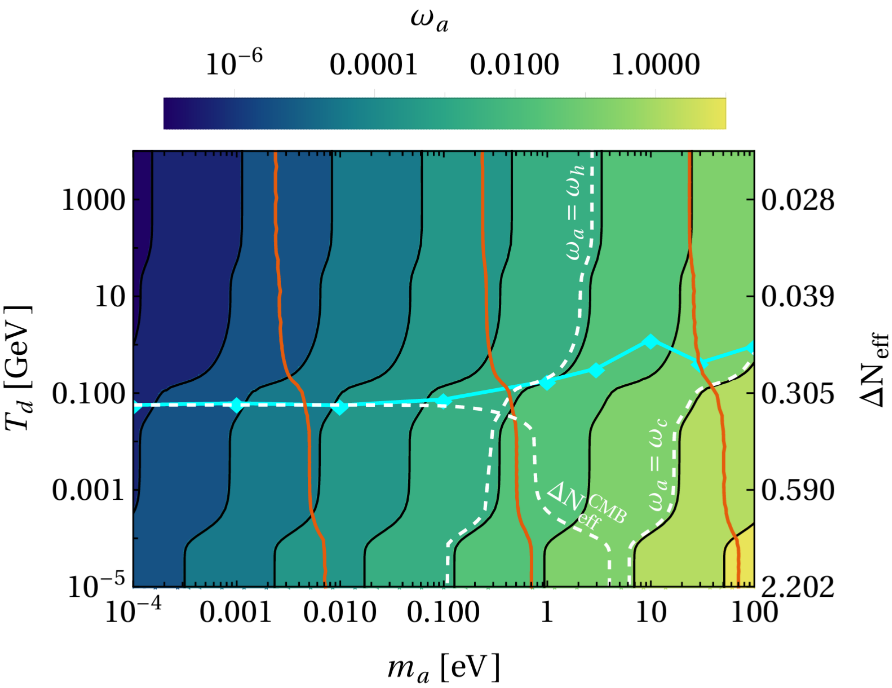


Figure 5.3: Plot from Ref. [62] showing the relic abundance of axions as a function of axion mass $m_a$ and the decoupling temperature $T_d$. The cyan line shows the bound on the axion decoupling temperature as a function of axion mass, which we have used for the bounds on the hot astrophobic axions. For small $m_a$, the bound coincides with the usual $\Delta N_{\rm eff}$ bounds from Planck. For larger mass, $m_a \simeq 1$ eV, axions behave as warm dark matter, and the bound coincides with the contour $\omega_h$, while for heavier axions the bound approaches the cold dark matter bound, contour $\omega_c$.

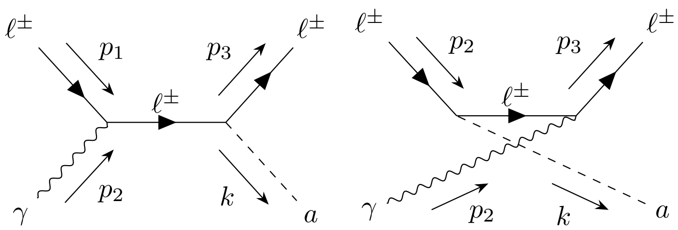


First, let's calculate the cross-section for a). This process has contributions from $s$ and $u$ channels and the corresponding amplitudes are given by

$$\begin{aligned}\mathcal{M}^s_{\ell^\pm\gamma\to\ell^\pm a} &= \frac{iC_\ell e}{2f_a}\epsilon_\mu(p_2)k_\nu\overline{u}(p_3)\gamma^\nu\gamma^5\frac{\not{p}_1-\not{p}_2+m_\ell}{s-m_\ell^2}\gamma^\mu u(p_1)\,,\\ \mathcal{M}^u_{\ell^\pm\gamma\to\ell^\pm a} &= \frac{iC_\ell e}{2f_a}\epsilon_\mu(p_2)k_\nu\overline{u}(p_3)\gamma^\mu\frac{\not{p}_1-\not{k}+m_\ell}{u-m_\ell^2}\gamma^\nu\gamma^5 u(p_1)\,.\end{aligned} \tag{5.29}$$

Accounting for the average over initial polarizations of fermion (1/2) and photon (1/2), the square of the amplitude is given by

$$\frac{1}{4}|\mathcal{M}|^2_{\ell^\pm\gamma\to\ell^\pm a} = \frac{C_\ell^2 e^2}{4f_a^2}\frac{1}{(s-m_\ell^2)(u-m_\ell^2)} \times \Big(m_\ell^2\Big(s^2+2s(3t+u)+t^2+6tu-3u^2\Big) \\ -2m_\ell^4(s+5t-u) - u\Big(s^2+2st+t^2-u^2\Big)\Big)\,, \tag{5.30}$$

which simplifies considerably by removing $u$ using $s+u+t=\sum_i m_i^2 = 2m_\ell^2 + m_a^2 \simeq 2m_\ell^2$

$$\frac{1}{4}|\mathcal{M}|^2_{\ell^\pm+\gamma\to\ell^\pm+a} = \frac{C_\ell^2 e^2}{4f_a^2}\frac{m_\ell^2 t^2}{(s-m_\ell^2)(s+t-m_\ell^2)}\,. \tag{5.31}$$

To find the cross section we follow Ref. [13], for details and definitions of $p_1^{\rm CM}$, $p_2^{\rm CM}$, $t_0$ and $t_1$ see Appendix A.3. The momenta in the centre of the mass frame are

$$p_1^{\rm CM} = p_2^{\rm CM} = \frac{s-m_\ell^2}{2\sqrt{s}}\,, \tag{5.32}$$

from which it follows that $t$ varies between

$$\begin{aligned} t_0 &= 0\,,\\ t_1 &= -\frac{(s-m_\ell^2)^2}{s}\,. \end{aligned} \tag{5.33}$$

Finally, we find the cross section as a function of the centre of mass energy $s$

$$\sigma_{\ell^\pm\gamma\to\ell^\pm a}(s) = \frac{C_\ell^2 e^2}{32\pi f_a^2}\frac{m_\ell^2(2s^2\log(s/m_\ell^2)+4m_\ell^2 s - 3s^2 - m_\ell^4)}{s^2(s-m_\ell^2)}\,. \tag{5.34}$$

Note, that the cross section at first glance seems to be divergent in limit $s\to m_f^2$. However, the numerator also vanishes in this limit and using the l'Hospital rule

$$\begin{aligned}\lim_{s\to m_\ell^2}\sigma_{\ell^\pm\gamma\to\ell^\pm a}(s) =& \frac{C_\ell^2 e^2 m_\ell^2}{32\pi f_a^2}\lim_{s\to m_\ell^2}\frac{(2s^2\log(s/m_\ell^2)+4m_\ell^2 s-3s^2-m_\ell^4)}{s^2(s-m_\ell^2)} = \\ & \frac{C_\ell^2 e^2 m_\ell^2}{32\pi f_a^2}\lim_{s\to m_\ell^2}\frac{(4s\log(s/m_\ell^2)+4m_\ell^2-4s)}{2s(s-m_\ell^2)+s^2} = 0\,,\end{aligned} \tag{5.35}$$

where in the last limit clearly the denominator is finite while the numerator vanishes.

We can perform a similar calculation for process b), to which $t$- and $u$- channels contribute.

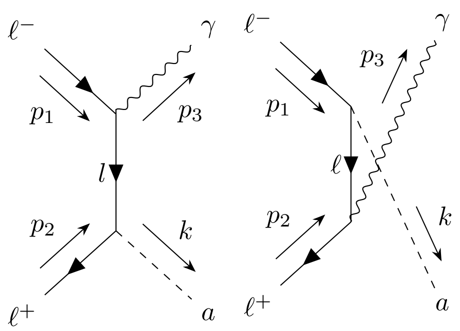

The amplitudes are

$$\begin{aligned}\mathcal{M}^t_{\ell^+\ell^-\to\gamma a} &= \frac{iC_\ell e}{2f_a}\epsilon_\mu(p_3)k_\nu\overline{v}(p_2)\gamma^\nu\gamma^5\frac{\not p_1-\not p_3+m_\ell}{t-m_\ell^2}\gamma^\mu u(p_1)\,,\\ \mathcal{M}^u_{\ell^+\ell^-\to\gamma a} &= \frac{iC_\ell e}{2f_a}\epsilon_\mu(p_3)k_\nu\overline{v}(p_2)\gamma^\mu\frac{\not p_1-\not k+m_\ell}{u-m_\ell^2}\gamma^\nu\gamma^5 u(p_1)\,.\end{aligned}\tag{5.36}$$

Accounting for the average over initial polarizations of fermions ($1/2\times 1/2$), the square of the amplitude is given by

$$\begin{aligned}\frac{1}{4}|\mathcal{M}|^2_{\ell^+\ell^-\to\gamma a} =&\frac{C_\ell^2e^2}{4f_a^2}\frac{1}{(m_\ell^2-t)(m_\ell^2-u)}\Big(2m_\ell^4(5s+t-u)+u\Big(s^2+2st+t^2-u^2\Big)\\ &-m_\ell^2\Big(s^2+6s(t+u)+t^2+2tu-3u^2\Big)\Big)\,.\end{aligned}\tag{5.37}$$

It again simplifies greatly upon using $s+u+t=\sum_i m_i^2=2m_\ell^2$

$$\frac{1}{4}|\mathcal{M}|^2_{\ell^+\ell^-\to\gamma a} = \frac{C_\ell^2e^2}{f_a^2}\frac{m_\ell^2s^2}{(m_\ell^2-t)(s+t-m_\ell^2)}\,.\tag{5.38}$$

The momenta in the centre of the mass frame are

$$\begin{aligned}p_1^{\mathrm{CM}} &= \sqrt{\frac{s}{4}-m_\ell^2}\,,\\ p_2^{\mathrm{CM}} &= \frac{\sqrt{s}}{2}\,.\end{aligned}\tag{5.39}$$

The variable $t$ varies between

$$\begin{aligned}t_0 &= -\frac{1}{4}\Big(\sqrt{s}-\sqrt{s-4m_\ell^2}\Big)^2\,,\\ t_1 &= -\frac{1}{4}\Big(\sqrt{s}+\sqrt{s-4m_\ell^2}\Big)^2\,.\end{aligned}\tag{5.40}$$

Finally, we find the cross section as a function of the centre of mass energy $s$ by integrating over $t$ from $t_1$ to $t_0$

$$\sigma_{\ell^+\ell^-\to\gamma a}(s) = \frac{C_\ell^2e^2}{8\pi f_a^2}\frac{m_\ell^2}{s-4m_\ell^2}\log\left(\frac{\sqrt{s(s-4m_\ell^2)}+s-2m_\ell^2}{2m_\ell^2}\right)\,.\tag{5.41}$$

The above formula can be further simplified by multiplying the numerator and denominator by $2/s$

$$\begin{aligned}&\log\left(\frac{\sqrt{s(s-4m_\ell^2)}+s-2m_\ell^2}{2m_\ell^2}\right) = \log\left(\frac{2\sqrt{1-\frac{2m_\ell^2}{s}}+2-\frac{4m_\ell^2}{s}}{1-1+\frac{4m_\ell^2}{s}}\right) =\\ &\log\left(\frac{2\sqrt{1-\frac{2m_\ell^2}{s}}+1+1-\frac{4m_\ell^2}{s}}{1-1+\frac{4m_\ell^2}{s}}\right) = \log\left(\frac{2\sqrt{1-\frac{2m_\ell^2}{s}}+2-\frac{4m_\ell^2}{s}}{1-1+\frac{4m_\ell^2}{s}}\right) =\\ &\log\left(\frac{\left(1+\sqrt{1-\frac{4m_\ell^2}{s}}\right)^2}{\left(1+\sqrt{1-\frac{4m_\ell^2}{s}}\right)\left(1-\sqrt{1-\frac{4m_\ell^2}{s}}\right)}\right) =\\ &\log\left(\frac{\left(1+\sqrt{1-\frac{4m_\ell^2}{s}}\right)}{\left(1-\sqrt{1-\frac{4m_\ell^2}{s}}\right)}\right) = 2\operatorname{arc\,tg}\sqrt{1-\frac{4m_\ell^2}{s}}\,,\end{aligned}\tag{5.42}$$

where in last line we have used the identity $\operatorname{arc\,tg} x = \log((1+x)/(1-x))/2$ for $x < 1$, justified since the centre of mass energy is bounded $s > 4m_\ell^2$. Expressing the cross section via inverse hyperbolic function, in agreement with Ref. [241] gives

$$\sigma_{\ell^+\ell^-\to\gamma a}(s) = \frac{C_\ell^2 e^2}{4\pi f_a^2}\frac{m_\ell^2}{s-4m_\ell^2}\operatorname{arc\,tg}\left(\sqrt{1-\frac{4m_\ell^2}{s}}\right). \tag{5.43}$$

Note that the formulas analogical to Eq. (5.43) and Eq. (5.34) can be used for quark scatterings with gluons by changing $e \to g_s$ and multiplying by a factor $(2\times(1/3))^2 = 4/9$, where 2 comes from the trace of Gell-Mann matrices and 1/3 from normalization of quark fields.

### 5.3.2 Flavor violating lepton decay

Flavor-violating couplings present in the astrophobic models induce flavor-violating lepton decays. A simple diagram

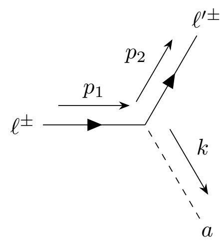


gives amplitude

$$i\mathcal{M}_{\ell\to\ell' a} = \frac{k_\mu}{2f_a}\bar{u}(p_2)\gamma^\mu\Big(C^V_{\ell\ell'} + C^A_{\ell\ell'}\gamma^5\Big)u(p_1). \tag{5.44}$$

The averaged square of the amplitude after Dirac algebra becomes

$$\frac{1}{2}|\mathcal{M}_{\ell\to\ell' a}| = \frac{\left(C^V_{\ell\ell'}\right)^2 + \left(C^A_{\ell\ell'}\right)^2}{f_a}(k\cdot p_1)(k\cdot p_2)\,. \tag{5.45}$$

The scalar products of this two-body decay are fixed by the kinematics

$$\begin{aligned}(p_1-k)^2 = p_2^2 = m_{\ell'}^2 = m_\ell^2 - 2p_1\cdot k \to p_1\cdot k = \frac{1}{2}\Big(m_\ell^2 - m_{\ell'}^2\Big)\,,\\ (k+p_2) = p_1^2 = m_\ell^2 = m_{\ell'}^2 + p_2\cdot k \to p_2\cdot k = \frac{1}{2}\Big(m_\ell^2 - m_{\ell'}^2\Big)\,.\end{aligned} \tag{5.46}$$

We finally find the square of the amplitude averaged over initial spins to be

$$\begin{aligned}\frac{1}{2}|\mathcal{M}_{\ell\to\ell' a}| &= \frac{\left(C^V_{\ell\ell'}\right)^2 + \left(C^A_{\ell\ell'}\right)^2}{4f_a}m_\ell^4\left(1-\frac{m_{\ell'}^2}{m_\ell^2}\right)^2\\ &= \frac{C^2_{\ell\ell'}}{4f_a}m_\ell^4\left(1-\frac{m_{\ell'}^2}{m_\ell^2}\right)^2,\end{aligned} \tag{5.47}$$

where in the last line we have used the definition of the flavor violating coupling, Eq. (3.49), $C^2_{\ell\ell'} = (C^V_{\ell\ell'})^2 + (C^A_{\ell\ell'})^2$. Note, that for relatively large mass splitting of fermions $m_\ell > m_{\ell'}$, we have

$$|\overline{\mathcal{M}_{\ell\to\ell' a}}|^2 = \frac{1}{2}|\mathcal{M}_{\ell\to\ell' a}| = \frac{C^2_{\ell\ell'}}{4f_a}m_\ell^4\,. \tag{5.48}$$

Using formulas from Appendix A.3, we have

$$\begin{aligned}\Gamma_{\ell\to\ell' a} &= \frac{1}{32\pi^2}|\overline{\mathcal{M}_{\ell\to\ell' a}}|^2 \frac{|\vec{p_2}|}{m_\ell^2}(4\pi)\,,\\ |\vec{p_2}| &= \frac{m_\ell^2 - m_{\ell'}^2}{2m_\ell}\,,\end{aligned} \tag{5.49}$$

where we have already performed integration over solid angle of $\ell'$ momentum, which simply gives $4\pi$. We finally have the decay width

$$\begin{aligned}\Gamma_{\ell\to\ell' a} =& \frac{1}{8\pi}\frac{C_{\ell\ell'}^2}{4f_a}m_\ell^4\left(1-\frac{m_{\ell'}^2}{m_\ell^2}\right)^2\frac{m_\ell}{2m_\ell^2}\left(1-\frac{m_{\ell'}^2}{m_\ell^2}\right) = \\ =& \frac{C_{\ell\ell'}^2}{64 f_a}m_\ell^3\left(1-\frac{m_{\ell'}^2}{m_\ell^2}\right)^3.\end{aligned} \tag{5.50}$$

One would expect that FV scatterings $\gamma\ell\to a\ell'$ and $\ell\ell'\to a\gamma$ contribute to the thermalization of the axion. Those scatterings have IR divergence as $p_\gamma\to 0$ related to soft particle emissions. Some authors, e.g. in Ref. [247], regularize the scattering rate by introducing the photon thermal mass $m_\gamma^2(T)\simeq e^2T^2$, however, this method greatly overestimates the rate. In fact, those IR divergences are canceled by real and virtual corrections to the tree-level decays, as demonstrated in Ref. [248]. As a result of this cancellation, FV scatterings give only a subleading contribution to the thermalization rate suppressed with respect to tree-level decay by $\alpha_{\rm EM}$. While results from Ref. [248] are completely applicable to our case, the general theorem analogous to Kinoshita-Lee-Nauenberg theorem [249, 250] is yet not proven in thermal field theory.

### 5.3.3 Pion scattering

In axion models with unsuppressed coupling to pions, the main production channel of thermal axions is via pion scattering [206, 251, 252]. The LO effective lagrangian (3.98) generates a derivative interaction between axion and all three pions. In the following, we will neglect the pion mass splitting $m_{\pi^\pm}\simeq m_{\pi^0}$, see Tab. 2.2. There are three channels of production via pion scatterings:

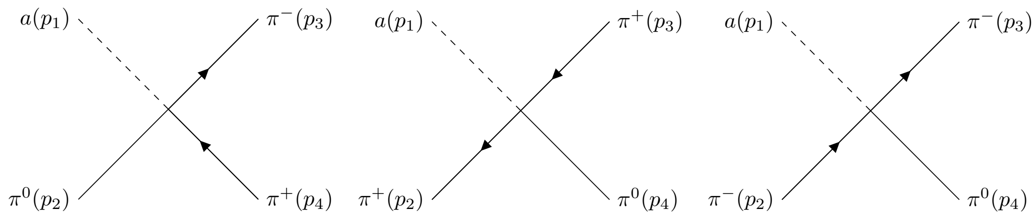


The amplitude of $a\pi^0\to\pi^+\pi^-$ diagram is given by

$$\begin{aligned} i\mathcal{M}_1 =& i\left(\frac{c_{a\pi}}{f_af_\pi}\right)(-ip_1^\mu)\Big(2(-ip_2^\mu)-(ip_3^\mu)-(ip_4^\mu)\Big) = \\ & i\left(\frac{c_{a\pi}}{f_af_\pi}\right)\frac{2s-t-u}{2} = i\left(\frac{c_{a\pi}}{f_af_\pi}\right)\frac{3}{2}(s-m_\pi^2)\,,\end{aligned} \tag{5.51}$$

where in the last equality we have used $2s-t-u=3s-(s+t+u)=3s-3m_\pi^2$, neglecting small axion mass. The square of the amplitude is

$$|\mathcal{M}_{a\pi^0\to\pi^+\pi^-}|^2 = \frac{9}{4}\left(\frac{c_{a\pi}}{f_af_\pi}\right)^2(s-m_\pi^2)^2\,. \tag{5.52}$$

The remaining two diagrams can be found by exchanging the momenta. Firstly, we can exchange $p_2 \leftrightarrow p_3$, remembering to change of sign due to change of outgoing pion to incoming pion $s_{a\pi^+\to\pi^0\pi^-} = p_1 + (-p_3) = t_{a\pi^0\to\pi^+\pi^-}$. We have explicitly written a process to which the Mandelstam variable corresponds and noted that it can expressed by the Mandelstam variable of the first process. Similarly, the exchange $p_2 \leftrightarrow p_4$ gives $s_{a\pi^-\to\pi^0\pi^+} = p_1 + (-p_4) = u_{a\pi^0\to\pi^+\pi^-}$.

Hence, the other scatterings give

$$\begin{aligned} |\mathcal{M}_{a\pi^+\to\pi^0\pi^+}|^2 &= \frac{9}{4}\left(\frac{c_{a\pi}}{f_a f_\pi}\right)^2 (t - m_\pi^2)^2\,, \\ |\mathcal{M}_{a\pi^-\to\pi^0\pi^-}|^2 &= \frac{9}{4}\left(\frac{c_{a\pi}}{f_a f_\pi}\right)^2 (u - m_\pi^2)^2\,, \end{aligned} \tag{5.53}$$

where we have simplified the notation such that Mandelstam variables correspond to $a\pi^0 \to \pi^+\pi^-$. Combining all amplitudes, we find results in agreement with Ref. [206, 252]

$$\begin{aligned} &|\mathcal{M}_{a\pi\to\pi\pi}|^2 = |\mathcal{M}_{a\pi^0\to\pi^+\pi^-}|^2 + |\mathcal{M}_{a\pi^+\to\pi^0\pi^+}|^2 + |\mathcal{M}_{a\pi^-\to\pi^0\pi^-}|^2 = \\ =&\frac{9}{4}\left(\frac{c_{a\pi}}{f_a f_\pi}\right)^2 \Big(s^2 + t^2 + u^2 + 3m_\pi^4 - 2m_\pi^2(s+t+u)\Big) = \\ =&\frac{9}{4}\left(\frac{c_{a\pi}}{f_a f_\pi}\right)^2 \Big(s^2 + t^2 + u^2 - 3m_\pi^4\Big)\,. \end{aligned} \tag{5.54}$$

We can now express the total square of the amplitude using only $s$ and $t$

$$|\mathcal{M}_{a\pi\to\pi\pi}|^2 = \frac{9}{2}\left(\frac{c_{a\pi}}{f_a f_\pi}\right)^2 (3m_\pi^4 - 3m_\pi^2(s+t) + s^2 + st + t^2)\,. \tag{5.55}$$

The momenta in the centre of the mass frame are

$$\begin{aligned} p_1^{\mathrm{CM}} &= \frac{s - m_\pi^2}{2\sqrt{s}}\,, \\ p_3^{\mathrm{CM}} &= \sqrt{\frac{s}{4} - m_\pi^2}\,. \end{aligned} \tag{5.56}$$

The range of the $t$ is bounded by

$$\begin{aligned} t_0 &= \frac{m_\pi^4}{4s} - \left(\frac{s - m_\pi^2}{2\sqrt{s}} - \sqrt{\frac{s}{4} - m_\pi^2}\right)^2\,, \\ t_1 &= \frac{m_\pi^4}{4s} - \left(\frac{s - m_\pi^2}{2\sqrt{s}} + \sqrt{\frac{s}{4} - m_\pi^2}\right)^2\,. \end{aligned} \tag{5.57}$$

Finally the cross section, according to Appendix A.3 is

$$\begin{aligned} \sigma_{a\pi\to\pi\pi}(s) &= \int_{t_1}^{t_0} \frac{1}{64\pi s p_1^{\mathrm{CM}}} |\mathcal{M}_{a\pi\to\pi\pi}|^2 = \\ &= \frac{3}{64\pi}\left(\frac{c_{a\pi}}{f_a f_\pi}\right)^2 \frac{1}{s^{3/2}} \Big(2m_\pi^2 - 5s\Big)\Big(m_\pi^2 - s\Big)\sqrt{s - 4m_\pi^2}\,. \end{aligned} \tag{5.58}$$

Note, that the cross section diverges linearly with $s \to \infty$. It is a consequence of the fact, that Eq. (3.98) is an effective lagrangian valid up to ChPT cut-off around $\sqrt{s} = \Lambda_{\mathrm{ChPT}} = 4\pi f_\pi = 1160$ MeV.

### 5.3.4 Kaon scattering

Scatterings with kaons involve 8 processes: $\pi^0 K^\pm, K^0\pi^\pm \to a\pi^\pm$; $\pi^0 K^0, \pi^- K^+ \to aK^0$; $\pi^+ K^-, \pi^0 \overline{K}^0 \to a\overline{K}^0$ represented by diagram of type:

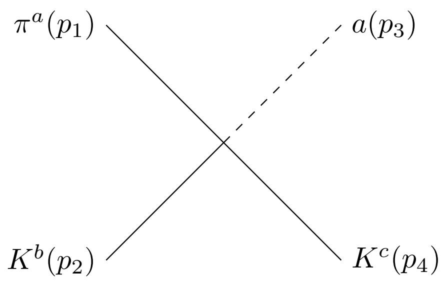


where indices $\pi^a = \pi^\pm, \pi^0$ and $K^{b/c} = K^0, K^\pm, \overline{K}^0$. Neglecting the mass splitting of pions, $m_\pi \equiv m_{\pi^\pm} = m_{\pi^0}$, and kaons, $m_K \equiv m_{K^\pm} = m_{K^0} = m_{\overline{K}^0}$, allows us to derive a simple formula for total square of amplitude in astrophobic axion models in limit $z = 1/2$, $w = 0$ using Eq. (3.103):

$$\sum_{\text{processes}} |\mathcal{M}|^2_{\pi K \to aK} = \left(\frac{C_s}{2\sqrt{3} f_a f_\pi}\right)^2 \left(3t - m_\pi^2\right)^2 \simeq \left(\frac{\sqrt{3} C_s}{2 f_\pi f_a}\right)^2 t^2 \,. \tag{5.59}$$

where in the last equality we have dropped pion mass, which is small compared to the momentum transfer of the scattering and gives only a few percent correction, since $(m_K/m_\pi)^2 \simeq 0.07$. Using definitions from Appendix A.3 we have

$$\begin{aligned} E_1^{\text{CM}} &= \frac{s - m_K^2}{2\sqrt{s}} \,, \\ E_3^{\text{CM}} &= \frac{s - m_K^2 + m_\pi^2}{2\sqrt{s}} \,, \end{aligned} \tag{5.60}$$

which gives the integration limit of $t$

$$\begin{aligned} t_0 &= \frac{m_\pi^4}{4s} - \left(\frac{s - m_K^2}{2\sqrt{s}} - \sqrt{\frac{s - m_K^2 + m_\pi^2}{4s}} - m_\pi^2\right)^2 \,, \\ t_1 &= \frac{m_\pi^4}{4s} - \left(\frac{s - m_K^2}{2\sqrt{s}} + \sqrt{\frac{s - m_K^2 + m_\pi^2}{4s}} - m_\pi^2\right)^2 \,. \end{aligned} \tag{5.61}$$

Using the formula for cross section Eq.(A.56) and expanding in $(m_\pi/m_K)$ we find

$$\sigma_{\pi K \to aK}(s) \simeq \frac{C_s^2}{64\pi f_a^2 f_\pi^2 s^3} \left(s - m_K^2\right)^2 \left(\left(s - m_K^2\right)^2 + \left(\frac{m_\pi}{m_K}\right)^2 \left(3m_K^4 + 2m_K^2 s\right)\right) , \tag{5.62}$$

which linearly diverges in large $s$, as expected from effective interaction Eq. (3.103). Similarly to scattering rate with pions, this cross section should be integrated using Eq. (B.4.64) up to validity scale of ChPT, $\sqrt{s} = \Lambda_{\text{ChPT}} = 4\pi f_\pi = 1160$ MeV.

The scattering rate with kaons has been calculated before for hadronic axion [63]. We have extended the calculation to include effects on non-vanishing strange quark couplings.

## 5.4 Freeze-in and freeze-out production of axions

Axions always thermalize for sufficiently small $f_a$, meaning their final abundance is fixed by the time the freeze-out temperature $T_d$. On the other hand, in the limit of weak interactions with the thermal bath, large $f_a$, axions never reach thermal equilibrium and are produced via freeze-in. For lepton scatterings and decays approximate formulas for the values of couplings at which the transition occurs are [209]

$$\begin{aligned}(f_a/C_{\ell\ell})_S^{\mathrm{eq}} &\approx \left(\frac{\alpha m_\ell M_{\mathrm{Pl}}}{\pi^2 1.66\zeta(3)\sqrt{g_{*s}^{\mathrm{UV}}}}\log 2\right)^{1/2} = 2\times 10^7\ \mathrm{GeV}\sqrt{\frac{m_\ell}{\mathrm{GeV}}}\,, \\ (f_a/C_{\ell\ell'})_D^{\mathrm{eq}} &\approx \left(\frac{m_\ell M_{\mathrm{Pl}}}{32\pi 1.66\zeta(3)\sqrt{g_{*s}^{\mathrm{UV}}}}\right)^{1/2} = 8\times 10^7\ \mathrm{GeV}\sqrt{\frac{m_\ell}{\mathrm{GeV}}}\,.\end{aligned} \tag{5.63}$$

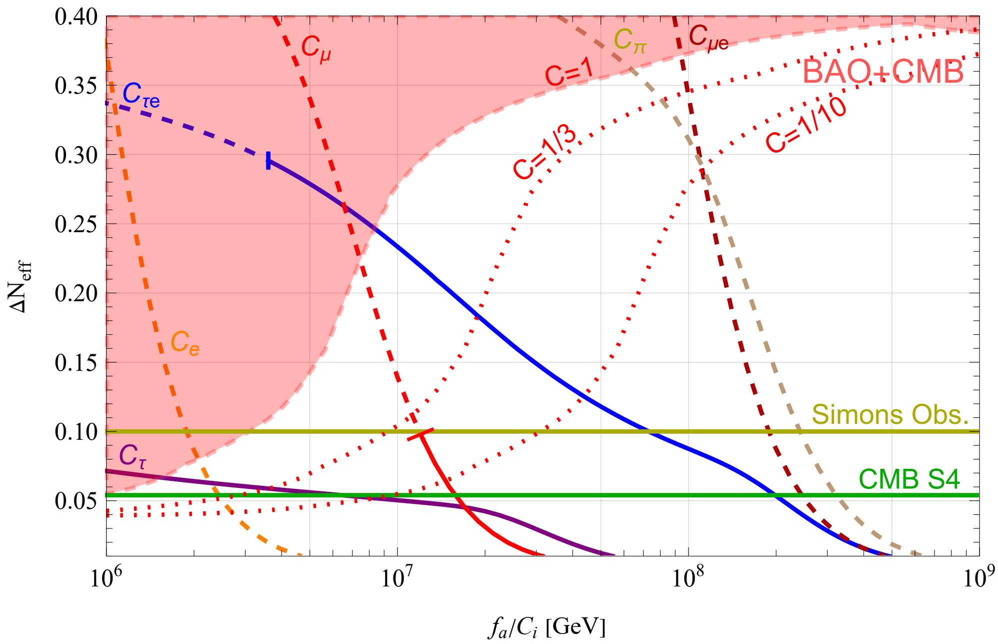


Figure 5.4: Model-independent axion contribution to the additional effective number of neutrinos $\Delta N_{\rm eff}$ as a function of $f_a/C_i$, for $i = \pi, \tau, \mu, e, \mu e, \tau e$. The red region is excluded by BAO+CMB [62] assuming $C_i = 1$, while dotted curves show the bound for the representative values $C_i = 1/3$ and $C_i = 1/10$. Dashed (solid) lines indicate ranges of excluded (viable) values of $f_a/C_i$ for a given type of coupling discussed in Section 3.4. Horizontal lines denote the predicted sensitivities of Simons Observatory (dark yellow) [237], CMB-S4 (green) [238].

## 5.5 Axion contribution to the effective number of neutrinos

In this section, we will finally present the original results, first published in Ref. [209]. Firstly, in Sec. 5.5.1 we will present a model-independent discussion of the thermal production of axions. In Sec. 5.5.2 we present results for the minimal astrophobic axion models, emphasizing the interplay between thermal abundance and signals in (baby)IAXO experiment. Finally, in Sec. 5.5.3, we analyze the production of astrophobic axions in models extended to 3 Higgs doublets which allow for additional suppression of couplings, in correspondence with Sec. 4.4.2.

### 5.5.1 Model-independent analysis of axion contribution to $\Delta N_{\rm eff}$

Let us first consider model-independent thermal production of axions coupled to leptons, taking into account experimental and astrophysical constraints described in Section 3.4. We intentionally neglect production from quarks, which is affected by non-perturbative effects which we will carefully examine in Section 5.5.4, where non-perturbative effects may dominate the axion production. This analysis will be useful for further examination of specific astrophobic axion models.

In Fig. 5.4 we show predicted $\Delta N_{\rm eff}$ as a function of $f_a/C_i$, for each coupling $C_i$ separately. Solid lines denote allowed values of couplings, and we mark the constraints from Section 3.4 by dashing the ruled-out ranges of $f_a/C_i$. We show axion-lepton couplings $C_\tau, C_\mu, C_e, C_{\mu e}, C_{\tau e}$ ($C_{\tau\mu}$ gives the same prediction as for $C_{\tau e}$, cf. Eq. (5.50)) along axion-pion coupling $C_\pi$ for comparison.

Along the predicted values of $\Delta N_{\rm eff}$, we also show BAO+CMB bound from [62], taking into account that for small $f_a$ axion can no longer be considered a massless particle. Note, that since this is a model-independent plot, we need to fix $C_i$. The red region assumes $C_i = 1$, and red dotted lines show bound for representative values $C_i = 1/3, 1/10$. The bound becomes strongly dependent on $f_a/C_i$ for $f_a/C_i < \mathcal{O}(10^7)$ GeV, corresponding to $m_a > \mathcal{O}(0.6)$ eV, where the axion becomes non-relativistic around recombination. We also supplement the plot with predicted sensitivities of Simons Observatory $\Delta N_{\rm eff}^{\rm Simons}(2\sigma) = 0.1$ [237], and CMB-S4 $\Delta N_{\rm eff}^{\rm CMB\text{-}S4}(2\sigma) = 0.054$ [238], conservatively assuming massless axion. Dependence of bounds on $f_a$, similar to BAO+CMB, is expected, however estimation of this effect is unreliable.

As mentioned before, in generic axion models, thermal production is dominated by late production from pion scatterings $\pi\pi \to \pi a$, which can be understood by the fact, that after QCDPT, freeze-out predicts large $\Delta N_{\rm eff}$ due to a small number of entropic degrees of freedom Eq. (5.15). In hadronic axion models, e.g. KSVZ with $C_\pi \approx 0.1$, this results in the hot dark matter bound $f_a \gtrsim 2 \times 10^7$ GeV, which is expected to be improved up to $f_a \gtrsim 6 \times 10^7$ GeV by CMB-S4 experiments [63]. However, astrophysical constraints set $f_a/C_\pi \gtrsim 2 \times 10^9$ GeV, which yields unobservable $\Delta N_{\rm eff} < 0.01$. On the other hand, in astrophobic models, axion-pion coupling is suppressed since $C_\pi \sim C_n - C_p$, Eq. (3.112), and other channels may overtake axion production.

Firstly, let's consider flavor-conserving axion-lepton scatterings. Electron scatterings give contribution only at small values of $f_a$, since they must overcome the cross section suppression Eq. (5.34) and Eq. (5.43). Because the production takes place at very late times, $\Delta N_{\rm eff}$ changes rapidly with $f_a/C_e <$ few $\times 10^6$ GeV. However, astrophysical constraint, Eq.(3.114), rules out parameter space with any observable axion population produced via electron scatterings.

On the other hand, muon scatterings are less limited by astrophysical constraints and sizable contributions $\Delta N_{\rm eff} = 0.1$ are consistent with SN1987A bound. Again, rapid change of $\Delta N_{\rm eff}$ with $f_a/C_\mu$ is a result of axion production at $T \sim m_\mu$, when the number of entropic degrees of freedom is already small.

Finally, the axion-tau coupling isn't constrained and the whole range of $f_a/C_\tau$ is allowed. However, because production takes place at high temperatures, the contribution from those scatterings can be $\Delta N_{\rm eff} > 0.05$ only for $f_a/C_\tau \lesssim 10^7$ GeV.

For flavor violating couplings, a large axion population may be produced in lepton decays. Muon decays give the largest contribution to $\Delta N_{\rm eff}$, however strong limits on flavor violating muon decays result in $f_a/C_{\mu e} > 5 \times 10^8$ GeV, which leads to unobservable axion abundance from this channel.

On the other hand, tau decays controlled by $C_{\tau\ell}$ are much less constrained by experiments and can give sizable contributions to $\Delta N_{\rm eff}$. Note, that there is no difference in $\Delta N_{\rm eff}$ between $\tau \to ea$ or $\tau \to \mu a$, as mass splitting between $\ell$ and $\tau$ is always large, Eq. (5.50). The current bound can be read off from the plot and is about $8 \times 10^6$ GeV for $C_{\tau\ell} = 1$, which is stronger than Belle-II bounds on tau decays Eq. (3.121) and Eq. (3.122). Our bound remains strong even for $C_{\tau\ell} = 1/10$, when it reads about $4 \times 10^6$ GeV. The reason this bound remains so strong is that, for $f_a \simeq 10^7$ GeV axions quickly become non-relativistic at recombination and the constraint tightens. Note, that CMB-S4 will be sensitive to $f_a/C_{\tau\ell} \simeq 2 \times 10^8$ GeV, which is an order magnitude stronger than the forecasted sensitivity of Belle-II, cf. Eq. (3.123).

To conclude, results from Fig. 5.4 show that sizable $\Delta N_{\rm eff}$ is possible in models with suppressed axion-pion and axion-electron couplings and sizable flavor violating axion couplings. Those conditions are already satisfied in the astrophobic models, which motivates our discussion in the following sections.

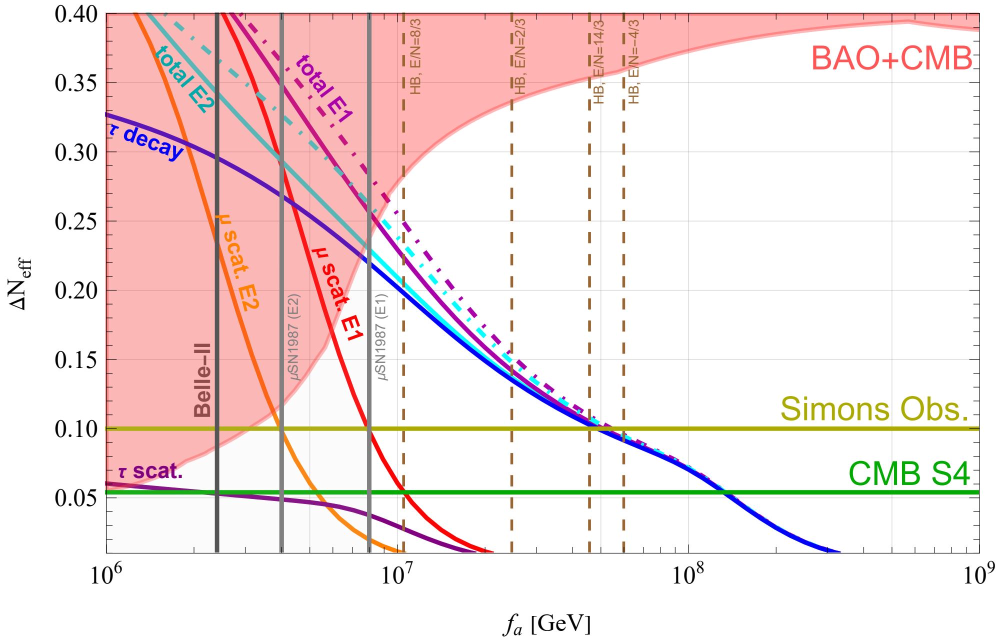


Figure 5.5: Additional effective number of neutrinos $\Delta N_{\rm eff}$ as a function of $f_a$ in astrophobic 2HDM. The total prediction without axion-kaon scatterings in for E1 (solid dark magenta) and E2 (solid light blue) are shown. Dashed-dotted lines are predictions for $\Delta N_{\rm eff}$ taking into account the production from kaon scatterings for $C_s = -2/3$ for $z = 0.49$. We also show the contribution to additional effective number of neutrinos coming from tau decays (solid blue), tau scatterings (solid purple) and muon scatterings in E1 (solid red) and E2 (solid orange). Moreover, vertical lines correspond to relevant constraints from Section 3.4 on $C_\mu$ from SN1987A [56] (grey), on $C_{\tau e}$ from the Belle-II [223] (cyan) and on $g_{a\gamma\gamma}$ from HB [53] (brown, dashed). Horizontal lines denote the predicted sensitivities of Simons Observatory (dark yellow) [237], CMB-S4 (green) [238].

### 5.5.2 2HDM

Let us now proceed to discuss the axion contribution to effective number of neutrinos in minimal implementation of astrophobic models, which includes 2 Higgs doublets. There are four different coupling choices in the astrophobic 2HDM, as discussed in section 4.4.1, differing by the muon and strange couplings.

We show the resulting prediction for $\Delta N_{\rm eff}$ as a function of $f_a$ in Fig. 5.5 for two possible choices of lepton sector: E1 and E2, which differ by $|C_\mu| = 1/3, 2/3$, respectively. Solid lines denote contributions coming solely from the lepton sector, while dashed-dotted lines include also contributions from kaon scatterings. We fix $C_s = 2/3$ and $z = 0.49$, which we motivate by noting that it gives the largest axion-kaon coupling, cf. approximate Eq. (3.103). In a sense, because the calculation involving kaons is intrinsically uncertain at the leading order of ChPT, we may think of this estimate as a quantifier of the uncertainty of our calculations. Note, that even though this contribution can alter the $\Delta N_{\rm eff}$ by 10%, the bound on $f_a$ changes only slightly. Moreover, we also include production from separate lepton channels on Fig. 5.5: flavor-violating $\tau$-decays and flavor-diagonal $\tau$- and $\mu$-scattering. We can read off the hot axion bound in astrophobic 2HDM to be:

$$
\begin{aligned}
&f_a > 7.8 \times 10^6 \text{ GeV} \quad (m_a < 0.73 \text{ eV}) \qquad \text{for E1,}\\
&f_a > 8.5 \times 10^6 \text{ GeV} \quad (m_a < 0.67 \text{ eV}) \qquad \text{for E2,}
\end{aligned}
\tag{5.64}
$$

which are comparable to the predicted sensitivity of future Belle-II searches for $\tau \to ea$, $f_a \sim 8 \times 10^6$ GeV, Eq. (3.123). Those bounds should be improved by future CMB observations, in particular Simons Observatory will probe 2HDM astrophobic axions up to $f_a \simeq 5 \times 10^7$ GeV ($m_a \simeq 0.1$ eV), while CMB-S4 should reach sensitivity to $f_a \simeq 10^8$ GeV ($m_a \simeq 0.06$ eV).

We can compare those bounds with constraints from Section 3.4, also shown on the plot. In particular, the Belle-II limit on flavor-violating $\tau e$ couplings, which requires $f_a \gtrsim 2 \times 10^6$ GeV. The bounds on muon coupling from SN1987A are also depicted as grey vertical lines, giving $f_a > 8 \times 10^6$ GeV ($4 \times 10^6$ GeV) in E1 (E2) model. As it turns out, the strongest bound in those models come from HB stars on $g_{a\gamma\gamma}$ controlled by electromagnetic anomaly $E/N \in \{14/3, 8/3, 2/3, -4/3\}$. On the plot we show those bounds in vertical, dashed, brown lines which vary between $f_a \simeq 10^7$ GeV (for Q1E1) to $f_a \gtrsim 6 \times 10^7$ GeV (for Q4E1).

Hence, current constraints on $f_a$ allow for $\Delta N_{\rm eff}$ as large as 0.20 (0.22) for E2 (E1) models with $E/N = 8/3$, including only leptonic production. Including the leading order of kaon production increases the allowed values of $\Delta N_{\rm eff}$ to about 0.23 (0.25) for E2 (E1) with $E/N = 8/3$. However, this result is uncertain due to possibly large correction to the kaon scattering rate from NLO ChPT. For $E/N = -4/3$ all models give the same maximal contribution to the $\Delta N_{\rm eff}$, as production is dominated by tau decays. The allowed contribution to additional effective number of neutrinos is about 0.09, just below the reach of Simons observatory, but within predicted sensitivity of CMB-S4.

Future helioscopes provide complementary searches for astrophobic axions, leveraging axion photon coupling. In Fig. 5.6 we show predictions for this couplings in 2HDM in $(m_a, g_{a\gamma\gamma})$ plane. Besides current bound from HB stars we also include the predicted sensitivities of BabyIAXO and IAXO [218]. For completeness, we include vertical lines denoting the predicted production of axions $\Delta N_{\rm eff}$ in E1 (magenta) and E2 (cyan).

BabyIAXO will only constrain models with $E/N = 14/3$ or $E/N = -4/3$, probing up to $f_a \simeq 10^8$ GeV ($\Delta N_{\rm eff} \simeq 0.07$). On the other hand, IAXO will probe those models up to $f_a \simeq 10^9$ GeV, well beyond the reach of CMB-S4.

For the models with $E/N = 2/3$ and $E/N = 8/3$, axion photon coupling is smaller, and IAXO will probe the parameter space up to $f_a \simeq 2 \times 10^8$ GeV and $f_a \simeq 8 \times 10^7$ GeV, respectively. Models with $E/N = 8/3$ are at the verge of sensitivity of IAXO for $f_a \in [5 \times 10^7, 10^8]$ GeV, but CMB-S4 will probe them down to $m_a \simeq 0.04$ eV ($f_a \simeq 1.5 \times 10^8$ GeV).

### Subsequent freeze-in

In 2HDM, the main channel of axion production are tau decays, which in wide range of $f_a$ bring axions into thermal equilibrium. However, at $f_a < 3 \times 10^7$ GeV, the total $\Delta N_{\rm eff}$ exceeds the value coming solely from $C_{\tau e}$ coupling. The reason is that the subleading muon scatterings take place at different temperature, leading to subsequent freeze-in of axions.

In the left panel of Fig. 5.7 we show the evolution of decay and scattering rates for representative $f_a = 2 \times 10^7$ GeV in E1 model, compared with the Hubble. Clearly, tau decays keep axions in thermal equilibrium for $1 \lesssim x \lesssim 10$, and $\Delta N_{\rm eff}$ only from those interactions is determined by the decoupling temperature, Eq. (5.15). On the other hand, muon scatterings never bring axions into thermal equilibrium and lead only to freeze-in production. On the right panel of Fig. 5.7 we show the corresponding evolution of the axion comoving number density for both channels separately, and the total $Y_a(x)$. The changes in $Y_a^{\rm eq}$, Eq. (5.14), are due to rapid changes in entropic degrees of freedom, $g_{*s}(x)$ around QCDPT, $m_\tau/T_{\rm QCDPT} \simeq 11$. We can clearly see, that tau (inverse) decays keep axions in thermal equilibrium, and as soon as the rate drops below Hubble the comoving

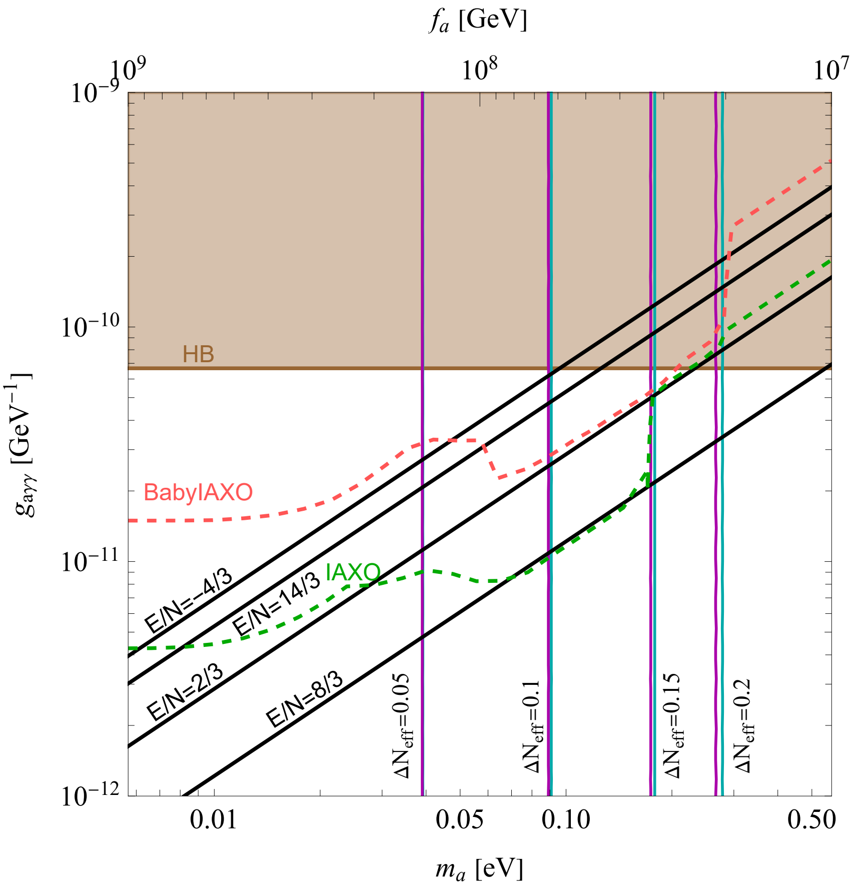


Figure 5.6: Predictions for the axion-photon coupling $g_{a\gamma\gamma}$ in the astrophobic models described in Section 4.4.1. The coupling is controlled by values of $E/N = \{14/3, 8/3, 2/3, -4/3\}$. Vertical lines denote predition for $\Delta N_{\rm eff}$ in E1 (magenta) and E2 (cyan), including axion kaon scatterings. Brown region is excluded by observation of population of HB stars. The predicted sensitivities of BabyIAXO and IAXO [218] are indicated by dashed light red and green, respectively.

number density ceases to change. On the other hand, muon scatterings only produce significant abundance of axions after $x \sim 10$, when the ratio of rate to Hubble is largest.

If both channels are active, the muon scatterings contribute to comoving number density after tau (inverse) decays freeze-out. As a result, the production from scatterings adds on top of the existing axion population. We will call it a subsequent freeze-in, highlighting that production takes place at different times. Note, that because the collision term of the Boltzmann equation is proportional to $Y_a^{\rm eq} - Y_a$, subsequent freeze-in is less efficient than freeze-in without previous tau (inverse) decay production. As a result, axion freeze-in production solely from $\mu$-scattering gives $\Delta Y \sim 1.5 \times 10^{-3}$, while the subsequent freeze-in gives only $\Delta Y \sim 0.5 \times 10^{-3}$.

### 5.5.3 3HDM

We have shown that in 2HDM there is the possibility of a sizable astrophobic axion contribution to the effective number of neutrinos, which can be within reach of Simons Observatory. However, the possible production of axions is restricted by bounds from axion-photon couplings.

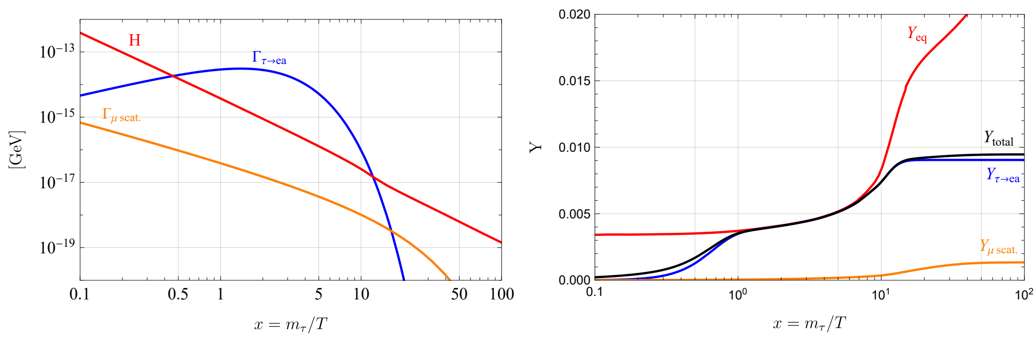


Figure 5.7: Left panel: Axion production rates from $\mu$-scatterings (orange) and $\tau$-decays (blue) as a function of $x = m_\tau/T$ compared to the Hubble rate (red) for E1 models ($C_\mu = -2/3$) at $f_a = 2 \times 10^7$ GeV. Right panel: Axion yield obtained by numerically solving the Boltzmann equation, Eq. (5.28) taking into account scattering and decays simultaneously (black) and separately (orange/green), compared to the equilibrium yield (red). The result is an example of subsequent freeze-in production of axions from muon scatterings on top of pre-existing population of axions produced through freeze-out.

We have seen in Section 4.4.2 that the generalization of the astrophobic axion model to 3HDM allows for additional coupling suppression without much fine-tuning, which results in a suppressed bound on $f_a$. This suppression results in the opening of the parameter space, possibly allowing for observable contribution to the $\Delta N_{\text{eff}}$. As we will see, in some models the CMB+BAO bound is the strongest constraint. This is in contrast to the hot axion bound in hadronic scenario, when the state-of-the-art constraint is $f_a \gtrsim 2.38 \times 10^7$ GeV [63], well below typical supernova, Eq. (3.109), or white dwarf bounds, Eq. (3.114), $f_a \gtrsim (\text{few}) \times 10^8$ GeV.

Similarly to Section 4.4.2 we will consider each class of models based on suppressed, phenomenologically relevant couplings.

### Muonphobic models $|C_\mu| \ll 1$

As discussed in Section 4.4.2, generalizations of astrophobic axion models to three Higgs doublets allow for additional suppression of $C_\mu$. In the Fig. 5.8 we show the prediction for $\Delta N_{\text{eff}}$ for a sample of such models. In particular, we show the largest possible contribution to effective number of neutrinos, obtained in models with $C_s = C_\tau = -2/3$, which is realized by Q2E1 and Q4E1. We can read off the bound from CMB+BAO, $f_a \gtrsim 7 \times 10^6$ GeV, which is always weaker than the HB constraints. This bound is expected to be improved by CMB-S4 to $f_a \gtrsim 2 \times 10^7$ GeV. Depending on specific model, the contribution to effective number of neutrinos compatible with HB bound is $\Delta N_{\text{eff}} \simeq 0.13$ ($E/N = 8/3$), $\Delta N_{\text{eff}} \simeq 0.1$ ($E/N = 4/3$) or below 0.01 ($E/N = 16/3$).

We also display total contribution in model with $C_s = 0$ $C_\tau = -2/3$ (Q5E1), where the bound is $f_a \gtrsim 10^6$ GeV. Taking into account HB bound, their contribution to $\Delta N_{\text{eff}}$ is always below sensitivity of CMB-S4. In model with $C_s = 0$, $C_\tau = 1/3$ (Q5E2) similar conclusions hold.

Those models will be most efficiently probed by IAXO, exploiting relatively large axion-photon coupling. Models with $E/N = 8/3$ will not be probed completely by IAXO, in analogy to Fig. 5.6, but will be complementary to CMB observations.

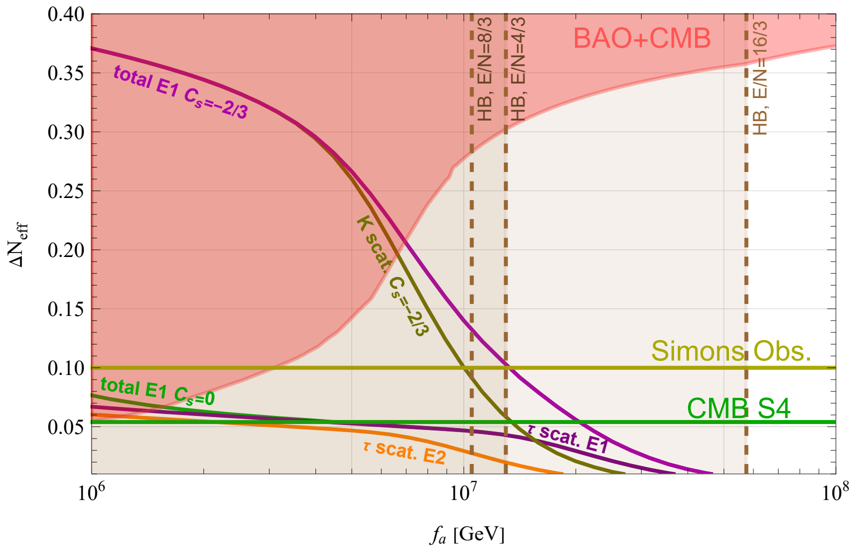


Figure 5.8: Additional effective number of neutrinos $\Delta N_{\text{eff}}$ as a function of $f_a$ in astrophobic 3HDM with suppressed muon coupling. Any quark sector from Tab. 4.7 combined with E1, E2 or E3 is muonphobic. The only differences in $\Delta N_{\text{eff}}$ between the models come from different values of $C_\tau$ and $C_s$. On the plot we show the total contribution to $\Delta N_{\text{eff}}$ in Q3E1, $C_\tau = C_s = -2/3$ (dark magenta) and in Q5E1, $C_\tau = -2/3$ $C_s = 0$. Vertical brown lines correspond to constraints on $g_{a\gamma\gamma}$ from HB [53] for $E/N = 8/3, 16/3$. Horizontal lines denote the predicted sensitivities of Simons Observatory (dark yellow) [237], CMB-S4 (green) [238].

### Photophobic models $C_\gamma \ll 1$

As discussed in Section 4.4.2, Q1E4 and Q4E5 models have electromagnetic anomaly $E/N = 2$, so their coupling to photons is suppressed, relaxing the HB cooling bound down to $f_a \sim \mathcal{O}(10^6)$ GeV. The strongest astrophysical bound comes from SN1987A constraint on axion-muon coupling $C_\mu = -2/3(1/3)$ in Q1E4 (Q4E5) model and allows for $f_a \simeq 8 \times 10^6 (4 \times 10^6$ GeV) in Q1E4 (Q4E5).

There is no LFV in those models, thus contributions to the $\Delta N_{\text{eff}}$ come from axion-kaon scatterings with coupling determined by $C_s = -2/3(0)$ Q1E4 (Q4E5) and muon and tau scatterings $C_\mu = C_\tau = -2/3(1/3)$ in Q1E4 (Q4E5) model. We show contributions to $\Delta N_{\text{eff}}$ on Fig. 5.9 together with SN1987A bound. In particular, the axion contribution to effective number of neutrinos is the largest in Q1E4 due to larger absolute values of lepton couplings, as well as non-zero strange coupling.

In Q1E4 model, $\Delta N_{\text{eff}}$ compatible with SN1987A bound can be as large as 0.23. Interestingly, the two constraints give similar bounds $f_a \gtrsim 8 \times 10^6$ GeV. The total contribution to $\Delta N_{\text{eff}}$ significantly deviates from production from either muon or kaon scatterings, because of subsequent freeze-in discussed in the second part of Section 5.5.2. Simons Observatory will probe those models up to $f_a \simeq 10^7$ GeV, and CMB-S4 will improve that bound up to $f_a \simeq 2 \times 10^7$ GeV.

On the other hand, our bound in Q4E5, $f_a \gtrsim 5 \times 10^6$ GeV, is even slightly stronger than SN1987A bound on the muon coupling. This is mainly due to the mass of the axion around 1 eV, which yields it non-relativistic at the recombination, significantly enhancing the bound in this region. Simons Observatory will probe those models up to $f_a \simeq 7 \times 10^6$ GeV, while CMB-S4 will improve that bound up to $f_a \simeq 10^7$ GeV. Due to

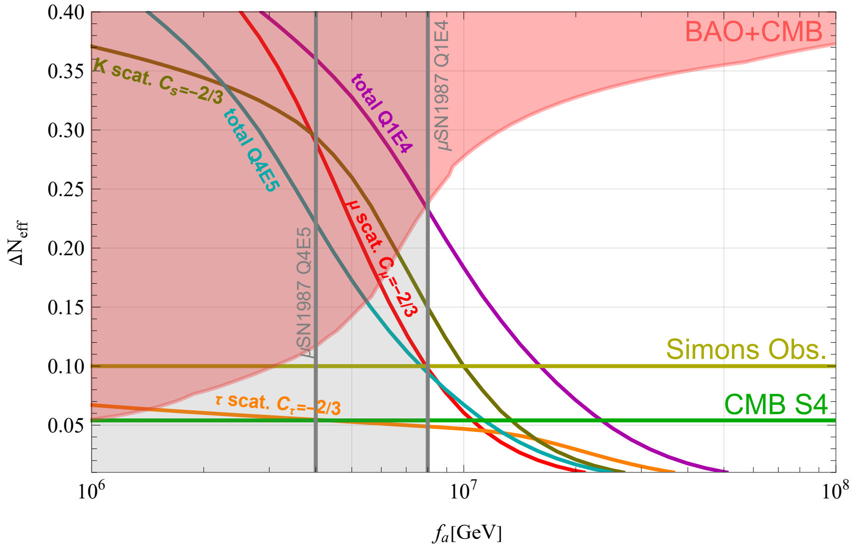


Figure 5.9: Additional effective number of neutrinos $\Delta N_{\rm eff}$ as a function of $f_a$ in astrophobic 3HDM with suppressed photon coupling, realized in Q1E4 and Q4E5 models. The vertical grey lines denote the limit on the muon coupling from SN1987A [56] for $C_\mu = -2/3, 1/3$, while red, brown and orange lines denote separate contributions from scattering with muons, kaons and taus, respectively. Horizontal lines denote the predicted sensitivities of Simons Observatory (dark yellow) [237], CMB-S4 (green) [238].

suppressed axion-photon coupling, those models will not be probed by IAXO.

However, for $f_a < 10^7$ GeV JWST could be potentially sensitive to the axion decay emission lines. The projected sensitivity of JWST on axion-photon coupling is $g_{a\gamma\gamma} \sim \mathcal{O}(10^{-11})$ [211]. However, due to theoretical uncertainty in contribution of axion-pion mixing Eq. (3.108) it is difficult to assess exactly if JWST will probe astrophobic photophobic axions. For the central value of axion-pion mixing contribution to $C_\gamma$ and $f_a = 8\times10^6$ GeV, we have $g_{a\gamma\gamma} \simeq 10^{-11}$, which is at the verge of JWST sensitivity. It is worth noting that the theoretical uncertainty allows for vanishing axion-photon coupling.

### Muonphobic and photophobic models $C_\gamma, C_\mu \ll 1$

Moving on to properly astrophobic axion models, suppressing coupling both to muons and to photons, which are realized in Q2E6 and Q3E6 models, as discussed in Section 4.4.2.

On the Fig. 5.10 we show the minimal prediction for $\Delta N_{\rm eff}$ realized in Q2E6 ($C_s = 1/3$), while very similar bound would be found in Q3E6 ($C_s = -2/3$). The main axion production channel is tau decay with coupling $C_{\tau\mu} = 2/3$, and kaon scatterings give subleading contribution.

The only constraint on the model is the Belle-II search for LFV tau decays [223], $f_a > 2\times10^6$ GeV. Interestingly, the cosmological CMB+BAO bound from thermal production is the strongest constraint on those models, $f_a > 8\times10^6$ GeV, surpassing the direct LFV searches. This is mainly due to the fact that for $f_a \lesssim 10^7$ GeV axion population acts as warm dark matter rather than dark radiation, and the CMB+BAO bound rapidly tightens.

Simons observatory is expected to probe models up to $f_a = 5\times10^7$ GeV, while CMB-S4 will improve that up to $f_a \simeq 10^8$ GeV. The predicted sensitivity of Belle-II should probe those model to $f_a \simeq 10^7$ GeV, which corresponds to $\Delta N_{\rm eff} = 0.21$. Hence, future

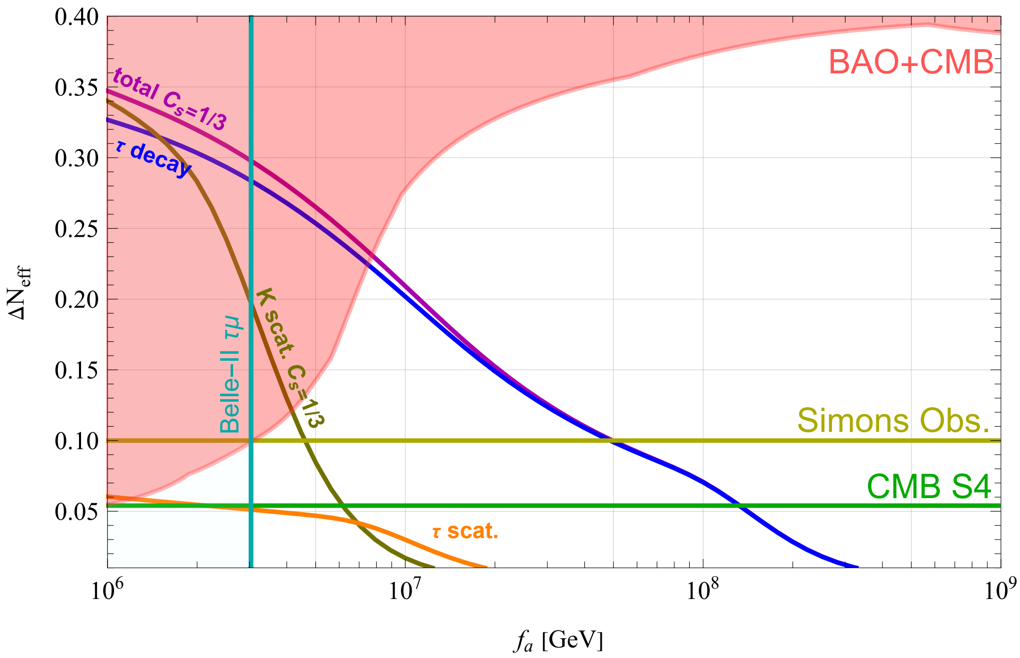


Figure 5.10: Additional effective number of neutrinos $\Delta N_{\rm eff}$ as a function of $f_a$ for proper astrophobic 3HDM, realized by the Q2E6 and Q3E6 models. On the plot we show the total prediction in the Q2E6 model (dark magenta) with the smallest kaon contribution determined by $C_s = 1/3$ and $z = 0.49$. The maximal contribution to $\Delta N_{\rm eff}$ in model Q3E6 for $C_s = -2/3$ is slightly larger, but the resulting bound on $f_a$ from cosmology is similar. We also show separate contributions to $\Delta N_{\rm eff}$ from $\tau$ decays (blue), kaon scatterings (brown) and tau scatterings (orange). The vertical cyan line indicates the lower bound on $f_a$ from searches for flavor-violating $\tau \to \mu a$ decays at Belle-II [223]. Horizontal lines denote the predicted sensitivities of Simons Observatory (dark yellow) [237], CMB-S4 (green) [238].

CMB experiments will be complementary to direct LFV searches in probing the proper astrophobic axion models.

Similarly to the discussion above, JWST could potentially be sensitive to this scenario, with details depending on theoretical prediction for axion-pion contribution to axion-photon coupling.

### 5.5.4 $\Delta N_{\rm eff}$ from the Naturally Astrophobic QCD Axion

Finally, let's consider the naturally astrophobic axion model introduced in Ref. [60] and discussed in Section 4.4.2.

In Fig. 5.11 we show $\Delta N_{\rm eff}$ in various scenarios of the naturally astrophobic axion model. In the minimal setup, axions couple only to up and down quarks, with couplings $C_u = 2/3$ and $C_d = 1/3$. The only relevant astrophysical constraint comes from the bound on axion-nucleon coupling, generated by the corrections to vanishing leading order, and allows for $f_a$ as small as $10^6$ GeV, if $z \approx 0.49$ [60]. Because axion couplings to leptons, pions, and kaons are suppressed, there is essentially no axion production below QCDPT. The only contribution to $\Delta N_{\rm eff}$ comes from the deconfined phase when up- and down-quark scatterings are present. However, the scattering rates cannot be reliably calculated using perturbative methods at temperatures below 1 TeV [63, 253, 254] Assumption, that non-

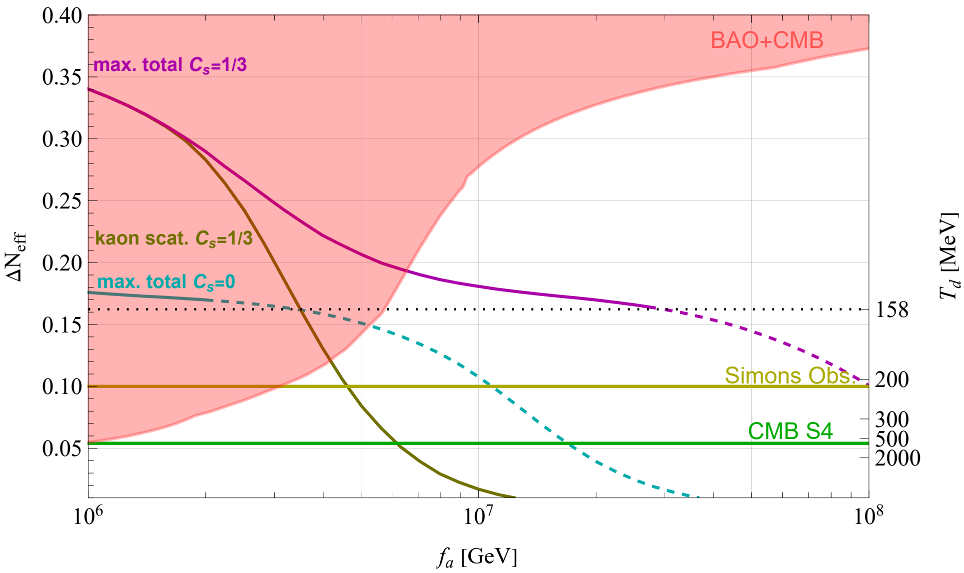


Figure 5.11: Additional effective number of neutrinos $\Delta N_{\rm eff}$ as a function of $f_a$ for the naturally astrophobic axion, realized e.g. by the E3Q5 model. The right vertical axis marks the decoupling temperature of axions under assumption that thermalization occurs, using Eq. (5.15). The dark magenta (dark cyan) shows production of axions from tree-level quark scattering for $C_s = 1/3(0)$, dashed regions marking the values of $f_a$ when production takes place via freeze-in. The model is muon- and photophobic, hence other constraints are absent. Horizontal lines denote the predicted sensitivities of Simons Observatory (dark yellow) [237], CMB-S4 (green) [238].

perturbative processes keep axion in thermal equilibrium, allows for estimating the possible contribution to $\Delta N_{\rm eff}$ by means of Eq. (5.15). Therefore, we indicate this contribution by setting one of the axes of Fig. 5.11 to decoupling temperature $T_d$. We denote the largest possible contribution, $\Delta N_{\rm eff} = 0.16$, by a dotted horizontal line corresponding to the non-perturbative freeze-out at the temperature of QCDPT, $T_d = 158$ MeV [255]. Even in the case when strange quark charge vanishes, $C_s = 0$ there is a small hadronic contribution to $\Delta N_{\rm eff}$ from kaon scatterings below $f_a \simeq 3 \times 10^6$ GeV. However, if non-perturbative effects don't keep axions in equilibrium down to QCDPT, which would be the case if the production rate is smooth, the production can be substantially smaller. In particular, if axions decouple around 1 GeV, $\Delta N_{\rm eff} \simeq 0.05$.

We provide another estimate for the axion production shown in Fig. 5.11 obtained by approximating the non-perturbative production rate with the leading order up- and down-quark scattering rates, setting strong coupling $g_s = 4\pi$. The cross sections for the axion production are analogous to Eq. (5.34) and Eq. (5.43), with an additional factor 4/9 and lepton coupling exchanged for quark coupling. In our calculation, we treat quarks as if they were present in SM plasma down to QCDPT, multiplying the rate by $\theta(T - T_{\rm QCD})$. In the minimal scenario, $C_s = 0$, those $u$ and $d$ scatterings thermalize axion only below $f_a \simeq 3 \times 10^6$ GeV, however freeze-in is potent enough to yield an observable contribution to the effective number of neutrinos resulting in bound $f_a > 5 \times 10^6$ GeV.

For the model with $C_s = C_d = 1/3$, where flavor-violating axion coupling of $s$ and $d$ quarks is suppressed [60], there is a contribution to $\Delta N_{\rm eff}$ from kaon scatterings which are no longer suppressed. Moreover, the strange quark scatterings provide an additional thermalization channel of the axion. Using the same method of estimation of non-perturbative production as before, we show prediction for maximal total $\Delta N_{\rm eff}$ in Fig. 5.11 for $C_s = 1/3$. As a result, axion is kept in equilibrium till QCDPT through quark scatterings for $f_a$ up to $3 \times 10^7$ GeV, and below QCDPT it is produced via freeze-in through kaon scatterings. The bound from CMB+BAO in this scenario is $f_a > 7 \times 10^6$ GeV.

Note, that while other axion-quark couplings might be present, they don't influence the prediction for $\Delta N_{\rm eff}$. The reason is that at QCDPT processes with charm and bottom quarks are Boltzmann suppressed and give negligible contribution to the production rate. This is crucial, as suppressing the axion-nucleon couplings to allow for $f_a$ much below $10^7$ GeV requires the presence of charm and bottom couplings [60].

Moreover, we have checked how our bound depends on the parametrization of non-perturbative effects. Firstly, we check that the bound is independent of the choice of strong coupling $g_s = 4\pi, \sqrt{4\pi}$. On the other hand, the reach of Simons Observatory for $f_a$ varies between $10^7$ and $10^8$ GeV if one changes $g_s$ from $\sqrt{4\pi}$ to $4\pi$ in strange scattering rate. Secondly, we checked the estimate proposed in Ref. [63] with the thermally averaged rate parameterized as $\bar{\Gamma} = \kappa T^3/f^2$ for $T \in [158 \text{ MeV}, 2 \text{ GeV}]$ and $\kappa = 0.1, 0.01$. We confirm that the lower bound on $f_a$ is independent of the parametrization.

We emphasize that naturally astrophobic axion is the least constrained model by CMB, and $f_a$ well below $10^7$ GeV is consistent with all bounds. As a result, axion as heavy as $\mathcal{O}(1)$ eV is allowed, which at recombination is non-relativistic. In future CMB experiments, this feature can help distinguish the naturally astrophobic axion from other axion models.

Those results are particularly interesting for baryon asymmetry generation via minimal axiogenesis [36]. The rotation of the PQ symmetry-breaking field $\Phi$ corresponds to the asymmetry in the PQ charge, which is converted into quark chiral asymmetry via strong sphalerons. Due to the EW anomaly, the chiral asymmetry is again converted into $B + L$ asymmetry via EW sphalerons. However, the rotation of the field $\Phi$ also generates the dark matter abundance via kinetic misalignment mechanism [35]. In the minimal setup, for $f_a \gg 10^7$ GeV, axiogenesis cannot account for whole baryon asymmetry due to the overproduction of axion DM, and additional model-building is required. On the other hand, in the minimal astrophobic axion model, $f_a \lesssim 10^7$ GeV is not excluded and observed baryon asymmetry can be generated without overproduction of dark matter. Our estimate of the axion production rate implies, that CMB-S4 should probe the parameter space of the successful minimal axiogenesis from the minimal astrophobic model.

## 5.6 Summary

In this chapter, we have discussed the $\Delta N_{\rm eff}$ bound on astrophobic axion models, where astrophysical bounds are relaxed. We have demonstrated that a sizable population of astrophobic axions may be produced in LFV decays and lepton scatterings. Results on Fig. 5.4 are model-independent results that may be applied to non-astrophobic axion models. We have found that the cosmological bound in 2HDM is around $f_a \gtrsim 8 \times 10^6$ GeV, which is comparable to the forecasted sensitivity of ground-based experiments. However, axion-photon coupling is constrained by HB star cooling constraints which vary between $(1 : 6) \times 10^7$ GeV, corresponding to $\Delta N_{\rm eff}$ between 0.1 and 0.25 and within reach of the Simons observatory.

Moreover, we have discussed the bound in generalization of astrophobic axions to 3HDM introduced in Chapter 4. Those models generally predict smaller $\Delta N_{\rm eff}$ due to ineffective axion production in flavor-conserving axion-lepton scatterings, with potentially sizable contribution from kaon scatterings. We have demonstrated that in the naturally astrophobic axion model the lower bound on $f_a$ can be as strong as $5 \times 10^6$ GeV, which can potentially allow minimal axiogenesis which explains both baryon and DM abundances.

However, in order to reliably extract the lower bound on $f_a$ in the naturally astrophobic axion models improvements in understanding non-perturbative phenomena above the QCD phase transition are necessary.

# Chapter 6

# Supersymmetry and Twin Higgs mechanism

In Sec. 2.3 we have discussed large corrections to the mass of the Higgs boson, suggesting a special form of new physics which from naturalness arguments should enter at energies not far beyond the EW scale. In this chapter, we will introduce Supersymmetry in Sec. 6.2 and Twin Higgs in Sec. 6.1, which alleviate the hierarchy problem. Finally, in Sec. 6.3 we will present SUSY TH models, which yield the EW scale natural without a need for fine-tuning.

## 6.1 Twin Higgs mechanism

The Twin Higgs mechanism [75] features an accidental global $SU(4)$ symmetry, which is protected from large explicit symmetry breaking coming from loop corrections. This protection relies on an introduction to the SM a set of particles, related to SM particle content by a $\mathbb{Z}_2$ symmetry. The two distinct sectors, which are denoted by superscript $A$ and $B$, will later be called 'visible' or 'SM', and 'twin' sectors, respectively. Each sector includes a gauge group analogous to the SM, hence the total gauge symmetry of the model is $G^A \times G^B = SU_C^A(3) \times SU_L^A(2) \times U_Y^A(1) \times SU_C^B(3) \times SU_L^B(2) \times U_Y^B(1)$. All particles in sector A are singlets under $G^B$ and vice versa. The $\mathbb{Z}_2$-symmetry, transforming any particle $\mathbb{Z}_2 : \phi_A \to \phi_B$, ensures that the corresponding couplings are the same, in particular gauge couplings $g_A = g_B$ and Yukawas $y_A = y_B$.

For now, let's just focus on the scalar sector of the model, which includes two Higgs doublets $H_A$ and $H_B$. Moreover, the Higgs doublets are collected into a single field in the fundamental representation of a global $SU(4)$ symmetry, $\mathcal{H} = (H_A, H_B)^T$. The potential is chosen so that the symmetry is spontaneously broken down to $SU(3)$, which results in the emergence of $15 - 8 = 7$ Goldstone bosons, see Appendix A.5.1. Out of those, six are eaten giving masses to gauge bosons in each sector, three for each sector. The remaining Goldstone is identified with the LHC-observed Higgs with mass $m_h \simeq 125$ GeV. The mass is generated by the explicit breaking of $SU(4)$ symmetry, either present at tree level or generated by loop corrections. To match the couplings of the Goldstone boson to the observed couplings of the Higgs boson, it is necessary to introduce a soft $\mathbb{Z}_2$ breaking in the potential. As we will shortly see, the quadratic correction to the masses of Higgs doublets is still present in the model, however, due to $\mathbb{Z}_2$ symmetry they contribute only to the $SU(4)$ symmetric term of the potential. As a result, those corrections do not contribute to the mass of the Goldstone and the mass of Higgs is natural up to the scale of $SU(4)$ breaking.

Following the Ref. [76], the scalar potential of TH is just the most general $SU(4)$ symmetric potential

$$V(\mathcal{H}) = \lambda\left(\mathcal{H}^\dagger\mathcal{H} - \frac{f_0^2}{2}\right)^2, \tag{6.1}$$

where $f_0$ is a scale of SSB. Including explicit $SU(4)$ breaking and hard $\mathbb{Z}_2$ breaking, and expressing the potential in terms of $H_A$ and $H_B$ we have

$$V(H_A, H_B) = \lambda\left(|H_A|^2 + |H_B|^2 - \frac{f_0^2}{2}\right)^2 + \kappa\left(|H_A|^4 + |H_B|^4\right) - \sigma f_0^2 |H_A|^2 + \rho |H_A|^4 \,. \tag{6.2}$$

The first term leads to SSB and is $SU(4)$ symmetric, $\kappa$ parametrizes the explicit symmetry breaking, $SU(4)$ breaking $\sigma$ term softly breaks $\mathbb{Z}_2$, which is required for compatibility of Higgs couplings to those measured at LHC [67] while $SU(4)$ breaking $\rho$ parametrizes hard $\mathbb{Z}_2$ breaking and is not necessary for TH mechanism to work. We can parametrize the scalar fields as

$$\mathcal{H} = \begin{pmatrix} H_A \\ H_B \end{pmatrix}, \qquad H_I = \begin{pmatrix} \chi^+ \\ \frac{1}{\sqrt{2}}(h_I + i\chi_I^0) \end{pmatrix}, \tag{6.3}$$

where index $I = A, B$ and $\chi$'s are would-be-Goldstone bosons, eaten to give masses to gauge bosons. In particular, in unitary gauge, we can simply set $\chi = 0$ to find the potential

$$V(h_A, h_B) = \frac{\lambda}{4}\left(h_A^2 + h_B^2 - f_0^2\right)^2 + \frac{\kappa}{4}\left(h_A^4 + h_B^4\right) - \frac{\sigma f_0^2}{2} h_A^2 + \frac{\rho}{4} h_A^4 \,. \tag{6.4}$$

Minimizing the above potential, we can find the VEVs

$$\langle h_A \rangle^2 = v_A^2 = \frac{f_0^2(\kappa\lambda + \sigma(\kappa + \lambda))}{\rho(\kappa + \lambda) + \kappa(\kappa + 2\lambda)}, \qquad f^2 = \frac{f_0^2(\kappa(2\lambda + \sigma) + \lambda\rho)}{\rho(\kappa + \lambda) + \kappa(\kappa + 2\lambda)}, \tag{6.5}$$

which satisfy $v_A^2 + v_B^2 = f^2$. In the limit of no $\mathbb{Z}_2$ breaking, $\sigma = \rho = 0$, we have $v_A^2 = f^2/2$. Equivalently, the vacuum misalignment between sectors vanishes, $v_A^2 = v_B^2$, as expected. We can now expand the potential around the minima, to find the mass matrix of the Higgses

$$M_h^2 = \begin{pmatrix} 2v_A^2(\lambda + \kappa + \rho) & 2\lambda v_A v_B \\ 2\lambda v_A v_B & 2v_B^2(\lambda + \kappa) \end{pmatrix}. \tag{6.6}$$

The mass matrix is diagonalized by orthogonal rotation $\mathcal{R}$

$$M_{\text{diag}}^2 = \mathcal{R}^{-1} M_h^2 \mathcal{R} = \begin{pmatrix} m_h^2 & 0 \\ 0 & m_{h'}^2 \end{pmatrix}, \tag{6.7}$$

where $h$ is SM-like Higgs with VEV $v$ and $h'$ twin Higgs with VEV $v'$, in physical basis. In particular, in the limit $v_A/f \ll 1$ the masses are [76]

$$m_h^2 = 2\rho v^2 + \frac{2v^2(\kappa^2 + 2\kappa\lambda)}{\kappa + \lambda}, \qquad m_{h'}^2 = 2f^2(\kappa + \lambda) - \frac{2v^2(\kappa^2 + 2\kappa\lambda)}{\kappa + \lambda}, \tag{6.8}$$

where we have exchanged $v_A$ and $v_B$ for $v$ and $v'$. Clearly, in the limit of vanishing explicit symmetry breaking, $\kappa, \rho \to 0$ the mass of the SM-like Higgs vanishes, and the mass of $h'$ approaches the mass of the $SU(4)$ fundamental $\mathcal{H}$. Moreover, the mixing angle from Eq. (6.7) can be found to be

$$\sin^2\alpha \simeq \frac{\lambda^2}{(\lambda + \kappa)^2}\frac{v^2}{f^2} \simeq \frac{v^2}{f^2}, \tag{6.9}$$

which holds for small breaking of $SU(4)$. Hence, SM Higgs is a mixture of $h_A$ and $h_B$, where proportions are controlled by the splitting of VEVs between the sectors. This mixing induces couplings of SM-like Higgs to the twin particles, in particular to twin fermions.

Note that since phenomenologically $v/f \ll 1$ and $v^2 + v'^2 = f^2$ we have $v/f \simeq v/v'$. As a result, the masses of twin particles, controlled by VEV of the twin Higgs $v'$, are simply rescaled with respect to the visible sector. Besides the mass of the heavy twin Higgs $m_{h'}$, the twin Higgs mechanism introduces only a single parameter, $v/v'$. We can see that by noting that there are 4 parameters of the potential Eq. (6.2) which must reproduce the mass of the SM Higgs and its VEV. The remaining parameters can be traded for the ratio of VEVs and the mass of twin Higgs.

The quadratically divergent corrections to the potential at 1-loop have the following form [75, 84]

$$\delta V = \sum_i \frac{3}{8\pi^2}\Lambda^2\Big(y_i^2|H_A|^2 + y_i'^2|H_B|^2\Big) + \sum_a \frac{9}{64\pi^2}\Lambda^2\Big(g_a^2|H_A|^2 + g_a'^2|H_B|^2\Big)\,, \qquad (6.10)$$

where the first sum runs over all (twin) fermions and the second sum runs over (twin) gauge couplings. Full correction also includes quartic scalar couplings parametrized by $\kappa$ and $\rho$ in Eq. (6.2), but including those would only increase clutter. Therefore, we will drop those corrections without losing the generality of the conclusions. Because of $\mathbb{Z}_2$ symmetry, couplings are equal between the sectors and the corrections contribute only to the $SU(4)$ symmetric part of the potential. Explicitly,

$$\begin{aligned}\delta V &= \sum_i \frac{3}{8\pi^2} y_i^2\Lambda^2\Big(|H_A|^2 + |H_B|^2\Big) + \sum_a \frac{9}{64\pi^2} g_a^2\Lambda^2\Big(|H_A|^2 + |H_B|^2\Big) = \\ &= \left(\sum_i \frac{3}{8\pi^2} y_i^2\Lambda^2 + \frac{9}{64\pi^2} g_a^2\Lambda^2\right)\mathcal{H}^\dagger\mathcal{H}\,,\end{aligned} \qquad (6.11)$$

which does not contribute to the mass of the Goldstone boson. Hence, the mass of the Higgs boson is protected from the quadratically divergent corrections. However, the hierarchy problem in the TH model is just postponed to larger scales, as the mass of $\mathcal{H}$ is now sensitive to UV scales. In other words, the Twin Higgs mechanism solves the little hierarchy problem and still requires UV completion.

The hierarchy between the sectors requires some tuning of the $\mathbb{Z}_2$-breaking parameter $\sigma$. For simplicity, let us drop the $SU(4)$ and $\mathbb{Z}_2$-breaking term parametrized by $\rho$ and reparameterize the lagrangian according to Ref. [68]

$$\mathcal{L} = \lambda\Big(|H_A|^2 + |H_B|^2\Big)^2 - m^2\Big(|H_A|^2 + |H_B|^2\Big) + \Delta\lambda\Big(|H_A|^4 + |H_B|^4\Big) + \Delta m^2 |H_A|^2\,. \quad (6.12)$$

The above parameters relate to Eq. (6.2) via $m^2 = \lambda f_0^2$, $\Delta m^2 = \sigma f_0^2$ and $\Delta\lambda = \kappa$. In this parametrization, the VEVs are given by [68]

$$v_B^2 = \frac{m^2}{4\lambda}\frac{1 + \frac{\lambda\Delta m^2}{\Delta\lambda m^2}}{1 + 2\Delta\lambda/\lambda}, \qquad v_A^2 = \frac{m^2}{4\lambda}\frac{1 - \frac{\lambda\Delta m^2}{\Delta\lambda m^2} - \frac{\Delta m^2}{m^2}}{1 + 2\Delta\lambda/\lambda}\,. \qquad (6.13)$$

The scale of $SU(4)$ breaking is

$$f^2 = \frac{m^2}{4\lambda}\frac{2 - \frac{\Delta m^2}{m^2}}{1 + 2\Delta\lambda/\lambda}\,. \qquad (6.14)$$

Using Barbieri-Giudice measure of fine-tuning, Eq. (2.111), we have [66]

$$
\begin{aligned}
\Delta_{v_A/f} &= \left|\frac{\partial \ln(v^2/f^2)}{\partial \ln \Delta m^2}\right| = \left|\Delta m^2 \frac{f^2}{v^2}\frac{\partial(v^2/f^2)}{\partial \Delta m^2}\right| = \\
&= \left|\Delta m^2 \frac{f^2}{v^2}\left(\left(-\frac{\Delta m^2}{m^2} - \frac{\lambda}{\Delta\lambda m^2}\right)\frac{1}{2-\frac{\Delta m^2}{m^2}} + \left(1 - \frac{\Delta m^2 \lambda}{\Delta\lambda m^2} - \frac{\Delta m^2}{m^2}\right)\frac{1}{\left(2-\frac{\Delta m^2}{m^2}\right)^2 m^2}\right)\right| = \\
&= \left|\frac{f^2}{v^2}\left(\frac{v_A^2}{f^2} - \frac{1}{2-\frac{\Delta m^2}{m^2}} + \frac{v_A^2}{f^2}\frac{\frac{\Delta m^2}{m^2}}{\left(2-\frac{\Delta m^2}{m^2}\right)^2}\right)\right| = \left|\frac{f^2}{v_A^2}\left(\frac{v_A^2}{f^2}\left(1+\frac{\frac{\Delta m^2}{m^2}}{(2-\frac{\Delta m^2}{m^2})}\right) - \frac{1}{(2-\frac{\Delta m^2}{m^2})}\right)\right| = \\
&= \left|\frac{1}{(2-\frac{\Delta m^2}{m^2})}\left(2-\frac{f^2}{v^2}\right)\right| \simeq \frac{1}{2}\left(\frac{f^2}{v^2}-2\right),
\end{aligned}
\tag{6.15}
$$

where in the last line we have assumed $m^2 \gg \Delta m^2$. For values allowed by the LHC, $v/f \simeq v/v' \gtrsim 3$ the tuning is worse than $\mathcal{O}(20\%)$. As a result, the twin Higgs mechanism stabilizes the electroweak scale with mild tuning up to scales $\Lambda \sim 4\pi f = 5-10$ TeV.

The twin Higgs mechanism does not solve the Hierarchy Problem and while the mass of the SM Higgs is protected, the mass of the twin Higgs obtains quadratic corrections from loop diagrams. This is another source of fine-tuning in the twin Higgs models, in analogy to Eq. (2.116). Assuming that the largest correction to $m_{h'}$ comes from the twin top loop the tuning of the TH breaking scale $f$ is given by

$$\Delta_f = \frac{3}{8\pi^2}\frac{y_t^2}{2\lambda v'^2}\Lambda_{\rm TH}^2\,, \tag{6.16}$$

where $\Lambda_{\rm TH}$ is the cut-off of the Twin Higgs model, and we implicitly set $y_{t'} = y_t$ using the $\mathbb{Z}_2$ symmetry. The total tuning is obtained via Eq. (2.114), $\Delta_{\rm TH} = \Delta_f \times v'^2/2v^2$. Compared to the tuning in the SM Eq. (2.116), the improvement in the naturalness is given by

$$\Delta_{\rm SM}/\Delta_{\rm TH} = \frac{2\lambda}{\lambda_{\rm SM}}\frac{\Lambda_{\rm SM}^2}{\Lambda_{\rm TH}^2}\,. \tag{6.17}$$

Since $\lambda_{\rm SM} \simeq 0.13$, it is possible to significantly relax the tuning, while keeping $\Lambda_{\rm TH}$ above the reach of the LHC. The Twin Higgs models have been UV completed, to extend the applicability to higher energy scales, with composite Higgs model [100–103], as well as supersymmetry [64–66, 68–71], which we cover in Sec. 6.3.

A minimal mirror twin Higgs mechanism requires a complete $\mathbb{Z}_2$ symmetry between the sectors, which implies the existence of massless (or nearly massless) states in the twin sector. Because the Higgs portal keeps both sectors in thermal equilibrium down to $T \simeq 3$ GeV [256], relativistic twin photons and twin fermions contribute to the radiation energy density in the early Universe, leaving the imprint in the CMB parameterized by the effective number of neutrinos [256, 257]

$$\Delta N_{\rm eff}^{\rm TH} \simeq 5.6\,, \tag{6.18}$$

which severely exceeds bounds from CMB+BAO, $\Delta N_{\rm eff} \lesssim 0.3$ at 95% C.L. [21].

Several solutions to the $\Delta N_{\rm eff}$ problem in TH models have been proposed. Most notably the Fraternal Twin Higgs, which extends the SM not with a mirror copy, but only with twin particles participating in the solving of the little hierarchy problem. As a result, only heavy SM particles, third-generation quarks, and leptons have twin partners, while twin photons and two of the twin neutrinos are absent.

Another possibility of reducing the $\Delta N_{\text{eff}}$ problem is by late entropy production, diluting the dark radiation, [256, 257]. The asymmetric injection of entropy into the twin sector at temperatures between 10 MeV (avoiding bound from BBN [258]) and 3 GeV (that is, after decoupling of twin sector from SM) results in suppression of the comoving number density of relativistic twin particles. The most common mechanism is the out-of-equilibrium decay of a particle dominantly into the SM, heating the SM sector and effectively diluting the energy density of relativistic twin particles.

Another solution is breaking of the $\mathbb{Z}_2$ symmetry in the Yukawa sector which mitigates the $\Delta N_{\text{eff}}$ problem by increasing the masses of light twin fermions [78, 87]. Another motivation for considering the $\mathbb{Z}_2$ breaking in the Yukawas is potential baryogenesis in the first-order phase transition [259].

## 6.2 Supersymmetry

Supersymmetry is a framework in which bosons and fermions are related by a spacetime symmetry. The main motivation for considering supersymmetry is the solution to the hierarchy problem, which we will cover in this section.
Another motivation for SUSY is the unification of the gauge interaction [260–262]. The beta functions of gauge couplings are altered by the new loop contribution from SUSY partners, leading to their convergence at a high scale, around $10^{16}$ GeV. This is theoretically pleasing, as it suggests that all gauge interactions emerge from a single fundamental force in a grand unified theory (GUT).

Moreover, if SUSY is promoted to local symmetry, similarly to gauge Yang-Mills theories, a new interaction field is introduced. The quantum of this field is a massless spin-2 particle, the graviton, accompanied by its superpartner, the spin-3/2 gravitino. This construction is known as supergravity [263–270] and is a low-energy limit of the string theory, one of the leading candidates for quantum gravity.

Besides those, the introduction of new particles, with minimal additional assumptions, provides candidates for the DM in the form of the lightest supersymmetric particle (LSP) [104]. Most notable examples of the DM candidates in SUSY are the lightest neutralino [135, 271–274] and gravitino [271, 274]. However, in the MSSM, neutralino DM is tightly constrained and can be DM only in highly fine-tuned portions of the parameter space [105, 275–277].
The exact SUSY in minimal implementation has only a few parameters since many interactions are related to each other via supersymmetry transformation. However, the most general parametrization of the SUSY breaking introduces 110 parameters [278]. In specific models of SUSY breaking, those parameters are calculable and depend on a few parameters of the assumed SUSY breaking mechanism.

We will start a discussion of SUSY by considering a toy model for supersymmetric theory

$$\begin{aligned}\mathcal{L} = &-\nabla_\mu \phi_i^* \nabla^\mu \phi^i + i\psi_i^\dagger \overline{\sigma}^\mu \nabla_\mu \psi^i + F_i^* F^i \\ &- \frac{1}{2}\Big(W^{ij}\psi_i\psi_j + W^{*ij}\psi_i^\dagger\psi_j^\dagger\Big) + W_i F^i + W_i^* F^{*i} \\ &+ \frac{1}{4}F_{\mu\nu}^a F^{a\mu\nu} + i\lambda^{\dagger a}\overline{\sigma}^\mu \nabla_\mu \lambda^a + \frac{1}{2}D_a D^a \\ &- \sqrt{2}g(\phi_i^* T^a \psi^i)\lambda^a - \sqrt{2}g\lambda^{\dagger a}(\psi_i^\dagger T^a \phi^i) + g(\phi_i^* T^a \phi^i)D^a\,,\end{aligned} \tag{6.19}$$

where in the first line are kinetic terms of complex scalar fields $\phi_i$ and their supersymmetric partners $\psi_i$ together with auxiliary complex fields $F_i$, which guarantee that the number of degrees of freedom off-shell matches their number on-shell. In the second line, we include all possible non-gauge interactions expressed in terms of superpotential $W$ defined and discussed below. In the third line we include the kinetic term of gauge fields, $F_{\mu\nu} = \partial_\mu A_\nu - \partial_\nu A_\mu + ig[A_\mu, A_\nu]$ and covariant derivative $\nabla_\mu \lambda^a = \partial_\mu \lambda^a + g f^{abc} A^b_\mu \lambda^c$, their supersymmetric partners called gauginos, $\lambda^a$, and an auxiliary field $D^a$ which ensures closing of the SUSY algebra. In the fourth line, we have included renormalizable gaugino couplings not included in the D-term.

The equations of motion of the auxiliary fields $F_i$ are

$$F_i = -W_i^*, \qquad F_i^* = -W_i\,, \tag{6.20}$$

which upon inserting into the lagrangian contributes to the scalar potential of the theory known as F-term

$$\begin{aligned} V(\phi_i, \phi^{*i})_{\text{F-term}} = F_i F^{*i} = W_i^* W^i = M^*_{ik} M^{kj} \phi^{*i} \phi_j + \frac{1}{2} M^{in} y^*_{jkn} \phi_i \phi^{*j} \phi^{*k} + \\ + \frac{1}{2} M^*_{in} y^{jkn} \phi^{*i} \phi_j \phi_k + \frac{1}{4} y^{ijn} y^*_{kln} \phi_i \phi_j \phi^{*k} \phi^{*l}\,. \end{aligned} \tag{6.21}$$

The superpotential is a gauge invariant, holomorphic function of the scalar fields $\phi_i$. In renormalizable theories the most general form of superpotential is [279]

$$W = W_0 + L^i \phi_i + \frac{1}{2} M^{ij} \phi_i \phi_j + \frac{1}{6} y^{ijk} \phi_i \phi_j \phi_k\,, \tag{6.22}$$

and we define its derivatives, used in Eq. (6.19) as

$$W^i = \frac{\delta W}{\delta \phi_i}, \qquad W^{ij} = \frac{\delta W}{\delta \phi_i \delta \phi_j}\,. \tag{6.23}$$

Similarly, the equations of motion of the auxiliary fields $D^a = -g(\phi^* T^a \phi)$, which gives contribution to the scalar potential called D-term

$$V(\phi_i, \phi^{*i})_{\text{D-term}} = \frac{1}{2} \sum_a g_a^2 (\phi^* T^a \phi)^2\,. \tag{6.24}$$

The supersymmetry transformation is given by

$$\begin{aligned} \delta\phi_i &= \epsilon\psi_i\,, \\ \delta\phi_i^* &= \psi_i^\dagger \epsilon^\dagger\,, \\ \delta\psi_i &= -i\sigma^\mu \epsilon_1^\dagger \nabla_\mu \phi_i + \epsilon_1 F_i\,, \\ \delta\psi_i^\dagger &= i\epsilon_1 \sigma^\mu \nabla_\mu \phi_i^* + \epsilon_1^\dagger F_i^*\,, \\ \delta F_i &= -i\epsilon_1^\dagger \overline{\sigma}^\mu \nabla_\mu \psi_i + \sqrt{2} g (T^a \phi)_i \epsilon_1^\dagger \lambda^{\dagger a}\,, \\ \delta F_i^* &= i\nabla_\mu \psi_i^\dagger \sigma^\mu \epsilon_1 + \sqrt{2} g (T^a \phi^*)_i \epsilon_1 \lambda^a\,, \\ \delta A^a_{i\mu} &= -\frac{1}{\sqrt{2}} \left( \epsilon_2^\dagger \overline{\sigma}_\mu \lambda_i^a + \lambda_i^{\dagger a} \overline{\sigma}_\mu \epsilon_2 \right), \\ \delta\lambda_i^a &= \frac{i}{2\sqrt{2}} (\sigma^\mu \overline{\sigma}^\nu) F^a_{i\mu\nu} + \frac{1}{\sqrt{2}} \epsilon_2 D_i^a\,, \\ \delta D_i^a &= \frac{i}{\sqrt{2}} \left( -\epsilon_2^\dagger \overline{\sigma}^\mu \nabla_\mu \lambda_i^a + \nabla_\mu \lambda_i^{\dagger a} \overline{\sigma}^\mu \epsilon_2 \right), \end{aligned} \tag{6.25}$$

where $\epsilon_1, \epsilon_2$ are infinitesimal, two-component Weyl fermions parametrizing the supersymmetric transformation.

We can now go back to the Hierarchy Problem discussed in Section 2.3 to see how supersymmetric particles contribute to the mass of the Higgs. The loop diagrams involving sfermions, higgsinos, and gauginos are

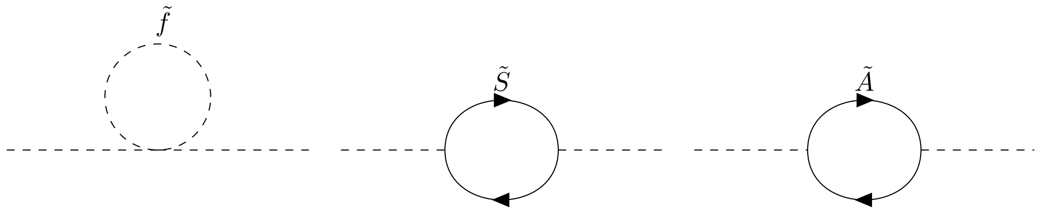


Recall, that the corrections to the mass of the Higgs were of type

$$\delta m_H^2 = -\frac{|\lambda_f|^2}{8\pi^2}\Lambda_{\rm UV}^2 + \frac{\lambda_s^2}{16\pi^2}\Lambda_{\rm UV}^2 + \frac{g_i^2}{16\pi^2}\Lambda_{\rm UV}^2\,, \tag{6.26}$$

where $\lambda_f$ is Yukawa couplings, $\lambda_s$ is the quartic Higgs self-coupling and $g_i$ is a gauge coupling.

In light of those results, the contribution from sparticles to the mass of the Higgs is

$$\delta m_H^2 = 2\frac{|\lambda_{\tilde{f}}|^2}{16\pi^2}\Lambda_{\rm UV}^2 - \frac{1}{2}\frac{|\lambda_{\tilde{s}}|^2}{8\pi^2}\Lambda_{\rm UV}^2 - \frac{1}{2}\frac{g_i^2}{8\pi^2}\Lambda_{\rm UV}^2\,, \tag{6.27}$$

where we have accounted for two scalars for each Dirac fermion, one for each Weyl component. The change of signs is the result of swapping a fermion to a scalar in the loop or vice versa. Note that Yukawa coupling $y_f$ implies that the 4-point vertex from the last term of Eq. (6.21) with coupling $y_f^2/4$, which after accounting for the combinatoric factors gives simply $\lambda_{\tilde{s}} = \lambda_f^2$. Hence, the quadratic contribution from fermion cancels against a quadratic contribution from sfermions, and similarly for scalars and gauge bosons. As a result, the mass of the Higgs boson is not quadratically sensitive to UV scales, and the Hierarchy Problem is solved.

In light of null LHC results, the scale of the SUSY must necessarily be above 1 TeV [280, 281], which means that the cancellation of quadratic divergencies becomes efficient well above the EW scale. For the mass of the Higgs to reproduce the observed 125 GeV, the cancellation between the bare Higgs mass and the corrections of the order of new physics scales require fine-tuning, which at best is around 1% for the low scale of SUSY breaking mediation [282]. However, the fine-tuning quickly gets worse as the mediation scale increases due to RG running of the soft Higgs masses [283, 284]. This issue is known as the little hierarchy problem, as it concerns a mild hierarchy between the electroweak and SUSY scales.

The largest correction to the Higgs soft mass is due to top and stop loops [64]

$$\delta m_{H_u}^2 = -\frac{3y_t^2}{8\pi^2}m_{\tilde{t}}^2 \log\left(\frac{\Lambda_{\rm UV}^2}{m_{\tilde{t}}^2}\right)\,, \tag{6.28}$$

where $\Lambda_{\rm UV}$ is the SUSY cut-off and $m_{\tilde{t}}$ is stop mass. Assuming, that $\Lambda_{\rm UV} = M_{\rm pl} \simeq 10^{19}$ GeV results in cancellation between loop suppression $1/8\pi^2$ and large logarithm. This indicates, $m_{H_u}^2 \sim m_{\tilde{t}}^2$. On the other hand, the minimization of the scalar potential in the MSSM gives

$$-\mu^2 - m_{H_u}^2 \simeq \frac{m_Z^2}{2}\,, \tag{6.29}$$

where $m_Z \simeq 90$ GeV. Hence, for $m_{H_u} \simeq 1$ TeV, the tuning required to obtain the EW scale is at best 1%. The little hierarchy problem could be solved by canceling the correction Eq. (6.28) and thus invalidating $m_{H_u}^2 \sim m_{\tilde{t}}^2$. That would imply $m_{H_u}^2 \sim 100$ GeV and Eq. (6.29) could be more naturally satisfied.

### 6.2.1 Minimal Supersymmetric Standard Model

The Minimal Supersymmetric Standard Model is a minimal extension of the SM invariant under SUSY transformation. The particle content of the theory is extended by including SUSY partners of elementary particles, as well as a second Higgs doublet to give masses to up-type quarks. We specify the interactions in terms of superpotential

$$W_{\mathrm{MSSM}} = \bar{u}\mathbf{y_u}QH_u - \bar{d}\mathbf{y_d}QH_d - \bar{e}\mathbf{y_e}LH_d + \mu H_u H_d\,, \tag{6.30}$$

where $u, d, e$ are triplets in the generation space in up-type quarks, down-type quarks, and leptons, while $Q, L$ are also $SU_L(2)$ doublets. We have chosen not to denote scalars with a tilde to emphasize the simplicity of the model. Note that $\mathbf{y_u}, \mathbf{y_d}, \mathbf{y_e}$ are Yukawa matrices in flavour space. Higgs doublets obtain VEVs

$$\langle H_u\rangle = v_u, \qquad \langle H_d\rangle = v_d\,, \tag{6.31}$$

which break EW symmetry and satisfy $v_u^2 + v_d^2 = v^2 \simeq (246\text{ GeV})^2$. Importantly, the EWSB is induced by the radiative corrections to the Higgs masses, as opposed to the SM where the scalar potential is chosen by hand to spontaneously break $SU_L(2)\times U_Y(1)$. The ratio of VEVs defines an angle

$$\mathrm{tg}\,\beta = \frac{v_u}{v_d}\,. \tag{6.32}$$

In the MSSM, discrete R-parity symmetry [285] is assumed, which is defined in terms of known quantum numbers

$$P_R = (-1)^{3(B-L)+2s}\,, \tag{6.33}$$

where $B$ is baryon number, $L$ is lepton number and $s$ is spin. This guarantees that every vertex of MSSM contains an even number of sparticles with $P_R = -1$. This discrete symmetry ensures the stability of the lightest supersymmetric particle, crucial for the validity of SUSY candidates for dark matter. Besides, R-parity conservation also ensures B and L conservation, suppressing the proton decay [286–288], which would otherwise be induced by dimension 5 operators, leading to observable proton lifetime.

### 6.2.2 Soft supersymmetry breaking

By definition, the spontaneous supersymmetry breaking occurs when the vacuum of the theory is not invariant under SUSY transformations. This condition is equivalent to the non-vanishing VEV of the scalar potential, which implies that the expectation value of the D-terms or F-terms is non-zero.

The general form of soft supersymmetry breaking terms is [73]

$$\mathcal{L}_{\mathrm{soft}} = -\left(\frac{1}{2}M_a\lambda^a\lambda^a + \frac{1}{6}a^{ijk}\phi_i\phi_j\phi_k + \frac{1}{2}b^{ij}\phi_i\phi_j\right) + c.c - (m^2)^{ij}\phi_i^*\phi_j\,, \tag{6.34}$$

where $M_a$ is the mass of each gaugino, $a^{ijk}$ is contribution to the interaction of three scalar fields, $m_{ij}^2$ and $b_ij$ are soft masses of the scalar particles. While those terms do not preserve SUSY, they do not reintroduce the quadratic corrections to the mas of the Higgs preserving the motivation from hierarchy problem. Specifying to the MSSM, the soft supersymmetry breaking lagrangian is

$$\begin{aligned}
\mathcal{L}_{\mathrm{soft}}^{\mathrm{MSSM}} = &-\frac{1}{2}\Big(M_3\tilde{g}\tilde{g} + M_2\tilde{W}\tilde{W} + M_3\tilde{B}\tilde{B}\Big) \\
&-\Big(\tilde{\bar{u}}\mathbf{A_u}\tilde{Q}H_u - \tilde{\bar{d}}\mathbf{A_d}\tilde{Q}H_d - \tilde{\bar{e}}\mathbf{A_e}\tilde{L}H_d + h.c.\Big) \\
&-\tilde{Q}^\dagger\mathbf{m_Q^2}\tilde{Q} - \tilde{L}^\dagger\mathbf{m_L^2}\tilde{L} - \tilde{\bar{u}}\mathbf{m_u^2}\tilde{\bar{u}}^\dagger - \tilde{\bar{d}}\mathbf{m_d^2}\tilde{\bar{d}}^\dagger - \tilde{\bar{e}}\mathbf{m_R^2}\tilde{\bar{e}}^\dagger \\
&-m_{H_u}^2H_u^*H_u - m_{H_d}^2H_d^*H_d - (bH_uH_d + b^*H_u^*H_d^*)\,,
\end{aligned} \tag{6.35}$$

where $M_3, M_2, M_1$ are gluino, wino, and bino soft masses, respectively. In the second line $\mathbf{A_f}$ are trilinear soft coupling matrices in flavor space, analogous to the Yukawa couplings. In the third line, the soft mass matrices of the squarks and sleptons are included in the flavor space. The final line includes contributions to the Higgs potential of the MSSM.

Randall:1998uk Giudice:1998xp, Randall:1998uk Giudice:1998xp, In principle, the scale of those parameters is set by the supersymmetry breaking scale, though various soft SUSY breaking scenarios predict different spectrum signatures. The possible scenarios of SUSY breaking include the Fayet-Iliopoulos mechanism (non-vanishing D-term) [289, 290] or O'Raifeartaigh (non-vanishing F-term) mechanism [291]. Since those mechanisms are not efficient in the MSSM, the SUSY breaking is usually assumed to happen in a dark sector and be mediated to the MSSM. The main categories of SUSY breaking include gravity mediation [292–295], gauge mediation [296–299], extra-dimensional mediation [300–303], and anomaly mediation [304, 305].

In the thesis we do not assume any specific SUSY breaking pattern, however, we make some common, simplifying assumptions. To avoid flavor violation, the matrices $\mathbf{A_f}$ and $\mathbf{m_f^2}$ are set to be diagonal in the flavor space. The CP-violation is assumed to come solely from the CKM matrix, which fixes masses of gauginos and trilinear couplings to be real.

For our purposes, we choose to parametrize the MSSM with the set of parameters defined below the weak scale and given in Tab. 6.1. Note, that by using the minimization condition of the scalar potential parameters $m_{H_u}$, $m_{H_d}$ and $b$ from Eq. (6.35) have been traded to $\mu$, $\mathrm{tg}\,\beta$ and $m_{A^0}$.

| **Parameter** | **Description** |
|---|---|
| $\mu$ | higgsino mass parameter |
| $M_1, M_2, M_3$ | bino, wino, gluino masses $M_1, M_2, M_3$ |
| $m_{L1}, m_{L2}, m_{L3}$ | Left-handed selectron, smuon, and stau masses |
| $m_{R1}, m_{R2}, m_{R3}$ | Right-handed selectron, smuon, and stau masses |
| $m_{Q1}, m_{Q2}, m_{Q3}$ | Left-handed squark masses |
| $m_{\bar{u}1}, m_{\bar{u}2}, m_{\bar{u}3}$ | Right-handed up-type squark masses |
| $m_{\bar{d}1}, m_{\bar{d}2}, m_{\bar{d}3}$ | Right-handed down-type squark masses |
| $A_t, A_b, A_\tau$ | Trilinear coupling for third generation fermions |
| $m_{A^0}$ | Mass of pseudoscalar Higgs |
| $\mathrm{tg}\,\beta$ | Ratio of the VEVs of the Higgses |

Table 6.1: MSSM parametrization used throughout the thesis, in correspondence with Ref. [306].

## 6.3 Supersymmetric Twin Higgs

Supersymmetry solves the hierarchy problem, by introducing the SUSY partners, which cancel quadratic divergences above the SUSY breaking scale. However, the expected mass of the scalar partners is around the mass of the Higgs, 125 GeV. The LHC searches for SUSY particles put bounds of order 1 TeV on the SUSY partners, and the observed mass of the Higgs can only be obtained by fine-tuning of the parameters. This is called the little hierarchy problem, which is less severe as it only requires some parameters to be Dirac unnatural.

On the other hand, the Twin Higgs model allows for postponing the scale at which the hierarchy problem arises. However, the $SU(4)$ fundamental obtains quadratically divergent corrections to its mass, just as the SM Higgs does. In other words, the Twin Higgs model is not UV complete and requires more model building to be valid at large energy scales.

This motivates combining the SUSY with Twin Higgs mechanism, by means of the double protection of the EW scale. The Twin Higgs mechanism should reduce the fine-tuning present in SUSY by postponing the scale at which Higgs emerges. On the other hand, the SUSY will provide the UV completion of the Twin Higgs model, cutting off quadratically divergent contributions to the mass of the $SU(4)$ fundamental $\mathcal{H}$.

We have seen, that in SUSY the scalar potential is fixed by particle content and gauge interaction in terms of F-term and D-term, respectively. In particular, the $SU(4)$-invariant part of potential Eq. (6.2) can be either generated by an F-term of a new supermultiplet, or a D-term of a new gauge interaction. This distinction provides a natural categorization of the SUSY TH models.

### 6.3.1 F-term SUSY TH

This realization of the TH mechanism in the SUSY has first been proposed in Refs. [64,65] and later studied in Refs. [66,67]. Besides two copies of the MSSM, the model consists of a singlet $S$ with superpotential

$$W = \lambda_s S\Big(H_u^A H_d^A + H_u^B H_D^B\Big) = \lambda_s S\mathcal{H}_u\mathcal{H}_d\,, \tag{6.36}$$

where we have defined the $SU(4)$ fundamental as $\mathcal{H}_{u/d} = (H^A_{u/d}, H^B_{u/d})$. The $\mathbf{Z}_2$-symmetry ensures that the potential is $SU(4)$ symmetric. Explicitly, the quartic term is

$$V(\mathcal{H}_u, \mathcal{H}_d) \supset \lambda_s^2(\mathcal{H}_u\mathcal{H}_d)^2 \simeq \lambda_s^2 \sin^2\beta\cos^2\beta\mathcal{H}^4\,, \tag{6.37}$$

where we have used $\mathcal{H}_u = \mathcal{H}\sin\beta$ and $\mathcal{H}_d = \mathcal{H}\cos\beta$ in the last line. Consequently, the quartic coupling is [66]

$$\lambda = \lambda_s^2\frac{\sin^2 2\beta}{4}\,. \tag{6.38}$$

The $SU(4)$ is broken at tree-level by the D-term contributions, Eq. (6.24), from the EW gauge interactions [64,65,73]

$$V(H_u^A, H_d^A, H_u^B, H_d^B) = \frac{g^2+g'^2}{8}\left(\left(\left|H_u^A\right|^2 - \left|H_d^A\right|^2\right)^2 + \left(\left|H_u^B\right|^2 - \left|H_d^B\right|^2\right)^2\right), \tag{6.39}$$

which generates the mass of the Goldstone boson identified by the SM Higgs

$$m_h^2 = 2m_Z^2\cos^2 2\beta\left(1-\frac{v^2}{f^2}\right) + \mathcal{O}(\Delta\lambda)\,, \tag{6.40}$$

neglecting the loop contribution $\Delta\lambda$ in Eq. (6.12). Note, that the mass of the Higgs is enhanced by a factor of $\sqrt{2}$ with respect to the result from MSSM [73]. Nonetheless, the mass of the Higgs is proportional to $\cos 2\beta = (1-\mathrm{tg}^2\beta)/(1+\mathrm{tg}^2\beta)$, which vanishes for $\mathrm{tg}\,\beta = 1$. Therefore, this relation can be exploited to set a lower limit on the $\mathrm{tg}\,\beta$ using $m_h = 125$ GeV. However, the quartic term is proportional to $\sin^2 2\beta = 4\,\mathrm{tg}^2\beta/(1+\mathrm{tg}^2\beta)^2$, and hence the lower bound of $\mathrm{tg}\,\beta$ from Higgs mass gives an upper limit on the magnitude of the quartic term. We will come back to this issue when discussing the fine-tuning of SUSY TH models.

Besides the quartic term, the $SU(4)$ invariant part of lagrangian also includes the Higgs soft masses

$$\begin{aligned} V_{\text{soft}}^{SU(4)} =& m_{H_u}^2\left(\left|H_u^A\right|^2 + \left|H_u^B\right|^2\right) + m_{H_d}^2\left(\left|H_d^A\right|^2 + \left|H_d^B\right|^2\right) - b\Big(H_u^A H_d^A + H_u^B H_d^B + \text{h.c.}\Big) = \\ =& m_{H_u}^2|\mathcal{H}_u|^2 + m_{H_d}^2|\mathcal{H}_d|^2 - b\Big(\mathcal{H}_u\mathcal{H}_d + \mathcal{H}_d^\dagger\mathcal{H}_u^\dagger\Big)\,, \end{aligned} \tag{6.41}$$

where $SU(4)$ invariance is guaranteed by the $\mathbb{Z}_2$ symmetry enforcing equal soft masses.

### 6.3.2 D-term SUSY TH

Another possibility of realizing the Twin Higgs mechanism is by generating the quartic term via the D-term of a new gauge symmetry with appropriately assigned charges, proposed in Ref. [68] and further explored in Refs. [69–71]. The new symmetry must be spontaneously broken so that the gauge boson is massive.

We extend the particle content with chiral multiplets $Z$, $P$ and $\bar{P}$ with $U(1)_X$ charges 0, $+q$ and $-q$, respectively. The superpotential is

$$W = \kappa Z\Big(P\bar{P} - M^2\Big)\,, \tag{6.42}$$

and assume that the soft masses of $P$ and $\bar{P}$ are equal

$$V = m_P^2\Big(|P|^2 + |\bar{P}|^2\Big)\,. \tag{6.43}$$

As a result, the $P$ and $\bar{P}$ obtain VEVs found via $\partial V/\partial P = 0$ and $\partial V/\partial\bar{P} = 0$:

$$v_p = \langle P\rangle = \langle\bar{P}\rangle = \sqrt{M^2 - \frac{m_P^2}{\kappa^2}}\,, \tag{6.44}$$

which in turn induces the mass of the gauge boson via the Higgs mechanism

$$m_X^2 = 4g_X^2 q^2 v_p^2\,. \tag{6.45}$$

If all the Higgses are charged under $U(1)_X$ symmetry, the D-term after integrating out heavy $P$ and $\bar{P}$ fields is

$$\begin{aligned} V =& \frac{g_X^2}{8}\left(\left|H_u^A\right|^2 - \left|H_d^A\right|^2 + \left|H_u^B\right|^2 - \left|H_d^B\right|^2\right)^2\Big(1-\epsilon^2\Big) = \\ =& \frac{g_X^2}{8}\Big(|\mathcal{H}_u|^2 - |\mathcal{H}_d|^2\Big)^2\Big(1-\epsilon^2\Big) = \frac{g_X^2}{8}\Big(|\mathcal{H}|^2\sin^2\beta - |\mathcal{H}|^2\cos^2\beta\Big)^2\Big(1-\epsilon^2\Big)\,, \end{aligned} \tag{6.46}$$

where

$$\epsilon^2 = \frac{m_X^2}{2m_P^2 + m_X^2} \tag{6.47}$$

comes from integrating out $P$ and $\bar{P}$, and in principle depends upon details of the model. However, it is possible to naturally have $\epsilon \ll 1$ [68].

Consequently, the quartic coupling in the D-term SUSY is

$$\lambda = g_X^2 \frac{\cos^2 2\beta}{8}\left(1-\epsilon^2\right), \tag{6.48}$$

which, as opposed to Eq. (6.38), is now increasing with $\operatorname{tg}\beta$.

The magnitude of the quartic term is bounded by the requirement that the Landau pole of $U(1)_X$ is avoided at low scales. The authors in Ref. [68] found that under mild assumptions, the gauge coupling is $g_X < 1.6(1.9)$ in the mirror (fraternal) Twin Higgs model. Moreover, the consistency requires that the Landau pole is above the mediation scale of SUSY breaking, $\Lambda$. This limits the validity of the $U(1)_X$ D-term SUSY to low mediation scales of SUSY breaking. This requirement may be slightly reduced if the first and second-generation fermions are not coupled to the $U(1)_X$, called the non-universal SUSY D-term TH model. By altering the $U(1)_X$ charges, the beta function of the $g_X$ is reduced and the Landau pole is pushed towards UV. As a consequence, in the non-universal D-term TH model, the gauge coupling can be as large as 2.4 [68].

Besides the tuning, large degeneracy in masses of the scalar CP-even heavy Higgses is expected in D-term SUSY TH, when compared with F-term models. Details concerning the spectrum of the models can be found in Ref. [68] for the D-term and in Refs. [66, 67] for the F-term model.

### 6.3.3 Fine-tuning in SUSY TH models

We can now proceed to the effect of double protection on naturalness. The SUSY TH models require the same fine-tuning as the Twin Higgs model, Eq. (6.15), of $\mathbb{Z}_2$ breaking to misalign the VEVs $v_A$ and $v_B$. Moreover, there is another source of fine-tuning present due to the corrections to the TH scale $f$

$$\delta f^2 = \frac{1}{32\pi^2}\left(\frac{3y_t^2}{\lambda}\Lambda_t^2 - 5\Lambda_\lambda^2\right), \tag{6.49}$$

where $\Lambda_t^2$ comes from loops involving stops, while $\Lambda_\lambda^2$ is generated by the Higgs self-interactions. Since the bounds on colorless particles are less constrained by the LHC, we will assume that $\Lambda_\lambda \ll \Lambda_t$. The total fine-tuning is thus, according to Eq. (2.114) given by

$$\Delta^{\text{tot}} = \frac{\partial \log f^2}{\partial \log \Lambda_t^2}\Delta_{v/f} = \frac{3y_t^2}{32\pi^2\lambda}\frac{\Lambda_t^2}{f^2}\frac{f^2}{2v^2} = \frac{3y_t^2}{32\pi^2}\frac{\Lambda_t^2}{v^2}\frac{1}{2\lambda}, \tag{6.50}$$

which should be compared to the fine-tuning in MSSM Eq. (6.28). Neglecting the log, exchanging physical threshold $m_{\tilde{t}}^2 \leftarrow \Lambda_{\text{UV}}^2$ and using $v = m_H^2/4\lambda$, the fine-tuning is relaxed by a factor

$$\Delta^{\text{MSSM}}/\Delta^{\text{tot}} = \frac{2\lambda}{\lambda_{\text{SM}}}, \tag{6.51}$$

where $\lambda_{\text{SM}} \simeq 0.13$ is the quartic coupling in the SM. Hence, the naturalness in the SUSY TH can be improved with respect to the MSSM as long as relatively large quartic $\lambda$ is generated. This result highlights the key difference between the SUSY TH discussed in the previous section, as the quartic coupling in the F-term model is bounded by the observed mass of the Higgs. On the other hand, the magnitude of the Higgs quartic in the D-term model is only bounded by the unitarity and allows for large improvements in the naturalness.

In particular, the fine-tuning in the F-term SUSY TH, for $\mu = 100$ GeV, $f/v = 3$, $\mathrm{tg}\,\beta = 3$ and $\lambda_S = 1.4$ is of order 1-2% in the region reproducing the observed mass of the Higgs [68]. Small higgsino mass is also preferred in the F-term model, as for $\mu = 500$ GeV, the required tuning is at the sub-percent level.

Meanwhile, in the D-term SUSY TH for $\mu = 500$ GeV, $f/v = 3$, $g_X \simeq 1.5$ and $\mathrm{tg}\,\beta = \mathcal{O}(5)$ the observed mass of the Higgs is obtained with about 10% fine-tuning for stops around 1 TeV. Stops as heavy as 2 TeV can be accommodated with tuning of order 2%. If more complexity is introduced by coupling only the heaviest fermions to the new $U(1)_X$ gauge boson, larger values of gauge coupling are compatible with the absence of the Landau pole. In the non-universal D-term SUSY TH model, the tuning can be as low as 20% for stops below 1 TeV, and heavy stops around 2 TeV require only 10% tuning.

The plots in Fig. 6.1 from Ref. [68] show the fine-tuning of the F-term SUSY TH (left panel) and D-term SUSY TH (right panel). The reduction of fine-tuning in the D-term SUSY TH model is significant and $m_h = 125$ GeV can be accommodated with $\Delta^{\mathrm{tot}} \simeq 8$.

The fine-tuning may be further reduced if larger values of the gauge couplings $g_X$ are allowed. However, larger couplings induce low-scale Landau pole, which in turn implies that low mediation scale of SUSY breaking (see discussion below Eq. (6.48)). This limitation of D-term SUSY TH has been addressed in Ref. [69], which considered the D-term generated by the non-abelian $SU(2)_X$ gauge group. By coupling the new gauge group to only a few of the supermultiplets, the running of the $g_X$ is significantly reduced, and the mediation scale of SUSY breaking can be as large as $\mathcal{O}(10^9)$ GeV. The impact of the new gauge interaction on the running of the top Yukawa further reduces the fine-tuning, which can be as good as 10% for SUSY partners beyond the reach of the LHC, while preserving perturbativity up to $10^{10}$ GeV. The mediation scale of SUSY breaking around Planck mass can also be accommodated in the asymptotically free D-term SUSY TH model proposed in Ref. [70]. Introducing two new gauge groups, $SU(2)_X$ and its mirror partner $SU(2)_{X'}$, the beta functions of the gauge couplings are altered and $SU(2)_X$ becomes asymptotically free. As a result, $g_X$ is large at low scales, improving the tuning by generating large quartic term in the TH potential Eq. (6.17). At the same time, the absence of the Landau pole relaxes the constraint on the mediation scale of SUSY breaking. Consequently, fine-tuning of only around 5-10% is required to obtain the correct EW scale with $\Lambda \simeq M_{\mathrm{pl}}$ with stops and gluino above 2 TeV.

## 6.4 Summary

In this chapter, we have introduced supersymmetry and the Twin Higgs mechanism as potential solutions to the hierarchy problem. We have discussed how the quadratic sensitivity of the EW VEV to the UV scales is avoided in each model. However, supersymmetry must necessarily be fine-tuned to yield observed EW VEV, while the Twin Higgs model suffers its own hierarchy problem. The limitations of those solutions motivate the introduction of double protection of the Higgs mass realized by Supersymmetric Twin Higgs models. Using existing literature we have demonstrated that $SU(4)$ symmetric quartic term, necessary for the TH mechanism, can be generated in SUSY in two ways, most notably by D-term of new gauge interaction. We have reviewed existing literature on SUSY TH models with an emphasis on naturalness, showing that fine-tuning can be better than 10% in several realizations of the models.

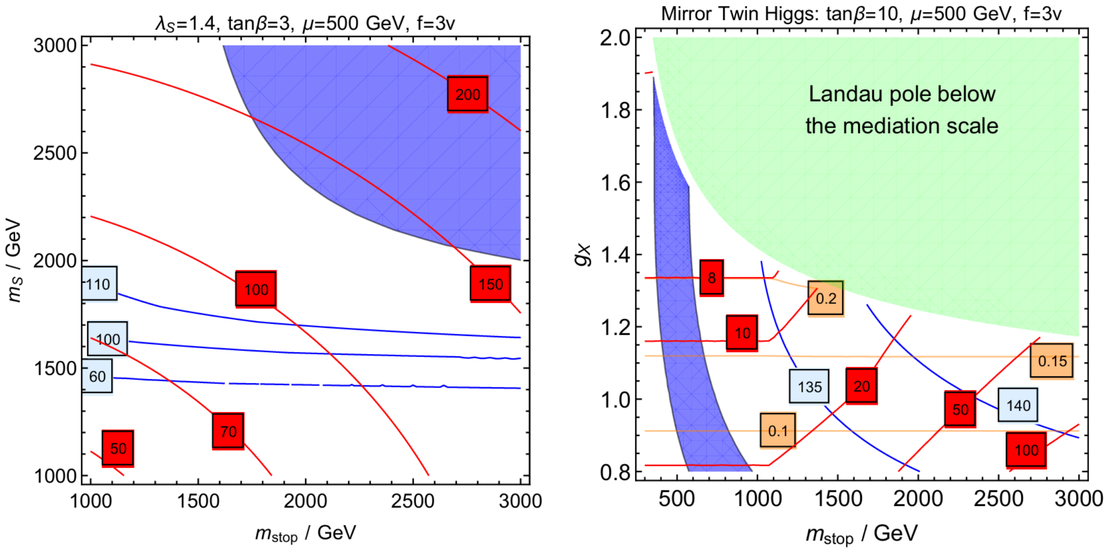


Figure 6.1: Fine-tuning contours (red) in F-term SUSY TH in $m_{\text{stop}} - m_S$ plane (left panel) and D-term SUSY TH in $m_{\text{stop}} - g_X$ plane (right panel) for $f = 3v$ and $\mu = 500$ GeV from Ref. [68]. On both plots, the gluino mass is $M_3 = 2$ TeV. The blue region reproduces $m_h = 125 \pm 3$ GeV, while blue contours denote the mass of the Higgs. Orange contours on the right panel mark the values of the $SU(4)$ quartic term Eq. (6.48), while in the green region the Landau pole of $U(1)_X$ is below the mediation scale of SUSY breaking assumed to be $\Lambda = 100 m_{\text{stop}}$.

# Chapter 7

# Twin supersymmetric dark matter

Many thermally produced dark matter candidates in the Twin Higgs models have been proposed [77–92], including twin tau, twin electron, twin pions, twin baryons and twin atoms.

Similarly, supersymmetric particles have long been considered as dark matter candidates [104]. In the R-parity conserving supersymmetric theories, the lightest supersymmetric particle is naturally stable. Most notable examples of the DM candidates in SUSY are the lightest neutralino [135, 271–274] and gravitino [271, 274]. However, in the MSSM, neutralino DM is tightly constrained and can be DM only in highly fine-tuned portions of the parameter space [105, 275–277].

Supersymmetric Twin Higgs models are primarily motivated by the naturalness of the electroweak scale. However, the plethora of new particles in those models allows for the accommodation of solutions to other problems of particle physics and cosmology. In particular, a stable sparticle in the twin sector is a cold relic and could be a candidate for dark matter, provided it meets all current constraints from direct detection experiments and astrophysical observations.

In this chapter, we will consider two dark matter candidates in the supersymmetric twin Higgs models, the twin stau in Sec. 7.1 and the twin neutralino in Sec. 7.2, the latter firstly discussed in [106]. As we will see, twin SUSY particles are quite naturally lighter than their MSSM counterparts due to mixing effects. We will discuss in detail their thermal production and implications for direct detection and collider searches.

## 7.1 Twin stau DM

In this section, we will consider twin stau, $\tilde{\tau}'$, as a candidate for the DM [60, 307]. Twin stau is $\mathbb{Z}_2$ partner of stau, $\tilde{\tau}$, which in turn is supersymmetric partner of tau lepton, $\tau$. Therefore, $\tilde{\tau}'$ is charged under twin electromagnetism and obtains soft masses from SUSY breaking, cf. Sec. 6.2.2. There are two twin stau states, corresponding to the two chiralities of the twin tau lepton.

In the following sections, we will consider the features of twin stau, including its mass in Sec. 7.1.1, its self-interactions in Sec. 7.1.2, the direct detection prospects of $\tilde{\tau}'$ DM in Sec. 7.1.3, the thermal relic abundance in Sec. 7.1.4 and the lifetime of MSSM stau in Sec. 7.1.5. Finally, in Sec. 7.1.6 we discuss the parameter space of twin stau DM.

### 7.1.1 Mass of (twin) stau

For twin stau to be stable, it must be the lightest supersymmetric particle (LSP), which implies that $m_{\tilde{\tau}'} < m_{\tilde{\tau}}$.

We assume that the SUSY breaking parameters do not break $\mathbb{Z}_2$, meaning that SUSY particles have the same soft masses in both the twin and MSSM sectors. For now, we will assume that the difference between sectors comes solely from the scalar sector and is captured by different values of VEVs, $v' \gtrsim v$. Later we will drop this assumption, allowing for $\mathbb{Z}_2$ breaking in the Yukawa sector, $y_{\tau'} \neq y_\tau$.

All below formulae will be given for stau, but analogous formulae for twin stau may be found by simply exchanging $v$ to $v'$, and $y_\tau$ to $y_{\tau'}$ if $\mathbb{Z}_2$ breaking in the Yukawa sector is present.

The stau mass matrix is

$$m^2_{\tilde{\tau}} = \begin{pmatrix} m^2_{3L} + \Delta_{\tilde{\tau}_L} + m^2_\tau & v(A_\tau \cos(\beta) - \mu y_\tau \sin(\beta)) \\ v(A_\tau \cos(\beta) - \mu y_\tau \sin(\beta)) & m^2_{3R} + \Delta_{\tilde{\tau}_R} + m^2_\tau \end{pmatrix}, \tag{7.1}$$

where $m^2_{3L}$, $m^2_3$ and $vA_\tau \cos(\beta) + c.c.$ are soft SUSY breaking contributions from Eq. (6.35), while diagonal $m^2_\tau$ and off-diagonal $y_\tau v \mu \sin(\beta)$ come from the superpotential Eq. (6.30), with Higgs field replaced with its VEV. The D-term contributions to the stau matrix are

$$\Delta_{\tilde{e}_i} = (T_{3e_i} - Q_{e_i} \sin^2\theta_W) \cos 2\beta m^2_Z\,, \tag{7.2}$$

where $T_3$ is the third component of weak isospin, $Q$ is the electric charge and $\theta_W$ is the Weinberg angle, $\sin^2\theta_W \simeq 0.22336 \pm 0.00010$ [13]. The explicit D-term contributions are [306, 308]

$$\begin{aligned} \Delta_{\tilde{e}3R} &= -m^2_Z \sin^2\theta_W \cos 2\beta\,, \\ \Delta_{\tilde{e}3L} &= m^2_Z\left(\sin^2\theta_W - \frac{1}{2}\right)\cos 2\beta\,. \end{aligned} \tag{7.3}$$

The mass eigenstates are found by diagonalizing the stau matrix with a unitary transformation, $\mathcal{R}_{\theta_{\tilde{\tau}}}$,

$$\mathcal{R}^\dagger_{\theta_{\tilde{\tau}}} m^2_{\tilde{\tau}} \mathcal{R}_{\theta_{\tilde{\tau}}} = \begin{pmatrix} m^2_{\tilde{\tau}_1} & 0 \\ 0 & m^2_{\tilde{\tau}_2} \end{pmatrix} \to \begin{pmatrix} \tilde{\tau}_1 \\ \tilde{\tau}_2 \end{pmatrix} = \begin{pmatrix} \cos\theta_{\tilde{\tau}} & -\sin\theta^*_{\tilde{\tau}} \\ \sin\theta_{\tilde{\tau}} & \cos\theta^*_{\tilde{\tau}} \end{pmatrix} \begin{pmatrix} \tilde{\tau}_L \\ \tilde{\tau}_R \end{pmatrix}, \tag{7.4}$$

where we defined stau mixing angle $\theta_{\tilde{\tau}}$. The preferred values of $\mathrm{tg}\,\beta$ are set by the unitarity of top Yukawa, $y_t = m_t/v \sin\beta \lesssim 1 \to \mathrm{tg}\,\beta \gtrsim 1$ [73]. Hence, the D-terms, $\Delta_{\tilde{e}3R}$ and $\Delta_{\tilde{e}3L}$, are both positive and proportional to the square of VEV, implying that for $v'/v \gtrsim 3$, diagonal entries are larger in the twin sector. However, the D-terms are suppressed by the gauge coupling, and for moderate values of $v'/v$, they give only a subleading contribution to the twin stau mass matrix. On the other hand, the off-diagonal terms are also proportional to the VEV and, for moderate values of higgsino mass $\mu$, lead to large mixing, pushing the mass of twin stau below the mass of stau.

The mass splitting between stau and sneutrino is given by [73]

$$m^2_{\tilde{\tau}_L} - m^2_{\tilde{\nu}_\tau} = -\cos(2\beta) m^2_W\,, \tag{7.5}$$

which implies that for $\mathrm{tg}\,\beta > 1$ sneutrino is always lighter than purely left-handed stau.

Combining the above insights, we conclude that mostly right-handed twin stau with large mixing, $m^2_{L_3} \gtrsim m^2_{\tilde{e}_3}$, is the preferred region of twin stau LSP.

### 7.1.2 Self-interactions of twin stau

Twin stau is characterized by an unsuppressed coupling to twin electromagnetism, resulting in long-range interaction mediated by the massless twin photon $\gamma'$.

Self-scatterings in the galactic halos lead to isotropization of the momenta of DM particles, reducing the ellipticity of the halo. The measurement of the ellipticity $\epsilon \simeq 0.3$ of the gravitational potential of NGC720 [309] allows for constraining the self-interaction of the DM. In the past, this bound has been overestimated by about an order of magnitude. The reason for that was using the linear approximation for the evolution of the ellipticity [310], which neglects the saturation effects, which substantially reduce the isotropization. A careful treatment of the velocity distribution of DM in the halo has been conducted in Ref. [311], which we will follow in this section.

Assume that there are two populations of DM particles, both described by Maxwell-Boltzmann distribution with different velocities, $v_h \gg v_c$. The distribution is therefore given by

$$f(v) = \frac{n_c}{\pi^{3/2} v_c^3} \exp\left(-\frac{v^2}{v_c^2}\right) + \frac{n_h}{\pi^{3/2} v_h^3} \exp\left(-\frac{v^2}{v_h^2}\right), \tag{7.6}$$

where $n_i$ is number density of $i$th population. The transfer of the energy between the populations is responsible for the isotropization of the DM halo and is modeled by the Boltzmann equation

$$\frac{df(v_1)}{dt} = \int d^3 v_2 d\Omega' |v_1 - v_2| \frac{d\sigma}{d\Omega'} (f(v_1)f(v_2) - f(v_3)f(v_4)), \tag{7.7}$$

where primes denote quantities in the CM frame. and unprimed denoted quantities in the galaxy frame. The differential cross section for the Møller, $e^- e^- \to e^- e^-$, and Bhabha scatterings, $e^- e^+ \to e^- e^+$, mediated by a twin photon is

$$\frac{d\sigma}{d\Omega'} = \frac{4\alpha_D^2}{m_{\rm DM}^2 |v_1 - v_2|^4 (1-\cos\theta')^2}, \tag{7.8}$$

where $\alpha_D = g^2/4\pi$ with gauge coupling $g$. Note that the cross section is the same for fermion and scalar DM in the non-relativistic limit, which justifies the use of the bound for twin stau. The cross-section is dominated by the $\theta' \simeq 0$, which allows authors to find a simple differential equation for the evolution of mean velocity

$$v_c \dot{v_c} = -\frac{8\sqrt{\pi}}{3} \frac{\alpha_D^2 n_h}{m_{\rm DM}^2 v_h^5} \left(v_c^2 - v_h^2\right)^2 \ln\Lambda, \tag{7.9}$$

where $\Lambda$ is the cut-off of divergent integration over angle, given in terms of the inter-particle spacing, $\lambda_p$, and the number density of the hot population, $n_h$. The solution of the equation is

$$v_c^2(t) = v_h^2 \left(1 - \frac{1}{\frac{t}{\tau} + \frac{v_h^2}{v_h^2 - v_{c,0}^2}}\right), \tag{7.10}$$

where $v_{c,0}$ is the initial velocity dispersion and the timescale of isotropization is

$$\tau = \frac{3 m_{\rm DM}^3 v_h^3}{16\sqrt{\pi} \alpha_D^2 n_h \ln\left(1 + \lambda_p^2 m_{\rm DM}^2 v_{0,c}^4/\alpha_D^2\right)}. \tag{7.11}$$

The ellipticity evolves as

$$\epsilon(t) \sim 1 - \frac{v_c^2(t)}{v_h^2} = \frac{\epsilon_0}{\frac{t}{\tau}\epsilon_0 + 1}, \tag{7.12}$$

saturating at late times, as $\epsilon$ approaches 0. Specifying to the case of the DM charged under twin electromagnetism, $\alpha_D = \alpha_{\rm em} = 1/137$, the ellipticity sets a lower bound on its mass

$$m_{\rm DM} \gtrsim 210 \text{ GeV}. \tag{7.13}$$

Satisfying this bound in the Twin Higgs models often requires breaking of twin electromagnetism [77–83, 83–86], since masses of twin particles have approximate scaling $m_{i'} = m_i v'/v$. However, in Twin SUSY the contributions from SUSY breaking can easily exceed $\mathcal{O}(100)$ GeV, and thus the bound can easily be satisfied without more model building. In particular, in the following sections, we show, that the observed relic abundance is reproduced by twin stau with mass $m_{\tilde{\tau}'} \gtrsim 400$ GeV.

### 7.1.3 Direct detection

The interaction between twin stau and the nucleons is mediated by the Higgs portal and Yukawa couplings to quarks

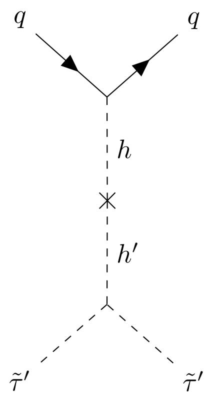


Each such diagram generates an effective twin stau-quark coupling

$$\mathcal{L}_{q\tilde{\tau}'} = S \sum_q c_q \bar{q} q \,, \tag{7.14}$$

where $S = \tilde{\tau}' \tilde{\tau}'^*$ and the couplings are

$$c_{u_i} = -\frac{\lambda_{h\tilde{\tau}'\tilde{\tau}'}}{m_h^2} \frac{m_{u_i}}{v} \frac{\sin\alpha}{\cos\beta}, \qquad c_{d_i} = \frac{\lambda_{h\tilde{\tau}'\tilde{\tau}'}}{m_h^2} \frac{m_{d_i}}{v} \frac{\cos\alpha}{\sin\beta} \,, \tag{7.15}$$

for up- and down-type quarks. In the above equations $m_h$ is the mass of SM Higgs, $\alpha$ is the mixing angle diagonalizing neutral CP-even Higgs mass matrix, and $\beta$ is defined by Eq. (6.32). The twin stau-Higgs coupling reads

$$\begin{aligned} \lambda_{h\tilde{\tau}'\tilde{\tau}'} &= \frac{g}{m_{W'}} \left[ \left( -\frac{1}{2} c^2_{\theta_{\tilde{\tau}'}} + s^2_W c_{2\theta_{\tilde{\tau}'}} \right) m^2_{Z'} s_{\alpha+\beta} + m^2_{\tau'} \frac{s_\alpha}{c_\beta} + \frac{m_{\tau'}}{2} \left( A_\tau \frac{s_\alpha}{c_\alpha} + \mu \frac{c_\alpha}{c_\beta} \right) s_{2\theta_{\tilde{\tau}'}} \right] \frac{v}{v'} \\ &\simeq \frac{g}{m_{W'}} \left[ \left( \frac{1}{2} c^2_{\theta_{\tilde{\tau}'}} - s^2_W c_{2\theta_{\tilde{\tau}'}} \right) m^2_{Z'} c_{2\beta} - m^2_{\tau'} - \frac{m_{\tau'}}{2} (A_\tau - \mu \,\mathrm{tg}\,\beta) s_{2\theta_{\tilde{\tau}'}} \right] \frac{v}{v'} \,, \end{aligned} \tag{7.16}$$

where the factor $v/v'$ comes from Higgs-twin Higgs mixing Eq. (6.9) (setting $v' \simeq f$, which holds for $v' \gg v$), $s_x = \sin x$ and $c_x = \cos x$, $m_{\tau'}$, $m_{W'}$ and $m_{Z'}$ are masses of the twin tau, W, and Z, respectively, $s_W$ is the sine of Weinberg angle and $g$ is electroweak coupling constant. In the second line, we go to the decoupling limit using $\cos(\beta - \alpha) = 0$. This result is obtained from stau-Higgs coupling, found e.g. in Ref. [308], corrected by the Higgs-twin Higgs mixing factor.

The twin stau-quark couplings generate effective twin stau-nucleon coupling [312]

$$\frac{c_N}{m_N} = \sum_q \frac{c_q f^N_{T_q}}{m_q} + \frac{2 f^N_{T_G}}{27} \sum_Q \frac{c_Q}{m_Q} \,, \tag{7.17}$$

where $m_N \simeq 940$ GeV is nucleon mass and $f_{T_G}$ is the form factor from gluon contribution to the coupling given by

$$f_{TG} = 1 - \sum_{q=u,d,s} f_q^N \,. \tag{7.18}$$

The quark form factors, $f_q^N$, are defined by

$$m_N f_q^N = \langle N | m_q \bar{q} q | N \rangle \,. \tag{7.19}$$

For the numerical values of the neutron form factors we use $f_u^N = 0.0191, f_d^N = 0.0153$, and $f_s^N = 0.0447$ [313]. Numerically, the difference in coupling $c_N$ to nucleons and protons is negligible.

The DD process $\tilde{\tau}'N \to \tilde{\tau}'N$ is represented by the diagram

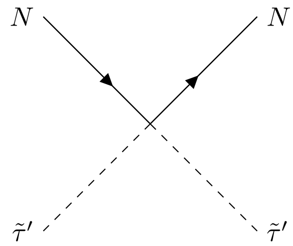


where non-relativistic amplitude reads [314]

$$|\mathcal{M}|^2 \simeq c_N^2 \left(2m_N\right)^2 . \tag{7.20}$$

The differential cross section is

$$\frac{d\sigma}{d\Omega} = \frac{1}{64\pi^2 (E_{\tilde{\tau}'} + E_N)^2} \frac{|\vec{p}_{\tilde{\tau}'}|}{|\vec{p_N}|} |\mathcal{M}|^2 \,, \tag{7.21}$$

where $\vec{p}_{\tilde{\tau}'}, \vec{p}_N$ are momenta of twin stau and nucleon, and $E_{\tilde{\tau}'}, E_N$ are corresponding energies. Taking the non-relativistic limit $E_i \simeq m_i$ in the centre of mass frame, $|\vec{p}_{\tilde{\tau}'}|/|\vec{p_N}| \simeq 1$, and integrating over the solid angle, we find the cross section

$$\sigma = \frac{c_N^2 \mu_{\tilde{\tau}'N}^2}{4\pi m_{\tilde{\tau}'}^2} \,, \tag{7.22}$$

where we have introduced the reduced mass of the system $\mu_{\tilde{\tau}'N} = m_{\tilde{\tau}'} m_N / (m_{\tilde{\tau}'} + m_N)$.

There are a few features of the direct detection cross section, which we will now highlight.

Firstly, the twin stau-Higgs coupling is proportional to the Higgs-twin Higgs mixing and hence can be suppressed by the hierarchy of electroweak and twin Higgs scales, $v \ll f \simeq v'$. Secondly, the form of the coupling Eq. (7.16) allows for cancellation between the first and third terms in the parenthesis, implying the existence of a blind spot in the DD searches for twin stau for $\theta_{\tilde{\tau}'} \sim 1/2$.

### 7.1.4 Thermal abundance

The R-parity conservation ensures that eventually, all odd particles decay into the LSP. As a result, the calculation of the relic density of DM involves calculation of the effective annihilation rate, as discussed in Appendix B.5.

In SUSY TH models, the Higgs portal is the most potent mechanism of thermalization between the sectors. In particular, even particles are kept in thermal equilibrium down to temperatures around 3 GeV [256], and hence we can describe both sectors with common temperature. At high temperatures, all particles are assumed to be in thermal equilibrium. As temperature drops and interactions are not sufficient to maintain thermalization, heavy unstable particles eventually decay, leaving behind the only stable LSP.

Since all processes involving particles from both sectors must include the Higgs-twin Higgs mixing, the scattering rates are suppressed at least by $(v/v')^2$. Therefore, we assume that only twin particles enter the effective annihilation cross section of the twin stau. This allowed us to use the `Micromegas` [306,315,316], which we have adapted for the twin sector by adjusting the masses of twin SM particles using scaling $m_{i'} = m_i v'/v$ or in presence of the $\mathbb{Z}_2$ breaking in the Yukawa sector $m_{f'} = m_f(v'/v)\,(y_{f'}/y_f)$. Unless stated otherwise, in our analysis, we set all soft masses, except $m_{3R}$ and $m_{3L}$ to $m_{\rm soft} = 10$ TeV. The reason is that squarks and sleptons affect relic abundance only when they are nearly degenerate with twin stau, and coannihilations become important.

This assumption is satisfied in most parts of the parameter space. However, in the absence of additional $\mathbb{Z}_2$-breaking the mass splitting between stau and twin stau may be small, $\Delta = (m_{\tilde\tau} - m_{\tilde\tau'})/m_{\tilde\tau'} \lesssim 0.05$, and coannihilation might play a role. To account for that, we follow Ref. [317]. The effective annihilation cross section, discussed and derived in Appendix B.5, is given by

$$\sigma_{\rm eff} = \sum_{ij} \sigma_{ij} \frac{g_i g_j}{g_{\rm eff}^2} (1+\Delta_i)^{3/2} (1+\Delta_j)^{3/2} \exp(-x(\Delta_i + \Delta_j))\,, \tag{7.23}$$

where sum runs over all particles, $\Delta_i$ is the mass splitting between LSP and $i$th particle, $g_i$ is the number of degrees of freedom of $i$th particle and $g_{\rm eff}$ is defined

$$g_{\rm eff} = \sum_i g_i (1+\Delta_i)^{3/2} \exp(-x\Delta_i)\,. \tag{7.24}$$

Assuming that only stau mass is in the proximity of the twin stau mass and leveraging the $\mathbb{Z}_2$ symmetry we set $\sigma_{\tilde\tau\tilde\tau} = \sigma_{\tilde\tau'\tilde\tau'} \equiv \sigma$. Denoting $\Delta \equiv \Delta_{\tilde\tau}$, we have

$$\sigma_{\rm eff} = \frac{\sigma}{g_{\rm eff}^2} \Big(1 + (1+\Delta)^3 \exp(-2x\Delta)\Big)\,, \tag{7.25}$$

where we have neglected the cross terms $\sigma_{\tilde\tau\tilde\tau'}$ for processes such as $\tilde\tau'\tilde\tau \to XX'$, which are suppressed by the Higgs-twin Higgs mixing $(v/v')^2$ and loop factor $1/16\pi^2$. Note, that $\tilde\tau - \tilde\tau'$ coannihilation cannot be a number-changing process at the tree level due to diagonal Higgs and twin Higgs couplings. Such coannihilation is also induced by the Higgsino and bino mixing or X gaugino portal (discussed in Sec. 7.1.5), however those processes are suppressed by large masses of mediators. Finally, the effective annihilation cross section at the time of freeze-out is

$$\sigma_{\rm eff} = \sigma \frac{1 + (1+\Delta)^3 e^{-2x_f\Delta}}{[1 + (1+\Delta)^{3/2} e^{-x_f\Delta}]^2}\,, \tag{7.26}$$

where $x_f = m_{\tilde\tau'}/T_f \sim 25$, with $T_f$ the freeze-out temperature. If the coannihilation with stau is subdominant, we can assume that the resulting relic abundance is simply scaled, according to Eq. (2.126), as

$$\Omega_{\rm coann} h^2 = \Omega h^2 \frac{\sigma}{\sigma_{\rm eff}}\,, \tag{7.27}$$

where $\Omega h^2$ is relic abundance calculated within the twin sector. Finally, we note, that the effect of the coannihilation with stau is just controlled by the mass splitting, which can be easily calculated. The largest possible enhancement is obtained for $\Delta = 0$ when stau acts as an additional degree of freedom of twin stau and relic density is increased by a factor of 2.

In the analysis, we differentiate between three cases of twin stau DM, allowing for $\Omega_{\tilde{\tau}'}h^2 \neq \Omega_{\rm obs} = 0.12$ for generality. We will refer to twin stau reproducing the observed relic density, $\Omega_{\tilde{\tau}'}h^2 = \Omega_{\rm obs} = 0.12$ as the thermal scenario, which is phenomenologically most interesting.

The multicomponent DM scenario refers to the region of parameter space with $\Omega^{\rm th}h^2 \leqslant 0.12$, where some additional source of DM is assumed. Most importantly, the DD bounds are weakened if twin stau does not constitute all of DM, which we take into account by rescaling the DD cross section by $\Omega^{\rm th}h^2/0.12$.

Finally, if twin stau is overproduced and $\Omega^{\rm th}h^2 > 0.12$, we will assume that an additional source of entropy injection suppresses the relic density so that $\Omega_{\tilde{\tau}'}h^2 = 0.12$. As a consequence, the DD bounds cross section is not rescaled in the region with $\Omega^{\rm th}h^2 > \Omega^{\rm obs}h^2$. We will refer to this as the non-thermal scenario.

### 7.1.5 Lifetime of stau

Because the mass splitting between twin stau and stau is relatively small, $\mathcal{O}(10)$ GeV, the signature of the twin stau DM scenario is relatively light stau with a mass of several hundred GeV. In particular, if the mass splitting is large enough, the stau decays into tau, twin tau, and twin stau

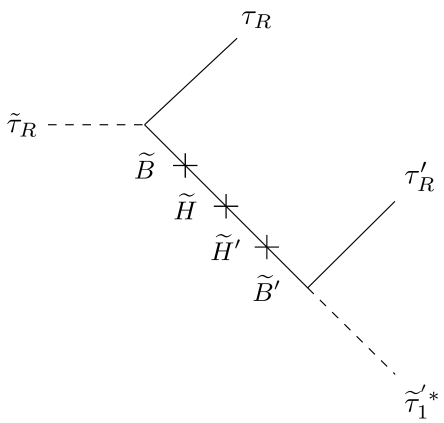


In the minimal scenario, this decay is mediated by the higgsino mass mixing. Such mixing must be present since Higgs and twin Higgs are coupled by a quartic term. In particular, in D-term Twin SUSY the mixing is

$$\mathcal{L}_{\text{ higgsino mix}} = -\epsilon_{\tilde{H}} \left( \tilde{H}_u - \frac{1}{\tan\beta} \tilde{H}_d \right) \left( \tilde{H}'_u - \frac{1}{\tan\beta} \tilde{H}'_d \right) , \tag{7.28}$$

which is generated by gaugino exchange from vertices generated by two first terms from the last line of Eq. (6.19) (setting the Higgs to its VEV). For concreteness, consider Twin SUSY D-term $U(1)_X$. We can estimate this mixing by considering the diagram

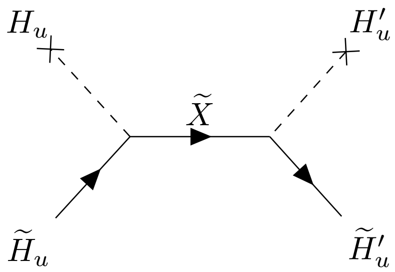


which in an effective theory, at scales below gaugino mass, contributes to the higgsino mass mixing

$$\epsilon_{\tilde{H}} \sim \frac{1}{m_{\tilde{X}}}\left(\sqrt{2}g_X\right)^2 Q_{H_u} Q_{H'_u} vv' \sim \frac{g_X vv'}{2v_P}\,, \tag{7.29}$$

where $m_{\tilde{X}} = g_X v_P$ is the mass of the $U(1)_X$ gaugino obtained from SSB after scalar field $P$ with charge $q = 1/2$ obtains VEV $\langle P\rangle = v_P$, cf. Eq. (6.45). The above result neglects soft gaugino mass , which alters the result by a factor of order $\mathcal{O}(1)$. $Q_{H_i}$ are gauge $U(1)_X$ charges of the Higgs doublets. The VEV $v_S$ generates a large mass of the gauge boson $X$ and the electroweak precision measurements give lower bound $v_S > 4$ TeV. In the numerical calculations we have adopted $g_X = 2$, $v_S = 5$ TeV which roughly gives

$$\epsilon_{\tilde{H}} \approx \left(\frac{v'/v}{3}\right) 20 \text{ GeV}\,. \tag{7.30}$$

Of course, those results depend on the details of the UV model and could be altered by an order of magnitude by changing the parameters by order $\mathcal{O}(1)$. An alternative derivation of the above estimate can be found in Ref. [307].

The effective lagrangian of stau, twin stau, tau, and twin tau from the first diagram in this section is

$$\mathcal{L} \supset \frac{1}{M}\bar{\tau}\bar{\tau}'\tilde{\tau}\tilde{\tau}'\,, \tag{7.31}$$

where the coupling is approximately

$$\frac{1}{M} = \frac{(g'^2 s_\beta v)\cdot(g'^2 s_\beta v')\epsilon_{\tilde{H}}(M_1^2 + m_{\tilde{\tau}}^2)m_{\tilde{\tau}}^2}{(M_1^2 - m_{\tilde{\tau}}^2)^2\cdot(\mu^2 - m_{\tilde{\tau}}^2)^2}\,. \tag{7.32}$$

In above formula, $(g'^2 s_\beta v)$ accounts for bino-stau-tau vertex $(g')$ and the bino-higgsino mixing $(g' s_\beta v)$, assuming large $\operatorname{tg}\beta$ which results in larger mixing with $\tilde{H}_u$. The term $(g'^2 s_\beta v')$ follows analogously and $\epsilon_{\tilde{H}}$ comes from higgsino mixing. The remaining factors come from the bino and higgsino propagators.

The 3-body decay width of particle with mass $M$ to particles with masses $m_1, m_2, m_3$ can be calculated using Eq. (A.67)

$$d\Gamma = \frac{1}{(2\pi)^3}\frac{1}{32M^3}|\mathcal{M}|^2 dm_{12}^2 dm_{23}^2\,, \tag{7.33}$$

where momentum variables $m_{ij}$ are defined in Appendix A.3. In our case we have $M = m_{\tilde{\tau}}$, $m_1 = m_{\tilde{\tau}'}$, $m_2 = m_{\tau'}$ and $m_3 = m_\tau$, which allows us to express the amplitude in the limit of large $\operatorname{tg}\beta$ and for $\mu, M_1 \gg g'v'$ as [307]

$$|\mathcal{M}|^2 = \left(\frac{g'^4 s_\beta^2 vv'\epsilon_{\tilde{H}}(M_1^2 + m_{\tilde{\tau}}^2)m_{\tilde{\tau}}^2}{(M_1^2 - m_{\tilde{\tau}}^2)^2\cdot(\mu^2 - m_{\tilde{\tau}}^2)^2}\right)^2 \left(m_{23}^2 - (m_\tau + m_{\tau'})^2\right)\,. \tag{7.34}$$

where $m_{23}^2 - (m_\tau + m_{\tau'})^2$ comes from the Dirac trace over the fermions in the effective interaction.

Neglecting the masses of tau and twin tau we find approximate decay width

$$\Gamma \simeq \frac{1}{480\pi^3} \frac{(m_{\tilde\tau} - m_{\tilde\tau'})^5}{m_{\tilde\tau}^2} \left( \frac{g'^4 s_\beta^2 v v' \epsilon_{\tilde H} (M_1^2 + m_{\tilde\tau}^2) m_{\tilde\tau}^2}{(M_1^2 - m_{\tilde\tau}^2)^2 \cdot (\mu^2 - m_{\tilde\tau}^2)^2} \right)^2 , \tag{7.35}$$

which numerically gives the decay length

$$d_{\tilde\tau} \simeq 2.7\text{m} \left( \frac{m_{\tilde\tau}}{300 \text{ GeV}} \right)^2 \left( \frac{M}{10^6 \text{ GeV}} \right)^2 \left( \frac{10 \text{ GeV}}{m_{\tilde\tau} - m_{\tilde\tau'}} \right)^5 . \tag{7.36}$$

We include $m_\tau$ and $m_{\tau'}$ in our calculations by numerically integrating Eq. (A.67) over $dm_{12}$.

From Eq. (7.36) it is clear that the decay length can be above 1 m for heavy bino and higgsino. This can be mitigated by increasing the mass splitting between stau and twin stau, which is maximized in the region of large mixing.

### Bino mixing

Let us comment on possible suppression of the stau decay length by introducing the bino mass mixing

$$\mathcal{L}_{\tilde B \tilde B'} = -\epsilon_{\tilde B} M_1 \tilde B \tilde B' , \tag{7.37}$$

which induces the effective coupling

$$\frac{1}{M} \bar\tau \bar\tau' \tilde\tau \tilde\tau', \qquad \frac{1}{M} = \frac{2 g'^2 \epsilon_{\tilde B}}{M_1} . \tag{7.38}$$

The decay is then simply

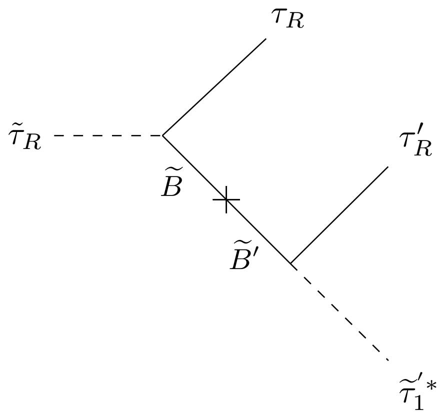


The stau decay length is then

$$d_{\tilde\tau} = 0.6 \text{ m} \left( \frac{m_{\tilde\tau}}{300 \text{ GeV}} \right)^2 \left( \frac{M_1}{10^3 \text{ GeV}} \right)^2 \left( \frac{10 \text{ GeV}}{m_{\tilde\tau} - m'_{\tilde\tau}} \right)^5 \left( \frac{10^{-2}}{\epsilon_M} \right)^2 , \tag{7.39}$$

which even for moderate values of the bino mixing allows for the stau decay length below 1 m even for heavy bino. However, the inclusion of bino mass mixing must not allow sizeable kinetic mixing of twin photon with photon

$$\mathcal{L}_{\gamma\gamma'} = -\frac{\epsilon}{2} F_{\mu\nu} F'^{\mu\nu}, \tag{7.40}$$

which would induce interaction between twin stau DM and nucleons, and is constrained by Xenon1T [165, 318]

$$\epsilon < 10^{-10}\left(\frac{m_{\tilde{\tau}'}}{100 \text{ GeV}}\right)^{1/2}. \tag{7.41}$$

We will distinguish short- and long-lived stau separately, as the phenomenology of those cases differ substantially.

### Short-lived stau in collider searches

The product of the stau decay is tau, which for short-lived stau is even softer than in MSSM, as in TH SUSY it decays into three particles: tau, twin tau, and twin stau. Short-lived stau is thus poorly constrained, as the soft tau leptons are difficult to observe [307]. At the time of writing Ref. [307] LHC was not sensitive to the direct production of right-handed stau, even in the limit of massless LSP [319, 320]. Since then, the search for direct production of stau pair performed in Ref. [321] found that the LHC is sensitive to stau pair production for mass splitting between LSP and stau, of order 100 GeV [321]. However, the mass splitting between stau and twin stau is typically of order few GeV, and thus the LHC searches for stau pair production do not constrain our scenario.

The LHC bounds on neutralino decays into stau may be relevant. Firstly, consider wino decays

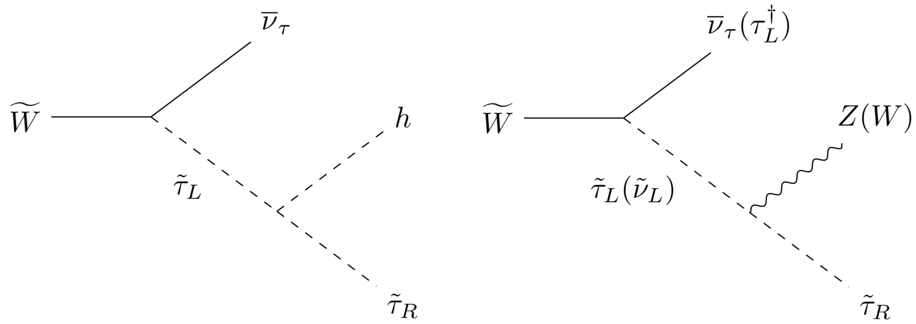


which can be probed by the search for taus and missing energy. However, the bounds are only applicable for $m_{\text{LSP}} < 100$ GeV [322], which is far below the mass of twin stau reproducing correct relic abundance, around $m_{\tilde{\tau}'} \sim 450$ GeV (discussed in Sec. 7.1.6). Similarly, the search for bosons $Z/W/h$ and the missing energy may also be relevant, however for $m_{\text{LSP}} > 300$ GeV, generically realized by the thermal scenario of twin stau DM, the constraint on wino mass is also absent. If the other two sleptons are also lighter than wino, the lower bound on wino mass becomes 1300 GeV in the limit of massless LSP, but it completely relaxes if the mass of LSP is above 800 GeV. For short-lived stau, this is essentially the only constraint relevant in the region of parameter space realizing twin stau DM. Nonetheless, there is no necessity for light wino for the validity of $\tilde{\tau}'$ as a DM candidate and this constraint should be viewed as a complementarity check for this scenario.

The higgsino decays

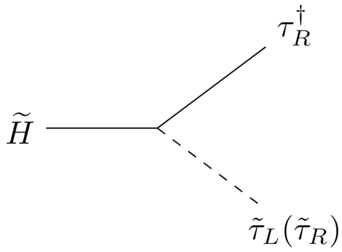


are analogous to the wino decays but does not involve Z/W/h in the final state. The cross section for such decays is even smaller due to Yukawa suppression, and consequently, the bound on higgsino mass is even weaker than bounds on wino mass.

Henceforth, generically, the masses of neutralinos are not constrained in our scenario as long as stau is short-lived.

### Long-lived stau

On the other hand, long-lived stau has important consequences not only for collider searches but also for cosmology.

If stau lifetime is larger than about 10 ns, corresponding to the decay length $d_{\tilde{\tau}} \sim \mathcal{O}(1)$m, LHC searches for long-lived charged particles become sensitive [323]. In particular, the bound on the mass of right-handed stau is [324]

$$m_{3R} \gtrsim 430 \text{ GeV}\,, \tag{7.42}$$

which sets tight constraints on the parameter space of twin stau DM. Moreover, the decay of heavy MSSM particles into stau exclude masses of stop, gluino, wino, higgsino, and left-handed slepton above 1600, 2200, 1300, 1200, and 500 GeV, respectively [307].

The stau with decay length below 1 m but above 0.1 m could be observed as a disappearing charged track at LHC [325, 326]. The upper limit on the production cross-section of stau with $d_{\tilde{\tau}} \sim \mathcal{O}(1)$ m at LHC with $\sqrt{s} = 13$ TeV is about 10 fb [325]. This sets a lower limit on the mass of right-handed stau of about 200 GeV [307], which is comparable to the ellipticity bound Eq. (7.13). This implies that LHC disappearing charged tracks searches will not play an important role in constraining the parameter space of twin stau DM.

If stau becomes very long-lived, it could decay after Big Bang Nucleosynthesis (BBN), altering the abundance of light elements including deuterium, $^3$He and $^4$He [145]. From Eq. (7.36) we see that the lifetime of stau is generically much shorter than $10^5$ s, corresponding to $d_{\tilde{\tau}} \sim \mathcal{O}(10^3)$ m, unless the mass splitting between stau and twin stau becomes small. The lifetime of stau can only alter BBN if the kinematic condition, $m_{\tilde{\tau}} > m_\tau + m_{\tau'} + m_{\tilde{\tau}'}$ is nearly saturated. Therefore, for the sake of plots, we adapt the BBN condition as

$$m_{\tilde{\tau}} < m_\tau + m_{\tau'} + m_{\tilde{\tau}'}. \tag{7.43}$$

If stau decays after the twin stau freeze-out around $T \simeq m_{\tilde{\tau}'}/25$, the DM abundance is enhanced by up to factor 2. However, as the stau decay is inefficient, the coannihilation between twin stau and stau ceases. The stau decays after twin stau freeze-out if its decay length is larger than

$$0.2\frac{M_{\rm pl}}{(m_{\tilde{\tau}}/25)^2} \simeq \mathcal{O}(1)\text{m}\left(\frac{300 \text{ GeV}}{m_{\tilde{\tau}}}\right)^2. \tag{7.44}$$

Stau decay length is above 1 m for nearly degenerate stau and twin stau, therefore our inclusion of coannihilations via Eq. (7.27) already mimics this effect, slightly underestimating the thermal relic abundance.

### 7.1.6 Results

In this section, we will consider $\mathbb{Z}_2$ breaking only in the Higgs potential and in the Yukawa sector. In particular $m_{3R'} = m_{3R}$, $m_{3L'} = m_{3L}$, $\mathrm{tg}\,\beta' = \mathrm{tg}\,\beta$ and $\mu = \mu'$. Moreover, throughout the analysis, we will set $A_\tau = 0$, as its effect on the $m_{\tilde{\tau}'}$ can be mitigated by adjusting $\mathrm{tg}\,\beta$ and $\mu$, while the effect on the effective annihilation cross section is subdominant.
We show that for the minimal hierarchy of EW and TH scales, $v'/v = 3$, twin stau is a valid candidate for the DM.

We will present the results from Ref. [307] and Ref. [60], updated with the first bound from the LZ experiment [168]. In cases when $v'/v = 3$ is excluded by the 2022 null results from LZ, we will also include plots with enhanced scalar $\mathbb{Z}_2$ breaking, $v'/v = 5$.

#### Decoupling limit

Firstly, let us consider the simplest scenario when all SUSY particles except for (twin) stau are decoupled. In particular, it means that bino and wino masses are set to $M_1 = M_2 = m_{\text{soft}} = 10$ TeV and they don't participate in the thermalization of twin stau. This simplifying assumption allows an understanding of the basic features of twin stau parameter space. The higgsino mass $\mu$ enters the mass matrix of twin stau, Eq. (7.1), so to avoid large contributions to the mass of twin stau we will set it to the natural value, which in TH models can be as large as $\mu = 1.5$ TeV. To maximize the mixing, we choose $\mathrm{tg}\,\beta = 10$, so that $\sin\beta \simeq 1$ in off-diagonal entries of (twin) stau matrix. On Fig. 7.1 we show the resulting parameter space in the plane of the right and left soft stau masses $m_{3R}$, $m_{3L}$. In some parts of the parameter space twin stau is not the LSP, corresponding to small mixing, as expected from the discussion in Sec. 7.1.1. For the lighter, mostly right-handed twin stau, the stau is always the lightest, while for the lighter, mostly left-handed twin stau the twin sneutrino is the lightest. Also, for sufficiently small soft masses, twin stau becomes tachyonic due to the large off-diagonal term in Eq. (7.1).

The correct relic density is obtained for twin stau masses between 250 and 400 GeV. In the region of mostly right-handed twin stau LSP, $m_{3L} > m_{3R}$, the mass splitting between stau and twin stau becomes small and coannihilation with MSSM plays an important role in decreasing the effective cross section, which increases the relic abundance. At the boundary of the BBN bound, the relic abundance is boosted by a factor of 1.8. Consequently, the correct relic abundance is obtained for smaller twin stau mass. Note, that the whole region with correct relic abundance is consistent with the self-interaction bound, $m_{\tilde{\tau}'} > 210$ GeV, Eq. (7.13).

On the plot, we also show the direct detection bounds from Xenon1T and LZ, and the predicted sensitivity of the LZ experiment. Solid curves assume $\Omega_{\tilde{\tau}'} h^2 = 0.12$ throughout the whole parameter space, while the dashed lines are rescaled by a factor $\Omega^{\text{th}} h^2/0.12$ whenever $\Omega^{\text{th}} h^2 < 0.12$, covering non-thermal and thermal scenarios, respectively (see discussion at the end of Sec. 7.1.4). Constrained by the Xenon1T and 2022 LZ results, twin stau explains all DM in part of parameter space with $m_{3L} > m_{3R}$. Note, that the LZ at full run should probe the whole parameter space shown on the plot, consistent with the BBN bound.

However, the simplifying assumptions used in the plot result in generically long-lived stau, $d_{\tilde{\tau}} > 1$ m, due to large higgsino and bino masses. Stau is electrically charged and is the subject of the ATLAS bound on long-lived charged particles, $m_{3R} > 430$ GeV, see discussion in Sec. 7.1.5. Together with DD bounds, this excludes the whole parameter space shown on the plot, unless bino-twin bino mixing is introduced to shorten the stau lifetime, see Eq. (7.39).

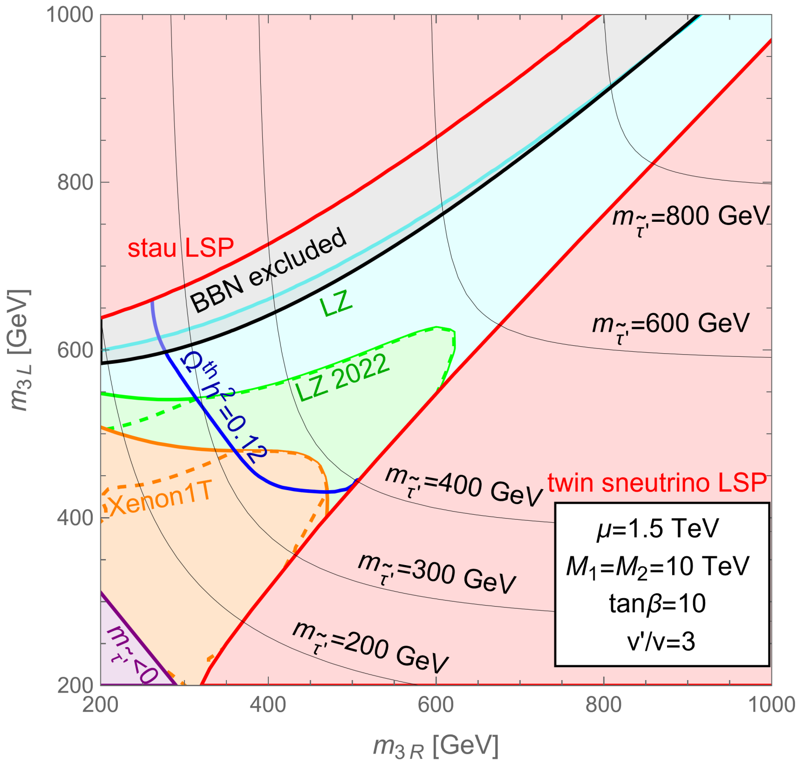


Figure 7.1: Twin stau parameter space in the plane of the right and left soft stau masses ($m_{3R}$, $m_{3L}$, respectively) for $\mu = 1.5$ TeV, $\mathrm{tg}\,\beta = 10$, $v'/v = 3$ and the bino and wino masses $M_1 = M_2 = 10$ TeV. The blue contour represents the observed relic abundance $\Omega^{\rm th}h^2 = 0.12$, and the black contours correspond to the mass of the lightest twin stau. In the red regions, twin stau is not LSP, while in the purple region twin stau is tachyonic. The orange region is excluded by Xenon1T [165], while the green region is excluded by the first results from the LZ experiment [168]. The predicted sensitivity of the LZ experiment [167] is colored cyan. The dashed DD lines assume scaling of the bound with the thermal abundance if $\Omega_{\tilde{\tau}'}h^2 = \Omega^{\rm th}h^2 < 0.12$.

### Light neutralinos

On the left (right) panel of Fig. 7.2 we show the parameter space for $v'/v = 3(5)$ with bino mass $M_1 = 1$ TeV and varying higgsino mass $\mu$ with $m_{3R} = m_{3L} - 100$. The wino remains decoupled, $M_2 = 10$ TeV. Higgsino mass $\mu$ enters the mass matrix of twin stau, and thus changing it results in changing of the twin stau mixing angle $\theta_{\tilde{\tau}'}$. To isolate the effect of light higgsino on the annihilation cross section, we set $\mathrm{tg}\,\beta = 15~\mathrm{TeV}/\mu$. We have kept the same coloring as in Fig. 7.1.

Purple curves show the contours of stau decay contours $d_{\tilde{\tau}} = 0.1, 1, 10$ m. Clearly, a large portion of the parameter space with $\mu \lesssim 600$ GeV allows for $d_{\tilde{\tau}} < 1$ m, which evades all collider constraints. For the minimal, allowed hierarchy of EW and TH scales, $v'/v = 3$ the correct relic abundance is obtained for $m_{\tilde{\tau}'} \simeq 400$ GeV. Note, that changing the mass of the higgsino does not affect the relic abundance as long as the higgsino is not nearly degenerate with the twin stau, reflecting the fact that higgsino-mediated processes do not dominate the freeze-out of twin stau. The correct relic abundance is obtained for parameters excluded by the 2022 results from the LZ experiment, $m_{3R} \gtrsim 470$ GeV.

On the right panel of Fig. 7.2 we show that by increasing the hierarchy between TH and EW scales to $v'/v = 5$, it is possible to avoid DD bounds by suppressing the twin stau-nucleon cross section Eq. (7.16). In that case, the correct relic abundance is obtained for slightly larger masses $m_{\tilde{\tau}'} \simeq 420$ GeV, due to enhanced mixing (note that in Fig. 7.1 $\Omega^{\rm th}h^2 = 0.12$ is obtained for heavier twin stau if $m_{3R} \simeq m_{3L}$). Larger misalignment, $v'/v = 5$, reduces significantly the decay length of stau by enhancing the higgsino mixing Eq. (7.29), but also by increasing the mixing between left- and right-handed twin stau and hence increasing the mass splitting between stau and twin stau. The decay length of stau can be below 1 m for higgsino masses as large as 850 GeV. The full run of the LZ experiment with expected sensitivity will probe the whole parameter space with correct thermal relic abundance, leaving out only the blind spot in the DD with $\Omega^{\rm th}h^2 > 0.12$.

The difference between the left and right panel in the shape of the contour $\Omega h^2 = 0.12$ comes mostly from different coannihilation effects. Note, that the mass splitting between neutralinos, $m_{\chi_i^0} - m_{\chi_1^0}$, and between the lightest neutralino and charginos, $m_{\chi_i^\pm} - m_{\chi_1^0}$, is proportional to the mass of the $Z$ boson and the higgsino mass $\mu$ [327]. Consequently, the coannihilations with neutralinos and charginos play an important role near $\mu \sim m_{3R}$, where mass splitting is smallest. However, the coannihilations are exponentially suppressed by the mass splitting, which for $v'/v = 5$ is strong enough to cancel contributions from channels involving neutralinos and charginos. Moreover, as the ratio $v'/v$ increases, as long as the ratio of VEVs is relatively small, the mass splitting between twin stau and stau is enhanced as well. The effect is further amplified by our choice $m_{3R} = m_{3L} + 100$ GeV, which already lies in the region around $m_{\tilde{\tau}'} \simeq m_{\tilde{\tau}}$. Consequently, for $v'/v = 3$ the enhancement in Eq. (7.27) is around 1.6, while for $v'/v = 5$ it is only around 1.1.

On the Fig. 7.3 we show analogous plots with varying bino mass $M_1$ for $\mu = 1$ TeV, $\mathrm{tg}\,\beta = 15$, $v'/v = 3(5)$ on left (right) panel. In the region with $M_1 \lesssim m_{3R}$ twin bino is the LSP. Light bino enhances the twin stau annihilation into twin fermions, hence the observed relic density is achieved for larger twin stau masses as we decrease $M_1$. For both $v'/v = 3$ and $v'/v = 5$, the correct relic abundance is obtained for twin stau as heavy as $m_{\tilde{\tau}'} \simeq 470$ GeV, which for former (later) is obtained for $m_{3R} = 490(510)$ GeV.

In the region $M_1 \gtrsim m_{3R}$, where twin bino is nearly degenerate with twin stau coannihilations result in suppression of the effective annihilation cross section Eq. (B.5.92). The reason is that in the limit $m_{\tilde{\tau}'} \to m_{\tilde{B}}$ twin bino contributes to the effective number of degrees of freedom $g_{\rm eff}$, defined below Eq. (B.5.91), but the cross section for processes $\tilde{\tau}'\tilde{B}' \to XY$ is relatively small. Therefore, the second term of the sum in Eq. (B.5.92) has only subleading contribution to $\langle\sigma_{\rm eff}v\rangle$, while the annihilation term, $\langle\sigma_{\rm ann}v\rangle$ is suppressed by a factor $g_{\tilde{\tau}'}g_{\tilde{\chi}^0}/g_{\rm eff}^2 \leqslant 4$.

For $v'/v = 3$ the stau decay length below 1 m requires $M_1 \lesssim 600$ GeV. For $v'/v = 5$, due to larger higgsino mixing and stau mass splitting, this is significantly relaxed and stau decay length can be smaller than 1 m even for $M_1 \simeq 900$ GeV. The 2022 LZ results probe the thermal twin stau scenario for a minimal hierarchy between EW and TH scales. With mild tuning, $v'/v = 5$, the DD bounds are significantly reduced, but the thermal twin stau scenario remains within the range of LZ.

For $v'/v = 3(5)$, the non-thermal scenario will be probed by LZ up to $m_{\tilde{\tau}'} \simeq 800(600)$ GeV. For $v'/v = 3$, the larger twin stau mass is in conflict with the BBN, while for $v'/v = 5$ there is a blind spot in the DD for 570 GeV $< m_{\tilde{\tau}'} <$ 710 GeV, discussed in Sec. 7.1.3.

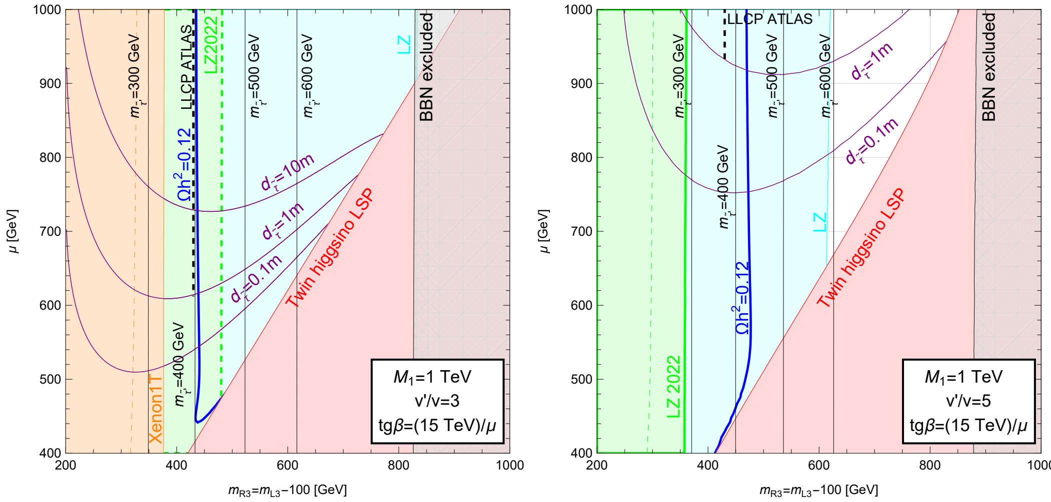


Figure 7.2: Twin stau parameter space in the plane of the right soft stau mass $m_{3R} = m_{3L}$ and higgsino mass $\mu$ for bino mass $M_1 = 1$ TeV, $v'/v = 3$ (left panel) and $v'/v = 5$ (right panel). To keep the twin stau mixing constant while varying $\mu$, we set $\mathrm{tg}\,\beta = 15$ TeV$/\mu$ and $m_{3L} = m_{3R} + 100$ GeV. The blue contour represents the observed relic abundance $\Omega^{\rm th}h^2 = 0.12$, and the black contours correspond to the mass of the lightest twin stau. In the red region, twin higgsino is lighter than twin stau, while the grey region is excluded by the BBN, Eq. (7.43). The orange region is excluded by Xenon1T [165], while the green region is excluded by the first results from the LZ experiment [168]. The predicted sensitivity of the LZ experiment [167] is colored cyan. The dashed DD lines assume scaling of the bound with the thermal abundance if $\Omega_{\tilde{\tau}'}h^2 = \Omega^{\rm th}h^2 < 0.12$. The purple contours represent the decay length of stau, discussed in Sec. 7.1.5

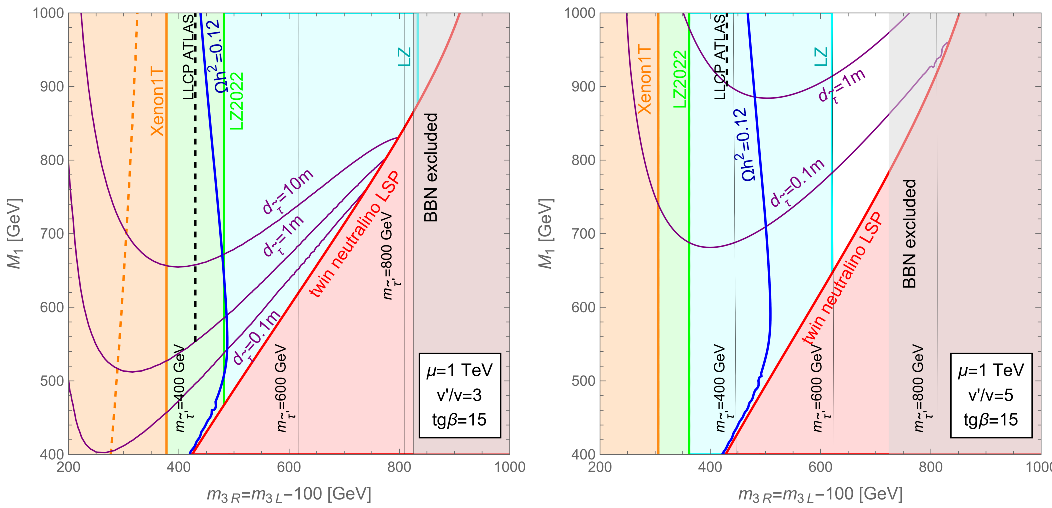


Figure 7.3: Twin stau parameter space in the plane of the right soft stau mass $m_{3R}$ and bino mass $M_1$ for higgsino mass $\mu = 1$ TeV, $\mathrm{tg}\,\beta = 15$, $v'/v = 3$ (left panel) and $v'/v = 5$ (right panel). We set $m_{3L} = m_{3R} + 100$ GeV. The blue contour represents the observed relic abundance $\Omega^{\rm th}h^2 = 0.12$, and the black contours correspond to the mass of the lightest twin stau. In the red region, twin bino is lighter than twin stau, while the grey region is excluded by the BBN, Eq. (7.43). The orange region is excluded by Xenon1T [165], while the green region is excluded by the first results from the LZ experiment [168]. The predicted sensitivity of the LZ experiment [167] is colored cyan. The dashed DD lines assume scaling of the bound with the thermal abundance if $\Omega_{\tilde{\tau}'}h^2 = \Omega^{\rm th}h^2 < 0.12$. The purple contours represent the decay length of stau, discussed in Sec. 7.1.5

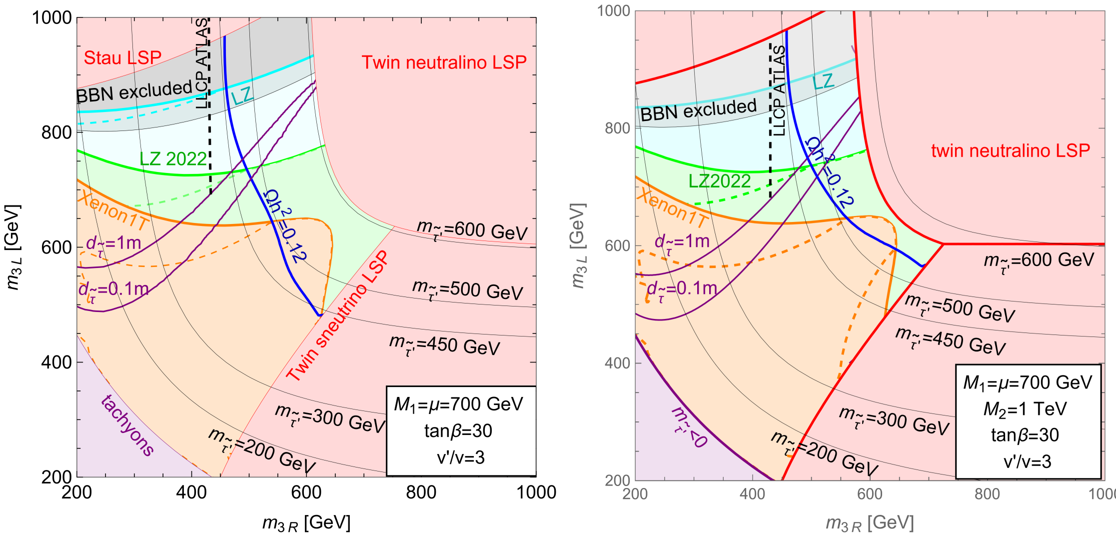


Figure 7.4: Twin stau parameter space in the plane of the right soft stau masses $m_{3R}$ and $m_{3L}$ for higgsino and bino masses $\mu = M_1 = 700$ GeV, $\mathrm{tg}\,\beta = 30$, $v'/v = 3$ and wino mass $M_2 = 8$ TeV (left panel) and $M_2 = 1$ TeV (right panel). The blue contour represents the observed relic abundance $\Omega^{\mathrm{th}}h^2 = 0.12$, and the black contours correspond to the mass of the lightest twin stau. In the red region, twin bino is lighter than twin stau, while the grey region is excluded by the BBN, Eq. (7.43). The dashed black line denotes the LHC bound for long-lived charged particles, Eq. (7.42). In the purple region, twin stau becomes tachyonic. The orange region is excluded by Xenon1T [165], while the green region is excluded by the first results from the LZ experiment [168]. The predicted sensitivity of the LZ experiment [167] is colored cyan. The dashed DD lines assume scaling of the bound with the thermal abundance if $\Omega_{\tilde{\tau}'}h^2 = \Omega^{\mathrm{th}}h^2 < 0.12$. The purple contours represent the decay length of stau, discussed in Sec. 7.1.5.

### Realistic and minimal twin stau dark matter

In Fig. 7.4 we show how the parameter space of twin stau dark matter opens up for $\mu = M_1 = 700$ GeV with wino mass $M_2 = 8(1)$ TeV in the left (right) panel. We call this case realistic, as it does not artificially decouple any of the particles involved in the thermalization of twin stau. To compensate for small higgsino mass while maintaining large mixing, we set $\mathrm{tg}\,\beta = 30$. Because of light neutralinos, the stau decay length is below 1 m in a large portion of the parameter space. At the same time, the DD bounds are moderate, and mostly right-handed twin stau is allowed. We have explicitly highlighted the ATLAS bound $m_{3R} > 430$ GeV for long-lived charged particles, Eq. (7.42), which is relevant only if stau decay length is above 1 m. Note, that the LHC bound also requires $\mu > 1.2$ TeV and $M_2 > 1.3$ TeV, but increasing $\mu$ does not affect the relic abundance while increasing bino mass does not change significantly $\Omega^{\mathrm{th}}h^2$ in the region with $d_{\tilde{\tau}} > 1$ m.

On the right panel of Fig. 7.4 we present the effect of allowing for relatively light wino. Because wino couples only to the left-handed twin stau, the contour $\Omega^{\mathrm{th}}h^2 = 0.12$ does not change in the region dominated by right-handed twin stau, $m_{3R} < m_{3L}$. However, in the proximity of twin sneutrino LSP region, $m_{3R} \lesssim m_{3L}$ light wino increases the effective annihilation cross section, and $\Omega^{\mathrm{th}}h^2 = 0.12$ is obtained for larger twin stau masses, about 550 GeV compared to 450 GeV for decoupled wino. Before the 2022 LZ results, it allowed for the possibility of highly mixed twin stau DM, just escaping the Xenon1T

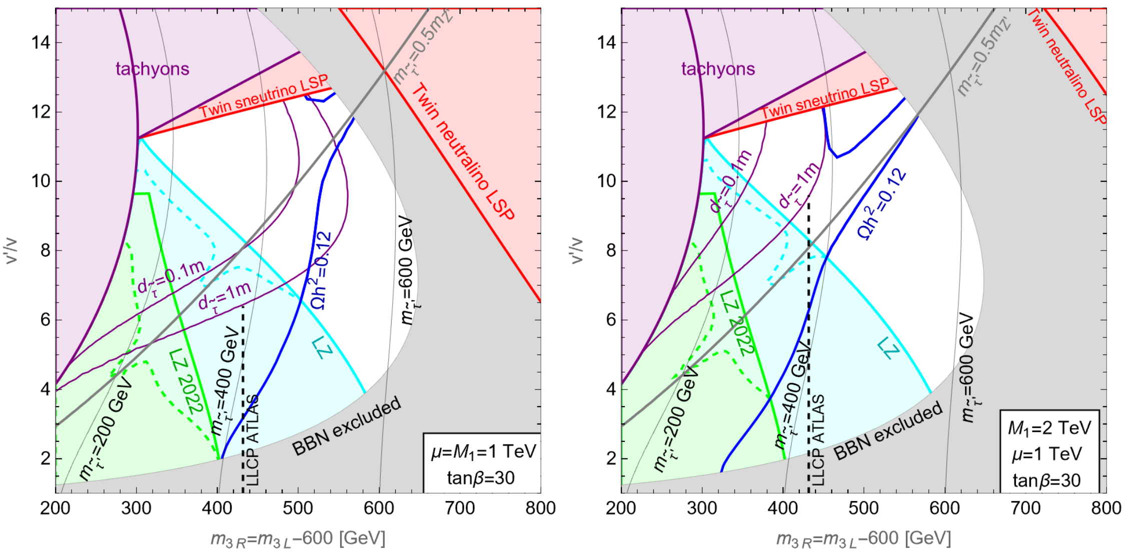


Figure 7.5: Twin stau parameter space in the plane of the right soft stau masses $m_{3R}$ and $v'/v$ for higgsino mass $\mu = 1$ TeV, $\mathrm{tg}\,\beta = 30$ and bino masses $M_1 = 1$ TeV (left panel) and $M_1 = 2$ TeV (right panel). The blue contour represents the observed relic abundance $\Omega^{\mathrm{th}}h^2 = 0.12$, and the black contours correspond to the mass of the lightest twin stau. In the red region, twin bino is lighter than twin stau, while the grey region is excluded by the BBN, Eq. (7.43). In the purple region, there are tachyons in the spectrum. The dashed black line denotes the LHC bound for long-lived charged particles, Eq. (7.42). The grey line corresponds to a resonance at $m_{\tilde{\tau}'} = m_{Z'}/2$. The orange region is excluded by Xenon1T [165], while the green region is excluded by the first results from the LZ experiment [168]. The predicted sensitivity of the LZ experiment [167] is colored cyan. The dashed DD lines assume scaling of the bound with the thermal abundance if $\Omega_{\tilde{\tau}'}h^2 = \Omega^{\mathrm{th}}h^2 < 0.12$. The purple contours represent the decay length of stau, discussed in Sec. 7.1.5

bound. We should note here, that the region with $d_{\tilde{\tau}} > 1$ m is excluded due to wino mass $M_2 = 1$ TeV $< 1.3$ TeV, which, combined with the LZ bound, excludes all the parameter space shown on the plot in the absence of the bino mixing. We show this plot as a demonstration of the mild effect light wino has on the twin stau relic abundance.

### Enhanced $\mathbb{Z}_2$ breaking

On the Fig. 7.5 we show the effect of allowing larger $\mathbb{Z}_2$ breaking in the scalar sector, $v'/v$, parametrized by $\sigma$ in Eq. (6.2), or $\Delta m^2$ in Eq. (6.12). By setting $m_{3R} = m_{3L} - 600$ GeV, we consider mostly right-handed twin stau LSP, with mixing enhanced by sizable higgsino mass $\mu = 1$ TeV. The left (right) panel shows the result for $M_1 = 1(2)$ TeV. For large $v'/v$ and $m_{3R} < 300$ GeV, the off-diagonal terms drive the mass of twin stau negative. Also, for large $v'/v$ the mass splitting between sneutrino and left-handed twin stau mass, Eq. (7.5), becomes so large that twin sneutrino becomes tachyonic.

Interestingly, the BBN bound Eq. (7.43) sets an upper limit on the $\mathbb{Z}_2$ breaking. The D-term contribution to the mass of twin stau is $\propto v'^2$, while the diagonal term is only $\propto v'$, so for sufficiently large VEV misalignment the gauge coupling suppression is overcome, reducing the mass splitting between stau and twin stau. For our choice of parameters, BBN requires $v'/v \lesssim 12$, which corresponds to the worst possible tuning of the model with twin stau DM around 1%.

The thermal relic abundance $\Omega^{\rm th}h^2 = 0.12$, for $M_1 = 1$ TeV, is obtained for twin stau masses between 400 GeV at $v'/v = 3$, up to about 550 GeV for $v'/v \simeq 11$. Large $v'$ decreases the mass splitting between twin stau and stau, leading to enhanced coannihilation yielding correct relic abundance for heavier twin stau. Around line $m_{\tilde{\tau}'} \simeq m_{Z'}/2$, the resonant annihilation into twin fermions significantly increases the effective annihilation cross section, boosting $m_{\tilde{\tau}'}$ required for $\Omega^{\rm th}h^2 = 0.12$.

On the other hand, for $M_2 = 2$ TeV, shown on the right panel of Fig. 7.5, the relic abundance is enhanced due to decreased effective annihilation rate for heavier bino. The correct relic abundance is obtained for twin stau masses between 350 GeV at $v'/v = 3$ and up to 550 GeV for $v'/v \simeq 11$. Since stau decay is mediated by the bino and higgsino, the decay length is also enhanced, leading to stronger bound from the search for long-lived charged particles.

As expected, the increase in the $v'$ leads to the suppression of DD bounds. For our choice of parameters, the 2022 results from LZ can probe up to $v'/v \simeq 8$, for multicomponent DM scenario. For light bino, the 2022 LZ bound doesn't constrain the thermal twin stau DM with $\Omega^{\rm th}h^2 = 0.12$, while for heavy bino, $M_1 = 2$ TeV, LZ excludes $v'/v \lesssim 4$. The full run of the LZ experiment will probe the thermal twin stau DM up to $v'/v = 6.5(8)$ for $M_1 = 1(2)$ TeV, which corresponds to EW tuning around 5(3)%.

Note, that at this point, the twin stau DM is more constrained by the ATLAS search for long-lived charged particles than by the 2022 LZ searches. However, the full run of LZ will probe a large portion of parameter space with $m_{3R} > 430$ GeV.

### $\mathbb{Z}_2$-breaking in the Yukawa sector

Finally, let us consider a $\mathbb{Z}_2$-breaking in the Yukawa sector, which does not spoil the TH solution to the Hierarchy Problem, while potentially alleviating the dark radiation problem, see Sec. 6.1.

One of the effects of enhanced tau Yukawa is an increase in the left-right twin stau mixing, as the off-diagonal term is proportional to $y_{\tau'}$. This opens up the possibility of smaller values of $\operatorname{tg}\beta$, motivating our choice $\operatorname{tg}\beta = 5$ on the Fig. 7.6. For $v'/v = 3$ shown on the left panel, twin stau becomes LSP for $y_{\tau'}/y_\tau \simeq 2$, however, to evade the BBN bound $y_{\tau'}/y_\tau \gtrsim 3.5$ is required. The stau lifetime strongly depends on the ratio of Yukawas and rapidly drops below 1 m for $y_{\tau'}/y_\tau \gtrsim 4$ (along $\Omega^{\rm th}h^2 = 0.12$ contour). Therefore, in the presence of the $\mathbb{Z}_2$ breaking in the tau Yukawa, the bino mass mixing is in general not required for reducing the $d_{\tilde{\tau}}$.

The correct relic abundance is thermally produced for twin stau masses as heavy as $m_{\tilde{\tau}'} = 600$ GeV for $y_{\tau'}/y_\tau \simeq 13$, due to enhanced annihilation into SM Higgs and twin tops. However, the large Yukawa contributes to the twin stau-Higgs coupling, and $y_{\tau'}/y_\tau \lesssim 6$ is excluded by Xenon1T, while LZ constraints $y_{\tau'}/y_\tau \lesssim 4$. For minimal hierarchy between EW and TH scales, $v'/v = 3$, only thermally underproduced twin stau is allowed by LZ, and the ATLAS searches for the long-lived charged particles. Combining the predicted sensitivity of the LZ experiment with the ATLAS bounds, the whole parameter space of thermal twin stau DM will be probed.

On the right panel of Fig. 7.6 we show the parameter space for the same choice of $\operatorname{tg}\beta = 5$ and $\mu = M_1 = 700$ GeV, but with enhanced $\mathbb{Z}_2$ breaking in the scalar sector, $v'/v = 5$. Twin stau becomes LSP for at least $y'/y \simeq 3$, but BBN excludes thermal scenario below $y'/y \simeq 4$. The larger mass splitting between twin stau and twin sneutrino, Eq. (7.5), results in twin sneutrino LSP at low $m_{3L}$, which was not visible on plot with $v'/v = 3$.

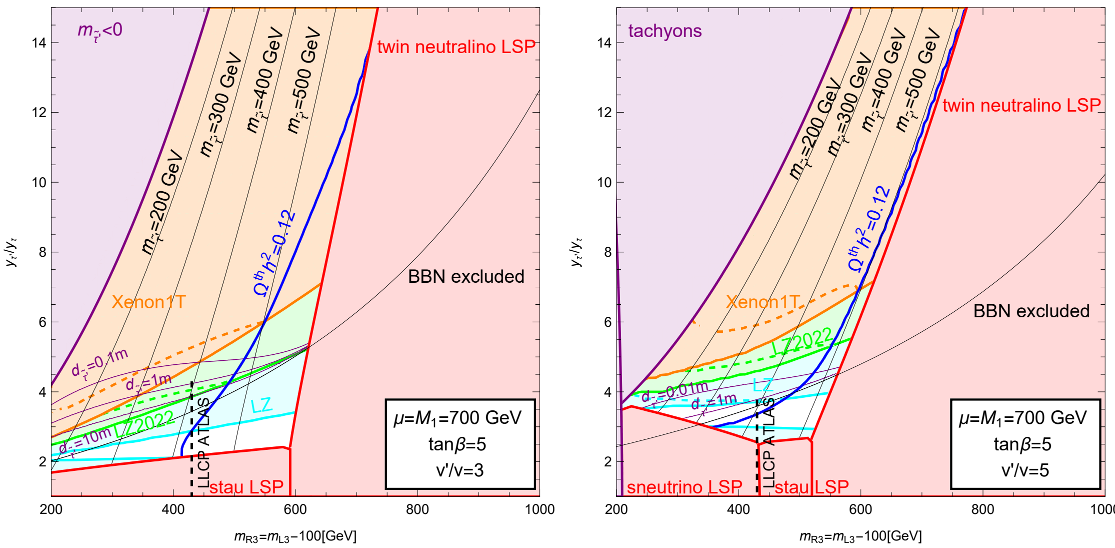


Figure 7.6: Twin stau parameter space in the plane of the right soft stau mass $m_{3R} = m_{3L} + 100$ GeV and ratio of Yukawas between sectors $y_{\tau'}/y_\tau$ for higgsino and bino masses $\mu = M_1 = 700$ GeV, $\mathrm{tg}\,\beta = 5$, wino mass $M_2 = 8$ TeV and $v'/v = 3(5)$ on left (right) panel. The blue contour represents the observed relic abundance $\Omega^{\rm th}h^2 = 0.12$, and the black contours correspond to the mass of the lightest twin stau. In the red regions, twin stau is not LSP, while the region below the black line is excluded by the BBN, Eq. (7.43). The dashed black line denotes the LHC bound for long-lived charged particles, Eq. (7.42). In the purple region, twin stau or twin sneutrino becomes tachyonic. The orange region is excluded by Xenon1T [165], while the green region is excluded by the first results from the LZ experiment [168]. The predicted sensitivity of the LZ experiment [167] is colored cyan. The dashed DD lines assume scaling of the bound with the thermal abundance if $\Omega_{\tilde{\tau}'}h^2 = \Omega^{\rm th}h^2 < 0.12$. The purple contours represent the decay length of stau, discussed in Sec. 7.1.5

Correct thermal relic abundance is obtained for twin stau masses between 300 and 500 GeV, but Xenon1T (LZ) rules out a large portion of parameter space with $\Omega^{\rm th}h^2 = 0.12$ with $y'/y \gtrsim 7(5)$. With the predicted sensitivity of LZ, the whole parameter space of thermal twin stau DM will be covered for this set of parameters, complemented by the BBN bound and ATLAS searches for long-lived charged particles. Only a tiny fraction of the parameter space, with $\Omega^{\rm th}h^2 \ll 0.12$, will remain unprobed by the LZ, corresponding to the blind spot in the DD cross section, discussed in Sec. 7.1.3. Due to reduced Higgs-twin Higgs mixing, a large portion of parameter space has $d_{\tilde{\tau}}$ below 1 m, and ATLAS bound is never stronger than BBN bound for thermal twin stau.

### Summary

We have demonstrated that a mostly right-handed twin stau with a mass around 450 GeV is a successful candidate for DM and can potentially constitute whole relic abundance $\Omega^{\rm obs}h^2$. This scenario is realized for a wide range of parameters and does not require fine-tuning, however, relatively light neutralinos are favored. Twin stau DM is constrained by the DD experiments, which also provide the best future probe of the scenario. There is a straightforward relation between the DD bounds and the naturalness of the model parametrized by the ratio of VEVs $v'/v$. Interestingly, the BBN constrains the visible stau lifetime and leads to an upper limit of that ratio, resulting in the worst possible tuning of the scenario at the percent level.

At the time of writing the thesis, new null LZ results have been published [328], nearly achieving the predicted sensitivity of the experiment. For DM mass of 400 GeV the new LZ constraint is stronger than LZ2022 by a factor of 10, but it is still weaker than the projected final sensitivity by a factor of 1.5 Consequently, the contours on plots denoted as predicted sensitivity of LZ can now be regarded as overestimated bounds from the last run of the LZ experiment. This implies that the most natural realization of the twin stau DM is already excluded and relatively large vacuum misalignment is required, as can be seen from Fig. 7.5. However, natural $v'/v = 3$ is allowed in the presence of late entropy production that alleviates the $\Delta N_{\rm eff}$ problem in TH models. Entropy injection dilutes the twin stau relic abundance requiring twin stau DM mass as large as 1 TeV, consequently requiring larger bino and higgsino masses, and suppressing the DD bounds.

## 7.2 Twin neutralino DM

MSSM neutralino has been one of the most studied candidates for DM, as discussed at the beginning of the chapter. There are four neutralinos composed of bino, wino, and two higgsinos.

Pure wino is a promising candidate for the DM [105, 327]. Wino states coannihilates into gauge bosons, mediated by wino exchange, with vertex $\tilde{W}^0\tilde{W}^{\pm}W^{\mp}$ determined by the gauge coupling $\mathcal{O}(0.5)$. Therefore, to sufficiently suppress the cross section for this process, a large $M_2 \simeq 2.5$ TeV is required. This implies that for the wino to be the LSP Higgsino mass $\mu > 2.5$ TeV, which requires tuning of order 0.1%, cf. Eq. (6.29).

Higgsino can also be a DM candidate, with mass reproducing observed relic abundance around 1 TeV [105, 327]. However, $\mu \simeq 1$ TeV requires considerable fine-tuning in the MSSM as discussed around Eq. (6.29). The main annihilation channel is into gauge bosons, and coannihilation with near degenerate higgsino plays a critical role in determining the relic abundance.

While pure bino DM does not require the tuning of the EW scale, observed relic abundance is possible only in fine-tuned regions of the parameter space where resonances or coannihilations are efficient. The main annihilation channel of bino is t-channel sfermion exchange $\tilde{B}\tilde{B} \to f\bar{f}$, and the approximate formula for the thermally averaged cross section is [329]

$$\langle \sigma_{\tilde{B}\tilde{B}\to f\bar{f}} \rangle = \left(1 - \frac{m_f^2}{m_{\tilde{B}}^2}\right)^{1/2} \frac{g_1^4}{128\pi} \left( \left(Y_L^2 + Y_R^2\right)^2 \left(\frac{m_f}{\Delta_f}\right)^2 + \left(Y_L^4 + Y_R^4\right) \left(\frac{4m_{\tilde{B}}^2}{\Delta_f^2}\right)^2 x \right), \tag{7.45}$$

where $Y_{L/R}$ is hypercharge of the left- or right-handed fermion, $\Delta_f = m_{\tilde{f}}^2 + m_{\tilde{B}}^2 - m_f^2$ and $x = m_{\tilde{B}}/T$. The first term, the s-wave contribution, is chirality suppressed by $m_f^2/m_{\tilde{f}}^4$. On the other hand, the p-wave contribution, proportional to $x$, is suppressed by $M_1^2/m_{\tilde{f}^4}$, which for bino LSP is also small unless sfermion is degenerate with bino. The least constrained sfermion mass is the stau, which can be as light as 90 GeV [330–333], but unless the masses of stau and bino are tuned to maximize coannihilations bino decouples too late, overclosing the Universe [105, 329, 334, 335].

Therefore, in the MSSM the neutralino DM always requires either tuning of the EW scale or tuning of the SUSY spectrum. Therefore, in this section, we will investigate the neutralino mainly composed of twin bino with a small admixture of twin higgsino as a candidate for DM. Focusing on the parameter space that avoids fine-tuning of the EW scale requires relatively small $\mu$, which induces small mixing between bino and higgsino.

The reason twin bino is a potentially valid DM candidate is the possibility of breaking the $\mathbb{Z}_2$ symmetry in the Yukawa sector, avoiding chirality suppression of the s-wave contribution to the thermally averaged cross section. Such breaking is motivated by alleviating the TH dark radiation problem, as discussed in Sec. 6.1, and does not introduce additional tuning to the model as long as top Yukawa $y_{t'} = y_t$. Spontaneous $\mathbb{Z}_2$ breaking in the Yukawa sectors can be accommodated in TH models via Froggatt-Nielsen mechanism [78, 336]. Moreover, the different Yukawa couplings can radiatively generate the misalignment of VEVs, $v' > v$, which may further reduce the fine-tuning of TH models.

### 7.2.1 Mass of (twin) neutralino

Neutralinos obtain masses from soft supersymmetry breaking, Eq. (6.35) and mixing terms are generated by the higgsino mass in the superpotential, Eq. (6.30). Moreover, interaction from the 4th line of Eq. (6.19) gives contributions from the gaugino-higgs-higgsino coupling, with Higgs replaced by its VEV. The neutralino mass matrix in the $(\widetilde{B}, \widetilde{W}, \widetilde{H}_d, \widetilde{H}_u)^T$ space is

$$m_\chi^2 = \begin{pmatrix} M_1 & 0 & -m_Z c_\beta s_{\theta_W} & m_Z s_\beta s_{\theta_W} \\ 0 & M_2 & m_Z c_\beta c_{\theta_W} & -m_Z s_\beta c_{\theta_W} \\ -m_Z c_\beta s_{\theta_W} & m_Z c_\beta c_{\theta_W} & 0 & -\mu \\ m_Z s_\beta s_{\theta_W} & -m_Z s_\beta c_{\theta_W} & -\mu & 0 \end{pmatrix}, \tag{7.46}$$

where $\theta_W$ is Weinberg angle, $c_\alpha = \cos\alpha$ and $s_\alpha = \sin\alpha$, $M_1$, $M_2$ are bino and wino soft masses. The twin neutralino mass matrix can be obtained from above by replacing $m_Z \to m_{Z'} \simeq m_Z v'/v$. Therefore, under the assumption that there is no $\mathbb{Z}_2$ breaking in SUSY breaking, the neutralino mixing is larger in the twin sector.

The physical neutralinos are obtained by diagonalization of the mass matrix with unitary transformation

$$\psi_i \to \tilde{\chi_0} = N_{ij}\psi_j\,. \tag{7.47}$$

Throughout the analysis, we will consider mostly bino LSP, with a small higgsino component, $\mu \gtrsim M_1$. Note, that $\mu$ cannot be arbitrarily large due to naturalness, requiring fine-tuning at the level of approximately 10 (1)% for $\mu = 1(3)$ TeV. Moreover, we will assume that wino is decoupled, $M_2 = 10$ TeV, therefore there is no mixing between bino and wino, $N_{12} \simeq 0$.

### 7.2.2 Direct detection

Twin neutralino interacts with the quarks via the Higgs portal, represented by a diagram

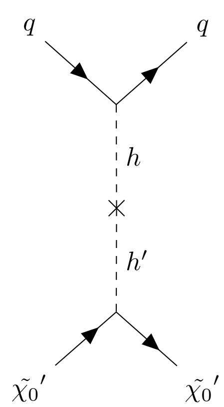

Therefore, similarly to the twin stau case, the effective twin neutralino-quark coupling is

$$\mathcal{L}_{q\tilde{\chi}_0'} = S\sum_q c_q \bar{q}q\,, \tag{7.48}$$

where $S = \tilde{\chi}_0'\tilde{\chi}_0'^\dagger$ and the couplings can be written in terms of twin neutralino-twin neutralino-Higgs coupling $C_{\tilde{\chi}_0'\tilde{\chi}_0'h}$ and the Yukawa couplings $C_{qqh}$

$$c_q = \frac{C_{\tilde{\chi}_0'\tilde{\chi}_0'h}C_{qqh}}{m_h^2}\,. \tag{7.49}$$

Using receipt from Ref. [312], the effective coupling to nucleons is

$$\frac{c_N}{m_N} = \sum_q \frac{c_q f^N_{T_q}}{m_q} + \frac{2f^N_{T_G}}{27}\sum_Q \frac{c_Q}{m_Q}\,, \tag{7.50}$$

therefore Yukawa couplings cancel, and each quark contribution is set by the form factors defined in Eq. (7.19):

$$c_N = \frac{C_{\tilde{\chi}_0'\tilde{\chi}_0'h}}{m_h^2}\left(\sum_q \frac{m_N}{\sqrt{2}v}f_q + \frac{2}{27}f_{TG}\sum_Q\frac{m_N}{\sqrt{2}v}\right) = \frac{C_{\tilde{\chi}_0'\tilde{\chi}_0'h}}{m_h^2}\left(\frac{6}{27}+\frac{21}{27}\sum_q f_q\right). \tag{7.51}$$

The twin neutralino-higgs coupling in general is given by [327]

$$C_{\tilde{\chi}_0'\tilde{\chi}_0'h} = \frac{v}{2v'}(g_2N'_{12} - g_1N'_{11})(s_\beta N'_{14} - c_\beta N'_{13})\,, \tag{7.52}$$

where factor $v/v'$ comes from Higgs-twin Higgs mixing. In our calculations we use Eq. (7.52) with numerically obtained mixing parameters $N_{ij}$. For bino-like LSP, in the limit $\mu \gg M_1$, the coupling simplifies to

$$C_{\tilde{\chi}_0'\tilde{\chi}_0'h} \approx \frac{g_1^2 v'}{2\sqrt{2}\mu}\left(s_{2\beta} + \frac{M_1}{\mu}\right)\frac{v}{v'}\,, \tag{7.53}$$

where dependence on $v'$ cancelles. This is in contrast to Eq. (7.16), which can be suppressed by enhancing the $\mathbb{Z}_2$ breaking in the scalar potential. On the other hand, the twin neutralino-Higgs coupling can be suppressed by a large hierarchy $\mu \gg M_1$ and the first term is also suppressed by large $\operatorname{tg}\beta$, $s_{2\beta} \sim 1/\operatorname{tg}\beta$.

The DD event $\tilde{\chi}_0'N \to \tilde{\chi}_0'N$ is represented by the diagram

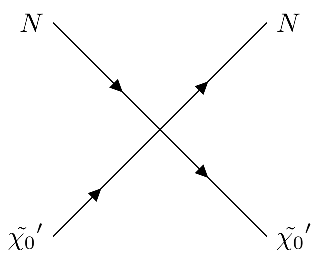


which gives the non-relativistic amplitude [314]

$$|\mathcal{M}|^2 \simeq \Big(2c_N(2m_{\tilde{\chi}_0'})(2m_N)\Big)^2\,, \tag{7.54}$$

where the first factor 2 comes from the two possible ways of attaching the Majorana neutralino. Using Eq. (7.21) the cross section is

$$\sigma = \frac{|\mathcal{M}|^2}{64\pi^2(E_{\tilde{\chi}_0'}+E_N)^2}\frac{|\vec{p}_{\tilde{\chi}_0'}|}{|\vec{p}_N|}4\pi \simeq \frac{4}{\pi}c_N^2\frac{m^2_{\tilde{\chi}_0'}m_N^2}{(m_N+m_{\tilde{\chi}_0'})^2}\,, \tag{7.55}$$

where in the last step we have gone to the non-relativistic $E_i \simeq m_i$ limit in the center of mass $|\vec{p}^{\,\mathrm{CM}}_{\tilde{\chi}_0'}| = |\vec{p}^{\,\mathrm{CM}}_N|$.

### 7.2.3 Thermal abundance

Similarly to the relic abundance of the twin stau in Sec. 7.1.4, the R-parity conservation ensures the stability of the twin neutralino LSP, which is a final product of all odd particles decays, see Appendix B.5.

The mass splitting between neutralino and twin neutralino is typically large, $(m_{\tilde{\chi}_0} - m_{\tilde{\chi}_0'})/m_{\tilde{\chi}_0} > 0.1$, hence the coannihilation gives at most $\mathcal{O}(5\%)$ correction to the $\Omega^{\rm th} h^2$. We assume that other SUSY particles are much heavier, therefore, we neglect the coannihilation between the sectors completely [106]. We find the the relic abundance using `Micromegas` for MSSM [306, 315, 316] with adjusted mass spectrum by rescaling $m_i \to m_i' = m_i v'/v$ or in case of $\mathbb{Z}_2$ breaking in the Yukawa $m_{f'} = m_f (v'/v)\,(y_{f'}/y_f)$. We decouple all SUSY particles, besides stau and neutralino masses, by setting their values at $m_{\rm soft} = 10$ TeV. They could only influence the relic abundance if nearly degenerate when coannihilations could become important.

### 7.2.4 Results

To avoid the chirality suppression of the s-wave contribution to the thermally averaged cross-section, discussed below Eq. (7.45), we break the $\mathbb{Z}_2$ symmetry in the Yukawa by setting $m_{\tau'} = 0.6 M_1$, see Fig. 1 in Ref. [106].

The plot on Fig. 7.7 shows the parameter space in the $\mu$-$M_1$ plane. Since the relic density necessarily depends on the mass of the (twin) stau, see Eq. (7.45), we fix it at every point of the plot so that $\Omega h^2 = 0.12$, with blue contours marking the benchmark value of stau mass. The purple region denotes the region in which $m_{\tilde{\tau}} < 90$ GeV is required to obtain correct relic density, in tension with the LEP limits [330–333]. The orange and green regions show the DD bounds from Xenon1T and the first results from LZ experiments, respectively. Since twin neutralino-Higgs coupling is inversely proportional to the higgsino mass, Eq. (7.53), the bounds become weaker with increasing $\mu$. The bound also weakens with an increase of neutralino mass, even though the coupling to Higgs is enhanced. The reason for that is that the DD bounds fall off faster with $m_{\rm DM} \simeq M_1$ than the Higgs coupling grows. For the smallest neutralino soft mass compatible with LEP, $M_1 \simeq 60$ GeV Xenon1T excludes $\mu < 700$ GeV and LZ $\mu < 1200$ GeV. The predicted sensitivity of LZ will probe neutralino DM up to $\mu \simeq 3$ TeV (not shown on the plot, which will be completely probed by LZ).

There is a resonant suppression of the relic density at $m_{\tilde{\chi}_0'} \simeq m_{Z'}/2 \simeq 135$ GeV, where twin neutralino annihilation into twin fermions is enhanced. A similar enhancement is expected at $m_{\tilde{\chi}_0'} \simeq m_h/2 \simeq 62.5$ GeV, marked with a thick, dashed line. We do not include this, as it only affects relic abundance within a few hundred MeV range around the center of the resonance, and is not required to realize $\Omega h^2 = 0.12$. On the contrary, the $Z'$ resonance is effective for a wide range of the twin neutralino masses, between 125 and 145 GeV.

The plot in Fig. 7.8 shows the twin neutralino parameter space in $M_1$-$\mathrm{tg}\,\beta$ plane for $m_{\tau'} = 0.6 M_1$, $v'/v = 3$ and $\mu = 1$ TeV. The correct relic abundance is obtained at every point of the parameter space, with blue contours marking the values of stau mass for which $\Omega h^2 = 0.12$. The $Z'$ resonance enhances the effective annihilation cross section, and in the proximity of $m_{\tilde{\chi}_0'} = m_{Z'}/2$, for fixed $\mathrm{tg}\,\beta$, the correct relic abundance is obtained for heavier stau. Alternatively, for fixed stau mass, $\Omega h^2 = 0.12$ is achieved for smaller $\mathrm{tg}\,\beta$ as the neutralino-Z coupling is proportional to $\cos 2\beta$. In the plot, we neglect the Higgs resonance but acknowledge it with a thick dashed line.

The DD bounds weaken with increasing $\mathrm{tg}\,\beta$, approaching a constant bound on $M_1$, as the first term in Eq. (7.53) vanishes. The increase in neutralino soft mass also weakens

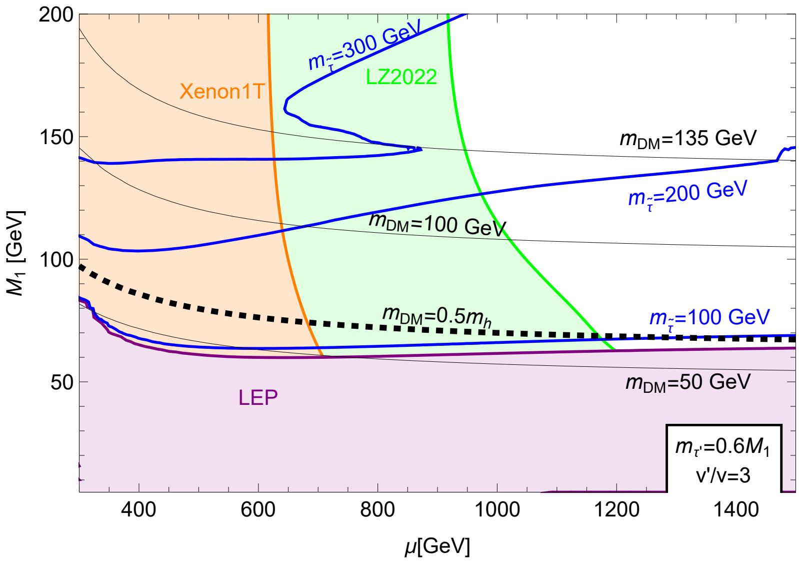


Figure 7.7: Twin neutralino DM parameter space in $\mu$-$M_1$ plane for $\mathrm{tg}\,\beta = 5$, $m_{\tau'} = 0.6M_1$ and $v'/v = 3$, with contours of stau mass $m_{\tilde{\tau}} = 100, 200, 300$ GeV (blue), which reproduce the observed relic abundance $\Omega h^2 = 0.12$. Orange region is excluded by the Xenon1T experiment [165], green region is excluded by the LZ experiment [168] and purple region is excluded by the LEP bound on stau mass [330–333]. Black, thin contours denote the mass of the twin neutralino and the thick dashed line denotes the Higgs resonance.

the bound, due to the increase in the mass of DM, which reduces the sensitivity of DD experiments, see Fig. 2.5. For $m_{\tilde{\chi}_0'} = 50$ GeV the LZ allows for $\mathrm{tg}\,\beta > 7$, while for $m_{\tilde{\chi}_0'} = 200$ GeV the bound is $\mathrm{tg}\,\beta > 5$. The sensitivity of the full run of LZ will probe the whole parameter space shown on the plot.

The dotted lines indicate the values of the twin tau Yukawa couplings, $y_{\tau'} = m_{\tau'}/v' \cos\beta$, which must be below 1.6 (0.8) at EW scale to avoid Landau pole below $10^4(10^{16})$GeV [106]. From the plot, we can observe that for twin neutralino around 100 GeV, perturbativity below $10^4(10^{16})$GeV requires $\mathrm{tg}\,\beta < 6(13)$. This quickly changes with the increase of neutralino mass to 180 GeV, where perturbativity below $10^4$ GeV is ruled out by LZ, and below $10^{16}$ GeV is possible only for $\mathrm{tg}\,\beta < 7$.

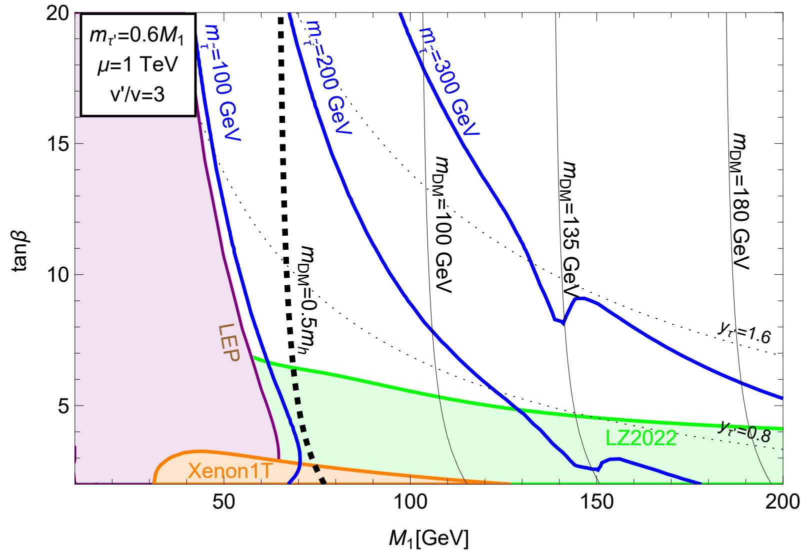


Figure 7.8: Twin neutralino DM parameter space in $M_1$-tg $\beta$ plane for $\mu = 1$ TeV, $m_{\tau'} = 0.6M_1$ and $v'/v = 3$, with contours of stau mass $m_{\tilde{\tau}} = 100, 200, 300$ GeV (blue), which reproduce the observed relic abundance $\Omega h^2 = 0.12$. Orange region is excluded by the Xenon1T experiment [165], green region is excluded by the LZ experiment [168] and purple region is excluded by the LEP bound on stau mass [330–333]. Black, thin contours denote the mass of the twin neutralino and the black, thick, dashed line denotes the Higgs resonance. Dotted lines correspond to the value of twin tau Yukawa, $y_{\tau'} = 0.8, 1.6$.

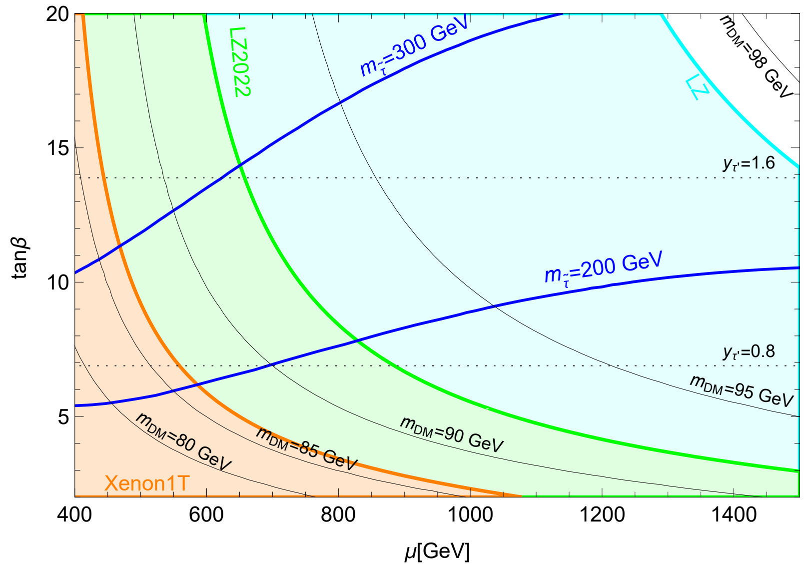


Figure 7.9: Twin neutralino DM parameter space in $\mu$-tg $\beta$ plane for $M_1 = 100$ GeV , $m_{\tau'} = 0.6M_1$ and $v'/v = 3$, with contours of stau mass $m_{\tilde{\tau}} = 100, 200, 300$ GeV (blue), which reproduce the observed relic abundance $\Omega h^2 = 0.12$. Orange region is excluded by the Xenon1T experiment [165], green region is excluded by the 2022 LZ experiment [168] and purple region is excluded by the LEP bound on stau mass [330–333]. The cyan region denoted the predicted sensitivity of the LZ experiment [167]. Black, thin contours denote the mass of the twin neutralino and dotted lines correspond to the value of twin tau Yukawa, $y_{\tau'} = 0.8, 1.6$.

The plot on Fig. 7.9 shows twin neutralino parameter space in $\mu - \mathrm{tg}\,\beta$ plane for $M_1 = 100$ GeV, $v'/v = 3$ and $m_{\tau'} = 0.6M_1$. Once again, all points reproduce $\Omega h^2 = 0.12$, with blue contours indicating the required mass of the stau. In correspondence to Fig. 7.7, the LEP bound is absent, and correct relic abundance requires relatively heavy stau.

The DD bounds on higgsino mass rapidly change with $\mathrm{tg}\,\beta$, as the first term in Eq. (7.53) vanishes for large $\mathrm{tg}\,\beta$. Consequently, for $\mathrm{tg}\,\beta = 10$, LZ rules out $\mu \lesssim 750$ GeV, which for $\mathrm{tg}\,\beta = 5$ gives bound $\mu \lesssim 1050$ GeV. With dotted lines, we indicate the values of twin tau Yukawa, $y_{\tau'} = 1.6(0.8)$ (corresponding to $\mathrm{tg}\,\beta = 14(7)$) which avoid Landau pole below $10^4(10^{16})$GeV. Note, that the running of Yukawa may be influenced by the BSM above the EW scale. In particular, in the presence of extra gauge symmetry, required in SUSY D-term TH the low-scale Landau pole may be avoided for values as large as $\mathrm{tg}\,\beta = 20$.

The full run of LZ will be sensitive to twin neutralino DM up to $\mu \simeq 1300$ GeV for $\mathrm{tg}\,\beta = 20$ and $\mu \simeq 3$ TeV for $\mathrm{tg}\,\beta = 5$.

**Summary**

In this section, we have demonstrated that twin bino-dominated twin neutralino is a successful candidate for DM. Contrary to the MSSM bino DM, no tuning in the spectrum is required to obtain observed relic abundance in the present of $\mathbb{Z}_2$ breaking in the tau Yukawa. Moreover, there is a simple relation between the naturalness of the model captured by higgsino mass parameter $\mu$ and the reach of the DD experiments.

At the time of writing the thesis, new null LZ results have been published [328], nearly achieving the predicted sensitivity of the experiment. For DM mass of 400 GeV the new LZ constraint is stronger than LZ2022 by a factor of 10, but it is still weaker than the projected final sensitivity by a factor of 1.5 Consequently, the contours on plots denoted as predicted sensitivity of LZ can now be regarded as overestimated bounds from the last run of the LZ experiment. This implies that new results exclude natural values of $\mu$ for small $\mathrm{tg}\,\beta$, but for $\mathrm{tg}\,\beta \gtrsim 10$ $\mu \gtrsim 1.5$ TeV is still allowed, as can be seen from Fig. 7.9.

# Chapter 8

# Conclusions

In this thesis, we have analyzed the phenomenology of two models motivated by naturalness criterium featuring the thermal production of dark relics. We have demonstrated the freeze-in mechanism in astrophobic axion models, which for large axion masses also feature a freeze-out mechanism. Axions constitute a hot relic since they decouple while relativistic, subsequently redshifting. On the other hand, we have discussed thermal productions of WIMP-like DM in SUSY TH models solving hierarchy problem without fine-tuning the parameters. Since DM candidates in this model thermalize primarily via annihilation, they freeze-out when non-relativistic and are therefore cold relics.

We have introduced the notion of astrophobic axion models, which avoid stringent astrophysical bounds by suppressing electron and nucleon couplings rather than increasing the axion decay constant $f_a$. Furthermore, we detailed the construction of astrophobic axion models, emphasizing axion-pion coupling suppression, providing derivation of couplings, and introducing 3HDM generalization of the model. In particular, we have shown that the LFV present in 2HDM can be avoided by introducing another Higgs doublet. Suppression of muon or photon coupling is possible within 3HDM, further relaxing astrophysical bounds, at the cost of reintroduction of the LFV. The exception is the naturally astrophobic model, whose only non-vanishing axion couplings are to up and down quarks without the need for LFV. Furthermore, we have collected all relevant constraints on axion-muon, axion-photon, and LFV couplings and categorized the 3HDM astrophobic axion models by the suppressed couplings, emphasizing their phenomenologies.

We have discussed the general thermal production of axions, which in the considered range of masses play the role of warm dark matter or dark radiation. The energy density of axions is historically parametrized by an additional effective number of neutrinos, $\Delta N_{\text{eff}}$, even though axions may be non-relativistic at the recombination. We have demonstrated that taking into account all present constraints, the contribution of axions to the $\Delta N_{\text{eff}}$ from pion scatterings is undetectable in benchmark models such as DFSZ or KSVZ. For large $f_a$ axion production takes place through the freeze-in mechanism, while for small $f_a$ axions can thermalize. A population of axions in equilibrium does not hold information about the past, and the production mechanism is the freeze-out, with $\Delta N_{\text{eff}}$ determined by the decoupling temperature.

We have discussed in detail the processes involved in the production of astrophobic axion including lepton scatterings, LFV lepton decays, and kaon scatterings for non-vanishing axion-strange coupling. By avoiding the most stringent astrophysical constraints, astrophobic axions can give an observable contribution to $\Delta N_{\text{eff}}$. In the 2HDM astrophobic axion model, we found that the lower bound on the axion decay constant from the production of hot axions is around $8 \times 10^6$ GeV. The bound is comparable to the astrophysical bounds on axion-muon and axion-photon couplings. Interestingly, the efficiency of axion production via LFV tau decays results in the hot axion bound stronger than the constraints from ground-based LFV searches at Belle-II. Moreover, the axion decay constant consistent with astrophysical bounds allows for $\Delta N_{\rm eff}$ as large as 0.25, within reach of Simons Observatory, which will probe astrophobic axion models up to $f_a \simeq 5 \times 10^7$ GeV. The CMB-S4 will be sensitive to hot axions with $f_a \simeq 1.5 \times 10^8$ GeV. We have demonstrated that the IAXO experiment will be complementary to CMB observations and could be used in distinguishing between astrophobic models.

We have determined the hot bound in astrophobic 3HDM models suppressing axion-muon coupling, which is usually weaker than the astrophysical bound on axion-photon coupling. However, in models with modest axion-photon coupling a sizable contribution of axions may be produced, $\Delta N_{\rm eff} \simeq 0.15$, mainly through scatterings with kaons, bringing them within the detection capabilities of the Simons Observatory. The CMB-S4 will allow for the detection of axions with $f_a \lesssim 2 \times 10^7$ GeV.

In the photophobic models the cosmological bound is comparable to the supernova constraint on the axion-muon coupling and sizable population of axions, $\Delta N_{\rm eff} \simeq 0.2$ is consistent with all observations. Depending on specific model, CMB-S4 will be sensitive to $f_a \in [8 \times 10^6, 2 \times 10^7]$ GeV.

In the properly astrophobic 3HDM, which suppresses both axion-muon and axion-photon coupling, axions are efficiently produced in the LFV tau decays while astrophysical bounds are easily satisfied. As a result, the cosmological bound is the strongest constraint on the model, of order $f_a > 7 \times 10^6$ GeV. Simons Observatory should probe this model up to $f_a \simeq 5 \times 10^7$ GeV, while CMB-S4 will further improve on that by potentially reaching $f_a \simeq 10^8$ GeV.

In the naturally astrophobic model, axion production is dominated by mechanisms that require non-perturbative treatments, which, due to the absence of reliable non-perturbative tools, we have estimated. The derived conservative bound, as strong as $f_a \gtrsim 5 \times 10^6$ GeV, did not depend on the parameterization and is the strongest constraint on the model. However, the sensitivities of Simons Observatory and CMB-S4 cannot be reliably derived with simple estimates and depend on the parametrization of non-perturbative effects. This is a common problem in predicting the relic abundance of axions, which is most efficient around QCDPT and hence subject to unknown, strong dynamics. In the future, improvement in the treatment of the non-perturbative effects can lead to refinement of the bound. Our result is important for axiogenesis, which requires the axion decay constant below $10^7$ GeV to simultaneously produce baryon asymmetry and account for all dark matter via the kinetic misalignment mechanism.

We have studied the parameter spaces of two dark matter candidates produced via freeze-out in SUSY TH models: twin stau and twin bino.

For the twin stau to be the LSP, and thus stable, it must be a mixture of left- and right-handed components. In the absence of $\mathbb{Z}_2$ breaking in the Yukawa sector, enhancing mixing between left-handed and right-handed twin stau requires relatively large values of $\operatorname{tg}\beta$ are required, typically above 10. The parameter space of twin stau is constrained by DD experiments, collider searches for long-lived staus, BBN, and ellipticity measurements of dark matter halo. We have analyzed the thermal production of twin stau, explaining how variations in the parameters affect relic abundance. We have demonstrated that mostly right-handed twin stau is a successful candidate for dark matter for a wide range of parameters. Specifically, we found that twin stau with a mass between 400 and 500 GeV constitutes the whole observed dark matter. The thermal production of twin stau involves interesting phenomena such as coannihilations with twin neutralinos and resonances. However, in contrast with many MSSM DM candidates like bino, those are not mandatory to satisfy all constraints on the parameter space and no additional fine-tuning is required.

In the SUSY TH models, the cross section for the DD event is suppressed by the mixing between the Higgses in twin and visible sectors, controlled by ratio $v'/v$. However, the suppression comes at the prize of fine-tuning and DD experiments remain the most promising probe of the most well-motivated part of twin stau DM parameter space. Notably, mostly right-handed twin stau mixture is preferred by the DD experiments.

The twin stau DM is necessarily accompanied by a relatively light MSSM stau, with mass splitting below a couple of tens of GeV. Consequently, the stau can become long-lived, potentially giving signals in collider searches or affecting cosmology. As long as neutralinos are light and stau decay length is suppressed, no additional model building is required. Heavy neutralinos can be accommodated in the twin stau DM scenario if bino-twin bino mixing is introduced.

We have analyzed the effect of increasing the VEV misalignment between the sectors, on the parameter space of twin stau. Interestingly, we have found an upper limit on the ratio $v'/v$ through BBN bound on stau lifetime. This can be directly translated into a lower bound on the fine-tuning of the model, around 1%. We have shown, that the sensitivity of the LZ experiment will probe the most natural regions of the parameter space, corresponding to tuning better than 3-5%.

Intriguingly, the ellipticity bound on self-interactions of DM is satisfied in the preferred region of the parameter space, requiring no breaking of twin electromagnetism. This result is in contrast to the TH candidates for charged DM, which usually require massive twin photon to suppress self-interactions.

The other DM candidate considered in the thesis and produced in freeze-out is twin bino-dominated twin neutralino. In contrast to the MSSM bino, overproduction can be mitigated by introducing $\mathbb{Z}_2$ breaking in the Yukawa sector and avoiding chiral suppression of annihilation cross section. Additional $\mathbb{Z}_2$ breaking alleviates the dark radiation problem present in TH extensions of the SM and does not compromise the TH solution to the little hierarchy problem.

Similar to the twin stau, the twin bino DM scenario is best probed by the DD experiment, which set a lower bound on the higgsino mass $\mu$. In particular, we found that the LZ experiment rules out the most natural values of $\mu \lesssim 1$ TeV for twin bino with a mass around 100 GeV, corresponding to fine-tuning of about 10%. We have shown that the full run of LZ will probe twin bino up to $\mu = 3$ TeV for small $\operatorname{tg}\beta$, and up to $\mu = 1.3$ TeV for large $\operatorname{tg}\beta$.

Using these two examples of DM candidates in SUSY TH models, we have demonstrated, that upcoming DD experiments, like LZ, will probe the most natural part of the parameter space. Therefore, in the following years, we will learn whether the SUSY TH model can simultaneously explain the stability of the EW scale and provide a viable DM candidate.

The limitations of our study include assumptions made when solving the Boltzmann equation. In the thesis, we have solved the integrated Boltzmann equation for the evolution of number densities assuming kinetic equilibrium. However, this assumption may not hold across the entire parameter space. In particular, corrections are expected in the proximity of resonances or when elastic scatterings are not efficient to maintain kinetic equilibrium. We expect those effects to be subdominant, but it remains interesting for future work to consider the full evolution of the distribution functions in the freeze-out production of DM in SUSY TH models and the freeze-in production of astrophobic axions.

In the thesis, we have presented two models featuring the thermal production of dark relics. We have shown that cosmological observations allowed for constraining the models by probing energies often unreachable by modern ground-based experiments. Due to the thermal history of the Universe, the search for dark relics produced through scatterings within the thermal bath remains a promising avenue in particle cosmology. Bounds set by cosmological observations are complementary to astrophysical observations and ground-based experiments searching for new physics. We have demonstrated that thermal production allows for constraining high-energy models such as SUSY TH, as well as models of very light and weakly coupled particles such as axions.

In astrophobic axion models, we have demonstrated the intricate interplay between astrophysical, laboratory, and cosmological observations. By focusing on specific scenarios of twin stau or twin bino DM in the SUSY TH model, we have been able to use DD experiments to set bounds on the SUSY TH model. Moreover, in the case of twin stau DM using cosmological hints on BBN we have derived a bound on the stau lifetime, which bounded the fine-tuning of the scenario from below. These are only some examples of the interplay between particle physics models and cosmology, which we have highlighted throughout the thesis. Combining astrophysical, laboratory, and cosmological observations, we have performed a complete analysis of three scenarios of thermal production in the early universe.

# Appendix A

# Elements of QFT

In this appendix, we will revisit some results from Quantum Field Theory. In Sec. A.1 we will prove an important relation between anomaly term and the Chern-Simons current, Sec. A.2 outlines the construction of LO of ChPT. Results from those two are heavily used in Chapter 3 and Sec. 2.2. Sec. A.3 presents the kinematics of basic processes, along with formulas used throughout the thesis. Sec. A.4 includes the derivation of Noether's theorem and a straightforward method for identifying conserved currents. Finally, in Sec. A.5 we derive the Goldstone theorem in two ways, discussing the effect of explicit symmetry breaking on the masses of Goldstone bosons.

## A.1 Divergence of Chern-Simons current

We will prove that the $G\tilde{G}$ term does not contribute to the perturbation theory by showing that

$$2\mathrm{Tr}\, G_{\mu\nu}\widetilde{G}^{\mu\nu} = \partial_\mu K^\mu \,. \tag{A.1}$$

The Chern-Simons current is defined by

$$K_\mu = 4\epsilon^{\mu\nu\alpha\beta}\mathrm{Tr}\Big(A_\nu\partial_\alpha A_\beta - \frac{2}{3}iA_\nu A_\alpha A_\beta, \Big)\,. \tag{A.2}$$

The author is not aware of any step-by-step derivation of this well-known equality in literature. We will start with rewriting the gauge fields in terms of their components, $A_\mu = A^a_\mu \lambda^a/2$. The CS current becomes

$$K_\mu = 4\epsilon^{\mu\nu\alpha\beta}\Big(\frac{1}{4}A^a_\nu\partial_\alpha A^b_\beta\mathrm{Tr}\Big(\lambda^a\lambda^b\Big) - \frac{i}{4}\frac{1}{3}A^a_\nu A^b_\alpha A^c_\beta\mathrm{Tr}\Big(\lambda^a\lambda^b\lambda^c\Big)\Big)\,. \tag{A.3}$$

The first trace is simply $\mathrm{Tr}(\lambda^a\lambda^b) = 2\delta^{ab}$, while to evaluate second trace note that:

$$\begin{aligned}\mathrm{Tr}\Big(\lambda^a\lambda^b\lambda^c\Big) &= \mathrm{Tr}\Big(\Big(\Big[\lambda^a\lambda^b\Big] + \lambda^b\lambda^a\Big)\lambda^c\Big) = \mathrm{Tr}\Big(\Big(2if^{abd}\lambda^d + \lambda^b\lambda^a\Big)\lambda^c\Big) = \\ &= 4if^{abc} + \mathrm{Tr}\Big(\lambda^b\lambda^a\lambda^c\Big)\,,\end{aligned} \tag{A.4}$$

where we have used the definition of structure constants, Eq. (2.3). Lastly, note that each of the Gell-Mann matrices is contracted with a gauge field, and each of those is contracted with a totally antisymmetric tensor. It means, that commuting $\lambda'$s generates a minus

$$\epsilon^{\mu\nu\alpha\beta}A^a_\nu A^b_\alpha A^c_\beta\mathrm{Tr}\Big(\lambda^a\lambda^b\lambda^c\Big) = -\epsilon^{\mu\nu\alpha\beta}A^a_\nu A^b_\alpha A^c_\beta\mathrm{Tr}\Big(\lambda^b\lambda^a\lambda^c\Big)\,, \tag{A.5}$$

so that we can substitute $\mathrm{Tr}\left(\lambda^a\lambda^b\lambda^c\right) = 2if^{abc}$ into Eq. (A.3). Finally, putting everything together, we obtain Chern-Simons current in the form

$$K^\mu = 2\epsilon^{\mu\nu\alpha\beta}\left(A^a_\nu\partial_\alpha A^a_\beta + \frac{1}{3}f^{abc}A^a_\nu A^b_\alpha A^c_\beta\right). \tag{A.6}$$

On the other hand, the LHS of Eq. (A.1) may be written as

$$2\mathrm{Tr}G_{\mu\nu}\widetilde{G}^{\mu\nu} = \frac{1}{2}G^a_{\mu\nu}G^a_{\alpha\beta}\epsilon^{\mu\nu\alpha\beta}, \tag{A.7}$$

where we have used definition $\widetilde{G}^{\mu\nu} = G_{\alpha\beta}\epsilon^{\alpha\beta\mu\nu}/2$ and $\mathrm{Tr}\lambda^a\lambda^b = 2\delta^{ab}$. Rescaling the gauge fields $A_\mu \to A_\mu/g$, the field strength becomes

$$G_{\mu\nu} = \partial_\mu A_\nu - \partial_\nu A_\mu - i[A_\mu, A_\nu] = \partial_\mu A^a_\nu\frac{\lambda^a}{2} - \partial_\nu A^a_\mu\frac{\lambda^a}{2} + f^{abc}A^b_\mu A^c_\nu\frac{\lambda^a}{2}. \tag{A.8}$$

Putting everything together, Eq. (A.1) becomes

$$G^a_{\mu\nu}G^a_{\alpha\beta}\epsilon^{\mu\nu\alpha\beta} = 4\epsilon^{\mu\nu\alpha\beta}\partial_\mu\left(A^a_\nu\partial_\alpha A^a_\beta + \frac{1}{3}f^{abc}A^a_\nu A^b_\alpha A^c_\beta\right). \tag{A.9}$$

Beginning with the LHS of the equation, we expand

$$\begin{aligned}
G^a_{\mu\nu}G^a_{\alpha\beta}\epsilon^{\mu\nu\alpha\beta} =&\epsilon^{\mu\nu\alpha\beta}\left(\partial_\mu A^a_\nu - \partial_\nu A^a_\mu + f^{abc}A^b_\mu A^c_\nu\right)\left(\partial_\alpha A^a_\beta - \partial_\beta A^a_\alpha + f^{ade}A^d_\alpha A^e_\beta\right)\\
=&\epsilon^{\mu\nu\alpha\beta}\Big(\partial_\mu A^a_\nu\partial_\alpha A^a_\beta - \partial_\mu A^a_\nu\partial_\beta A^a_\alpha - \partial_\nu A^a_\mu\partial_\alpha A^a_\beta + \partial_\nu A^a_\mu\partial_\beta A^a_\alpha\\
&+\left(\partial_\mu A^a_\nu - \partial_\nu A^a_\mu\right)A^b_\alpha A^c_\beta f^{abc} + \left(\partial_\alpha A^a_\beta - \partial_\beta A^a_\alpha\right)A^d_\mu A^e_\nu f^{ade}\\
&+A^b_\mu A^c_\nu A^d_\alpha A^e_\beta f^{abc}f^{ade}\Big).
\end{aligned} \tag{A.10}$$

Firstly, let's consider the terms in the first line of the result. Consider contraction of antisymmetric tensor with arbitrary tensor $\epsilon^{\mu\nu\alpha\beta}T_{\mu\nu\alpha\beta}$ and rename indices as $\mu \leftrightarrow \nu$ and similarly $\alpha \leftrightarrow \beta$ so we have

$$\epsilon^{\nu\mu\beta\alpha}T_{\nu\mu\beta\alpha} = \epsilon^{\mu\nu\alpha\beta}T_{\nu\mu\beta\alpha}, \tag{A.11}$$

and similarly, if we change only one pair of indices

$$\epsilon^{\nu\mu\alpha\beta}T_{\nu\mu\alpha\beta} = -\epsilon^{\mu\nu\alpha\beta}T_{\nu\mu\alpha\beta}. \tag{A.12}$$

Using those two relations we find that all four terms in the first line of the result Eq. (A.10) are identical and in total give

$$\text{1st line} = 4\epsilon^{\mu\nu\alpha\beta}\partial_\mu A^a_\nu\partial_\alpha A^a_\beta. \tag{A.13}$$

Similar consideration can be applied to the second line of the result, where the second term can be rewritten by renaming $\mu \leftrightarrow \alpha$ and $\nu \leftrightarrow \beta$

$$\begin{aligned}
\epsilon^{\mu\nu\alpha\beta}\left(\partial_\alpha A^a_\beta - \partial_\beta A^a_\alpha\right)A^d_\mu A^e_\nu f^{ade} \xlongequal[\mu\leftrightarrow\alpha]{\nu\leftrightarrow\beta}&\epsilon^{\alpha\beta\mu\nu}\left(\partial_\mu A^a_\nu - \partial_\nu A^a_\mu\right)A^d_\alpha A^e_\beta f^{ade} =\\
=&\ \epsilon^{\mu\nu\alpha\beta}\left(\partial_\mu A^a_\nu - \partial_\nu A^a_\mu\right)A^d_\alpha A^e_\beta f^{ade}.
\end{aligned} \tag{A.14}$$

The two terms in the second line are now identical and in total give

$$\text{2nd line} = 4\epsilon^{\mu\nu\alpha\beta}\partial_\mu A^a_\nu A^b_\alpha A^c_\beta f^{abc}. \tag{A.15}$$

In the third line we can rename group indices $A^b_\mu A^c_\nu A^d_\alpha A^e_\beta f^{abc} f^{ade} = A^a_\mu A^b_\nu A^c_\alpha A^e_\beta f^{abd} f^{dce}$ to use Jacobi identity

$$f^{abd} f^{dce} + f^{bcd} f^{dae} + f^{cad} f^{dbe} = 0 \,. \tag{A.16}$$

Inserting this into the last term of Eq. (A.10) gives

$$\epsilon^{\alpha\beta\mu\nu} A^a_\mu A^b_\nu A^c_\alpha A^e_\beta f^{abd} f^{dce} = \epsilon^{\alpha\beta\mu\nu} A^a_\mu A^b_\nu A^c_\alpha A^e_\beta \Big( -f^{bcd} f^{dae} - f^{cad} f^{dbe} \Big) \,. \tag{A.17}$$

Renaming the $SU(3)$ indices in the first term $a \to c, b \to a, c \to b$ we find

$$\begin{aligned} &\epsilon^{\alpha\beta\mu\nu} A^a_\mu A^b_\nu A^c_\alpha A^e_\beta f^{bcd} f^{dae} \xlongequal[c\to b]{a\to c, b\to a} \epsilon^{\alpha\beta\mu\nu} A^c_\mu A^a_\nu A^b_\alpha A^e_\beta f^{abd} f^{dce} = \epsilon^{\alpha\beta\mu\nu} A^a_\nu A^b_\alpha A^c_\mu A^e_\beta f^{abd} f^{dce} \\ &\quad = \epsilon^{\nu\alpha\beta\mu} A^a_\nu A^b_\alpha A^c_\mu A^e_\beta f^{abd} f^{dce} = -\epsilon^{\alpha\beta\mu\nu} A^c_\mu A^a_\nu A^b_\alpha A^e_\beta f^{abd} f^{dce} \,, \end{aligned} \tag{A.18}$$

which thus vanishes. Summarizing, we find that

$$G^a_{\mu\nu} G^a_{\alpha\beta} \epsilon^{\mu\nu\alpha\beta} = 4\epsilon^{\mu\nu\alpha\beta} \Big( \partial_\mu A^a_\nu \partial_\alpha A^a_\beta + \partial_\mu A^a_\nu A^b_\alpha A^c_\beta f^{abc} \Big) \,. \tag{A.19}$$

We can now focus on the RHS of Eq. (A.9), where the evaluation of derivative yields

$$4\epsilon^{\mu\nu\alpha\beta} \bigg( \partial_\mu A^a_\nu \partial_\alpha A^a_\beta + A^a_\nu \partial_\mu \partial_\alpha A^a_\beta + \frac{1}{3} f^{abc} \Big( \partial_\mu A^a_\nu A^b_\alpha A^c_\beta + A^a_\nu \partial_\mu A^b_\alpha A^c_\beta + A^a_\nu A^b_\alpha \partial_\mu A^c_\beta \Big) \bigg) \,. \tag{A.20}$$

The second term vanishes upon contracting the double derivative and $\epsilon^{\mu\nu\alpha\beta}$. The second and third terms of the parenthesis can be rewritten as

$$\begin{aligned} &\frac{1}{3} f^{abc} \epsilon^{\mu\nu\alpha\beta} A^a_\nu \partial_\mu A^b_\alpha A^c_\beta \xlongequal[\alpha\leftrightarrow\nu]{a\leftrightarrow b} \frac{1}{3} f^{bac} \epsilon^{\mu\alpha\nu\beta} \partial_\mu A^b_\nu A^a_\alpha A^c_\beta = \frac{1}{3} f^{abc} \epsilon^{\mu\nu\alpha\beta} \partial_\mu A^a_\nu A^b_\alpha A^c_\beta \,, \\ &\frac{1}{3} f^{abc} \epsilon^{\mu\nu\alpha\beta} A^a_\nu A^b_\alpha \partial_\mu A^c_\beta \xlongequal[\beta\leftrightarrow\nu]{a\leftrightarrow c} \frac{1}{3} f^{cba} \epsilon^{\mu\nu\alpha\beta} A^a_\beta A^b_\alpha \partial_\mu A^c_\nu = \frac{1}{3} f^{abc} \epsilon^{\mu\nu\alpha\beta} \partial_\mu A^a_\nu A^b_\alpha A^c_\beta \,. \end{aligned} \tag{A.21}$$

As a result, three terms in the parenthesis add up and we have

$$\text{RHS} = 4\epsilon^{\mu\nu\alpha\beta} \Big( \partial_\mu A^a_\nu \partial_\alpha A^a_\beta + f^{abc} \partial_\mu A^a_\nu A^b_\alpha A^c_\beta \Big) \,, \tag{A.22}$$

which is the same as LHS, Eq. (A.19).

The fact that this term is a total derivative guarantees that it does not contribute to the perturbation theory, as any vertex emerging from that term would be proportional to the sum of momenta of participating particles, identically vanishing.

## A.2 Non-linear sigma model for mesons

The full symmetry of the chiral QCD is $SU_A(3) \times SU_V(3) \times U_V(1)$, where we have accounted for the anomalous character of $U_A(1)$. Since mesons are bound states of quark-antiquark pairs, their baryon number is always 0. Hence, mesons are singlet under $U_V(1)$ and any lagrangian involving only mesons should be automatically $U_V(1)$ invariant.

Let us focus on the non-abelian global symmetry of the chiral QCD, $G = SU_L(3) \times SU_R(3)$, with element $g = (L, R)$ such that $L \in SU_L(3)$ and $R \in SU_R(3)$. The ground state remains unbroken only under the vector subgroup with elements $v = (V, V) \in H$, which is isomorphic to $SU(3)$. By Goldstone theorem, we expect 8 NGBs, $\phi_i$, which are best studied in the non-linear realization of $G$. The goal is to find a mapping, which generalizes the representation to target spaces, which are not necessarily vector spaces. We will follow the construction in [110].

Let $M_1$ be a vector space spanned by the Goldstone bosons, that is

$$M_1 = \{\Phi : \mathrm{Mink}^4 \to R^8\} . \tag{A.23}$$

We require that the mapping $\varphi : (g, \Phi) \in G \times M_1 \to M_1$ obeys

$$\begin{aligned} \varphi(e, \Phi) &= \Phi, \text{where } e \text{ is identity in } G , \\ \varphi(g_1, \varphi(g_2, \Phi)) &= \varphi(g_1 g_2, \Phi) \, , \text{for all } g_1, g_2 \in G . \end{aligned} \tag{A.24}$$

Most importantly, we do not require linearity of the map, $\varphi(g, \alpha\Phi) \neq \alpha\varphi(g, \Phi)$. Consider a space obtained by embedding the Goldstone bosons in exponentials,

$$M_3 = \left\{ U : \mathrm{Mink}^4 \to SU(3) \middle| U(x) = \exp\left(\frac{i}{f_\pi}\lambda_a\phi_a\right)\right\} , \tag{A.25}$$

where $f_\pi$ is the cut-off scale of the non-linear sigma model. Since a sum of two $SU(3)$ matrices is not a $SU(3)$ matrix, $M_3$ is not a vector space. We will take this space to be a target of the mapping defining non-linear realization of the symmetry G

$$\varphi : \big((L, R), U(x)\big) \in G \times M_3 \to M_3 : \left\{\varphi\big((L, R), U(x)\big) = RU(x)L^\dagger\right\} . \tag{A.26}$$

Clearly, as $U(x) \in SU(3)$ and $L, R \in SU(3)$, the result is indeed an element of $SU(3)$ itself. Let us verify that requirements Eq. (A.24) are indeed satisfied:

$$\begin{aligned} \varphi(e = (\mathbb{1}, \mathbb{1}), U(x)) &= \mathbb{1}U(x)\mathbb{1} = U(x) \\ \varphi(g_1, \varphi(g_2, U(x)) &= \varphi(g_1, R_2U(x)L_2^\dagger) = R_1R_2U(x)L_2^\dagger L_1^\dagger = R_1R_2U(x)(L_1L_2)^\dagger \\ &= \varphi(L_1L_2, R_1R_2, U(x)) = \varphi(g_1g_2, U(x)) . \end{aligned} \tag{A.27}$$

Let us observe some properties of the introduced structure. The ground state corresponds to no meson excitation $\phi_i = 0$, which implies $U_0(x) = \mathbb{1}$. The ground state is invariant under vector transformations:

$$U_0(x) = \mathbb{1} \to V\mathbb{1}V^\dagger = \mathbb{1} = U_0(x) . \tag{A.28}$$

Which is not a case for axial transformations

$$U_0(x) = \mathbb{1} \to A^\dagger\mathbb{1}A^\dagger \neq U_0(x) . \tag{A.29}$$

To find the transformation properties of the Goldstone bosons under vector transformations we expand exponential to find

$$U(x) = 1 + \frac{i}{f_\pi}\phi + \frac{1}{2}\left(\frac{i}{f_\pi}\right)^2\phi^2 + ... \to VU(x)V^\dagger = 1 + \frac{i}{f_\pi}V\phi V^\dagger + \frac{1}{2}\left(\frac{i}{f_\pi}\right)^2 V\phi^2V^\dagger + ... . \tag{A.30}$$

In the second term, we can insert unit matrix: $V\phi^2V^\dagger = V\phi V^\dagger V\phi V^\dagger$, from which it is clear that $\phi \to V\phi V^\dagger$. Explicitly we have

$$\begin{aligned} \phi = \phi_a\lambda_a \to \exp\left(i\alpha_a\frac{\lambda_a}{2}\right)\phi_b\lambda_b \exp\left(-i\alpha_a\frac{\lambda_a}{2}\right) &= \phi - \frac{i}{2}\alpha^a\phi_c[\lambda_a, \lambda_b] + \mathcal{O}\Big(\alpha^2\Big) = \\ = \phi + f_{abc}\alpha_a\phi_b\lambda_c , \end{aligned} \tag{A.31}$$

whereas there is no simple form of transformation of Goldstone bosons under axial transformations. Explicitly the form of $U(x)$ is given by

$$U(x) = \exp\left(\frac{i}{f_\pi}\begin{pmatrix} \pi^0 + \eta/\sqrt{3} & \sqrt{2}\pi^+ & \sqrt{2}K^+ \\ \sqrt{2}\pi^- & -\pi^0 + \eta/\sqrt{3} & \sqrt{2}K^0 \\ \sqrt{2}K^- & \sqrt{2}\bar{K}^0 & -2\eta/\sqrt{3} \end{pmatrix}\right). \tag{A.32}$$

Now that we have already embedded the required symmetry-breaking pattern into a non-linear realization of the global group, we can write the general lagrangian invariant under the whole group $G$. For a kinetic term, the only combination with two derivatives, which is invariant under (A.26) is given by

$$\mathcal{L}_{\text{kin}} = \frac{f_\pi^2}{4}\text{Tr}(\partial_\mu U \partial^\mu U^\dagger)\,, \tag{A.33}$$

where factor $f_\pi^2/4$ ensures the correct normalization of the kinetic terms of NGBs. To verify the invariance we use the cyclic property of the trace

$$\frac{f_\pi^2}{4}\text{Tr}\Big(\partial_\mu U \partial^\mu U^\dagger\Big) \to \frac{f_\pi^2}{4}\text{Tr}\Big(R\partial_\mu L^\dagger L U \partial^\mu U^\dagger R^\dagger\Big) = \frac{f_\pi^2}{4}\text{Tr}\Big(R^\dagger R \partial_\mu U \partial^\mu U^\dagger\Big) = \mathcal{L}_{\text{kin}}\,. \tag{A.34}$$

To include the masses of quarks in lagrangian one observes that $\bar{q}_R M q_L + \bar{q}_L M^\dagger q_R$ would be invariant if the mass matrix $M$ had transformation law $M \to RML^\dagger$

$$\begin{aligned} \bar{q}_R M q_L + \bar{q}_L M q_R \to & \bar{q}_R R^\dagger RML^\dagger L q_L + \bar{q}_L L^\dagger LMR^\dagger R q_R = \\ & = \bar{q}_R M q_L + \bar{q}_L M q_R\,. \end{aligned} \tag{A.35}$$

This trick allows us to construct the mass term

$$\begin{aligned} \mathcal{L}_m = \frac{f_\pi^2 B_0}{2}\text{Tr}\Big(MU^\dagger + UM^\dagger\Big) \to & \frac{f_\pi^2 B_0}{2}\text{Tr}\Big(RML^\dagger L U^\dagger R^\dagger + RUL^\dagger LLM^\dagger R\Big) = \\ & = \frac{f_\pi^2 B_0}{2}\text{Tr}\Big(MU^\dagger + UM^\dagger\Big)\,, \end{aligned} \tag{A.36}$$

which is invariant only if $M$ is not invariant under $G$. Note, that the mass term should be even under the parity transformation P, which fixes the sign of the linear combination. To see this note that $P : \phi(\vec{x}, t) \to -\phi(-\vec{x}, t)$, hence $P : U(\vec{x}, t) \to U(-\vec{x}, t)^\dagger$. It follows that

$$\begin{aligned} P: \quad \frac{f_\pi^2 B_0}{2}\text{Tr}\Big(MU^\dagger - UM^\dagger\Big) \to & \frac{f_\pi^2 B_0}{2}\text{Tr}\Big(MU - U^\dagger M^\dagger\Big) = \\ & = -\frac{f_\pi^2 B_0}{2}\text{Tr}\Big(MU^\dagger - UM^\dagger\Big)\,, \end{aligned} \tag{A.37}$$

where in the last line we have used $M^\dagger = M$.

We can find the conserved currents corresponding to the global symmetries by allowing the transformations to be local, see Appendix A.4. Consider a symmetry transformation with $\theta_a^R = 0$, that is

$$\begin{aligned} & U \to UL^\dagger \simeq U\Big(1 + \frac{i}{2}\theta_a^L(x)\lambda^a\Big) \\ & \partial_\mu U \to \partial_\mu(UL^\dagger) \simeq \partial_\mu U\Big(1 + \frac{i}{2}\theta_a^L(x)\lambda^a\Big) + \frac{i}{2}\Big(\partial_\mu\theta_a^L\Big)U\lambda^a\,. \end{aligned} \tag{A.38}$$

Since we are interested only in the derivative with respect to $\partial_\mu \theta^a_L$, we can focus on variation of the kinetic term

$$\begin{aligned}
\delta\mathcal{L}_{\text{kin}} &= \frac{f_\pi^2}{4}\text{Tr}\Big(\frac{i}{2}\Big(\partial_\mu\theta_a^L\Big)U\lambda^a\partial^\mu U^\dagger + \partial^\mu U\Big(-\frac{i}{2}\partial_\mu\theta_a^L\lambda_a U^\dagger\Big)\Big) = \\
&= \frac{i}{2}\partial_\mu\theta_a^L\frac{f_\pi^2}{4}\text{Tr}\Big(\lambda^a\Big((\partial^\mu U^\dagger)U - U^\dagger\partial^\mu U\Big)\Big) = \\
&= i\partial_\mu\theta_a^L\frac{f_\pi^2}{4}\text{Tr}\Big(\lambda^a(\partial^\mu U^\dagger)U\Big)\,,
\end{aligned} \tag{A.39}$$

where we have used $U^\dagger U = 1 \to (\partial_\mu U^\dagger)U = -U^\dagger(\partial_\mu U)$ in last equality. We can now perform the same calculation for $\theta_a^L = 0$, letting $\theta_a^R = \theta_a^R(x)$

$$\begin{aligned}
&U \to RU \simeq \Big(1 - \frac{i}{2}\theta_a^R(x)\lambda^a\Big)U \\
&\partial_\mu U \to \partial_\mu(RU) \simeq -\frac{i}{2}\Big(\partial_\mu\theta_a^R\Big)\lambda^a U + \Big(1 - \frac{i}{2}\theta_a^R(x)\lambda^a\Big)\partial_\mu U\,.
\end{aligned} \tag{A.40}$$

Taking only the part involving a single power of $\partial_\mu\theta_a^R$ we find

$$\begin{aligned}
\delta\mathcal{L}_{\text{kin}} &= \frac{f_\pi^2}{4}\text{Tr}\Big(-\frac{i}{2}\Big(\partial_\mu\theta_a^R\Big)\lambda^a U\Big(\partial^\mu U^\dagger\Big) + \partial^\mu U\Big(\frac{i}{2}\partial_\mu\theta_a^R U^\dagger\lambda_a\Big)\Big) = \\
&= -\frac{i}{2}\partial_\mu\theta_a^R\frac{f_\pi^2}{4}\text{Tr}\Big(\lambda^a\Big(U\Big(\partial^\mu U^\dagger\Big) - (\partial^\mu U)U^\dagger\Big)\Big) = \\
&= -i\partial_\mu\theta_a^R\frac{f_\pi^2}{4}\text{Tr}\Big(\lambda^a U\Big(\partial^\mu U^\dagger\Big)\Big)\,.
\end{aligned} \tag{A.41}$$

Therefore, the conserved currents are

$$\begin{aligned}
J_a^{L,\mu} &= \frac{\partial\delta\mathcal{L}_{\text{kin}}}{\partial(\partial_\mu\theta_a^L)} = i\frac{f_\pi^2}{4}\text{Tr}\Big(\lambda^a(\partial^\mu U^\dagger)U\Big)\,, \\
J_a^{R,\mu} &= \frac{\partial\delta\mathcal{L}_{\text{kin}}}{\partial(\partial_\mu\theta_a^R)} = -i\frac{f_\pi^2}{4}\text{Tr}\Big(\lambda^a U(\partial^\mu U^\dagger)\Big)\,,
\end{aligned} \tag{A.42}$$

from which it follows from Eq. (2.25) that axial and vector currents are

$$\begin{aligned}
J_a^{V,\mu} &= -i\frac{f_\pi^2}{4}\text{Tr}\Big(\lambda^a[U,(\partial^\mu U^\dagger)]\Big)\,, \\
J_a^{A,\mu} &= -i\frac{f_\pi^2}{4}\text{Tr}\Big(\lambda^a\{U,(\partial^\mu U^\dagger)\}\Big)\,.
\end{aligned} \tag{A.43}$$

Putting Eq. (A.33) and Eq. (A.36) together we obtain the LO of ChPT lagrangian

$$\begin{aligned}
\mathcal{L}_{\text{LO}} =& \frac{f_\pi^2}{4}\text{Tr}(\partial_\mu U\partial^\mu U^\dagger) + \frac{f_\pi^2 B_0}{2}\text{Tr}\Big(MU^\dagger + UM^\dagger\Big) \\
&- iC^V\frac{f_\pi^2}{4}K_\mu\text{Tr}\Big(\lambda^a[U,(\partial^\mu U^\dagger)]\Big) - iC^A\frac{f_\pi^2}{4}K_\mu\text{Tr}\Big(\lambda^a\{U,(\partial^\mu U^\dagger)\}\Big)\,,
\end{aligned} \tag{A.44}$$

where we have also included possible coupling of generic, vector-like operator $K^\mu$, to the axial and vector currents with couplings $C^A$ and $C_V$, respectively.

## A.3 Cross sections, decay widths

In this appendix, we will review the kinematics of scatterings and decays following Ref. [13], by defining momentum variables and observables.

The differential cross section for a process $1+2 \to 3+...+n$ is defined

$$d\sigma = \frac{(2\pi)^4|\mathcal{M}|^2}{4\sqrt{(p_1\cdot p_2)^2 - m_1^2 m_2^2}}\delta^{(4)}\left(p_1+p_2-\sum_{i=3}^{n} p_i\right)\prod_{i=3}^{n}\frac{d^3p_i}{(2\pi)^3 2E_i}\,, \tag{A.45}$$

which in the center of the mass frame can be simplified using

$$\sqrt{(p_1\cdot p_2)^2 - m_1^2 m_2^2} = p_{1cm}\sqrt{s}\,. \tag{A.46}$$

The differential partial decay width for $1 \to 2+..+n$ is defined

$$d\Gamma = \frac{(2\pi)^4}{2m_1}|\mathcal{M}|^2\delta^{(4)}\left(p_1-\sum_{i=2}^{n} p_i\right)\prod_{i=2}^{n}\frac{d^3p_i}{(2\pi)^3 2E_i}\,. \tag{A.47}$$

### A.3.1 Scattering $2 \to 2$

Consider kinematics of $2 \to 2$ scattering represented by the diagram:

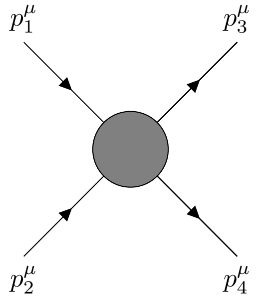


Mandelstam variables are Lorentz invariant combinations of momenta, convenient for the description of $2 \to 2$ scatterings. For incoming 4-momenta $p_1^\mu, p_2^\mu$ with masses $m_1, m_2$ and outgoing 4 momenta $p_3^\mu, p_4^\mu$ with masses $m_3, m_4$ Mandelstam variables are defined

$$\begin{aligned}
s &= (p_1+p_2)^2 = m_1^2 + m_2^2 + 2p_1^\mu p_2^\mu = (p_3+p_4)^2 = m_3^2+m_4^2+2p_3^\mu p_4^\mu\,,\\
t &= (p_1-p_3)^2 = m_1^2+m_3^2-2p_1^\mu p_3^\mu\,,\\
u &= (p_1-p_4)^2 = m_1^2+m_4^2-2p_1^\mu p_4^\mu\,.
\end{aligned} \tag{A.48}$$

We have used momenta conservation to express $s$ in terms of incoming and outgoing momenta. Mandelstam variables satisfy

$$s+t+u = m_1^2+m_2^2+m_3^2+m_4^2\,. \tag{A.49}$$

We compute the cross section in the center of mass frame, $\mathbf{p}_1^{\mathrm{CM}}+\mathbf{p}_2^{\mathrm{CM}} = \mathbf{p}_3^{\mathrm{CM}}+\mathbf{p}_4^{\mathrm{CM}} = 0$. From now on, we will omit the superscript CM for clarity of expressions. The following identities are useful

$$p_1^\mu p_2^\mu = E_1E_2 - \mathbf{p}_1\cdot\mathbf{p}_2 = E_1E_2 - \mathbf{p}_1^2 = E_1E_2-\mathbf{p}_2^2\,, \tag{A.50}$$

$$p_1^\mu p_2^\mu = \frac{1}{2}\left(s-m_1^2-m_2^2\right), \tag{A.51}$$

where in the first line we have used $|\mathbf{p}_1|^2 = |\mathbf{p}_2|^2$ and the second line follows from the definition of $s$. For later convenience, let us find the energy of the first particle expressed in terms of $s$

$$\begin{aligned}
E_1^2 =& E_1^2 \frac{(E_1+E_2)^2}{(E_1+E_2)^2} = \frac{(E_1^2+E_1E_2)^2}{(E_1+E_2)^2} = \frac{(m_1^2+\mathbf{p}_1^2+E_1E_2)^2}{E_1^2+E_2^2+2E_1E_2} = \\
=& \frac{(m_1^2+p_1^\mu p_2^\mu)^2}{m_1^2+\mathbf{p}_1^2+m_2^2+\mathbf{p}_2^2+2E_1E_2} = \frac{(m_1^2+p_1^\mu p_2^\mu)^2}{m_1^2+m_2^2+2p_1^\mu p_2^\mu} = \\
=& \frac{(2m_1^2+s-m_1^2-m_2^2)^2}{2s} = \frac{(s+m_1^2-m_2^2)^2}{2s}\,.
\end{aligned} \tag{A.52}$$

We have used Eq. (A.50) in going from the first to the second line, and we have used Eq. (A.51) to simplify to final line. By complete analogy, by using identities

$$p_3^\mu p_4^\mu = E_3E_4 - \mathbf{p}_3\cdot\mathbf{p}_4 = E_3E_4 - \mathbf{p}_3^2 = E_3E_4 - \mathbf{p}_4^2\,, \tag{A.53}$$

$$p_3^\mu p_4^\mu = \frac{1}{2}\Big(s - m_3^2 - m_4^2\Big)\,, \tag{A.54}$$

we find the energy of the third particle in the center of mass

$$\begin{aligned}
E_3^2 =& E_3^2 \frac{(E_3+E_4)^2}{(E_3+E_4)^2} = \frac{(E_3^2+E_3E_4)^2}{(E_3+E_4)^2} = \frac{(m_3^2+\mathbf{p}_3^2+E_3E_4)^2}{E_3^2+E_4^2+2E_3E_4} = \\
=& \frac{(m_3^2+p_3^\mu p_4^\mu)^2}{m_3^2+\mathbf{p}_3^2+m_4^2+\mathbf{p}_4^2+2E_3E_4} = \frac{(m_3^2+p_3^\mu p_4^\mu)^2}{m_3^2+m_4^2+2p_3^\mu p_4^\mu} = \\
=& \frac{(2m_3^2+s-m_3^2-m_4^2)^2}{2s} = \frac{(s+m_3^2-m_4^2)^2}{2s}\,.
\end{aligned} \tag{A.55}$$

We have now all the ingredients, which are necessary to find the cross section [113]. Using Eq. (A.49) we can express any $2\to 2$ amplitude in terms of $s$ and $t$. The cross section can be found by integrating

$$\frac{d\sigma}{dt} = \frac{1}{64\pi s}\frac{1}{|\mathbf{p}_1^{\mathrm{CM}}|^2}|\mathcal{M}|^2. \tag{A.56}$$

From the definition of Mandelstam variables we have

$$\begin{aligned}
t =& (p_1^{\mathrm{CM}} - p_3^{\mathrm{CM}})^2 = (E_1^{\mathrm{CM}} - E_3^{\mathrm{CM}})^2 - (\mathbf{p}_1^{\mathrm{CM}} - \mathbf{p}_3^{\mathrm{CM}})^2 = \\
=& (E_1^{\mathrm{CM}} - E_3^{\mathrm{CM}})^2 - (|\mathbf{p}_1^{\mathrm{CM}}|^2 + |\mathbf{p}_3^{\mathrm{CM}}|^2 - 2\mathbf{p}_1^{\mathrm{CM}}\cdot\mathbf{p}_3^{\mathrm{CM}}) = \\
=& (E_1^{\mathrm{CM}} - E_3^{\mathrm{CM}})^2 - (|\mathbf{p}_1^{\mathrm{CM}}|^2 + |\mathbf{p}_3^{\mathrm{CM}}|^2 - 2|\mathbf{p}_1^{\mathrm{CM}}||\mathbf{p}_3^{\mathrm{CM}}|\cos\theta_{\mathrm{CM}})\,,
\end{aligned} \tag{A.57}$$

where we have temporarily restored notation with CM superscript to emphasize the meaning of angle $\theta_{\mathrm{CM}}$, which is the angle between the momentum of the first and third particle in the center of the mass frame. Dropping CM superscripts we further have

$$\begin{aligned}
t &= (E_1 - E_3)^2 - (|\mathbf{p}_1| - |\mathbf{p}_3|)^2 - 2|\mathbf{p}_1||\mathbf{p}_3|(1-\cos\theta_{\mathrm{CM}}) = \\
&= (E_1 - E_3)^2 - (|\mathbf{p}_1| - \mathbf{p}_3|)^2 - 4|\mathbf{p}_1||\mathbf{p}_3|\sin^2\frac{\theta_{\mathrm{CM}}}{2}\,.
\end{aligned} \tag{A.58}$$

where we have used trigonometric identity $\cos(2x) = 1 - \sin^2 x$. Therefore, the limiting angles $\theta_{\mathrm{CM}} = 0, \pi$ correspond to

$$\theta_{\mathrm{CM}} = 0: \quad t_0 = (E_1 - E_3)^2 - (|\mathbf{p}_1| - |\mathbf{p}_3|)^2\,, \tag{A.59}$$

$$\theta_{\mathrm{CM}} = \pi: \quad t_1 = (E_1 - E_3)^2 - (|\mathbf{p}_1| + |\mathbf{p}_3|)^2\,. \tag{A.60}$$

$$\tag{A.61}$$

Note, that $t_0 > t_1$. Moreover, that since we expressed $E_1$ and $E_2$ in terms of $s$, we have

$$t_0 = \left(\frac{m_1^2 - m_3^2 - m_2^2 + m_4^2}{2\sqrt{s}}\right)^2 - (|\mathbf{p}_1| - |\mathbf{p}_3|)^2 , \tag{A.62}$$

$$t_1 = \left(\frac{m_1^2 - m_3^2 - m_2^2 + m_4^2}{2\sqrt{s}}\right)^2 - (|\mathbf{p}_1| + |\mathbf{p}_3|)^2 . \tag{A.63}$$

where magnitude of momenta can be found using (A.52) and (A.55):

$$|\mathbf{p}_i| = \sqrt{E_i^2 - m_i^2} . \tag{A.64}$$

**Two-body decays**

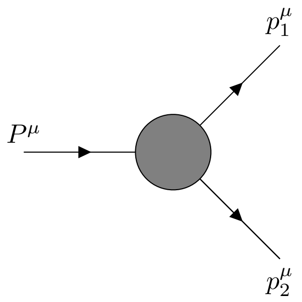


The differential of the decay width is defined

$$d\Gamma = \frac{1}{32\pi^2}|\mathcal{M}|^2 \frac{|\mathbf{p_1}|}{M^2} d\Omega , \tag{A.65}$$

where $M$ is mass of mother particle, $P^\mu P_\mu = M^2$, $\mathbf{p_1}$ is momentum of one of product particle and $d\Omega$ is the solid angle of particle 1. In the rest frame of the mother particle, the momentum is found via

$$|\mathbf{p}_1| = \frac{\Big(\big(M^2 - (m_1 + m_2)^2\big)\big(M^2 - (m_1 - m_2)^2\big)\Big)^{1/2}}{2M} . \tag{A.66}$$

**Three body decay**

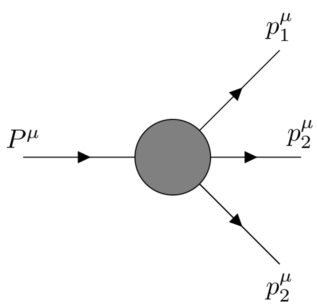


The 3-body decay width of particle with mass $M$ to particles with masses $m_1, m_2, m_3$ can be calculated using

$$d\Gamma = \frac{1}{(2\pi)^3}\frac{1}{32M^3}|\mathcal{M}|^2 dm_{12}^2 dm_{23}^2 , \tag{A.67}$$

where $m_{ij}^2 = (p_i + p_j)^2$. The range of $m_{23}^2$ for a given value of $m_{12}^2$ is determined by

$$\begin{aligned}(m_{23}^2)_{\max} &= (E_2^* + E_3^*)^2 - \left(\sqrt{E_2^{*2} - m_2^2} - \sqrt{\sqrt{E_3^{*2} - m_3^2}}\right)^2, \\ (m_{23}^2)_{\min} &= (E_2^* + E_3^*)^2 - \left(\sqrt{E_2^{*2} - m_2^2} + \sqrt{\sqrt{E_3^{*2} - m_3^2}}\right)^2,\end{aligned} \tag{A.68}$$

with $E_2^* = (m_{12}^2 - m_1^2 + m_2^2)/2m_{12}$ and $E_3^* = (M^2 - m_{12}^2 - m_3^2)/2m_{12}$ are energies in the rest frame of the decaying particle. The integration limits of $m_{12}^2$ are [13]

$$\begin{aligned}(m_{12}^2)_{\max} &= (M - m_3)^2, \\ (m_{12}^2)_{\min} &= (m_1 + m_2)^2.\end{aligned} \tag{A.69}$$

## A.4 Noether theorem

Following [110,337], consider a theory of fields $\Phi_i$ defined with lagrangian

$$\mathcal{L} = \mathcal{L}[\Phi_i, \partial_\mu \Phi_i], \tag{A.70}$$

which is invariant under internal symmetry transformation

$$\Phi_i \to \Phi_i + \delta\Phi_i = \Phi_i - i\epsilon^a(x) F_i^a[\Phi]. \tag{A.71}$$

We parametrize the symmetry transformation with generally spacetime dependent $\epsilon^a(x)$, and not necessarily linear functional $F_i^a[\Phi]$, where the index $a$ runs over all symmetry generators, e.g., $a = 1, \ldots, 8$ for $SU(3)$. The variation of lagrangian under this symmetry vanishes

$$\begin{aligned}\delta\mathcal{L} &= \frac{\partial \mathcal{L}}{\partial \Phi_i}\delta\Phi_i + \frac{\partial \mathcal{L}}{\partial(\partial_\mu \Phi_i)}\partial_\mu \delta\Phi_i = \\ &= \frac{\partial \mathcal{L}}{\partial \Phi_i}(-i\epsilon^a(x) F_i^a[\Phi]) + \frac{\partial \mathcal{L}}{\partial(\partial_\mu \Phi_i)}(-i\partial_\mu \epsilon^a F_i^a[\Phi] - i\epsilon^a \partial_\mu F_i^a[\Phi]) = \\ &= \epsilon^a\left(-iF_i^a[\Phi]\frac{\partial \mathcal{L}}{\partial \Phi_i} - i\partial_\mu F_i^a[\Phi]\frac{\partial \mathcal{L}}{\partial(\partial_\mu \Phi_i)}\right) + \partial_\mu \epsilon^a\left(-i\frac{\partial \mathcal{L}}{\partial(\partial_\mu \Phi_i)}F_i^a[\Phi_i]\right) = 0.\end{aligned} \tag{A.72}$$

Note, that the derivative of the second bracket is

$$\partial_\mu\left(-i\frac{\partial \mathcal{L}}{\partial(\partial_\mu \Phi_i)}F_i^a[\Phi_i]\right) = -i\partial_\mu\frac{\partial \mathcal{L}}{\partial(\partial_\mu \Phi_i)} - i\partial_\mu F_i^a[\Phi_i]\frac{\partial \mathcal{L}}{\partial(\partial_\mu \Phi_i)}, \tag{A.73}$$

which is equal to the first bracket in the last line of Eq. (A.72). Therefore, we might write Eq. (A.72) as

$$\delta\mathcal{L} = \epsilon^a \partial_\mu J^{\mu,a} + \partial_\mu \epsilon^a J^{\mu,a} = 0. \tag{A.74}$$

In particular, for global symmetries $\partial_\mu \epsilon^a(x) = 0$ and we obtain conservation of current

$$\partial_\mu J^{\mu,a} = 0. \tag{A.75}$$

On the other hand, we might use Eq. (A.74) to find the conserved currents and their divergences

$$J^{\mu,a} = \frac{\partial \delta\mathcal{L}}{\partial(\partial_\mu \epsilon^a)}, \tag{A.76}$$

$$\partial_\mu J^{\mu,a} = \frac{\partial \delta\mathcal{L}}{\partial \epsilon^a}. \tag{A.77}$$

Note, that since we have not assumed that $F_i^a[\Phi]$ is linear in fields, those equations might be used to find the current also in non-linear realizations of symmetries. In particular, we can use them to find conserved currents in ChPT, Eq. (A.42).

## A.5 Spontaneous symmetry breaking and Goldstone theorem

Spontaneous symmetry breaking arises when the ground state of symmetric theory is not symmetric itself. The symmetry breaking is a result of the dynamics of the system, which relaxes to the minimum, and thus is spontaneous. Ref. [115] proved that the SSB of continuous symmetry is accompanied by the presence of spinless, massless degrees of freedom.

Consider a theory of scalar fields $\phi_i$, with lagrangian

$$\mathcal{L} = \frac{1}{2}\partial_\mu \phi_i \partial^\mu \phi_i - V(\phi_i)\,, \tag{A.78}$$

where $V(\phi_i)$ is potential invariant under transformations of the continuous group $\mathcal{G}$. The action of $g \in \mathcal{G}$ on the fields is given by

$$\phi_i \to \phi_i + \delta\phi_i = \phi_i - i\epsilon_a T^a_{ij}\phi_j\,, \tag{A.79}$$

where $T^a$ are generators of the group. The minimum of the theory is found by considering the minima of the Hamiltonian $\mathcal{H} = \frac{1}{2}\partial_\mu\phi_i\partial^\mu\phi_i + V(\phi_i)$, which is minimized for static, homogenous field configurations $(\partial_\mu\phi_i)^2 = 0$. Hence, the minima of the theory are given by the minima of the potential.

Spontaneous symmetry breaking is present if the minimum $\langle\phi_i\rangle$ is invariant only under a subgroup of $\mathcal{H} \subset \mathcal{G}$. At this point, we can expand the potential around the minimum $\phi_i = \langle\phi_i\rangle + \chi_i$, which up to the first two terms reads

$$\begin{aligned} V(\phi_i) &= V(\langle\phi_i\rangle) + \left.\frac{\partial V}{\partial\phi_i}\right|_{\langle\phi_i\rangle}\chi_i + \left.\frac{\partial^2 V}{\partial\phi_i\partial\phi_j}\right|_{\langle\phi_i\rangle}\chi_i\chi_j = \\ &= V(\langle\phi_i\rangle) + \frac{1}{2}m^2_{ij}\chi^i\chi^j\,, \end{aligned} \tag{A.80}$$

where the second term trivially vanishes at the minimum and $m_{ij}$ is a symmetric, positive-definite mass matrix. The potential changes under infinitesimal $\mathcal{G}$ transformation according to

$$V(\langle\phi_i\rangle) \to V(\langle\phi_i\rangle + \delta\phi^0) = V(\langle\phi_i\rangle) + \frac{1}{2}m^2_{ij}\delta\phi^0_i\delta\phi^0_j\,. \tag{A.81}$$

On the other hand, the potential is assumed to be invariant under those transformations, so we have

$$m^2_{ij}\delta\phi^0_i\delta\phi^0_j = 0\,. \tag{A.82}$$

Since $m^2_{ij}$ is symmetric it implies

$$m^2_{ij}\delta\phi^0_j = 0 \to \epsilon^a m^2_{ij}T^a_{jk}\langle\phi_k\rangle = 0\,. \tag{A.83}$$

It follows directly that depending on whether $T^a$ belongs to $\mathcal{H}$ solutions belong to one of two categories.

1. for the generator $T^a$ of the subgroup $\mathcal{H}$ which leaves minimum invariant, we have $T^a_{ij}\langle\phi_j\rangle = 0$. Thus, the above equation is satisfied for arbitrary $m^2_{ij}$.
2. for each generator of $\mathcal{G}$, which is not a generator of $\mathcal{H}$, we have $T^a_{ij}\langle\phi_j\rangle \neq 0$. Hence, equation A.83 is an eigenvalue equation with zero eigenvalue. It follows that for each generator that does not preserve the minimum, there exists a massless state. The number of NGBs is determined by the symmetry groups and is given by dim$\mathcal{G}-$dim$\mathcal{H}$.

### A.5.1 Alternative proof of Goldstone theorem

We proved that if the ground state is invariant only under a subgroup of the symmetry group of the theory, new massless states appear. We will now prove it again in a more general form, following Ref. [113].
According to the Noether theorem, Appendix A.4, the invariance of lagrangian under continuous symmetry transformation, parametrized by $\alpha$, implies conservation of current Eq. (A.76)

$$J^\mu = \frac{\partial \delta \mathcal{L}}{\partial(\partial_\mu \delta\alpha)} = \sum_m \frac{\partial \mathcal{L}}{\partial \partial_\mu \phi_m} \frac{\delta \phi_m}{\delta \alpha} \,. \tag{A.84}$$

Each current is associated with the conserved charge, which can be found by integrating the zeroth component of the current

$$Q = \int d^3x \sum_m \frac{\partial \mathcal{L}}{\partial \partial_0 \phi_m} \frac{\delta \phi_m}{\delta \alpha} \,. \tag{A.85}$$

The conserved charges commute with Hamiltonian $[Q, H] = 0$. Consider the ground state $|\Omega\rangle$, which is not invariant only under a subgroup of the full symmetry group of the theory. In other words, the vacuum state has transformation law under the symmetry transformation which is specified by the non-vanishing charge of the state

$$Q|\Omega\rangle \neq 0 \,. \tag{A.86}$$

The eigenvalue equation for the energy of the ground state is simply $H|\Omega\rangle = E_0|\Omega\rangle$. It is easy to see that the energy of state $Q|\Omega\rangle$ is also $E_0$

$$HQ|\Omega\rangle = [H, Q]|\Omega\rangle + QH|\Omega\rangle = E_0 Q|\Omega\rangle \,. \tag{A.87}$$

Using the definition of the charge we can rewrite this state as

$$Q|\Omega\rangle = \int d^3x J_0(x)|\Omega\rangle \,. \tag{A.88}$$

We have explicitly displayed position dependence to emphasize momentum independence. Out of this state, we can construct the momentum eigenstate as

$$|\pi(\vec{p})\rangle = -\frac{2i}{F} \int d^3x e^{i\vec{x}\cdot\vec{p}} J_0(x)|\Omega\rangle \,, \tag{A.89}$$

where the arbitrary factor in front has been chosen for later convenience. Taking the limit of vanishing momentum $\vec{p} \to 0$ yields

$$|\pi(\vec{p}=0)\rangle = -\frac{2i}{F} \int d^3x J_0(x)|\Omega\rangle = -\frac{2i}{F} Q|\Omega\rangle \,, \tag{A.90}$$

which is an eigenstate of energy, degenerate with ground state. Momentum eigenstate degenerate with the ground state in the limit of vanishing momenta cannot be interpreted differently than a state of massless particle — the Goldstone boson. Furthermore, we can find that

$$\int \frac{d^3\vec{p}}{(2\pi)^3} e^{i\vec{p}\cdot\vec{y}} \langle \pi(\vec{q}) \,|\, \pi(\vec{p})\rangle = -\frac{2i}{F} \int d^3x \int \frac{d^3\vec{p}}{(2\pi)^3} e^{i\vec{p}\cdot(\vec{x}+\vec{y})} \langle \pi(\vec{q})|J_0(x)|\Omega\rangle \,, \tag{A.91}$$

Normalization of the field is given by $\langle \pi(\vec{q}) \,|\, \pi(\vec{p})\rangle = 2E_p(2\pi)^3\delta^{(3)}(\vec{p}-\vec{q})$, for energy $E_p$ of field with momentum $\vec{p}$, so on LHS of the equation we have

$$\int \frac{d^3p}{(2\pi)^3} e^{i\vec{p}\cdot\vec{y}} 2E_p(2\pi)^3\delta^{(3)}(\vec{p}-\vec{q}) = 2E_q e^{i\vec{q}\cdot\vec{y}} \,, \tag{A.92}$$

while the RHS of the equation simplifies to

$$-\frac{2i}{F}\int d^3x\delta^{(3)}(\vec{x}+\vec{y})\langle\pi(\vec{q})|J_0(x^0,\vec{x})|\Omega\rangle = \frac{2i}{F}\langle\pi(\vec{q})|J_0(x^0,-\vec{y})|\Omega\rangle\,. \tag{A.93}$$

Changing the spatial coordinates system $x^i \to -x^i$ does not change the scalar product, while $J_0(x^0,-\vec{y}) \to J_0(x^0,\vec{y}) \equiv J_0(y)$. Combining Eq. (A.92) and Eq. (A.93), we obtain the famous formula for the creation of Goldstone from the vacuum by a charge corresponding to the broken generator

$$\langle\pi(\vec{q})|J_0(y)|\Omega\rangle = iE_qFe^{i\vec{q}\cdot\vec{y}}\,. \tag{A.94}$$

By Lorentz invariance, the general formula is

$$\langle\pi(\vec{q})|J_\mu(y)|\Omega\rangle = iq_\mu e^{i\vec{q}\cdot\vec{y}}\,. \tag{A.95}$$

This result is useful for finding the composition of Goldstone bosons e.g. in the axion models, see Sec. 3.2.

### Example with explicit symmetry breaking

Consider a small correction to the above potential, which explicitly breaks $\mathcal{G}$. We will work out details on an example, however the conclusions are general. An example of a $SO(3)$ symmetric potential with small breaking is given by

$$V(\phi) = -\frac{m^2}{2}\phi_i\phi_i + \frac{\lambda}{4}(\phi_i\phi_i)^2 + a\phi_3\,, \tag{A.96}$$

where $\phi$ belongs to $SO(3)$ fundamental representation. For $a = 0$, the minimum of the theory is at $\langle\phi_i\phi_i\rangle = v^2 = m^2/\lambda$, and the minimum has only $SO(2)$ symmetry, which results in $3-1=2$ massless NGBs.
On the other hand, if $a \neq 0$ the minimization conditions for each component is

$$\begin{aligned} i=1,2: -m^2\langle\phi_i\rangle + \lambda\langle\phi_i\rangle^3 = 0 \to \phi_1 = \phi_2 = 0\,,\\ i=3: -m^2\langle\phi_3\rangle + \lambda\langle\phi_3\rangle^3 + a = 0\,. \end{aligned} \tag{A.97}$$

We can solve the second condition using ansatz $\langle\phi_3\rangle = \langle\phi_3\rangle^{(0)} + a\langle\phi_3\rangle^{(1)}$ and expanding up to linear order in $a$

$$\langle\phi_3\rangle^{(0)}(-m^2 + \lambda\langle\phi_3\rangle^{(0)}) + a(1 - m^2\langle\phi_3\rangle^{(1)} + 3\lambda\Big(\langle\phi_3\rangle^{(0)}\Big)^2\langle\phi_3\rangle^{(1)}) = 0\,. \tag{A.98}$$

At leading order ($a = 0$), the solution is $\langle\phi_3\rangle^{(0)} = \sqrt{m^2/\lambda}$, in agreement with result above. If we expand the potential around that minimum, $\phi_3 = \langle\phi_3\rangle^{(0)} + \chi_3$, we find

$$\begin{aligned} V(\phi_1,\phi_2,\chi_3) = &-\frac{m^4}{4\lambda} + \frac{\lambda}{4}(\phi_1^4+\phi_2^4+\chi_3^4) + \frac{\lambda}{2}(\phi_1^2\phi_2^2 + \phi_1^2\chi_3^2 + \phi_2^2\chi_3^2) + \\ &+ \sqrt{\lambda m^2}(\phi_1^2+\phi_2^2+\chi_3^2)\chi_3 + \frac{1}{2}(2m^2)\chi_3^2\,, \end{aligned} \tag{A.99}$$

which is a theory with two NGBs $\phi_1$ and $\phi_2$ and a massive $\chi_3$ corresponding to the generator of the remaining symmetry. Going beyond leading order in Eq. (A.98) we find that

$$\langle\phi_3\rangle^{(1)} = -\frac{1}{2m^2} \to \langle\phi_3\rangle = \sqrt{\frac{m^2}{\lambda}} - \frac{a}{2m^2}\,, \tag{A.100}$$

plugging that result into the potential the masses of the NGBs are generated, while the mass of $\chi_3$ is shifted

$$\begin{aligned} m_{\phi_1}^2 &= m_{\phi_2}^2 = a\sqrt{\frac{\lambda}{m^2}}\,, \\ m_{\chi_3}^2 &= 2m^2 + 3a\sqrt{\frac{\lambda}{m^2}}\,. \end{aligned} \tag{A.101}$$

An important feature of this result is that while massive, pNGBs are relatively light as long as the symmetry holds approximately. Any explicit symmetry breaking of spontaneously broken symmetry will generate masses of pNGBs. This result can be applied to approximate symmetries, such as chiral symmetry in QCD, and used to understand the low energy spectrum of the theory.

# Appendix B

# Cosmology of Homogenous Universe

In this appendix, we quote some known results in cosmology used throughout the thesis.

## B.1 Geometry of homogenous Universe

Under the assumption of homogeneity and isotropy the most general spacetime metric $g_{\mu\nu}$ in spherical coordinates $(t, r, \theta, \phi)$ is Friedmann-Lemaitre-Robertson-Walker (FLRW)

$$ds^2 = g_{\mu\nu}dx^\mu dx^\nu = g_{00}dx_0^2 - \gamma_{ij}dx^i dx^j = -dt^2 + a^2(t)\left(\frac{dr^2}{1-kr^2} + r^2 d\theta^2 + r^2 \sin^2\theta d\phi^2\right), \tag{B.1.1}$$

where we have implicitly defined the spatial part of the metric $\gamma_{ij}$. The Christoffel symbol(s?) is defined

$$\Gamma^\mu_{\alpha\beta} = \frac{1}{2}g^{\mu\lambda}(\partial_\alpha g_{\beta\lambda} + \partial_\beta g_{\alpha\lambda} - \partial_\lambda g_{\alpha\beta}), \tag{B.1.2}$$

which for FLRW metric has non-zero elements

$$\begin{aligned} \Gamma^0_{ij} &= a\dot{a}\gamma_{ij}, \\ \Gamma^i_{0j} &= \Gamma^i_{j0} = \frac{\dot{a}}{a}\delta^i_j, \\ \Gamma^i_{jk} &= \Gamma^i_{kj} = \frac{1}{2}\gamma^{il}(\partial_j\gamma_{kl} + \partial_k\gamma_{jl} - \partial_l\gamma_{jk}). \end{aligned} \tag{B.1.3}$$

The Ricci tensor is defined

$$R_{\mu\nu} = \partial_\lambda\Gamma^\lambda_{\mu\nu} - \partial_\nu\Gamma^\lambda_{\mu\lambda} + \Gamma^\lambda_{\lambda\rho}\Gamma^\rho_{\mu\nu} - \Gamma^\rho_{\mu\lambda}\Gamma^\lambda_{\nu\rho}, \tag{B.1.4}$$

from which we can obtain Ricci scalar by contracting the indices $R = R_{\mu\nu}g^{\mu\nu}$. The Einstein equation relates functions of the metric to the energy momentum tensor $T_{\mu\nu}$:

$$G_{\mu\nu} = R_{\mu\nu} - \frac{1}{2}Rg_{\mu\nu} = 8\pi G T_{\mu\nu}, \tag{B.1.5}$$

where we have defined the Einstein tensor $G_{\mu\nu}$, and $G$ is the gravitational constant. Homogeneity and isotropy fix the form of the energy-momentum tensor of a perfect fluid

$$T^0_0 = \rho, \qquad T^i_0 = 0, \qquad T^i_j = P\delta^i_j, \tag{B.1.6}$$

where $\rho$ is energy density and $P$ is pressure in the comoving frame. Finally, the Einstein equation for FLRW metric simplifies to two Friedmann equations

$$\begin{aligned} \left(\frac{\dot{a}}{a}\right)^2 &= \frac{8\pi G}{3}\rho - \frac{k}{a^2}\,, \\ \frac{\ddot{a}}{a} &= -\frac{4\pi G}{3}(\rho + 3P)\,. \end{aligned} \tag{B.1.7}$$

The Hubble parameter is defined as

$$H = \frac{\dot{a}}{a}\,. \tag{B.1.8}$$

Since the curvature vanishes in our Universe, $k = 0$ [21], by measuring the current Hubble, $H_0$, we can determine the critical energy density

$$\rho^0_{\text{crit}} = \frac{3H_0^2}{8\pi G}\,. \tag{B.1.9}$$

Critical energy density is used in convenient dimensionless parametrization of the energy densities measured today, $\rho_i^0$,

$$\Omega_i = \frac{\rho_i}{\rho^0_{\text{crit}}}\,. \tag{B.1.10}$$

In this way, we implicitly relate the energy density observable to the current Hubble, which is also observable. To cancel this redundancy, we define the dimensionless Hubble as $h = H_0/100\text{km/s/Mpc} \simeq 0.7$ and parameterize the energy density as

$$\Omega_i h^2 = \frac{\rho_i}{\rho^0_{\text{crit}}}\left(\frac{H_0}{100\text{km/s/Mpc}}\right)^2. \tag{B.1.11}$$

The components of the Universe are well approximated by a perfect fluid with energy-momentum tensor

$$T_{\mu\nu} = (\rho + P)U_\mu U_\nu + P g_{\mu\nu}\,, \tag{B.1.12}$$

where $\rho$ and $P$ are the energy density and pressure of the fluid, respectively, and the 4-velocity $U_\mu$ in the comoving frame. The continuity equation of the energy-momentum tensor reads

$$\nabla_\mu T^\mu_\nu = \partial_\mu T^\mu_\nu + \Gamma^\mu_{\mu\lambda}T^\lambda_\nu - \Gamma^\lambda_{\mu\nu}T^\mu_\lambda = 0\,, \tag{B.1.13}$$

which for a perfect fluid in FLRW gives

$$\dot{\rho} + 3\frac{\dot{a}}{a}(\rho + P) = 0\,. \tag{B.1.14}$$

Parametrizing the equation of state with a constant $\omega = P/\rho$ gives scaling of energy density

$$\rho \propto a^{-3(1+w)}\,. \tag{B.1.15}$$

For matter $\omega = 0$, for radiation $\omega = 1/3$ and for dark energy $\omega = -1$. Using this scaling, the dynamics of the expansion of the Universe can be found from Friedmann Eqs. (B.1.7). Using the above scaling and Eq. (B.1.11), the Hubble rate can be expressed in terms of energy densities and the scale factor

$$H^2 = H_0^2\left(\Omega_r\left(\frac{a}{a_0}\right)^{-4} + \Omega_m\left(\frac{a}{a_0}\right)^{-3} + \Omega_\Lambda\right), \tag{B.1.16}$$

where $H_0$ is the current Hubble rate and indices $r, m, \Lambda$ correspond to radiation, matter, and cosmological constant, respectively. It follows that evaluating the above expression now, at $t = t_0$, the densities are related via

$$\Omega_r + \Omega_m + \Omega_\Lambda = 1\,. \tag{B.1.17}$$

The measurements of the power spectrum of CMB temperature anisotropies give [21]

$$\Omega_m h^2 = 0.321 \pm 0.013, \qquad \Omega_\Lambda h^2 = 0.697 \pm 0.013\,, \tag{B.1.18}$$

while radiation gives negligible, though measurable in terms of an effective number of neutrinos Sec. 5.1, contribution to the energy budget of the Universe.

## B.2 Thermodynamics of early Universe

The equilibrium distribution function of a particle in the momentum space is

$$f^{\rm eq}(p,T) = \frac{1}{e^{(E(p)-\mu)/T} \pm 1}\,, \tag{B.2.19}$$

where + sign is for fermions (Fermi-Dirac distribution) and - sign is for bosons (Bose-Einstein distribution), $E(p) = \sqrt{p^2 + m^2}$ is the energy of the particle with momentum $p$, $\mu$ is chemical potential and $T$ is the temperature. Neglecting the quantum spin statistics and chemical potential in Eq. (B.2.19) gives Maxwell-Boltzmann distribution

$$f^{\rm eq}(p,T) \simeq e^{-E(p)/T}\,. \tag{B.2.20}$$

The number density of particles is defined as an integral over the distribution

$$n(T) = \frac{g}{(2\pi)^3} \int d^3p f(p,T)\,, \tag{B.2.21}$$

where $g$ is the number of internal degrees of freedom. Similarly, the energy density is defined as

$$\rho(T) = \frac{g}{(2\pi)^3} \int d^3p E(p) f(p,T)\,. \tag{B.2.22}$$

Substituting the Eq. (B.2.19) for vanishing chemical potential in the relativistic limit $(m \to 0)$ the above formulas yield

$$n^{\rm eq} = \frac{\zeta(3)}{\pi^2} g T^3 \begin{cases} 1 & \text{bosons} \\ \frac{3}{4} & \text{fermions} \end{cases}\,, \tag{B.2.23}$$

$$\rho^{\rm eq} = \frac{\pi^2}{30} g T^4 \begin{cases} 1 & \text{bosons} \\ \frac{7}{8} & \text{fermions} \end{cases}\,, \tag{B.2.24}$$

where $\zeta(x)$ is Riemann zeta function. For non-relativistic particles of mass $m$, Eqs. (B.2.21) and (B.2.22) give the same results for bosons and fermions

$$n^{\rm eq} = g\left(\frac{mT}{2\pi}\right)^{3/2} \exp^{-m/T}\,, \tag{B.2.25}$$

$$\rho^{\rm eq} = mn + \frac{3}{2} nT\,. \tag{B.2.26}$$

The entropy density of a single species of particles is

$$s = \frac{2\pi^2}{45} g_{*s} T^3 = \frac{2\pi^2}{45} g T^3 \begin{cases} 1 & \text{bosons} \\ \frac{7}{8} & \text{fermions} \end{cases} , \tag{B.2.27}$$

where $g$ is the number of internal degrees of freedom. The above formulas motivate the definition of total entropy density

$$s = \frac{2\pi^2 T^3}{45} g_{*s}(T)\,, \tag{B.2.28}$$

$$\rho = \frac{\pi^2}{30} T^4 g_*(T)\,. \tag{B.2.29}$$

where $g_{*s}(T)$ counts the number of degrees of freedom contributing to entropy and $g_*$ counts the number of relativistic degrees of freedom. We use results from [242] for both $g_{*s}$ and $g_*$.

## B.3 Boltzmann equation

In the previous appendix, we have discussed the cosmology of particles in equilibrium. However, the thermal history of the Universe is dynamic whenever a particle species is out of equilibrium with the SM heat bath. The exact dynamics of an out-of-equilibrium state are governed by the Boltzmann equation, which includes information about scatterings and decays in the form of collision terms.

Any particle species that is coupled to the SM must have necessarily been produced in the high-energy conditions of the early universe. This makes thermal production a particularly efficient probe of high-energy physics models, sensitive to deviations from the SM. In particular, the production of stable particles results in a potentially observable population still present today, e.g. in the form of DM.

Throughout the thesis, we use results from this appendix to study both relativistic and non-relativistic stable relics. In Sec. B.3 we discuss general properties of the Boltzmann equation, in Sec. B.3 introduce numerically convenient dimensionless variables. In Sec. B.4 we consider the collision term and derive it with standard methods for several representative cases. Finally, in Sec. B.5 we discuss the thermal history of a set of supersymmetric particles, governed by a system of Boltzmann equations.

### General discussion

Following the derivation from Ref. [143], we will discuss the basic properties of the Boltzmann equation before moving to a more detailed analysis in the following sections. Without interactions, the number density of a particle species $i$ has scaling $n_i \propto a^{-3}$. This allows us to write

$$\frac{d(n_i a^3)}{dt} = 0 \to \frac{dn_i}{dt} + 3Hn_i = 0\,, \tag{B.3.30}$$

where we used the definition of the Hubble constant $H = \dot{a}/a$. The inclusion of the interactions is done by letting the right-hand side of this equation be non-zero,

$$\frac{dn_i}{dt} + 3Hn_i = C[n_i, n_j]\,, \tag{B.3.31}$$

where the collision term $C[n_i, n_j, ...]$, in general, depends on number densities of all other particles. For a process $ij \to ab$, the collision term must be linear in $n_i$ and $n_j$, so that it vanishes in the limit $n_i, n_j \to 0$. Similarly, for the inverse process $ab \to ij$, the collision term must be linear in $n_a$ and $n_b$.

While throughout the thesis we will be considering this form of the equation, it is worth noting that number density is not a fundamental quantity but is rather defined as the integral of the distribution function, Eq. (B.2.21). Solving the integrated Boltzmann equation is often a good approximation, however in some cases, e.g. in the proximity of resonances or in case of Sommerfeld enhancement of annihilation cross section, can lead up to an order of magnitude difference in prediction for relic abundance [338, 339].

For a start, it is instructive to consider the Boltzmann equation for some generic $2 \leftrightarrow 2$ scattering process $ab \leftrightarrow ij$. The collision term consists of two competing processes, and the Boltzmann equation can be schematically written as

$$\frac{dn_i}{dt} + 3Hn_i = -\alpha n_i n_j + \beta n_a n_b \, . \tag{B.3.32}$$

In equilibrium, the right-hand side must vanish and changes in $n_i$ are solely due to dilution by expansion of the Universe. This condition is called detailed balance and implies that

$$\beta = \alpha \left( \frac{n_i n_j}{n_a n_b} \right)_{\text{eq}} , \tag{B.3.33}$$

which simplifies the Boltzmann equation

$$\frac{dn_i}{dt} + 3Hn_i = -\alpha \left( n_i n_j - \left( \frac{n_i^{\text{eq}} n_j^{\text{eq}}}{n_a^{\text{eq}} n_b^{\text{eq}}} \right) n_a n_b \right) . \tag{B.3.34}$$

This is particularly useful when particles $a$ and $b$ are in equilibrium with a thermal bath, $n_a = n_a^{\text{eq}}$ and $n_b = n_b^{\text{eq}}$, and the Boltzmann equation reads

$$\frac{dn_i}{dt} + 3Hn_i = -\alpha \left( n_i n_j - n_i^{\text{eq}} n_j^{\text{eq}} \right) . \tag{B.3.35}$$

From dimensional analysis, the parameter $\alpha$ must have dimension $[\mathrm{m}^3 \mathrm{s}^{-1}]$. The QFT observable of $2 \leftrightarrow 2$ is the cross section $\sigma$, with dimension $\mathrm{m}^2$, therefore $\alpha \sim \sigma v_{\text{rel}}$, where $v_{\text{rel}}$ is the relative velocity of initial particles. In the following sections, we will show an explicit derivation that $\alpha = \langle \sigma v_{\text{rel}} \rangle$ is a thermally averaged cross section.

For simplicity, let's consider a single particle production from the thermal bath, that is $n_j = n_j^{\text{eq}}$. The collision term is linear in the number density

$$\frac{dn_i}{dt} + 3Hn_i = -\alpha' (n_i - n_i^{\text{eq}}) \, , \tag{B.3.36}$$

where we have defined $\Gamma = \alpha n_j^{\text{eq}}$ with the same dimensions as the Hubble expansion rate. Since this is a first-order differential equation, we can look for the solutions of the homogenous equation

$$\frac{dn_i}{dt} = (\Gamma - 3H) n_i \, . \tag{B.3.37}$$

Integrating both sides reads

$$\log \left( \frac{n_i}{n_i^0} \right) = \int dt (\Gamma - 3H) \, , \tag{B.3.38}$$

which results in a fairly simple solution

$$n_i = n_i^0 \exp \left( \int dt (\Gamma - 3H) \right) , \tag{B.3.39}$$

which shows that the behavior of $n_i$ is in general exponential. Going back to the original Boltzmann equation, Eq. (B.3.36), we see that for sufficiently strong interaction, if we start with $n_i < n_i^{\rm eq}$, the derivative of number density is positive and $n_i$ exponentially grows towards equilibrium. On the contrary, if we start with $n_i > n_i^{\rm eq}$, the derivative of number density is negative, and $n_i$ exponentially drops towards equilibrium. For efficient interactions, $\Gamma \gtrsim H$ equilibrium is the attractor of the Boltzmann equation, while if $\Gamma \ll H$ particles are just redshifted by the expansion of the Universe, Eq. (B.3.30).

### Change to dimensionless variables

Let us focus on a single particle production, relevant in axion models, but similar calculation can be conducted in $2 \leftrightarrow 2$ scatterings. The evolution of number density $n$ is governed by the integrated Boltzmann equation [340]

$$\frac{dn}{dt} + 3Hn = \left(\sum_i \Gamma_i\right)\left(n^{\rm eq} - n\right), \tag{B.3.40}$$

where $n^{\rm eq}$ is the number at equilibrium, $H$ is the Hubble parameter and $\Gamma_i$ are scattering or decay rates parametrizing the collision term. It is numerically convenient to work in a dimensionless variable $x = m/T$ and yield $Y = n/s$, where $m$ is typically set to the mass of the heaviest particle or the DM candidate, and $s$ is the entropy density defined by Eq. (B.2.28). Note, that the equilibrium yield, $Y^{\rm eq}$, remains constant as long as $g_{*s}$ does not change. To relate the time derivative to the derivative with respect to $x$, we use entropy conservation

$$\begin{aligned} \frac{d(sa^3)}{dt} &= \frac{ds}{dt}a^3 + 3sa^2\frac{da}{dt} = 0\,, \\ \frac{ds}{dt} &= -3sH\,, \end{aligned} \tag{B.3.41}$$

where $a$ is the scale factor, and we have used the definition of Hubble, Eq. (B.1.8). Furthermore, we have

$$\begin{aligned} \frac{ds}{dt} &= \frac{ds}{dT}\frac{dT}{dx}\frac{dx}{dt} = \left(\frac{2\pi^2}{45}\left(\frac{dg_{*s}}{dT}T^3 + 3g_{*s}T^2\right)\right)\cdot\left(-\frac{m}{x^2}\right)\cdot\frac{dx}{dt} = \\ &= 3\frac{s}{T}\left(1 + \frac{T}{3g_{*s}}\frac{dg_{*s}}{dx}\frac{dx}{dT}\right)\cdot\left(-\frac{m}{x^2}\right)\cdot\frac{dx}{dt} = \\ &= 3s\frac{x}{m}\left(-\frac{m}{x^2}\right)\cdot\left(1 + \frac{m/x}{3g_{*s}}\frac{dg_{*s}}{dx}\left(-\frac{x^2}{m}\right)\right)\frac{dx}{dt} = \\ &= -3\frac{s}{x}\left(1 - \frac{x}{3g_{*s}}\frac{dg_{*s}}{dx}\right)\frac{dx}{dt} = -3Hs\,, \end{aligned} \tag{B.3.42}$$

from which it follows that derivative in time can be written as

$$\frac{d}{dt} = xH\left(\frac{T}{3s}\frac{ds}{dT}\right)^{-1}\frac{d}{dx} = xH\left(1 - \frac{x}{3g_{*s}}\frac{dg_{*s}}{dx}\right)^{-1}\frac{d}{dx}\,. \tag{B.3.43}$$

In particular, the time derivative of the number density, $n = Ys$, is

$$\frac{dn}{dt} = \frac{dY}{dt}s + Y\frac{ds}{dt} = \frac{dY}{dt}s - 3HsY = \frac{dY}{dt}s - 3Hn\,, \tag{B.3.44}$$

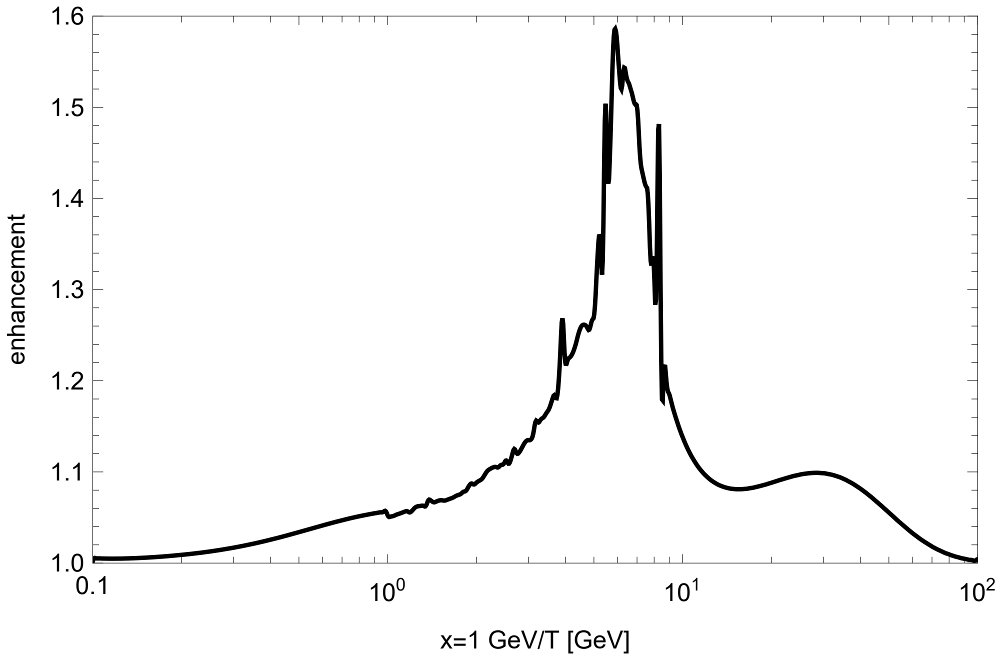


Figure B.1: Enhancement $\left(1 - \frac{x}{3g_{*s}}\frac{dg_{*s}}{dx}\right)$ of the collision term as a function of $x = 1\ \mathrm{GeV}/T[\mathrm{GeV}]$. The largest enhancement is possible at the QCDPT crossover $x \sim 6$, $T \simeq 170$ MeV.

where we have used Eq. (B.3.41). Finally, combining Eq. (B.3.43) and Eq. (B.3.44), the Boltzmann equation Eq. (B.3.40) in new variables takes form

$$\begin{aligned} sHx\frac{dY}{dx} =& \left(1 - \frac{x}{3g_{*s}}\frac{dg_{*s}}{dx}\right) \cdot \left(\sum_i \Gamma_i\right) s\left(Y^{\mathrm{eq}} - Y\right) = \\ =& \left(1 - \frac{x}{3g_{*s}}\frac{dg_{*s}}{dx}\right)\left(\sum_i \Gamma_i\right) n^{\mathrm{eq}}\left(1 - \frac{Y}{Y^{\mathrm{eq}}}\right), \end{aligned} \tag{B.3.45}$$

where sometimes in literature rates are rescaled $\gamma_i = n^{\mathrm{eq}}\Gamma_i$. Often, when production takes place at large temperatures, as is the case of WIMP freeze-out, we can set $dg_{*s}/dx \simeq 0$. However, during periods of rapid changes of entropic degrees of freedom, this term can lead to enhancement of the collision term. Notably, around the QCDPT, the enhancement can be as large as 50%, as shown in Fig B.1.

## B.4 Collision term

The collision term due to the process $\psi + a + b + ... \leftrightarrow i + j + ...$ in the integrated Boltzmann equation for the evolution of number density of the particle $\psi$ is given by [39]

$$\begin{aligned} C[f_\psi, f_a, f_i, ...] = -\int & d\Pi_\psi d\Pi_a d\Pi_b d\Pi_i d\Pi_j (2\pi)^4 \delta^{(4)}(p_\psi + p_i + p_j + ... - p_i - p_j - ...) \times \\ & \times \Big( |\mathcal{M}_{\psi+a+b+...\to i+j+...}|^2 f_\psi f_a f_b ... (1 \pm f_i)(1 \pm f_j) ... - \\ & - |\mathcal{M}_{i+j+...\to\psi+a+b+...}|^2 f_i f_j ... (1 \pm f_\psi)(1 \pm f_a)(1 \pm f_b) \Big), \end{aligned} \tag{B.4.46}$$

where $\delta^{(4)}(...)$ ensures 4-momentum conservation, $|\mathcal{M}|^2$ encodes information about the probability of the transition as a function of momenta, and $f_i, ..., f_a$ are distribution functions of particle species involved in the process. The first term accounts for transitions $\psi + a + b + ... \rightarrow i + j + ...$ and the second term accounts for inverse process $i + j + ... \rightarrow \psi + a + b + ....$ The blocking and stimulated emission factors $(1 \pm f_i)$, use $+$ for bosons and $-$ for fermions. Assuming that the temperature is well above Bose condensation temperature and Fermi blocking, we can approximate $(1 \pm f_i) \simeq 1$. Moreover, if the process is CP invariant, we have

$$|\mathcal{M}_{\psi+a+b+...\rightarrow i+j+...}|^2 = |\mathcal{M}_{i+j+...\rightarrow\psi+a+b+...}|^2 \,, \tag{B.4.47}$$

The collision term becomes

$$C[f_\psi, f_a, f_i, ...] = -\int d\Pi_\psi d\Pi_a d\Pi_b d\Pi_i d\Pi_j (2\pi)^4 \delta^{(4)}(p_\psi + p_i + p_j + ... - p_i - p_j - ...)\times \\ \times |\mathcal{M}_{\psi+a+b+...\rightarrow i+j+...}|^2 \Big( f_\psi f_a f_b ... - f_i f_j ... \Big) \,, \tag{B.4.48}$$

which, up to the distributions, resembles the definition of the cross section Eq. (A.45).

Note, that for particles in equilibrium, the collision term vanishes, therefore from Eq. (B.5.92) distribution functions must satisfy

$$f_\psi^{\rm eq} f_a^{\rm eq} f_b^{\rm eq} \cdots = f_i^{\rm eq} f_j^{\rm eq} \cdots \,, \tag{B.4.49}$$

named detailed balance condition.

An important assumption, that greatly simplifies solving the Boltzmann equation, is the kinetic equilibrium. In the presence of processes conserving the number of particles, e.g. elastic scattering $a + i \leftrightarrow a + i$, the distribution function is in local equilibrium. Note, that this condition is widely satisfied, since elastic scatterings are less Boltzmann suppressed in the collision term. We can then use an ansatz

$$f_\psi = f_\psi^{\rm eq} n_\psi / n_\psi^{\rm eq} \,, \tag{B.4.50}$$

trading an unknown distribution function depending on both time and momentum to an unknown function of time only. The collision term is then calculated by integrating the amplitude with a known equilibrium distribution function, while number densities factor out of the momentum integral. This allows us to solve ordinary differential equation instead of integro-differential equation.

### B.4.1 Special cases of collision term

In this section, we will derive the collision term of the Boltzmann equation for the most common processes: $2 \leftrightarrow 2$ scatterings and two-body decays. Each time we will make use of the detailed balance, Eq. (B.4.49) and assume CP invariance, Eq. (B.4.47), and kinetic equilibrium, Eq. (B.4.54).

#### $2 \leftrightarrow 2$ scatterings

Following Ref. [341], consider a scattering $12 \leftrightarrow 23$, whose collision term is given by

$$C[f] = -\int d\Pi_1 d\Pi_2 d\Pi_3 d\Pi_4 (2\pi)^4 \delta^4(p_1 + p_2 - p_3 - p_4) \Big( f_1 f_2 |\mathcal{M}_{12\rightarrow 34}|^2 - f_3 f_4 |\mathcal{M}_{34\rightarrow 12}|^2 \Big) \,, \tag{B.4.51}$$

where the amplitude is summed over initial and final spins. The CP invariance implies $|\mathcal{M}_{12\to 23}|^2 = |\mathcal{M}_{34\to 12}|^2$, and detailed balance gives

$$f_1^{\rm eq} f_2^{\rm eq} = f_3^{\rm eq} f_4^{\rm eq} \to \frac{f_1^{\rm eq} f_2^{\rm eq}}{f_3^{\rm eq} f_4^{\rm eq}} = 1\,, \tag{B.4.52}$$

which we may insert into the collision term

$$C[f] = -\int d\Pi_1 d\Pi_2 d\Pi_3 d\Pi_4 (2\pi)^4 \delta^4(p_1 + p_2 - p_3 - p_4) |\mathcal{M}_{12\to 34}|^2 \left( f_1 f_2 - f_3 f_4 \frac{f_1^{\rm eq} f_2^{\rm eq}}{f_3^{\rm eq} f_4^{\rm eq}} \right) . \tag{B.4.53}$$

Assuming the kinetic equilibrium, Eq. (B.4.50), for all particles

$$\frac{f_3 f_4}{f_3^{\rm eq} f_4^{\rm eq}} = \frac{n_3 n_4}{n_3^{\rm eq} n_4^{\rm eq}}, \qquad \frac{f_1 f_2}{f_1^{\rm eq} f_2^{\rm eq}} = \frac{n_1 n_2}{n_1^{\rm eq} n_2^{\rm eq}}\,, \tag{B.4.54}$$

allows us to factor out momentum-independent number densities out of the integral

$$C[f] = -\left( \frac{n_1 n_2}{n_1^{\rm eq} n_2^{\rm eq}} - \frac{n_3 n_4}{n_3^{\rm eq} n_4^{\rm eq}} \right) \int d\Pi_1 d\Pi_2 d\Pi_3 d\Pi_4 (2\pi)^4 \delta^4(p_1 + p_2 - p_3 - p_4) |\mathcal{M}_{12\to 34}|^2 f_1^{\rm eq} f_2^{\rm eq} . \tag{B.4.55}$$

Because the integrals over momenta of particles 3 and 4 do not enter the distributions, we can use the formula for Lorentz invariant cross section [113]

$$\sigma_{12\to 34} = \frac{1}{g_1 g_2} \frac{1}{4 p_1 \cdot p_2 v_{\rm rel}} \int d\Pi_3 d\Pi_4 (2\pi)^4 \delta^4(p_1 + p_2 - p_3 - p_4) |\mathcal{M}_{12\to 34}|^2\,, \tag{B.4.56}$$

where $v_{\rm rel}$ is the relative velocity, which in terms of center of mass energy $s = (p_1 + p_2)^2$ is

$$v_{\rm rel} = \frac{\lambda^{1/2}(s, m_1, m_2)}{2 p_1 \cdot p_2} = \frac{\sqrt{(s - (m_1 + m_2)^2)(s - (m_1 - m_2)^2)}}{2 p_1 \cdot p_2}\,, \tag{B.4.57}$$

where we implicitly defined the function $\lambda$. Plugging that into the collision term, we have

$$\begin{aligned} C[f] &= -\left( \frac{n_1 n_2}{n_1^{\rm eq} n_2^{\rm eq}} - \frac{n_3 n_4}{n_3^{\rm eq} n_4^{\rm eq}} \right) 2 g_1 g_2 \int d\Pi_1 d\Pi_2 \lambda^{1/2}(s, m_1, m_2) \sigma_{12\to 34}(s) f_1^{\rm eq} f_2^{\rm eq} = \\ &= -\left( \frac{n_1 n_2}{n_1^{\rm eq} n_2^{\rm eq}} - \frac{n_3 n_4}{n_3^{\rm eq} n_4^{\rm eq}} \right) \gamma_S\,, \end{aligned} \tag{B.4.58}$$

where in the last line we have defined the effective scattering rate $\gamma_S$. The remaining task is to perform the phase space integration. To do so analytically, we need to approximate both $f_i^{\rm eq}, f_j^{\rm eq}$ with Maxwell distributions, Eq. (B.2.20). This allows us to go to new variables

$$\begin{aligned} E_+ &= E_1 + E_2\,, \\ E_- &= E_1 - E_2\,, \\ s &= m_1^2 + m_2^2 - 2(E_1 E_2 - |\vec{p_1}||\vec{p_2}| \cos\theta)\,, \end{aligned} \tag{B.4.59}$$

which is advantageous because integrand does not depend on $E_-$. The jacobian of the transformation gives

$$\frac{d^3 p_1}{(2\pi)^3} \frac{d^3 p_2}{(2\pi)^3} = \frac{|\vec{p_1}||\vec{p_2}|}{32\pi^4} dE_1 dE_2 d(cos\theta) = \frac{1}{128\pi^4} dE_+ dE_- ds\,. \tag{B.4.60}$$

The new limits of integration are [341]

$$\begin{aligned} &(m_1+m_2)^2 \leqslant s \leqslant \infty\,, \\ &\sqrt{s} \leqslant E_+ \leqslant \infty\,, \\ &\left| E_- + E_- \frac{m_1^2 - m_2^2}{s} \right| \leqslant \lambda^{1/2}(s, m_1, m_2)\frac{(E_+^2 - s)^{1/2}}{s}\,. \end{aligned} \tag{B.4.61}$$

We have implicitly assumed that $m_1 + m_2 > m_3 + m_4$, otherwise $s_{\rm min} = (m_3 + m_4)^2$.

At this point the effective rate has the following form

$$\gamma_S = \frac{g_1 g_2}{64\pi^4}\int dE_+ dE_- ds f_1^{\rm eq} f_2^{\rm eq} \lambda^{1/2}(s, m_1, m_2)\sigma_{12\to34}(s)\,. \tag{B.4.62}$$

The integration over $E_-$ gives simply $2\lambda^{1/2}(s, m_1, m_2)(E_+^2 - s)^{1/2}/s$ and the effective rate is

$$\gamma_S = \frac{g_1 g_2}{32\pi^4}\int_{\sqrt{s}}^{\infty} dE_+ \exp\left(\frac{E_+}{T}\right)(E_+^2 - s)^{1/2}\int_{(m_1+m_2)^2}^{\infty} ds\frac{\lambda(s, m_1, m_2)}{s}\sigma_{12\to34}(s)\,. \tag{B.4.63}$$

We identify the first integral as the definition of the modified Bessel function of the second kind $K_1(\sqrt{s}/T)$. The final result for effective rate is thus given by

$$\gamma_S = \frac{g_1 g_2}{32\pi^4} T\int_{(m_1+m_2)^2}^{\infty} ds\frac{\lambda(s, m_1, m_2)}{s^{1/2}}\sigma_{12\to34}(s) K_1\left(\frac{\sqrt{s}}{T}\right)\,. \tag{B.4.64}$$

Thermally averaged cross section is defined by

$$\langle\sigma_{12\to34} v\rangle = \frac{\gamma_S}{n_1^{\rm eq} n_2^{\rm eq}}\,, \tag{B.4.65}$$

which in the Boltzmann equation gives

$$\frac{dn_1}{dt} + 3Hn_1 = -\langle\sigma_{12\to34} v\rangle\left(n_1 n_2 - n_3 n_4 \frac{n_1^{\rm eq} n_2^{\rm eq}}{n_3^{\rm eq} n_4^{\rm eq}}\right)\,, \tag{B.4.66}$$

A special case of the $2 \leftrightarrow 2$ scattering is the annihilation into thermal bath particles, $n_1 = n_2 \equiv n$, $n_3 = n_3^{\rm eq}$, $n_4 = n_4^{\rm eq}$. In this case, the Boltzmann equation takes the form

$$\frac{dn}{dt} + 3Hn = -\langle\sigma_{\rm ann} v\rangle\left(n^2 - (n^{\rm eq})^2\right)\,. \tag{B.4.67}$$

If $n_1 \neq n_2$, but $n_3 = n_3^{\rm eq}$ and $n_4 = n_4^{\rm eq}$, we have

$$\frac{dn_1}{dt} + 3Hn_1 = -\langle\sigma_{12\to34} v\rangle(n_1 n_2 - n_1^{\rm eq} n_2^{\rm eq})\,. \tag{B.4.68}$$

On the other hand, the Boltzmann equation for single particle 3 production, assuming 1,2 and 4 are in thermal equilibrium, reads

$$\frac{dn_3}{dt} + 3Hn_3 = \gamma_S\left(1 - \frac{n_3}{n_3^{\rm eq}}\right) = (n_3^{\rm eq} - n_3)\Gamma_S\,, \tag{B.4.69}$$

where we have implicitly defined the rate $\Gamma_S = \gamma_S/n_3^{\rm eq}$, which in terms of thermally averaged cross section is

$$\Gamma_S = \frac{n_1^{\rm eq} n_2^{\rm eq}}{n_3^{\rm eq}}\langle\sigma_{12\to34} v\rangle\,. \tag{B.4.70}$$

**Two-body decays**

The collision term induced by decays $1 \leftrightarrow 23$ has the following form

$$C[f] = \sum_{\text{spins}} \int d\Pi_1 d\Pi_2 d\Pi_3 (2\pi)^4 \delta^{(4)}(p_1 - p_2 - p_3)\Big(f_1 |\mathcal{M}_{1\to 23}|^2 - f_2 f_3 |\mathcal{M}_{23\to 1}|^2\Big)\,, \quad \text{(B.4.71)}$$

Assuming CP invariance, $|\mathcal{M}_{23\to 1}|^2 = |\mathcal{M}_{1\to 23}|^2 = |\mathcal{M}|^2$, the detailed balance has the following from

$$f_1^{\text{eq}} = f_2^{\text{eq}} f_3^{\text{eq}} \to \frac{f_1^{\text{eq}}}{f_2^{\text{eq}} f_3^{\text{eq}}} = 1\,, \quad \text{(B.4.72)}$$

which can be inserted into the collision, yielding

$$C[f] = \sum_{\text{spins}} \int d\Pi_1 d\Pi_2 d\Pi_3 (2\pi)^4 \delta^{(4)}(p_1 - p_2 - p_3)|\mathcal{M}|^2 \left(f_1 - \frac{f_1^{\text{eq}}}{f_2^{\text{eq}} f_3^{\text{eq}}} f_2 f_3\right). \quad \text{(B.4.73)}$$

Assuming kinetic equilibrium, Eq. (B.4.50), is maintained

$$\frac{f_2 f_3}{f_2^{\text{eq}} f_3^{\text{eq}}} = \frac{n_2 n_3}{n_2^{\text{eq}} n_3^{\text{eq}}}\,, \quad \text{(B.4.74)}$$

the collision term has form

$$C[f] = \sum_{\text{spins}} \int d\Pi_1 d\Pi_2 d\Pi_3 (2\pi)^4 \delta^{(4)}(p_1 - p_2 - p_3)|\mathcal{M}|^2 \left(f_1 - f_1^{\text{eq}} \frac{n_2 n_3}{n_2^{\text{eq}} n_3^{\text{eq}}}\right). \quad \text{(B.4.75)}$$

Let's assume that the mother particle and one of the products are in thermal equilibrium, $n_1 = n_1^{\text{eq}}$, $n_3 = n_3^{\text{eq}}$. Number densities are momentum-independent, and can be factored out

$$\begin{aligned} C[f] &= \sum_{\text{spins}} \int d\Pi_1 d\Pi_2 d\Pi_3 (2\pi)^4 \delta^{(4)}(p_1 - p_2 - p_3)|\mathcal{M}|^2 f_1^{\text{eq}} \left(1 - \frac{n_2 n_3^{\text{eq}}}{n_2^{\text{eq}} n_3^{\text{eq}}}\right) \\ &= (n_2^{\text{eq}} - n_2)\frac{1}{n_2^{\text{eq}}} \sum_{\text{spins}} \int d\Pi_1 d\Pi_2 d\Pi_3 (2\pi)^4 \delta^{(4)}(p_1 - p_2 - p_3)|\mathcal{M}|^2 f_1^{\text{eq}} \\ &= (n_2^{\text{eq}} - n_2)\frac{1}{n_2^{\text{eq}}} \gamma_D\,, \end{aligned} \quad \text{(B.4.76)}$$

The integral defines the effective decay rate $\gamma_D$, which can be simplified using the definition of decay width

$$\Gamma_{1\to 23} = \frac{1}{2m_1} \int d\Pi_2 d\Pi_3 (2\pi)^4 \delta^{(4)}(p_1 - p_2 - p_3)|\mathcal{M}_{1\to 23}|^2\,. \quad \text{(B.4.77)}$$

Since the momentum of the mother particle only enters via distribution, we can insert the width to the integral, yielding

$$\gamma_D = \Gamma_{1\to 23} g_1 \int \frac{d^3 p_1}{(2\pi)^3} \frac{m_1}{E_1} f_1^{\text{eq}}\,. \quad \text{(B.4.78)}$$

The sum over spins gave the number of internal degrees of freedom $g_1$. The rate can be evaluated analytically assuming Maxwell-Boltzmann distribution, which is justified at temperatures above Bose condensation or Fermi blocking. We have

$$\begin{aligned} \gamma_D =& \Gamma_{1\to 23} g_1 \int_0^\infty p_1^2 dp_1 \frac{4\pi}{(2\pi)^3} \frac{m_1}{E_1} \exp\left(-\frac{E_1}{T}\right) \\ =& \Gamma_{1\to 23} \frac{m_1}{2\pi^2} g_1 \int_{m_1}^\infty E_1 dE_1 \sqrt{E_1^2 - m_1^2} \frac{1}{E_1} \exp\left(-\frac{E_1}{T}\right) \\ =& \Gamma_{1\to 23} g_1 \frac{m_1^2}{2\pi^2} T K_1\left(\frac{m_1}{T}\right). \end{aligned} \quad \text{(B.4.79)}$$

Using $n_1^{\rm eq} = g_1(m_1^2/2\pi^2)TK_2(m_1/T)$, we have

$$\gamma_D = n_1^{\rm eq}\Gamma_{1\to 23}\frac{K_1(m_1/T)}{K_2(m_1/T)}\,. \tag{B.4.80}$$

Finally, the Boltzmann equation reads

$$\frac{dn_2}{dt} + 3Hn_2 = (n_2^{\rm eq} - n_2)\frac{1}{n_2^{\rm eq}}\gamma_D = (n_2^{\rm eq} - n_2)\Gamma_D\,, \tag{B.4.81}$$

where we have defined the decay rate by rescaling the effective rate

$$\Gamma_D = \gamma_D/n_2^{\rm eq} = \frac{n_1^{\rm eq}}{n_2^{\rm eq}}\Gamma_{1\to 23}\frac{K_1(m_1/T)}{K_2(m_1/T)}\,. \tag{B.4.82}$$

## B.5 Boltzmann equations in supersymmetric models

Following the classic paper in Ref. [317], consider a $R$-parity conserving theory of $N$ supersymmetric particles $\chi_i$. The dynamics of number densities $n_i$ is governed by a set of Boltzmann equations

$$\begin{aligned}\frac{dn_i}{dt} + 3Hn_i = &-\sum_j \langle\sigma_{ij}v\rangle\Big(n_in_j - n_i^{\rm eq}n_j^{\rm eq}\Big)\\ &-\sum_{j,X}\Big(\langle\sigma'_{ij}v\rangle(n_in_X - n_i^{\rm eq}n_X^{\rm eq}) - \langle\sigma'_{ji}v\rangle\Big(n_jn_X - n_j^{\rm eq}n_X^{\rm eq}\Big)\Big)\\ &-\sum_j \Gamma_{ij}(n_i - n_i^{\rm eq})\,,\end{aligned} \tag{B.5.83}$$

in analogy with Eq. (B.4.67) and Eq. (B.4.68). The first term on the right-hand side accounts for single production channels (for $i \neq j$) and annihilations (for $i = j$) of $\chi_i$ in processes $\chi_i\chi_j \leftrightarrow XY$, where $X, Y$ are SM particles. To account for all scatterings, we use a cross section defined as $\sigma_{ij} = \sum_X \sigma(\chi_i\chi_j \leftrightarrow X)$.
The second term accounts for conversions $\chi_iX \leftrightarrow \chi_jY$ through scattering with SM particles. The cross section again includes contributions from all possible channels $\sigma_{ij} = \sum_Y \sigma(\chi_iX \leftrightarrow \chi_jY)$, where usually, the choice of $\chi_i$, $\chi_j$ and $X$ completely determines $Y$.

The last line includes decays (and inverse decays) of the $i$th particles, and similarly, the decay rate includes sum over possible final states $\Gamma_{ij} = \sum_X \Gamma(\chi_i \to \chi_jX)$.

The assumption of $R$-parity allows us to simplify the problem. All particles except for LSP are unstable and must decay conserving the matter-parity charge. As a result, we can introduce a total number density of LSP after all decays are complete

$$n = \sum_i^N n_i\,. \tag{B.5.84}$$

Summing the Eq. B.5.83 we obtain

$$\begin{aligned}\frac{dn}{dt} + 3Hn = &-\sum_{i,j} \langle\sigma_{ij}v\rangle\Big(n_in_j - n_i^{\rm eq}n_j^{\rm eq}\Big)\\ &-\sum_{i,j\neq i}\Big(\langle\sigma'_{ij}v\rangle\Big(n_in_X - n_j^{\rm eq}n_X^{\rm eq}\Big) - \langle\sigma'_{ji}v\rangle\Big(n_jn_X - n_j^{\rm eq}n_X^{\rm eq}\Big)\Big)\\ &-\sum_{i,j\neq i} \Gamma_{ij}(n_i - n_i^{\rm eq})\,.\end{aligned} \tag{B.5.85}$$

Note, that the second line is antisymmetric with respect to the change of indices $i \leftrightarrow j$, therefore the sum vanishes. On the other hand, the last term might be written as

$$\begin{aligned}\sum_{i,j\neq i}\Gamma_{ij}(n_i-n_i^{\text{eq}}) =&\frac{1}{2}\sum_{i,j\neq i}\Big(\Gamma_{ij}(n_i-n_i^{\text{eq}})+\Gamma_{ji}\Big(n_j-n_j^{\text{eq}}\Big)\Big) = \\ =&\frac{1}{2}\sum_{i,j\neq i}\Gamma_{ij}(n_i-n_i^{\text{eq}})=0\,,\end{aligned} \tag{B.5.86}$$

where we have symmetrized the summed indices in the first step and used the fact that $j \to i$ is kinematically disallowed, implying $\Gamma_{ji} = 0$. Finally, the Boltzmann equation takes the form

$$\frac{dn}{dt}+3Hn=-\sum_{i,j}\langle\sigma_{ij}v\rangle\Big(n_in_j-n_i^{\text{eq}}n_j^{\text{eq}}\Big)\,. \tag{B.5.87}$$

Assuming the kinetic equilibrium, the ratio of number densities remains constant even after decoupling

$$\frac{n_i}{n}=\frac{n_i^{\text{eq}}}{n^{\text{eq}}}\to n_i=n\frac{n_i^{\text{eq}}}{n^{\text{eq}}}\,. \tag{B.5.88}$$

Plugging that into Eq. (B.5.87) gives

$$\begin{aligned}\frac{dn}{dt}+3Hn=&-\sum_{i,j}\langle\sigma_{ij}v\rangle\left(n^2\frac{n_i^{\text{eq}}n_j^{\text{eq}}}{(n^{\text{eq}})^2}-n_i^{\text{eq}}n_j^{\text{eq}}\right)= \\ =&-\Big(n^2-n_{\text{eq}}^2\Big)\sum_{i,j}\langle\sigma_{ij}v\rangle\frac{n_i^{\text{eq}}n_j^{\text{eq}}}{(n^{\text{eq}})^2}\,.\end{aligned} \tag{B.5.89}$$

This is particularly useful, as it has the form of Boltzmann equation for annihilations, with annihilation cross section replaced with effective annihilation cross section

$$\langle\sigma_{\text{eff}}v\rangle=\sum_{ij}\langle\sigma_{ij}v\rangle\frac{n_i^{\text{eq}}n_j^{\text{eq}}}{n_{\text{eq}}^2}\,. \tag{B.5.90}$$

For freeze-out of DM, we are interested in temperatures in which all SUSY particles are non-relativistic. Following the original paper, let $x = m_1/T$, $\Delta_i = (m_i - m_1)/m_1$, where $m_1$ is the mass of the LSP. Consider the ratio

$$\begin{aligned}\frac{n_i}{n^{\text{eq}}}=&\frac{g_i\Big(\frac{m_iT}{2\pi}\Big)^{3/2}\exp\left(\frac{-m_i}{T}\right)}{\sum_i g_i\Big(\frac{m_iT}{2\pi}\Big)^{3/2}\exp\left(\frac{-m_i}{T}\right)}=\frac{g_i\Big(\frac{(1+\Delta_i)mT}{2\pi}\Big)^{3/2}\exp\left(-(1+\Delta_i)x\right)}{\sum_i g_i\Big(\frac{(1+\Delta_i)mT}{2\pi}\Big)^{3/2}\exp\left(-(1+\Delta_i)x\right)}= \\ =&\frac{g_i(1+\Delta_i)^{3/2}\exp\left(-\Delta_ix\right)}{\sum_i g_i(1+\Delta_i)^{3/2}\exp\left(-\Delta_ix\right)}=\frac{1}{g_{\text{eff}}}g_i(1+\Delta_i)^{3/2}\exp\left(-\Delta_ix\right)\,,\end{aligned} \tag{B.5.91}$$

where in the last line we have implicitly defined $g_{\text{eff}}$ in the denominator. The effective cross section is now given by

$$\langle\sigma_{\text{eff}}v\rangle=\sum_{ij}\langle\sigma_{ij}v\rangle\frac{g_ig_j}{g_{\text{eff}}^2}(1+\Delta_i)^{3/2}(1+\Delta_j)^{3/2}\exp(-(\Delta_i+\Delta_j)x)\,. \tag{B.5.92}$$

Using the above formula, we can easily read off which particles are involved in the thermalization of the LSP. As long as the relative mass splitting $\Delta_i$ is small, it is possible that the process involving only one LSP, named coannihilation, contributes to the thermalization.

Possible resonances in scatterings of dark matter may play an important role in the determination of relic density. For concreteness, consider s-channel annihilation of LSP into some SM particles $X, Y$ mediated by particle $\phi$. The amplitude of such a process will involve a propagator $1/(s-m_\phi^2)$. Because dark matter is non-relativistic at freeze-out, we have $s=(p_1+p_2)^2 \simeq 4m_{\rm LSP}^2$. As a result, the thermally averaged cross section for this scattering is singular at $m_{\rm LSP}=m_\phi/2$. While this singularity is regulated by including the decay rate of $\phi$ in Breit-Wigner distribution $1/(s-m_\phi^2+i\Gamma_\phi m_\phi)$, the effect of the enhanced cross section can be dominant in portions of parameter space. However, the cross section enhancement usually requires some fine-tuning to have $m_{\rm LSP} \simeq m_\phi/2$. Therefore, models that require resonances to satisfy $\Omega h^2 = 0.12$ are usually considered unnatural.

# Bibliography


[1] **CMS** Collaboration, S. Chatrchyan et al., *Observation of a New Boson at a Mass of 125 GeV with the CMS Experiment at the LHC*, Phys. Lett. B **716** (2012) 30–61, [arXiv:1207.7235].

[2] **ATLAS** Collaboration, G. Aad et al., *Observation of a new particle in the search for the Standard Model Higgs boson with the ATLAS detector at the LHC*, Phys. Lett. B **716** (2012) 1–29, [arXiv:1207.7214].

[3] L. Di Lella and C. Rubbia, *The Discovery of the W and Z Particles*, Adv. Ser. Direct. High Energy Phys. **23** (2015) 137–163.

[4] **CDF** Collaboration, T. Aaltonen et al., *High-precision measurement of the W boson mass with the CDF II detector*, Science **376** (2022), no. 6589 170–176.

[5] J. de Blas, M. Pierini, L. Reina, and L. Silvestrini, *Impact of the Recent Measurements of the Top-Quark and W-Boson Masses on Electroweak Precision Fits*, Phys. Rev. Lett. **129** (2022), no. 27 271801, [arXiv:2204.04204].

[6] C.-T. Lu, L. Wu, Y. Wu, and B. Zhu, *Electroweak precision fit and new physics in light of the W boson mass*, Phys. Rev. D **106** (2022), no. 3 035034, [arXiv:2204.03796].

[7] A. Strumia, *Interpreting electroweak precision data including the W-mass CDF anomaly*, JHEP **08** (2022) 248, [arXiv:2204.04191].

[8] **CMS** Collaboration, "CMS Physics Analysis Summary: Measurement of the W boson mass in proton-proton collisions at at $\sqrt{s} = 13$ TeV." https://cds.cern.ch/record/2910372/files/SMP-23-002-pas.pdf, 9, 2024.

[9] M. Kobayashi and T. Maskawa, *CP Violation in the Renormalizable Theory of Weak Interaction*, Prog. Theor. Phys. **49** (1973) 652–657.

[10] **CDF** Collaboration, F. Abe et al., *Observation of top quark production in $\bar{p}p$ collisions*, Phys. Rev. Lett. **74** (1995) 2626–2631, [hep-ex/9503002].

[11] **D0** Collaboration, S. Abachi et al., *Observation of the top quark*, Phys. Rev. Lett. **74** (1995) 2632–2637, [hep-ex/9503003].

[12] D. Hanneke, S. Fogwell, and G. Gabrielse, *New Measurement of the Electron Magnetic Moment and the Fine Structure Constant*, Phys. Rev. Lett. **100** (2008) 120801, [arXiv:0801.1134].

[13] **Particle Data Group** Collaboration, C. Patrignani et al., *Review of Particle Physics*, Chin. Phys. C **40** (2016), no. 10 100001.

[14] **LIGO Scientific, Virgo** Collaboration, B. P. Abbott et al., *Observation of Gravitational Waves from a Binary Black Hole Merger*, Phys. Rev. Lett. **116** (2016), no. 6 061102, [arXiv:1602.03837].

[15] A. Friedman, *On the Curvature of space*, Z. Phys. **10** (1922) 377–386.

[16] A. Friedmann, *On the Possibility of a world with constant negative curvature of space*, Z. Phys. **21** (1924) 326–332.

[17] G. Lemaitre, *A Homogeneous Universe of Constant Mass and Increasing Radius accounting for the Radial Velocity of Extra-galactic Nebulæ*, Mon. Not. Roy. Astron. Soc. **91** (1931), no. 5 483–490.

[18] H. P. Robertson, *Kinematics and World-Structure*, Astrophys. J. **82** (1935) 284–301.

[19] H. P. Robertson, *Kinematics and World-Structure. 2*, Astrophys. J. **83** (1935) 187–201.

[20] H. P. Robertson, *Kinematics and World-Structure. 3*, Astrophys. J. **83** (1936) 257–271.

[21] **Planck** Collaboration, N. Aghanim et al., *Planck 2018 results. VI. Cosmological parameters*, Astron. Astrophys. **641** (2020) A6, [arXiv:1807.06209]. [Erratum: Astron.Astrophys. 652, C4 (2021)].

[22] B. D. Fields, *The primordial lithium problem*, Ann. Rev. Nucl. Part. Sci. **61** (2011) 47–68, [arXiv:1203.3551].

[23] L. J. Hall, K. Jedamzik, J. March-Russell, and S. M. West, *Freeze-In Production of FIMP Dark Matter*, JHEP **03** (2010) 080, [arXiv:0911.1120].

[24] **Planck** Collaboration, *The Scientific programme of Planck*, 4, 2006.

[25] R. D. Peccei and H. R. Quinn, *CP Conservation in the Presence of Instantons*, Phys. Rev. Lett. **38** (1977) 1440–1443.

[26] R. D. Peccei and H. R. Quinn, *Constraints Imposed by CP Conservation in the Presence of Instantons*, Phys. Rev. D **16** (1977) 1791–1797.

[27] S. Weinberg, *A New Light Boson?*, Phys. Rev. Lett. **40** (1978) 223–226.

[28] F. Wilczek, *Problem of Strong P and T Invariance in the Presence of Instantons*, Phys. Rev. Lett. **40** (1978) 279–282.

[29] J. E. Kim, *Weak Interaction Singlet and Strong CP Invariance*, Phys. Rev. Lett. **43** (1979) 103.

[30] M. A. Shifman, A. I. Vainshtein, and V. I. Zakharov, *Can Confinement Ensure Natural CP Invariance of Strong Interactions?*, Nucl. Phys. B **166** (1980) 493–506.

[31] J. Preskill, M. B. Wise, and F. Wilczek, *Cosmology of the Invisible Axion*, Phys. Lett. B **120** (1983) 127–132.

[32] L. F. Abbott and P. Sikivie, *A Cosmological Bound on the Invisible Axion*, Phys. Lett. B **120** (1983) 133–136.

[33] M. Dine and W. Fischler, *The Not So Harmless Axion*, Phys. Lett. B **120** (1983) 137–141.

[34] R. T. Co, L. J. Hall, and K. Harigaya, *QCD Axion Dark Matter with a Small Decay Constant*, Phys. Rev. Lett. **120** (2018), no. 21 211602, [arXiv:1711.10486].

[35] R. T. Co, L. J. Hall, and K. Harigaya, *Axion Kinetic Misalignment Mechanism*, Phys. Rev. Lett. **124** (2020), no. 25 251802, [arXiv:1910.14152].

[36] R. T. Co and K. Harigaya, *Axiogenesis*, Phys. Rev. Lett. **124** (2020), no. 11 111602, [arXiv:1910.02080].

[37] T. W. B. Kibble, *Topology of Cosmic Domains and Strings*, J. Phys. A **9** (1976) 1387–1398.

[38] R. L. Davis, *Cosmic Axions from Cosmic Strings*, Phys. Lett. B **180** (1986) 225–230.

[39] E. W. Kolb and M. S. Turner, The Early Universe, vol. 69. Addison-Wesley Publishing Company, 1990.

[40] T. Hiramatsu, M. Kawasaki, K. Saikawa, and T. Sekiguchi, *Production of dark matter axions from collapse of string-wall systems*, Phys. Rev. D **85** (2012) 105020, [arXiv:1202.5851]. [Erratum: Phys.Rev.D 86, 089902 (2012)].

[41] P. Sikivie, *Of Axions, Domain Walls and the Early Universe*, Phys. Rev. Lett. **48** (1982) 1156–1159.

[42] P. Sikivie, *Axion Cosmology*, Lect. Notes Phys. **741** (2008) 19–50, [astro-ph/0610440].

[43] R. T. Co, N. Fernandez, A. Ghalsasi, L. J. Hall, and K. Harigaya, *Lepto-Axiogenesis*, JHEP **03** (2021) 017, [arXiv:2006.05687].

[44] K. Harigaya and I. R. Wang, *Axiogenesis from $SU(2)_R$ phase transition*, JHEP **10** (2021) 022, [arXiv:2107.09679]. [Erratum: JHEP 12, 193 (2021)].

[45] R. T. Co, K. Harigaya, Z. Johnson, and A. Pierce, *R-parity violation axiogenesis*, JHEP **11** (2021) 210, [arXiv:2110.05487].

[46] R. T. Co, T. Gherghetta, and K. Harigaya, *Axiogenesis with a heavy QCD axion*, JHEP **10** (2022) 121, [arXiv:2206.00678].

[47] G. G. Raffelt, *Astrophysical methods to constrain axions and other novel particle phenomena*, Phys. Rept. **198** (1990) 1–113.

[48] M. S. Turner, *Axions from SN 1987a*, Phys. Rev. Lett. **60** (1988) 1797.

[49] A. Burrows, M. S. Turner, and R. P. Brinkmann, *Axions and SN 1987a*, Phys. Rev. D **39** (1989) 1020.

[50] G. Raffelt and D. Seckel, *Bounds on Exotic Particle Interactions from SN 1987a*, Phys. Rev. Lett. **60** (1988) 1793.

[51] G. G. Raffelt, *Particle physics from stars*, Ann. Rev. Nucl. Part. Sci. **49** (1999) 163–216, [hep-ph/9903472].

[52] G. G. Raffelt, *Astrophysical axion bounds*, Lect. Notes Phys. **741** (2008) 51–71, [hep-ph/0611350].

[53] A. Ayala, I. Domínguez, M. Giannotti, A. Mirizzi, and O. Straniero, *Revisiting the bound on axion-photon coupling from Globular Clusters*, Phys. Rev. Lett. **113** (2014), no. 19 191302, [arXiv:1406.6053].

[54] P. Carenza, T. Fischer, M. Giannotti, G. Guo, G. Martínez-Pinedo, and A. Mirizzi, *Improved axion emissivity from a supernova via nucleon-nucleon bremsstrahlung*, JCAP **10** (2019), no. 10 016, [arXiv:1906.11844]. [Erratum: JCAP 05, E01 (2020)].

[55] R. Bollig, W. DeRocco, P. W. Graham, and H.-T. Janka, *Muons in Supernovae: Implications for the Axion-Muon Coupling*, Phys. Rev. Lett. **125** (2020), no. 5 051104, [arXiv:2005.07141]. [Erratum: Phys.Rev.Lett. 126, 189901 (2021)].

[56] D. Croon, G. Elor, R. K. Leane, and S. D. McDermott, *Supernova Muons: New Constraints on Z' Bosons, Axions and ALPs*, JHEP **01** (2021) 107, [arXiv:2006.13942].

[57] M. Buschmann, C. Dessert, J. W. Foster, A. J. Long, and B. R. Safdi, *Upper Limit on the QCD Axion Mass from Isolated Neutron Star Cooling*, Phys. Rev. Lett. **128** (2022), no. 9 091102, [arXiv:2111.09892].

[58] L. Di Luzio, F. Mescia, E. Nardi, P. Panci, and R. Ziegler, *Astrophobic Axions*, Phys. Rev. Lett. **120** (2018), no. 26 261803, [arXiv:1712.04940].

[59] F. Björkeroth, L. Di Luzio, F. Mescia, E. Nardi, P. Panci, and R. Ziegler, *Axion-electron decoupling in nucleophobic axion models*, Phys. Rev. D **101** (2020), no. 3 035027, [arXiv:1907.06575].

[60] M. Badziak and K. Harigaya, *Naturally astrophobic QCD axion*, JHEP **06** (2023) 014, [arXiv:2301.09647].

[61] L. Di Luzio, F. Mescia, E. Nardi, and S. Okawa, *Renormalization group effects in astrophobic axion models*, Phys. Rev. D **106** (2022), no. 5 055016, [arXiv:2205.15326].

[62] L. Caloni, M. Gerbino, M. Lattanzi, and L. Visinelli, *Novel cosmological bounds on thermally-produced axion-like particles*, JCAP **09** (2022) 021, [arXiv:2205.01637].

[63] A. Notari, F. Rompineve, and G. Villadoro, *Improved Hot Dark Matter Bound on the QCD Axion*, Phys. Rev. Lett. **131** (2023), no. 1 011004, [arXiv:2211.03799].

[64] A. Falkowski, S. Pokorski, and M. Schmaltz, *Twin SUSY*, Phys. Rev. D **74** (2006) 035003, [hep-ph/0604066].

[65] S. Chang, L. J. Hall, and N. Weiner, *A Supersymmetric twin Higgs*, Phys. Rev. D **75** (2007) 035009, [hep-ph/0604076].

[66] N. Craig and K. Howe, *Doubling down on naturalness with a supersymmetric twin Higgs*, JHEP **03** (2014) 140, [arXiv:1312.1341].

[67] A. Katz, A. Mariotti, S. Pokorski, D. Redigolo, and R. Ziegler, *SUSY Meets Her Twin*, JHEP **01** (2017) 142, [arXiv:1611.08615].

[68] M. Badziak and K. Harigaya, *Supersymmetric D-term Twin Higgs*, JHEP **06** (2017) 065, [arXiv:1703.02122].

[69] M. Badziak and K. Harigaya, *Minimal Non-Abelian Supersymmetric Twin Higgs*, JHEP **10** (2017) 109, [arXiv:1707.09071].

[70] M. Badziak and K. Harigaya, *Asymptotically Free Natural Supersymmetric Twin Higgs Model*, Phys. Rev. Lett. **120** (2018), no. 21 211803, [arXiv:1711.11040].

[71] M. Badziak and K. Harigaya, *Natural supersymmetric Twin Higgs*, J. Phys. Conf. Ser. **1586** (2020), no. 1 012042, [arXiv:1903.11671].

[72] M. J. G. Veltman, *The Infrared - Ultraviolet Connection*, Acta Phys. Polon. B **12** (1981) 437.

[73] S. P. Martin, *A Supersymmetry primer*, Adv. Ser. Direct. High Energy Phys. **18** (1998) 1–98, [hep-ph/9709356].

[74] R. Haag, J. T. Lopuszanski, and M. Sohnius, *All Possible Generators of Supersymmetries of the s Matrix*, Nucl. Phys. B **88** (1975) 257.

[75] Z. Chacko, H.-S. Goh, and R. Harnik, *The Twin Higgs: Natural electroweak breaking from mirror symmetry*, Phys. Rev. Lett. **96** (2006) 231802, [hep-ph/0506256].

[76] A. Ahmed, *Heavy Higgs of the Twin Higgs Models*, JHEP **02** (2018) 048, [arXiv:1711.03107].

[77] V. Prilepina and Y. Tsai, *Reconciling Large And Small-Scale Structure In Twin Higgs Models*, JHEP **09** (2017) 033, [arXiv:1611.05879].

[78] R. Barbieri, L. J. Hall, and K. Harigaya, *Effective Theory of Flavor for Minimal Mirror Twin Higgs*, JHEP **10** (2017) 015, [arXiv:1706.05548].

[79] S. Koren and R. McGehee, *Freezing-in twin dark matter*, Phys. Rev. D **101** (2020), no. 5 055024, [arXiv:1908.03559].

[80] I. Garcia Garcia, R. Lasenby, and J. March-Russell, *Twin Higgs WIMP Dark Matter*, Phys. Rev. D **92** (2015), no. 5 055034, [arXiv:1505.07109].

[81] D. Curtin, S. Gryba, D. Hooper, J. Scholtz, and J. Setford, *Resurrecting the fraternal twin WIMP miracle*, Phys. Rev. D **105** (2022), no. 3 035033, [arXiv:2106.12578].

[82] M. Farina, *Asymmetric Twin Dark Matter*, JCAP **11** (2015) 017, [arXiv:1506.03520].

[83] I. Garcia Garcia, R. Lasenby, and J. March-Russell, *Twin Higgs Asymmetric Dark Matter*, Phys. Rev. Lett. **115** (2015), no. 12 121801, [arXiv:1505.07410].

[84] N. Craig and A. Katz, *The Fraternal WIMP Miracle*, JCAP **10** (2015) 054, [arXiv:1505.07113].

[85] H.-C. Cheng, L. Li, and R. Zheng, *Coscattering/Coannihilation Dark Matter in a Fraternal Twin Higgs Model*, JHEP **09** (2018) 098, [arXiv:1805.12139].

[86] Y. Hochberg, E. Kuflik, and H. Murayama, *Twin Higgs model with strongly interacting massive particle dark matter*, Phys. Rev. D **99** (2019), no. 1 015005, [arXiv:1805.09345].

[87] R. Barbieri, L. J. Hall, and K. Harigaya, *Minimal Mirror Twin Higgs*, JHEP **11** (2016) 172, [arXiv:1609.05589].

[88] Z. Chacko, D. Curtin, M. Geller, and Y. Tsai, *Cosmological Signatures of a Mirror Twin Higgs*, JHEP **09** (2018) 163, [arXiv:1803.03263].

[89] Z. Chacko, D. Curtin, M. Geller, and Y. Tsai, *Direct detection of mirror matter in Twin Higgs models*, JHEP **11** (2021) 198, [arXiv:2104.02074].

[90] H. Beauchesne and Y. Kats, *Cosmology of the Twin Higgs without explicit $\mathbb{Z}_2$ breaking*, JHEP **12** (2021) 160, [arXiv:2109.03279].

[91] M. Freytsis, S. Knapen, D. J. Robinson, and Y. Tsai, *Gamma-rays from Dark Showers with Twin Higgs Models*, JHEP **05** (2016) 018, [arXiv:1601.07556].

[92] C. Kilic, C. B. Verhaaren, and T. Youn, *Twin quark dark matter from cogenesis*, Phys. Rev. D **104** (2021), no. 11 116018, [arXiv:2109.03248].

[93] A. Birkedal, Z. Chacko, and M. K. Gaillard, *Little supersymmetry and the supersymmetric little hierarchy problem*, JHEP **10** (2004) 036, [hep-ph/0404197].

[94] P. H. Chankowski, A. Falkowski, S. Pokorski, and J. Wagner, *Electroweak symmetry breaking in supersymmetric models with heavy scalar superpartners*, Phys. Lett. B **598** (2004) 252–262, [hep-ph/0407242].

[95] Z. Berezhiani, P. H. Chankowski, A. Falkowski, and S. Pokorski, *Double protection of the Higgs potential in a supersymmetric little Higgs model*, Phys. Rev. Lett. **96** (2006) 031801, [hep-ph/0509311].

[96] T. S. Roy and M. Schmaltz, *Naturally heavy superpartners and a little Higgs*, JHEP **01** (2006) 149, [hep-ph/0509357].

[97] C. Csaki, G. Marandella, Y. Shirman, and A. Strumia, *The Super-little Higgs*, Phys. Rev. D **73** (2006) 035006, [hep-ph/0510294].

[98] P. Batra and Z. Chacko, *A Composite Twin Higgs Model*, Phys. Rev. D **79** (2009) 095012, [arXiv:0811.0394].

[99] M. Geller and O. Telem, *Holographic Twin Higgs Model*, Phys. Rev. Lett. **114** (2015) 191801, [arXiv:1411.2974].

[100] R. Barbieri, D. Greco, R. Rattazzi, and A. Wulzer, *The Composite Twin Higgs scenario*, JHEP **08** (2015) 161, [arXiv:1501.07803].

[101] M. Low, A. Tesi, and L.-T. Wang, *Twin Higgs mechanism and a composite Higgs boson*, Phys. Rev. D **91** (2015) 095012, [arXiv:1501.07890].

[102] C. Csaki, M. Geller, O. Telem, and A. Weiler, *The Flavor of the Composite Twin Higgs*, JHEP **09** (2016) 146, [arXiv:1512.03427].

[103] R. Contino, D. Greco, R. Mahbubani, R. Rattazzi, and R. Torre, *Precision Tests and Fine Tuning in Twin Higgs Models*, Phys. Rev. D **96** (2017), no. 9 095036, [arXiv:1702.00797].

[104] G. Jungman, M. Kamionkowski, and K. Griest, *Supersymmetric dark matter*, Phys. Rept. **267** (1996) 195–373, [hep-ph/9506380].

[105] N. Arkani-Hamed, A. Delgado, and G. F. Giudice, *The Well-tempered neutralino*, Nucl. Phys. B **741** (2006) 108–130, [hep-ph/0601041].

[106] M. Badziak, G. Grilli Di Cortona, and K. Harigaya, *Natural Twin Neutralino Dark Matter*, Phys. Rev. Lett. **124** (2020), no. 12 121803, [arXiv:1911.03481].

[107] P. A. M. Dirac, *New basis for cosmology*, Proc. Roy. Soc. Lond. A **165** (1938) 199–208.

[108] G. 't Hooft, *Naturalness, chiral symmetry, and spontaneous chiral symmetry breaking*, NATO Sci. Ser. B **59** (1980) 135–157.

[109] N. Craig, *Naturalness: past, present, and future*, Eur. Phys. J. C **83** (2023), no. 9 825, [arXiv:2205.05708].

[110] S. Scherer, *Introduction to chiral perturbation theory*, Adv. Nucl. Phys. **27** (2003) 277, [hep-ph/0210398].

[111] D. J. Gross and F. Wilczek, *Ultraviolet Behavior of Nonabelian Gauge Theories*, Phys. Rev. Lett. **30** (1973) 1343–1346.

[112] W. E. Caswell, *Asymptotic Behavior of Nonabelian Gauge Theories to Two Loop Order*, Phys. Rev. Lett. **33** (1974) 244.

[113] M. D. Schwartz, Quantum Field Theory and the Standard Model. Cambridge University Press, 3, 2014.

[114] **Particle Data Group** Collaboration, R. L. Workman and Others, *Review of Particle Physics*, PTEP **2022** (2022) 083C01.

[115] J. Goldstone, A. Salam, and S. Weinberg, *Broken Symmetries*, Phys. Rev. **127** (1962) 965–970.

[116] A. M. Polyakov, *Compact Gauge Fields and the Infrared Catastrophe*, Phys. Lett. B **59** (1975) 82–84.

[117] A. A. Belavin, A. M. Polyakov, A. S. Schwartz, and Y. S. Tyupkin, *Pseudoparticle Solutions of the Yang-Mills Equations*, Phys. Lett. B **59** (1975) 85–87.

[118] G. 't Hooft, *Symmetry Breaking Through Bell-Jackiw Anomalies*, Phys. Rev. Lett. **37** (1976) 8–11.

[119] R. Jackiw and C. Rebbi, *Vacuum Periodicity in a Yang-Mills Quantum Theory*, Phys. Rev. Lett. **37** (1976) 172–175.

[120] M. Srednicki, Quantum field theory. Cambridge University Press, 1, 2007.

[121] N. S. Manton and P. Sutcliffe, Topological solitons. Cambridge Monographs on Mathematical Physics. Cambridge University Press, 2004.

[122] T. Schäfer and E. V. Shuryak, *Instantons in QCD*, Rev. Mod. Phys. **70** (1998) 323–426, [hep-ph/9610451].

[123] S. R. Coleman, *The Fate of the False Vacuum. 1. Semiclassical Theory*, Phys. Rev. D **15** (1977) 2929–2936. [Erratum: Phys.Rev.D 16, 1248 (1977)].

[124] C. G. Callan, Jr., R. F. Dashen, and D. J. Gross, *The Structure of the Gauge Theory Vacuum*, Phys. Lett. B **63** (1976) 334–340.

[125] L. Di Luzio, M. Giannotti, E. Nardi, and L. Visinelli, *The landscape of QCD axion models*, Phys. Rept. **870** (2020) 1–117, [arXiv:2003.01100].

[126] F. A. Berezin, *The method of second quantization*, Pure Appl. Phys. **24** (1966) 1–228.

[127] C. Abel et al., *Measurement of the Permanent Electric Dipole Moment of the Neutron*, Phys. Rev. Lett. **124** (2020), no. 8 081803, [arXiv:2001.11966].

[128] K. Ottnad, B. Kubis, U. G. Meissner, and F. K. Guo, *New insights into the neutron electric dipole moment*, Phys. Lett. B **687** (2010) 42–47, [arXiv:0911.3981].

[129] J. Hisano, J. Y. Lee, N. Nagata, and Y. Shimizu, *Reevaluation of Neutron Electric Dipole Moment with QCD Sum Rules*, Phys. Rev. D **85** (2012) 114044, [arXiv:1204.2653].

[130] P. Binetruy, Supersymmetry. Oxford Graduate Texts. Oxford University Press, 7, 2012.

[131] F. Abu-Ajamieh, *Model-independent Veltman condition, naturalness and the little hierarchy problem **, Chin. Phys. C **46** (2022), no. 1 013101, [arXiv:2101.06932].

[132] R. Barbieri and G. F. Giudice, *Upper Bounds on Supersymmetric Particle Masses*, Nucl. Phys. B **306** (1988) 63–76.

[133] J. R. Ellis, K. Enqvist, D. V. Nanopoulos, and F. Zwirner, *Observables in Low-Energy Superstring Models*, Mod. Phys. Lett. A **1** (1986) 57.

[134] A. Arbey and F. Mahmoudi, *Dark matter and the early Universe: a review*, Prog. Part. Nucl. Phys. **119** (2021) 103865, [arXiv:2104.11488].

[135] J. L. Feng, *Dark Matter Candidates from Particle Physics and Methods of Detection*, Ann. Rev. Astron. Astrophys. **48** (2010) 495–545, [arXiv:1003.0904].

[136] K. G. Begeman, A. H. Broeils, and R. H. Sanders, *Extended rotation curves of spiral galaxies: Dark haloes and modified dynamics*, Mon. Not. Roy. Astron. Soc. **249** (1991) 523.

[137] F. Zwicky, *Die Rotverschiebung von extragalaktischen Nebeln*, Helv. Phys. Acta **6** (1933) 110–127.

[138] M. Persic, P. Salucci, and F. Stel, *The Universal rotation curve of spiral galaxies: 1. The Dark matter connection*, Mon. Not. Roy. Astron. Soc. **281** (1996) 27, [astro-ph/9506004].

[139] D. Clowe, M. Bradac, A. H. Gonzalez, M. Markevitch, S. W. Randall, C. Jones, and D. Zaritsky, *A direct empirical proof of the existence of dark matter*, Astrophys. J. Lett. **648** (2006) L109–L113, [astro-ph/0608407].

[140] G. W. Angus, B. Famaey, and H. Zhao, *Can MOND take a bullet? Analytical comparisons of three versions of MOND beyond spherical symmetry*, Mon. Not. Roy. Astron. Soc. **371** (2006) 138, [astro-ph/0606216].

[141] S. Dodelson, *The Real Problem with MOND*, Int. J. Mod. Phys. D **20** (2011) 2749–2753, [arXiv:1112.1320].

[142] M. Bradac, S. W. Allen, T. Treu, H. Ebeling, R. Massey, R. G. Morris, A. von der Linden, and D. Applegate, *Revealing the properties of dark matter in the merging cluster MACSJ0025.4-1222*, Astrophys. J. **687** (2008) 959, [arXiv:0806.2320].

[143] D. Baumann, Cosmology. Cambridge University Press, 7, 2022.

[144] B. D. Fields, K. A. Olive, T.-H. Yeh, and C. Young, *Big-Bang Nucleosynthesis after Planck*, JCAP **03** (2020) 010, [arXiv:1912.01132]. [Erratum: JCAP 11, E02 (2020)].

[145] M. Kawasaki, K. Kohri, T. Moroi, and Y. Takaesu, *Revisiting Big-Bang Nucleosynthesis Constraints on Long-Lived Decaying Particles*, Phys. Rev. D **97** (2018), no. 2 023502, [arXiv:1709.01211].

[146] **SDSS** Collaboration, D. G. York et al., *The Sloan Digital Sky Survey: Technical Summary*, Astron. J. **120** (2000) 1579–1587, [astro-ph/0006396].

[147] B. A. Reid et al., *Cosmological Constraints from the Clustering of the Sloan Digital Sky Survey DR7 Luminous Red Galaxies*, Mon. Not. Roy. Astron. Soc. **404** (2010) 60–85, [arXiv:0907.1659].

[148] S. Chabanier, M. Millea, and N. Palanque-Delabrouille, *Matter power spectrum: from Ly$\alpha$ forest to CMB scales*, Mon. Not. Roy. Astron. Soc. **489** (2019), no. 2 2247–2253, [arXiv:1905.08103].

[149] K. Griest, *The Search for dark matter: WIMPs and MACHOs*, Annals N. Y. Acad. Sci. **688** (1993) 390, [hep-ph/9303253].

[150] M. Kamionkowski, *WIMP and axion dark matter*, in ICTP Summer School in High-Energy Physics and Cosmology, pp. 394–411, 6, 1997. hep-ph/9710467.

[151] N. Arkani-Hamed, D. P. Finkbeiner, T. R. Slatyer, and N. Weiner, *A Theory of Dark Matter*, Phys. Rev. D **79** (2009) 015014, [arXiv:0810.0713].

[152] J. Cooley, *Overview of Non-Liquid Noble Direct Detection Dark Matter Experiments*, Phys. Dark Univ. **4** (2014) 92–97, [arXiv:1410.4960].

[153] T. Marrodán Undagoitia and L. Rauch, *Dark matter direct-detection experiments*, J. Phys. G **43** (2016), no. 1 013001, [arXiv:1509.08767].

[154] G. Bertone, ed., Particle Dark Matter: Observations, Models and Searches. Cambridge Univ. Press, Cambridge, 2010.

[155] **DAMA** Collaboration, R. Bernabei et al., *First results from DAMA/LIBRA and the combined results with DAMA/NaI*, Eur. Phys. J. C **56** (2008) 333–355, [arXiv:0804.2741].

[156] **DAMA, LIBRA** Collaboration, R. Bernabei et al., *New results from DAMA/LIBRA*, Eur. Phys. J. C **67** (2010) 39–49, [arXiv:1002.1028].

[157] **KIMS** Collaboration, H. S. Lee et al., *Limits on WIMP-nucleon cross section with CsI(Tl) crystal detectors*, Phys. Rev. Lett. **99** (2007) 091301, [arXiv:0704.0423].

[158] **KIMS** Collaboration, K. W. Kim et al., *Limits on Interactions between Weakly Interacting Massive Particles and Nucleons Obtained with NaI(Tl) crystal Detectors*, JHEP **03** (2019) 194, [arXiv:1806.06499].

[159] **COSINE-100** Collaboration, G. Adhikari et al., *Search for a Dark Matter-Induced Annual Modulation Signal in NaI(Tl) with the COSINE-100 Experiment*, Phys. Rev. Lett. **123** (2019), no. 3 031302, [arXiv:1903.10098].

[160] **COSINE-100** Collaboration, G. Adhikari et al., *Three-year annual modulation search with COSINE-100*, Phys. Rev. D **106** (2022), no. 5 052005, [arXiv:2111.08863].

[161] **CRESST** Collaboration, G. Angloher et al., *Results on light dark matter particles with a low-threshold CRESST-II detector*, Eur. Phys. J. C **76** (2016), no. 1 25, [arXiv:1509.01515].

[162] **CRESST** Collaboration, H. Kluck et al., *Search for low-mass Dark Matter with the CRESST Experiment*, in 13th Patras Workshop on Axions, WIMPs and WISPs, pp. 130–133, 2018. arXiv:1711.01285.

[163] **CDMS-II** Collaboration, Z. Ahmed et al., *Dark Matter Search Results from the CDMS II Experiment*, Science **327** (2010) 1619–1621, [arXiv:0912.3592].

[164] **CDMS** Collaboration, R. Agnese et al., *Silicon Detector Dark Matter Results from the Final Exposure of CDMS II*, Phys. Rev. Lett. **111** (2013), no. 25 251301, [arXiv:1304.4279].

[165] **XENON** Collaboration, E. Aprile et al., *Dark Matter Search Results from a One Ton-Year Exposure of XENON1T*, Phys. Rev. Lett. **121** (2018), no. 11 111302, [arXiv:1805.12562].

[166] **XENON** Collaboration, E. Aprile et al., *The XENONnT Dark Matter Experiment*, arXiv:2402.10446.

[167] **LZ** Collaboration, D. S. Akerib et al., *Projected WIMP sensitivity of the LUX-ZEPLIN dark matter experiment*, Phys. Rev. D **101** (2020), no. 5 052002, [arXiv:1802.06039].

[168] **LZ** Collaboration, J. Aalbers et al., *First Dark Matter Search Results from the LUX-ZEPLIN (LZ) Experiment*, Phys. Rev. Lett. **131** (2023), no. 4 041002, [arXiv:2207.03764].

[169] **PandaX-II** Collaboration, X. Cui et al., *Dark Matter Results From 54-Ton-Day Exposure of PandaX-II Experiment*, Phys. Rev. Lett. **119** (2017), no. 18 181302, [arXiv:1708.06917].

[170] **PandaX-4T** Collaboration, Y. Meng et al., *Dark Matter Search Results from the PandaX-4T Commissioning Run*, Phys. Rev. Lett. **127** (2021), no. 26 261802, [arXiv:2107.13438].

[171] **LZ Collaboration** Collaboration, J. Aalbers et al., *Dark Matter Search Results from 4.2 Tonne-Years of Exposure of the LUX-ZEPLIN (LZ) Experiment*, arXiv:2410.17036.

[172] J. M. Gaskins, *A review of indirect searches for particle dark matter*, Contemp. Phys. **57** (2016), no. 4 496–525, [arXiv:1604.00014].

[173] **Fermi-LAT** Collaboration, W. B. Atwood et al., *The Large Area Telescope on the Fermi Gamma-ray Space Telescope Mission*, Astrophys. J. **697** (2009) 1071–1102, [arXiv:0902.1089].

[174] **Fermi-LAT** Collaboration, M. Ackermann et al., *The Fermi Large Area Telescope On Orbit: Event Classification, Instrument Response Functions, and Calibration*, Astrophys. J. Suppl. **203** (2012) 4, [arXiv:1206.1896].

[175] **H.E.S.S.** Collaboration, F. Aharonian et al., *The h.e.s.s. survey of the inner galaxy in very high-energy gamma-rays*, Astrophys. J. **636** (2006) 777–797, [astro-ph/0510397].

[176] **H.E.S.S.** Collaboration, J. A. Hinton, *The Status of the H.E.S.S. project*, New Astron. Rev. **48** (2004) 331–337, [astro-ph/0403052].

[177] **H.E.S.S.** Collaboration, A. Abramowski et al., *Search for a Dark Matter annihilation signal from the Galactic Center halo with H.E.S.S*, Phys. Rev. Lett. **106** (2011) 161301, [arXiv:1103.3266].

[178] **MAGIC** Collaboration, J. Albert et al., *Observation of gamma-rays from the galactic center with the magic telescope*, Astrophys. J. Lett. **638** (2006) L101–L104, [astro-ph/0512469].

[179] J. Aleksić et al., *Optimized dark matter searches in deep observations of Segue 1 with MAGIC*, JCAP **02** (2014) 008, [arXiv:1312.1535].

[180] **VERITAS** Collaboration, J. Holder et al., *The first VERITAS telescope*, Astropart. Phys. **25** (2006) 391–401, [astro-ph/0604119].

[181] **AMS** Collaboration, M. Aguilar et al., *The Alpha Magnetic Spectrometer (AMS) on the International Space Station. I: Results from the test flight on the space shuttle*, Phys. Rept. **366** (2002) 331–405. [Erratum: Phys.Rept. 380, 97–98 (2003)].

[182] **AMS** Collaboration, M. Aguilar et al., *First Result from the Alpha Magnetic Spectrometer on the International Space Station: Precision Measurement of the Positron Fraction in Primary Cosmic Rays of 0.5–350 GeV*, Phys. Rev. Lett. **110** (2013) 141102.

[183] P. Picozza et al., *PAMELA: A Payload for Antimatter Matter Exploration and Light-nuclei Astrophysics*, Astropart. Phys. **27** (2007) 296–315, [astro-ph/0608697].

[184] **Pierre Auger** Collaboration, A. Aab et al., *The Pierre Auger Cosmic Ray Observatory*, Nucl. Instrum. Meth. A **798** (2015) 172–213, [arXiv:1502.01323].

[185] **Super-Kamiokande** Collaboration, Y. Fukuda et al., *The Super-Kamiokande detector*, Nucl. Instrum. Meth. A **501** (2003) 418–462.

[186] **Super-Kamiokande** Collaboration, S. Desai et al., *Search for dark matter WIMPs using upward through-going muons in Super-Kamiokande*, Phys. Rev. D **70** (2004) 083523, [hep-ex/0404025]. [Erratum: Phys.Rev.D 70, 109901 (2004)].

[187] **Super-Kamiokande** Collaboration, T. Tanaka et al., *An Indirect Search for WIMPs in the Sun using 3109.6 days of upward-going muons in Super-Kamiokande*, Astrophys. J. **742** (2011) 78, [arXiv:1108.3384].

[188] **IceCube** Collaboration, R. Abbasi et al., *Search for dark matter from the Galactic halo with the IceCube Neutrino Telescope*, Phys. Rev. D **84** (2011) 022004, [arXiv:1101.3349].

[189] **IceCube** Collaboration, R. Abbasi et al., *Search for Neutrinos from Annihilating Dark Matter in the Direction of the Galactic Center with the 40-String IceCube Neutrino Observatory*, arXiv:1210.3557.

[190] **IceCube** Collaboration, M. G. Aartsen et al., *Search for dark matter annihilations in the Sun with the 79-string IceCube detector*, Phys. Rev. Lett. **110** (2013), no. 13 131302, [arXiv:1212.4097].

[191] **IceCube-Gen2** Collaboration, M. G. Aartsen et al., *IceCube-Gen2: the window to the extreme Universe*, J. Phys. G **48** (2021), no. 6 060501, [arXiv:2008.04323].

[192] **ANTARES** Collaboration, M. Ageron et al., *ANTARES: the first undersea neutrino telescope*, Nucl. Instrum. Meth. A **656** (2011) 11–38, [arXiv:1104.1607].

[193] **ANTARES** Collaboration, S. Adrian-Martinez et al., *First results on dark matter annihilation in the Sun using the ANTARES neutrino telescope*, JCAP **11** (2013) 032, [arXiv:1302.6516].

[194] **ANTARES** Collaboration, S. Adrian-Martinez et al., *Limits on Dark Matter Annihilation in the Sun using the ANTARES Neutrino Telescope*, Phys. Lett. B **759** (2016) 69–74, [arXiv:1603.02228].

[195] C. Vafa and E. Witten, *Parity Conservation in QCD*, Phys. Rev. Lett. **53** (1984) 535.

[196] C. Vafa and E. Witten, *Restrictions on Symmetry Breaking in Vector-Like Gauge Theories*, Nucl. Phys. B **234** (1984) 173–188.

[197] I. B. Khriplovich, *Quark Electric Dipole Moment and Induced $\theta$ Term in the Kobayashi-Maskawa Model*, Phys. Lett. B **173** (1986) 193–196.

[198] J. E. Kim, *Light Pseudoscalars, Particle Physics and Cosmology*, Phys. Rept. **150** (1987) 1–177.

[199] K. Mimasu and V. Sanz, *ALPs at Colliders*, JHEP **06** (2015) 173, [arXiv:1409.4792].

[200] L. D. Landau, *On the angular momentum of a system of two photons*, Dokl. Akad. Nauk SSSR **60** (1948), no. 2 207–209.

[201] C.-N. Yang, *Selection Rules for the Dematerialization of a Particle Into Two Photons*, Phys. Rev. **77** (1950) 242–245.

[202] **Flavour Lattice Averaging Group (FLAG)** Collaboration, Y. Aoki et al., *FLAG Review 2021*, Eur. Phys. J. C **82** (2022), no. 10 869, [arXiv:2111.09849].

[203] G. Grilli di Cortona, E. Hardy, J. Pardo Vega, and G. Villadoro, *The QCD axion, precisely*, JHEP **01** (2016) 034, [arXiv:1511.02867].

[204] D. Lombardi, *The DFSZ axion: analysis and generalization*, laurea thesis, U. Bologna, DIFA, 2018.

[205] A. J. MacFarlane, A. Sudbery, and P. H. Weisz, *On Gell-Mann's lambda-matrices, d- and f-tensors, octets, and parametrizations of SU(3)*, Commun. Math. Phys. **11** (1968) 77–90.

[206] S. Chang and K. Choi, *Hadronic axion window and the big bang nucleosynthesis*, Phys. Lett. B **316** (1993) 51–56, [hep-ph/9306216].

[207] L. Di Luzio, G. Martinelli, and G. Piazza, *Breakdown of chiral perturbation theory for the axion hot dark matter bound*, Phys. Rev. Lett. **126** (2021), no. 24 241801, [arXiv:2101.10330].

[208] W. R. Inc., "Mathematica, Version 14.2." Champaign, IL, 2024.

[209] M. Badziak, K. Harigaya, M. Łukawski, and R. Ziegler, *Thermal production of astrophobic axions*, JHEP **09** (2024) 136, [arXiv:2403.05621].

[210] M. M. Miller Bertolami, B. E. Melendez, L. G. Althaus, and J. Isern, *Revisiting the axion bounds from the Galactic white dwarf luminosity function*, JCAP **10** (2014) 069, [arXiv:1406.7712].

[211] S. Roy, C. Blanco, C. Dessert, A. Prabhu, and T. Temim, *Sensitivity of JWST to eV-Scale Decaying Axion Dark Matter*, arXiv:2311.04987.

[212] T. Bessho, Y. Ikeda, and W. Yin, *Indirect detection of eV dark matter via infrared spectroscopy*, Phys. Rev. D **106** (2022), no. 9 095025, [arXiv:2208.05975].

[213] R. Janish and E. Pinetti, *Hunting Dark Matter Lines in the Infrared Background with the James Webb Space Telescope*, arXiv:2310.15395.

[214] W. Yin et al., *First Result for Dark Matter Search by WINERED*, arXiv:2402.07976.

[215] M. Kawasaki, K. Saikawa, and T. Sekiguchi, *Axion dark matter from topological defects*, Phys. Rev. D **91** (2015), no. 6 065014, [arXiv:1412.0789].

[216] K. Harigaya and L.-T. Wang, *More axions from diluted domain walls*, arXiv:2211.08289.

[217] **CAST** Collaboration, V. Anastassopoulos et al., *New CAST Limit on the Axion-Photon Interaction*, Nature Phys. **13** (2017) 584–590, [arXiv:1705.02290].

[218] **IAXO** Collaboration, A. Abeln et al., *Conceptual design of BabyIAXO, the intermediate stage towards the International Axion Observatory*, JHEP **05** (2021) 137, [arXiv:2010.12076].

[219] C. O'Hare, "cajohare/axionlimits: Axionlimits." https://cajohare.github.io/AxionLimits/, July, 2020.

[220] A. Jodidio et al., *Search for Right-Handed Currents in Muon Decay*, Phys. Rev. D **34** (1986) 1967. [Erratum: Phys.Rev.D 37, 237 (1988)].

[221] **TWIST** Collaboration, R. Bayes et al., *Search for two body muon decay signals*, Phys. Rev. D **91** (2015), no. 5 052020, [arXiv:1409.0638].

[222] L. Calibbi, D. Redigolo, R. Ziegler, and J. Zupan, *Looking forward to lepton-flavor-violating ALPs*, JHEP **09** (2021) 173, [arXiv:2006.04795].

[223] **Belle-II** Collaboration, I. Adachi et al., *Search for Lepton-Flavor-Violating $\tau$ Decays to a Lepton and an Invisible Boson at Belle II*, Phys. Rev. Lett. **130** (2023), no. 18 181803, [arXiv:2212.03634].

[224] A. D. Linde, *Axions in inflationary cosmology*, Phys. Lett. B **259** (1991) 38–47.

[225] M. Fairbairn, R. Hogan, and D. J. E. Marsh, *Unifying inflation and dark matter with the Peccei-Quinn field: observable axions and observable tensors*, Phys. Rev. D **91** (2015), no. 2 023509, [arXiv:1410.1752].

[226] G. Ballesteros, J. Redondo, A. Ringwald, and C. Tamarit, *Unifying inflation with the axion, dark matter, baryogenesis and the seesaw mechanism*, Phys. Rev. Lett. **118** (2017), no. 7 071802, [arXiv:1608.05414].

[227] G. Ballesteros, J. Redondo, A. Ringwald, and C. Tamarit, *Standard Model—axion—seesaw—Higgs portal inflation. Five problems of particle physics and cosmology solved in one stroke*, JCAP **08** (2017) 001, [arXiv:1610.01639].

[228] G. Ballesteros, J. Redondo, A. Ringwald, and C. Tamarit, *Several Problems in Particle Physics and Cosmology Solved in One SMASH*, Front. Astron. Space Sci. **6** (2019) 55, [arXiv:1904.05594].

[229] G. W. Gibbons and S. W. Hawking, *Action Integrals and Partition Functions in Quantum Gravity*, Phys. Rev. D **15** (1977) 2752–2756.

[230] D. J. E. Marsh, *Axion Cosmology*, Phys. Rept. **643** (2016) 1–79, [arXiv:1510.07633].

[231] M. Gorghetto, E. Hardy, and H. Nicolaescu, *Observing invisible axions with gravitational waves*, JCAP **06** (2021) 034, [arXiv:2101.11007].

[232] R. Holman, S. D. H. Hsu, T. W. Kephart, E. W. Kolb, R. Watkins, and L. M. Widrow, *Solutions to the strong CP problem in a world with gravity*, Phys. Lett. B **282** (1992) 132–136, [hep-ph/9203206].

[233] S. M. Barr and D. Seckel, *Planck scale corrections to axion models*, Phys. Rev. D **46** (1992) 539–549.

[234] M. Kamionkowski and J. March-Russell, *Planck scale physics and the Peccei-Quinn mechanism*, Phys. Lett. B **282** (1992) 137–141, [hep-th/9202003].

[235] J. Martin Camalich, M. Pospelov, P. N. H. Vuong, R. Ziegler, and J. Zupan, *Quark Flavor Phenomenology of the QCD Axion*, Phys. Rev. D **102** (2020), no. 1 015023, [arXiv:2002.04623].

[236] M. Cielo, M. Escudero, G. Mangano, and O. Pisanti, *Neff in the Standard Model at NLO is 3.043*, Phys. Rev. D **108** (2023), no. 12 L121301, [arXiv:2306.05460].

[237] **Simons Observatory** Collaboration, P. Ade et al., *The Simons Observatory: Science goals and forecasts*, JCAP **02** (2019) 056, [arXiv:1808.07445].

[238] **CMB-S4** Collaboration, K. N. Abazajian et al., *CMB-S4 Science Book, First Edition*, arXiv:1610.02743.

[239] F. D'Eramo, E. Di Valentino, W. Giarè, F. Hajkarim, A. Melchiorri, O. Mena, F. Renzi, and S. Yun, *Cosmological bound on the QCD axion mass, redux*, JCAP **09** (2022) 022, [arXiv:2205.07849].

[240] T.-H. Yeh, J. Shelton, K. A. Olive, and B. D. Fields, *Probing physics beyond the standard model: limits from BBN and the CMB independently and combined*, JCAP **10** (2022) 046, [arXiv:2207.13133].

[241] F. D'Eramo, R. Z. Ferreira, A. Notari, and J. L. Bernal, *Hot Axions and the $H_0$ tension*, JCAP **11** (2018) 014, [arXiv:1808.07430].

[242] K. Saikawa and S. Shirai, *Primordial gravitational waves, precisely: The role of thermodynamics in the Standard Model*, JCAP **05** (2018) 035, [arXiv:1803.01038].

[243] S. Borsanyi et al., *Calculation of the axion mass based on high-temperature lattice quantum chromodynamics*, Nature **539** (2016), no. 7627 69–71, [arXiv:1606.07494].

[244] M. Badziak and M. Laletin, *Precise predictions for the QCD axion contribution to dark radiation with full phase-space evolution*, arXiv:2410.18186.

[245] R. Mertig, M. Bohm, and A. Denner, *FEYN CALC: Computer algebraic calculation of Feynman amplitudes*, Comput. Phys. Commun. **64** (1991) 345–359.

[246] V. Shtabovenko, R. Mertig, and F. Orellana, *New Developments in FeynCalc 9.0*, Comput. Phys. Commun. **207** (2016) 432–444, [arXiv:1601.01167].

[247] F. D'Eramo and S. Yun, *Flavor violating axions in the early Universe*, Phys. Rev. D **105** (2022), no. 7 075002, [arXiv:2111.12108].

[248] A. Czarnecki, M. Kamionkowski, S. K. Lee, and K. Melnikov, *Charged Particle Decay at Finite Temperature*, Phys. Rev. D **85** (2012) 025018, [arXiv:1110.2171].

[249] T. Kinoshita, *Mass singularities of Feynman amplitudes*, J. Math. Phys. **3** (1962) 650–677.

[250] T. D. Lee and M. Nauenberg, *Degenerate Systems and Mass Singularities*, Phys. Rev. **133** (1964) B1549–B1562.

[251] R. Z. Ferreira, A. Notari, and F. Rompineve, *Dine-Fischler-Srednicki-Zhitnitsky axion in the CMB*, Phys. Rev. D **103** (2021), no. 6 063524, [arXiv:2012.06566].

[252] S. Hannestad, A. Mirizzi, and G. Raffelt, *New cosmological mass limit on thermal relic axions*, JCAP **07** (2005) 002, [hep-ph/0504059].

[253] P. Graf and F. D. Steffen, *Thermal axion production in the primordial quark-gluon plasma*, Phys. Rev. D **83** (2011) 075011, [arXiv:1008.4528].

[254] A. Salvio, A. Strumia, and W. Xue, *Thermal axion production*, JCAP **01** (2014) 011, [arXiv:1310.6982].

[255] S. Borsanyi, Z. Fodor, J. N. Guenther, R. Kara, S. D. Katz, P. Parotto, A. Pasztor, C. Ratti, and K. K. Szabo, *QCD Crossover at Finite Chemical Potential from Lattice Simulations*, Phys. Rev. Lett. **125** (2020), no. 5 052001, [arXiv:2002.02821].

[256] N. Craig, S. Koren, and T. Trott, *Cosmological Signals of a Mirror Twin Higgs*, JHEP **05** (2017) 038, [arXiv:1611.07977].

[257] Z. Chacko, N. Craig, P. J. Fox, and R. Harnik, *Cosmology in Mirror Twin Higgs and Neutrino Masses*, JHEP **07** (2017) 023, [arXiv:1611.07975].

[258] P. F. de Salas, M. Lattanzi, G. Mangano, G. Miele, S. Pastor, and O. Pisanti, *Bounds on very low reheating scenarios after Planck*, Phys. Rev. D **92** (2015), no. 12 123534, [arXiv:1511.00672].

[259] M. Badziak and I. Nałecz, *First-order phase transitions in Twin Higgs models*, JHEP **02** (2023) 185, [arXiv:2212.09776].

[260] U. Amaldi, W. de Boer, and H. Furstenau, *Comparison of grand unified theories with electroweak and strong coupling constants measured at LEP*, Phys. Lett. B **260** (1991) 447–455.

[261] P. Langacker and M.-x. Luo, *Implications of precision electroweak experiments for $M_t$, $\rho_0$, $\sin^2\theta_W$ and grand unification*, Phys. Rev. D **44** (1991) 817–822.

[262] C. Giunti, C. W. Kim, and U. W. Lee, *Running coupling constants and grand unification models*, Mod. Phys. Lett. A **6** (1991) 1745–1755.

[263] P. Nath and R. L. Arnowitt, *Generalized Supergauge Symmetry as a New Framework for Unified Gauge Theories*, Phys. Lett. B **56** (1975) 177–180.

[264] R. L. Arnowitt, P. Nath, and B. Zumino, *Superfield Densities and Action Principle in Curved Superspace*, Phys. Lett. B **56** (1975) 81–84.

[265] D. Z. Freedman, P. van Nieuwenhuizen, and S. Ferrara, *Progress Toward a Theory of Supergravity*, Phys. Rev. D **13** (1976) 3214–3218.

[266] S. Deser and B. Zumino, *Consistent Supergravity*, Phys. Lett. B **62** (1976) 335.

[267] D. Z. Freedman and P. van Nieuwenhuizen, *Properties of Supergravity Theory*, Phys. Rev. D **14** (1976) 912.

[268] E. Cremmer, B. Julia, J. Scherk, S. Ferrara, L. Girardello, and P. van Nieuwenhuizen, *Spontaneous Symmetry Breaking and Higgs Effect in Supergravity Without Cosmological Constant*, Nucl. Phys. B **147** (1979) 105.

[269] J. A. Bagger, *Coupling the Gauge Invariant Supersymmetric Nonlinear Sigma Model to Supergravity*, Nucl. Phys. B **211** (1983) 302.

[270] E. Cremmer, S. Ferrara, L. Girardello, and A. Van Proeyen, *Yang-Mills Theories with Local Supersymmetry: Lagrangian, Transformation Laws and SuperHiggs Effect*, Nucl. Phys. B **212** (1983) 413.

[271] J. R. Ellis, J. S. Hagelin, D. V. Nanopoulos, K. A. Olive, and M. Srednicki, *Supersymmetric Relics from the Big Bang*, Nucl. Phys. B **238** (1984) 453–476.

[272] J. Edsjo and P. Gondolo, *Neutralino relic density including coannihilations*, Phys. Rev. D **56** (1997) 1879–1894, [hep-ph/9704361].

[273] G. Bertone, D. Hooper, and J. Silk, *Particle dark matter: Evidence, candidates and constraints*, Phys. Rept. **405** (2005) 279–390, [hep-ph/0404175].

[274] J. Ellis and K. A. Olive, *Supersymmetric Dark Matter Candidates*, arXiv:1001.3651.

[275] M. Badziak, M. Olechowski, and P. Szczerbiak, *Is well-tempered neutralino in MSSM still alive after 2016 LUX results?*, Phys. Lett. B **770** (2017) 226–235, [arXiv:1701.05869].

[276] M. E. Cabrera, J. A. Casas, A. Delgado, S. Robles, and R. Ruiz de Austri, *Naturalness of MSSM dark matter*, JHEP **08** (2016) 058, [arXiv:1604.02102].

[277] H. Baer, V. Barger, and H. Serce, *SUSY under siege from direct and indirect WIMP detection experiments*, Phys. Rev. D **94** (2016), no. 11 115019, [arXiv:1609.06735].

[278] S. Dimopoulos and D. W. Sutter, *The Supersymmetric flavor problem*, Nucl. Phys. B **452** (1995) 496–512, [hep-ph/9504415].

[279] D. Tong, *Lectures on Supersymmetry*, 2022. Lecture notes, University of Cambridge.

[280] **ATLAS** Collaboration, G. Aad et al., *Search for a scalar partner of the top quark in the all-hadronic $t\bar{t}$ plus missing transverse momentum final state at $\sqrt{s} = 13$ TeV with the ATLAS detector*, Eur. Phys. J. C **80** (2020), no. 8 737, [arXiv:2004.14060].

[281] **CMS** Collaboration, A. M. Sirunyan et al., *Search for top squark production in fully-hadronic final states in proton-proton collisions at $\sqrt{s} = 13$ TeV*, Phys. Rev. D **104** (2021), no. 5 052001, [arXiv:2103.01290].

[282] M. van Beekveld, S. Caron, and R. Ruiz de Austri, *The current status of fine-tuning in supersymmetry*, JHEP **01** (2020) 147, [arXiv:1906.10706].

[283] M. R. Buckley, D. Feld, S. Macaluso, A. Monteux, and D. Shih, *Cornering Natural SUSY at LHC Run II and Beyond*, JHEP **08** (2017) 115, [arXiv:1610.08059].

[284] M. R. Buckley, A. Monteux, and D. Shih, *Precision Corrections to Fine Tuning in SUSY*, JHEP **06** (2017) 103, [arXiv:1611.05873].

[285] G. R. Farrar and P. Fayet, *Phenomenology of the Production, Decay, and Detection of New Hadronic States Associated with Supersymmetry*, Phys. Lett. B **76** (1978) 575–579.

[286] S. Weinberg, *Supersymmetry at Ordinary Energies. 1. Masses and Conservation Laws*, Phys. Rev. D **26** (1982) 287.

[287] N. Sakai and T. Yanagida, *Proton Decay in a Class of Supersymmetric Grand Unified Models*, Nucl. Phys. B **197** (1982) 533.

[288] S. Dimopoulos, S. Raby, and F. Wilczek, *Proton Decay in Supersymmetric Models*, Phys. Lett. B **112** (1982) 133.

[289] P. Fayet, *Supergauge Invariant Extension of the Higgs Mechanism and a Model for the electron and Its Neutrino*, Nucl. Phys. B **90** (1975) 104–124.

[290] P. Fayet, *Spontaneously Broken Supersymmetric Theories of Weak, Electromagnetic and Strong Interactions*, Phys. Lett. B **69** (1977) 489.

[291] L. O'Raifeartaigh, *Spontaneous Symmetry Breaking for Chiral Scalar Superfields*, Nucl. Phys. B **96** (1975) 331–352.

[292] A. H. Chamseddine, R. L. Arnowitt, and P. Nath, *Locally Supersymmetric Grand Unification*, Phys. Rev. Lett. **49** (1982) 970.

[293] R. Barbieri, S. Ferrara, and C. A. Savoy, *Gauge Models with Spontaneously Broken Local Supersymmetry*, Phys. Lett. B **119** (1982) 343.

[294] L. J. Hall, J. D. Lykken, and S. Weinberg, *Supergravity as the Messenger of Supersymmetry Breaking*, Phys. Rev. D **27** (1983) 2359–2378.

[295] N. Ohta, *GRAND UNIFIED THEORIES BASED ON LOCAL SUPERSYMMETRY*, Prog. Theor. Phys. **70** (1983) 542.

[296] M. Dine and A. E. Nelson, *Dynamical supersymmetry breaking at low-energies*, Phys. Rev. D **48** (1993) 1277–1287, [hep-ph/9303230].

[297] M. Dine, A. E. Nelson, and Y. Shirman, *Low-energy dynamical supersymmetry breaking simplified*, Phys. Rev. D **51** (1995) 1362–1370, [hep-ph/9408384].

[298] M. Dine, A. E. Nelson, Y. Nir, and Y. Shirman, *New tools for low-energy dynamical supersymmetry breaking*, Phys. Rev. D **53** (1996) 2658–2669, [hep-ph/9507378].

[299] G. F. Giudice and R. Rattazzi, *Theories with gauge mediated supersymmetry breaking*, Phys. Rept. **322** (1999) 419–499, [hep-ph/9801271].

[300] E. A. Mirabelli and M. E. Peskin, *Transmission of supersymmetry breaking from a four-dimensional boundary*, Phys. Rev. D **58** (1998) 065002, [hep-th/9712214].

[301] D. E. Kaplan, G. D. Kribs, and M. Schmaltz, *Supersymmetry breaking through transparent extra dimensions*, Phys. Rev. D **62** (2000) 035010, [hep-ph/9911293].

[302] Z. Chacko, M. A. Luty, A. E. Nelson, and E. Ponton, *Gaugino mediated supersymmetry breaking*, JHEP **01** (2000) 003, [hep-ph/9911323].

[303] M. Schmaltz and W. Skiba, *Minimal gaugino mediation*, Phys. Rev. D **62** (2000) 095005, [hep-ph/0001172].

[304] L. Randall and R. Sundrum, *Out of this world supersymmetry breaking*, Nucl. Phys. B **557** (1999) 79–118, [hep-th/9810155].

[305] G. F. Giudice, M. A. Luty, H. Murayama, and R. Rattazzi, *Gaugino mass without singlets*, JHEP **12** (1998) 027, [hep-ph/9810442].

[306] G. Belanger, F. Boudjema, A. Pukhov, and A. Semenov, *MicrOMEGAs: A Program for calculating the relic density in the MSSM*, Comput. Phys. Commun. **149** (2002) 103–120, [hep-ph/0112278].

[307] M. Badziak, G. Grilli di Cortona, K. Harigaya, and M. Łukawski, *Charged dark matter in supersymmetric twin Higgs models*, JHEP **10** (2022) 057, [arXiv:2202.10488].

[308] J. Rosiek, *Complete set of Feynman rules for the MSSM: Erratum*, hep-ph/9511250.

[309] D. A. Buote, T. E. Jeltema, C. R. Canizares, and G. P. Garmire, *Chandra evidence for a flattened, triaxial dark matter halo in the elliptical galaxy ngc 720*, Astrophys. J. **577** (2002) 183–196, [astro-ph/0205469].

[310] J. L. Feng, M. Kaplinghat, H. Tu, and H.-B. Yu, *Hidden Charged Dark Matter*, JCAP **07** (2009) 004, [arXiv:0905.3039].

[311] P. Agrawal, F.-Y. Cyr-Racine, L. Randall, and J. Scholtz, *Make Dark Matter Charged Again*, JCAP **05** (2017) 022, [arXiv:1610.04611].

[312] M. Cirelli, E. Del Nobile, and P. Panci, *Tools for model-independent bounds in direct dark matter searches*, JCAP **10** (2013) 019, [arXiv:1307.5955].

[313] G. Belanger, F. Boudjema, A. Pukhov, and A. Semenov, *micrOMEGAs_3: A program for calculating dark matter observables*, Comput. Phys. Commun. **185** (2014) 960–985, [arXiv:1305.0237].

[314] M. E. Peskin and D. V. Schroeder, An Introduction to quantum field theory. Addison-Wesley, Reading, USA, 1995.

[315] G. Belanger, F. Boudjema, A. Pukhov, and A. Semenov, *micrOMEGAs: Version 1.3*, Comput. Phys. Commun. **174** (2006) 577–604, [hep-ph/0405253].

[316] G. Belanger, F. Boudjema, A. Pukhov, and A. Semenov, *MicrOMEGAs 2.0: A Program to calculate the relic density of dark matter in a generic model*, Comput. Phys. Commun. **176** (2007) 367–382, [hep-ph/0607059].

[317] K. Griest and D. Seckel, *Three exceptions in the calculation of relic abundances*, Phys. Rev. D **43** (1991) 3191–3203.

[318] D. Dunsky, L. J. Hall, and K. Harigaya, *Higgs Parity, Strong CP, and Dark Matter*, JHEP **07** (2019) 016, [arXiv:1902.07726].

[319] B. Fuks, M. Klasen, D. R. Lamprea, and M. Rothering, *Revisiting slepton pair production at the Large Hadron Collider*, JHEP **01** (2014) 168, [arXiv:1310.2621].

[320] **CMS** Collaboration, A. M. Sirunyan et al., *Search for direct pair production of supersymmetric partners to the $\tau$ lepton in proton-proton collisions at $\sqrt{s} = 13$ TeV*, Eur. Phys. J. C **80** (2020), no. 3 189, [arXiv:1907.13179].

[321] **CMS** Collaboration, A. Tumasyan et al., *Search for direct pair production of supersymmetric partners of $\tau$ leptons in the final state with two hadronically decaying $\tau$ leptons and missing transverse momentum in proton-proton collisions at $\sqrt{s} = 13$ TeV*, Phys. Rev. D **108** (2023), no. 1 012011, [arXiv:2207.02254].

[322] **CMS** Collaboration, A. Tumasyan et al., *Search for electroweak production of charginos and neutralinos in proton-proton collisions at $\sqrt{s} = 13$ TeV*, JHEP **04** (2022) 147, [arXiv:2106.14246].

[323] **ATLAS** Collaboration, M. Aaboud et al., *Search for heavy charged long-lived particles in the ATLAS detector in 36.1 fb$^{-1}$ of proton-proton collision data at* $\sqrt{s} = 13$ *TeV*, Phys. Rev. D **99** (2019), no. 9 092007, [arXiv:1902.01636].

[324] J. A. Evans and J. Shelton, *Long-Lived Staus and Displaced Leptons at the LHC*, JHEP **04** (2016) 056, [arXiv:1601.01326].

[325] **ATLAS** Collaboration, G. Aad et al., *Search for long-lived charginos based on a disappearing-track signature using 136 fb$^{-1}$ of pp collisions at $\sqrt{s}$ = 13 TeV with the ATLAS detector*, Eur. Phys. J. C **82** (2022), no. 7 606, [arXiv:2201.02472].

[326] **CMS** Collaboration, A. M. Sirunyan et al., *Search for disappearing tracks in proton-proton collisions at $\sqrt{s}$ = 13 TeV*, Phys. Lett. B **806** (2020) 135502, [arXiv:2004.05153].

[327] M. Badziak, A. Delgado, M. Olechowski, S. Pokorski, and K. Sakurai, *Detecting underabundant neutralinos*, JHEP **11** (2015) 053, [arXiv:1506.07177].

[328] **LZ** Collaboration, J. Aalbers et al., *Dark Matter Search Results from 4.2 Tonne-Years of Exposure of the LUX-ZEPLIN (LZ) Experiment*, arXiv:2410.17036.

[329] J. R. Ellis, T. Falk, and K. A. Olive, *Neutralino - Stau coannihilation and the cosmological upper limit on the mass of the lightest supersymmetric particle*, Phys. Lett. B **444** (1998) 367–372, [hep-ph/9810360].

[330] **ALEPH** Collaboration, A. Heister et al., *Search for scalar leptons in e+ e- collisions at center-of-mass energies up to 209-GeV*, Phys. Lett. B **526** (2002) 206–220, [hep-ex/0112011].

[331] **DELPHI** Collaboration, J. Abdallah et al., *Searches for supersymmetric particles in e+ e- collisions up to 208-GeV and interpretation of the results within the MSSM*, Eur. Phys. J. C **31** (2003) 421–479, [hep-ex/0311019].

[332] **L3** Collaboration, P. Achard et al., *Search for scalar leptons and scalar quarks at LEP*, Phys. Lett. B **580** (2004) 37–49, [hep-ex/0310007].

[333] **OPAL** Collaboration, G. Abbiendi et al., *Search for anomalous production of dilepton events with missing transverse momentum in e+ e- collisions at s**(1/2) = 183-Gev to 209-GeV*, Eur. Phys. J. C **32** (2004) 453–473, [hep-ex/0309014].

[334] C. Boehm, A. Djouadi, and M. Drees, *Light scalar top quarks and supersymmetric dark matter*, Phys. Rev. D **62** (2000) 035012, [hep-ph/9911496].

[335] H. Baer, T. Krupovnickas, A. Mustafayev, E.-K. Park, S. Profumo, and X. Tata, *Exploring the BWCA (bino-wino co-annihilation) scenario for neutralino dark matter*, JHEP **12** (2005) 011, [hep-ph/0511034].

[336] C. D. Froggatt and H. B. Nielsen, *Hierarchy of Quark Masses, Cabibbo Angles and CP Violation*, Nucl. Phys. B **147** (1979) 277–298.

[337] M. Gell-Mann and M. Levy, *The axial vector current in beta decay*, Nuovo Cim. **16** (1960) 705.

[338] T. Binder, T. Bringmann, M. Gustafsson, and A. Hryczuk, *Early kinetic decoupling of dark matter: when the standard way of calculating the thermal relic density fails*, Phys. Rev. D **96** (2017), no. 11 115010, [arXiv:1706.07433]. [Erratum: Phys.Rev.D 101, 099901 (2020)].

[339] A. Hryczuk and M. Laletin, *Impact of dark matter self-scattering on its relic abundance*, Phys. Rev. D **106** (2022), no. 2 023007, [arXiv:2204.07078].

[340] D. Cadamuro, S. Hannestad, G. Raffelt, and J. Redondo, *Cosmological bounds on sub-MeV mass axions*, JCAP **02** (2011) 003, [arXiv:1011.3694].

[341] F. D'Eramo, N. Fernandez, and S. Profumo, *Dark Matter Freeze-in Production in Fast-Expanding Universes*, JCAP **02** (2018) 046, [arXiv:1712.07453].